Environmental Science

Wei Shan
Ying Guo
Fawu Wang
Hideaki Marui
Alexander Strom *Editors*

Landslides in Cold Regions in the Context of Climate Change

Springer

Environmental Science and Engineering

Environmental Science

For further volumes:
http://www.springer.com/series/3234

Wei Shan · Ying Guo · Fawu Wang
Hideaki Marui · Alexander Strom
Editors

Landslides in Cold Regions in the Context of Climate Change

Springer

Editors
Wei Shan
Ying Guo
Institute of Engineering Geology
Northeast Forestry University
Harbin
People's Republic of China

Fawu Wang
Faculty of Science and Engineering
Shimane University
Matsue
Japan

Hideaki Marui
Research Institute for Natural Hazards
Niigata University
Niigata
Japan

Alexander Strom
Geodynamics Research Center
JSC Institute Hydroproject
Moscow
Russia

ISSN 1431-6250
ISBN 978-3-319-00866-0 ISBN 978-3-319-00867-7 (eBook)
DOI 10.1007/978-3-319-00867-7
Springer Cham Heidelberg New York Dordrecht London

Library of Congress Control Number: 2013948752

Printed on acid-free paper

Springer is part of Springer Science+Business Media (www.springer.com)

Foreword

During the past 100 years, the global climate is changing and the geological disasters caused by it are growing. In the high-altitude permafrost regions, the degradation rate of glacier is accelerating, such as Qinghai-Tibet Plateau in China, the Alps in Europe and high mountain in Central Asia South America. On the other hand, in the high-latitude permafrost regions, such as Northern Canada, Alaska in USA, higher and lesser Khingan in Northeast of China, Siberia in Russia and the Nordic, the Southern boundary of permafrost is moving Northward gradually. Even in Kilimanjaro Mount in Africa which is located near the equator, also has been reported on permafrost degradation.

Many new geological problems are emerging with phenomena of permafrost degradation and extreme weather. Because repeated freeze-thaw cycle and the melting of surface and shallow slope, the geological disasters such as mountain collapse, mud-rock flow, and landslide are growing. All of above not only drastically changed the local geological and environmental conditions, but also caused huge losses to human lives and property, and threatened the security of local infrastructure.

In order to promote landslide research, as well as to contribute for the development of international community, environmental protection and capacity-building. On 21 January 2002, the International Consortium on Landslides (ICL) was established in Kyoto, Japan. ICL is a nonprofit and nongovernmental organization consisting (in 2012) of 51 member institutions from 32 countries; its International Program on Landslides (IPL) was jointly established by the United Nations Educational, Scientific, and Cultural Organization (UNESCO), World Meteorological Organization (WMO), Food and Agricultural Organization of the United Nations (FAO), United Nations International Strategy for Disaster Reduction (UNISDR), United Nations University (UNU), International Council for Science (ICSU), International Union of Geological Sciences (IUGS), and the World Federation of Engineering Organizations (WFEO).

In the ICL 10th Anniversary Conference (19 January 2012 in Kyoto, Japan), ICL decided to set up ICL Cold Regions Landslides Network (ICL-CRLN). The goal of it is, through exchanging and cooperation of the scientists coming from different countries and regions, as well as different professional field such as geography, geology, meteorology and so on, such problems as landslide mechanism, landforms distinguish, early warning and forecasting, disaster Assessment

were studied, which also could contribute to geological environment of the cold regions and safety of human life and property.

After legal procedures, ICL-CRLN announced its establishment in Harbin, China in July 2012. Currently, 15 scientists from Canada, Czech, China, Italy, Japan, Russia, and Switzerland joined ICL-CRLN. Wei Shan from Northeast Forestry University, China worked as the Network Coordinator, while Alexander Strom from Russia Geodynamic Research Center and Hideaki Marui from Niigata University, Japan served as the Deputy Coordinators.

At present, the study about landslides in cold region is not enough. However, this topic is likely to become concerns with the influence of climate changing on geological and environmental conditions in cold regions. This book we published now is a part of the study results of ICL-CRLN members, the content mainly is about landslides in cold region in the context of global climate changing. I appreciated their exploration spirit and their valuable research results, and also willing to recommend them to all the people interested in cold region landslide.

Florence, Italy, 15 June 2013

Paolo Canuti
President of International Consortium
on Landslides

Preface

As Prof. Canuti said, this book presents up-to-date research results of landslides in cold region. We define the cold region as the place where the monthly average temperature is less than −10 °C in the coldest month. In cold mountainous and hilly areas, the characteristics of mechanism, movement, and damage to environment of landslides are different with the landslides in noncold region. Moreover, these characteristics are closely related to climate change.

In order to strengthen the international cooperation and exchanges of landslide research in cold region, I proposed to launch the network of landslide research in cold region during the 10th council of the International Consortium on Landslides (ICL) in Rome in October 2011. This proposal was gotten the approval and support from Prof. Paolo Canuti (the president of the ICL), Prof. Sassa (the executive chairperson of the ICL), and the delegates participating in the council. In January 2012, the establishment of the network of landslide research in cold region was obtained by official approval of the ICL on 10th anniversary of the ICL in Kyoto University. After 6 months of preparation, the establishment of the network of landslide research in cold region of the ICL was proclaimed in Harbin, China on July 23, 2012. During the first meeting, we discussed and adopted the regulation and action plan of this network, published the declaration, and held the academic exchange of landslide research in cold region. Prof. Paolo Canuti, the president of the ICL, participated and delivered the congratulation. Dr. Alexander Strom who is the Researcher of the Geodynamic Research Centre (the branch of the JSC "Hydro-project Institute", Russia), Prof. Hideaki Marui who is the Director of the Research Institute for Natural Hazards and Disaster Recovery of Niigata University in Japan, Dr. Ying Guo from the Institute of Engineering Consulting and Design of Northeast Forestry University in China and other colleagues did fruitful work of developing the network of landslide research in cold region of the ICL. I really appreciate their supports and contributions.

At present, the members of the network of landslide research in cold region of the ICL and other colleagues from different countries and regions are using different research approaches to conduct comprehensive study on the landslides in cold region under climate change. This book is the summary of interim research results of colleagues and also a commemoration for the first anniversary of the network of landslide research in cold region of the ICL and the 3rd World Landslide Forum which will be hold in Beijing in June 2014.

Due to the differences from the regions and technical requirements, the topics, methods, and contents of colleagues' research are different. Dr. Filippo Catani, Prof. Paolo Canuti, and Prof. Nicola Casagli who are from the Department of Earth Sciences, University of Florence in Italy, and Dr. Chunjiao Wang and Prof. Wei Shan who are from the Northeast Forestry University in China studied the distribution of permafrost and slope movement before landslide using remote sensing. Their research results provide a scientific basis for early warning and prediction. Dr. Alexander Strom who is from the Geodynamic Research Centre (the branch of JSC "Hydroproject Institute", Russia) studied the process of landslide caused by the glacier of high-elevation mountain area in Central Asia from geological history. Prof. Hideaki Marui who is from the Niigata University and Prof. Fawu Wang who is from the Shimane University in Japan analyzed two landslides triggered by snowmelt in the North Central of Japan. Dr. Marten Geertsema and Dr. Menno van Hees who are from the Ministry of Forests, Lands and Natural Resource Operations in Canada, and Prof. Marta Chiarle who is from the Consiglio Nazionale delle Ricerche (Istituto di Ricerca per la Protezione Idrogeologica U.O.S. Torino, Italy) studied the debris flow triggered by snowmelt in the British Columbia of Canada. Italian scholars A. M. Ferrero, A. Godio, M. R. Migliazza, L. Sambuelli, A. Segalini, and A. Théodule et al., and Dr. Zhaoguang Hu who is from the Northeast Forestry University in China studied the geophysical characteristics of landslides in cold region. Prof. Adam Emmer and Prof. Vít Vilímek who are from the Charles University in Prague, Dr. Jan Klimeš who is from the Institute of Rock Structure and Mechanics, Academy of Sciences of the Czech Republic, Dr. Alejo Cochachin who is from the Unidad de Glaciologia y Recursos Hidricos in Peru, and Dr. Krivonogova and Dr. Stanislav Panov who are from the JSC Vedeneyev VNIIG in Russia studied the effect of landslides on reservoir safety in high-elevation mountain area in South America and the central Siberia permafrost in Russia. Marina Leibman who is the Chief Scientist of the Earth Cryosphere Institute SB RAS in Russia and her research team contributed four papers which presented the mechanism of permafrost landslides located in the northern Russia where is close to the Arctic Polar plains from geomorphology, vegetation and geochemistry. They also carried out the classification and risk assessment of landslides. Prof. Tonglu Li who is from Chang'an University in China and his team studied the mechanism of landslides in the permafrost of Qinghai-Tibet Plateau and the seasonal frozen region in the Northwest of China. Dr. Shiwei Shen and Prof. Lei Nie who are from the Jilin University presented a fast stability evaluation method of collapse in sliding type slopes. Prof. Wei Shan and Dr. Hua Jiang who are from the Northeast Forestry University studied the mechanism and movement characteristics of landslides located in the degraded areas of high-latitude permafrost in the Northeast China based on the data of climate change, geological survey, and monitoring. Dr. Ying Guo analyzed the effect of seasonal frozen-thaw process on the stability of soil slope according to the data of field monitoring and laboratory experiments.

In the occasion of completion of this edited book, I would like to thank all colleagues of the network of landslide research in cold region of the ICL.

Sincerely, I extend special thanks to my old friend, Prof. Fawu Wang who is one of the founders of the ICL. I appreciate his continued support and help for 10 years. Also, I would like to thank Agata Oelschläger, Kiruthika Poomalai, Fermine Shaly and Shine David of Springer. Without their excellent work, this book cannot be published on time and with high editing quality. Nonetheless, all errors and bias remain ours.

This book is the part of research results of my colleagues and me. Indeed, it is far from perfect. With the deepening of our research, more attention and more colleagues who plan to contribute to the landslide research in cold region, we will offer more high-quality research results, which will be the great contribution for global disaster mitigation.

Shan Wei

Harbin, China, 21 June 2013

Wei Shan
Coordinator of ICL Landslides
in Cold Regions Network,
Professor of Northeast Forestry University

Contents

Part I
Landslides Related to Climate and Environment Changes

Catastrophic Slope Processes in Glaciated Zones of Mountainous Regions

Alexander Strom

Abstract Catastrophic slope failures that occur in glaciated zones of mountain ranges at high altitudes can be considered as landslides in cold regions, since ice plays an important role in their origination and emplacement. Case studies of the XX Century rock avalanche that fell onto the glacier and of the extraordinary prehistoric ice-rock avalanche are described briefly. They demonstrate that presence of large quantities of ice in the glaciated zones of high mountains results in significant masking of the origin of debris accumulations that could be found either on glaciers or at the feet of heavily glaciated slopes.

Keywords Glacier · Landslide · Rock avalanche · Ice-rock avalanche

1 Introduction

Cold regions include not only areas at high latitudes (Siberia, Far East of Russia, North-Eastern China, Northern Canada, Alaska, Southern Chile) but also high mountains and, especially, glaciated zones of mountainous regions regardless of latitude. The specific character of such processes in glaciated areas is predetermined by presence of permafrost and ice. The latter form large portion of the collapsing masses on the one hand and of the bed over which they move on the other hand.

Such phenomena as rock and ice-rock avalanches attract researchers' attention for many years (Evans and Clague 1988; Reznichenko 2012). Besides direct threat posed to local communities and infrastructure they play an important role in general evolution of glaciers and, thus, affect water balance of the rivers that

A. Strom (✉)
Geodynamic Research Centre—Branch of JSC, Hydroproject Institute, Moscow, Russia
e-mail: a.strom@g23.relcom.ru

W. Shan et al. (eds.), *Landslides in Cold Regions in the Context of Climate Change*, Environmental Science and Engineering, DOI: 10.1007/978-3-319-00867-7_1,

originate from glaciers (Reznichenko et al. 2010). That is why study of various slope processes that take place in glaciated zones of mountainous ranges should be an important topic of the "Landslides in cold regions" ICL Network.

2 Catastrophic Slope Failures

Catastrophic slope failures that occur in the regions in question can be divided, at a large extent conventionally, in two main groups: (a) bedrock landslides that fell onto glaciers and move over them, and (b) slope failures that include large amount of ice.

The first group can be exemplified by 1964 Sherman Glacier rock avalanche (McSaveney 1975, 1978), 1986 Bualtar Glacier rock avalanche in Karakorum, Pakistan (Hewitt 1988), 1997 Mount Munday rock avalanche in British Columbia (Delaney and Evans 2008), rock avalanches that accompany the 2002 Denaly earthquake (Jubson et al. 2006; Schulz et al. 2008), and other historical case studies. Similar prehistoric event in Greenland was described by Kelly (1980). Comprehensive analysis of this type of rock avalanches was provided recently in the PhD thesis of Reznichenko (2012) and by Shugar and Clague (2011). Thorough review of slope stability in paraglacial environment was performed also by McColl (2012).

Second group can be exemplified by the catastrophic 1962 and 1970 Huaskaran ice-rock avalanches in Peru (Evans et al. 2009b) by the 2002 Kolka-Karmadon disaster in Northern Osetia (Petrakov et al. 2008; Evans et al. 2009a) and other less disastrous events (Huggel 2008).

Hereafter I present brief description of case studies related to both types of the phenomena—rock avalanche the caved onto glacier in northern Caucasus likely in 1959 or few years earlier and the extraordinary prehistoric ice-rock avalanche in the Alai valley (Kyrgyzstan).

2.1 Rock Avalanche Over Glacier

Looking over August 1959 aerial images of the glaciated zone of the Great Caucasus Range I found an impressive image of rock avalanche that fell on the glacier in the upper reaches of the Urukh river basin most likely same year or, may be, 1–2 years earlier (Fig. 1). This assumption is based on undisturbed shape of rock avalanche body without any evidence of reworking except some fractures at the upper and middle parts of the depositional zone that cross both ice and overlying debris. Rock avalanche debris with significant portion of large blocks up to several meters in size forms thin blanket that overlays minor irregularities of the underlying glacier relief (Fig. 2) in the same way as it was observed at the rock avalanches that accompanied the 2002 Denali earthquake (Jibson et al. 2006; Schulz et al. 2008).

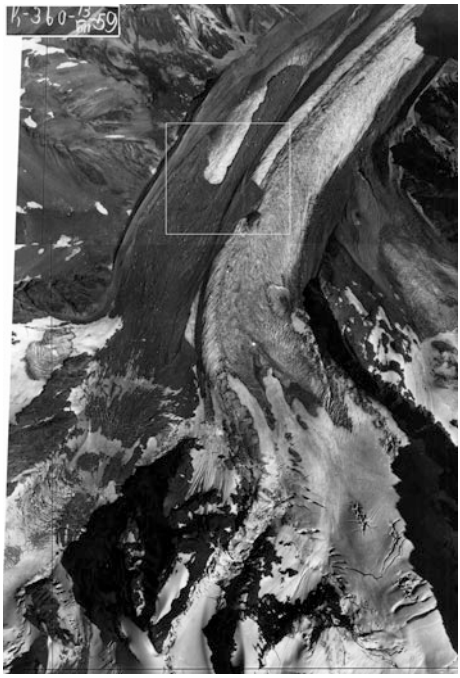

Fig. 1 Aerial photograph of rock avalanche deposits that form thin blanket of debris over glacier in the upper reaches of the Urukh River basin. Source zone of rock avalanche is in the *shadow*. Outlined fragment is shown on Fig. 2

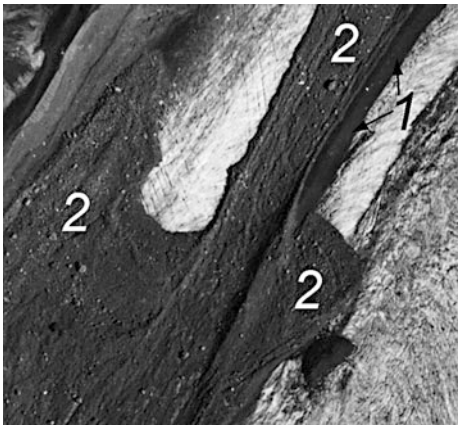

Fig. 2 Interaction of rock avalanche debris (2) with underlying glacier relief. 1—the moraine levee composed of much finer material. Note that diagonal fractures visible on ice in the *upper central* part of the image do not affect rock avalanche deposits

No historical records about this phenomenon were found in publications. However, fortunately, Goggle Earth provides high resolution space image of the same area obtained on November 23, 2004 (Fig. 3) allowing comparison of rock avalanche deposits shape and position after 45 years. If there would be no information about this rock avalanche, coarse deposits visible now on the surface of this glacier could be easily interpreted as "normal" moraine.

Fig. 3 Google Earth 2004 space image of the same area as shown on Fig. 1. Front of coarse rock avalanche material can be found on the glacier surface about 500 m downstream from its initial position, while the proximal part of rock avalanche almost disappeared being transformed into two levees very similar to lateral moraine

2.2 Prehistoric Extraordinary Ice-Rock Avalanche in the Alai Valley

Ice-rock avalanches carrying out large quantities of easily melting ice belong to the most hazardous natural phenomena in high mountains. They move very rapidly at an abnormally large distances (Petrakov et al. 2008; Evans et al. 2009a, b; Huggel 2008). However, the Komansu case study described briefly hereafter is extraordinary even among these outstanding events due to volume of material involved and runout distance (Fig. 4).

The site is located in the central part of the so called Alai valley—large intermountain depression between the Zaalay (Transalay) Range of the Northern Pamirs and the Alay Range of the Southern Tien Shan. The Zaalay Range, which was the source of this slope failure is up to 7 km a.s.l. high and rises up to 3.0–4.0 km above the depression bottom.

Zone of unusual irregular topography with hills and furrows (local term—"chukur") about 14 km long across the Alay valley and up to 8 km along it (see Fig. 4) was first described in the middle of 20th Century by K.V. Kurdiukov who proposed that it is the eroded body of the gigantic rock avalanche about 4–5 km^3 in volume. Later on, Nikonov and his co-authors (1983) argued that his interpretation is wrong and that this feature, along with several other "chukur" fields typical of

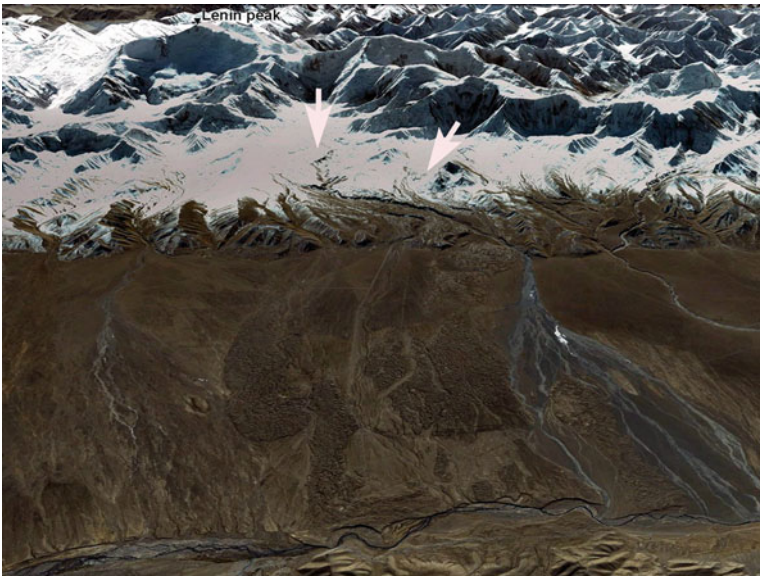

Fig. 4 The prehistoric Komansu ice-rock avalanche deposits in the central part of the Alai intermountain depression. 3D Google earth image. View from the north. *Arrows* indicate possible source zone of the slope failure. Distance from the watershed of the Zaalai range with the topmost summit—the Lenin Peak (7134 m a.s.l.) to the Kyzylsuu river at the foreground slightly exceeds 30 km. Traces of active faults pass along the foot of the range and at the frontal part of the avalanche body about 2.5 km south from the Kyzylsuu river

the Zaalay Range northern foothills have glacial origin. Indeed, microrelief of this feature is quite irregular, which is typical of moraines, rather then of rock avalanches. Some morphological and sedimentological peculiarities, however, contradict this interpretation.

First, the Komansu deposits front rises several tens of meters over the lowermost part of its base, indicating that it "climbed" on the opposite—northern slope of the valley, which is strange for the front of the glacier that had to move slowly being so far from its feeding zone. Second, material in some outcrops at this frontal part is completely unrounded, and represents breccia with sandy matrix typical of rock avalanches (Fig. 5). At some outcrops blocks of such material are mixed with moraine material but demonstrate jigsaw structure (Fig. 6). Third, at the outcrop along the right bank of Kyzylsuu River one can see at a distance of several hundreds meters that the Komansu body overlays two river terraces without any sign of their erosion by water (Fig. 7). Huge advancing glacier must produce large amount of melt water that would leave some signs of erosion at the terrace surface.

Besides, such overlaying, along with evidence of river damming visible at the north-eastern part of the Kumansu body where it is eroded by the Kyzylsuı river allows assumption that this feature is relatively young—Holocene. If so, it should occur later than maximal glaciation in this region took place.

Fig. 5 Crushed rock avalanche-style debris in the frontal part of the Komansu deposits

Fig. 6 The Jugsaw pazzle of breccia blocks in the moraine-like material. Outcrop at the left bank of the Kyzylsuu river

Most logical explanation of the totality of the observable features implies that the Kumansu body is the deposit of the gigantic extra-mobile ice-rock avalanche that originated on the glaciated northern slope of the Zaalay Range close to its watershed and travelled 27–33 km (depending on the location of its actual source) with elevation drop of about 3 km.

Large proportion of ice that was presented in the deposits, underwent intensive melting that led to formation of the chaotic moraine-like "chukur" relief. More recent glaciers degradation promoted significant erosion of the deposits of ice-rock avalanche. All these processes masked real origin of the studied feature producing relief more typical of glacial deposits rather then of those formed by purely gravitational processes.

Fig. 7 The Komansu body overlays two river terraces without any sign of water erosion

3 Conclusions

Case studies described herein briefly demonstrate that presence of large quantities of ice in the glaciated zones of high mountains results in significant masking of the origin of debris accumulations that could be found either directly on glaciers or at the feet of heavily glaciated slopes. Those that originated due to either bedrock or ice-bedrock slope failures often look like moraines even several decades after the event. It can explain the fact that source zones of most of large-scale bedrock landslides have been found not at the topmost parts of the ranges, but within the intermediate sections of their slopes (see, for example, Hewitt 2002).

Along with ongoing monitoring of slope failures in the remote hardly attainable glaciated areas that can be performed by use of the remote sensing data (Kaab et al. 2003) and seismological observations (McSaveney and Downes 2002) special studies focused on identification of significantly reworked slope failures in glaciated zones should be performed. They can provide important input data that will shed more light on interrelations between glaciers and rockslides.

Acknowledgments My study in the Alay valley was performed within the frames of the UNU PALM Project "Sustainable Land Management in the High Pamir and Pamir-Alai Mountains in Central Asia". During the 2009 field trip in this region I worked together with Mr. Alexander Meleshko, who passed away prematurely in 2010.

References

Delaney KB, Evans SG (2008) Application of digital cartographic techniques in the characterization and analysis of catastrophic landslides; the 1997 mount munday rock avalanche, British Columbia. In: Locat J, Perret D, Turmel D, Demers D, Leroueil S (eds) Proceedings of the 4th Canadian conference on geohazards: from causes to management. Presse de l'Université Laval, Québec

Evans SG, Clague JJ (1988) Catastrophic rock avalanches in glacial environments: proceedings, 5th international symposium on landslides, vol 2, pp 1153–1158, Lausanne, Switzerland

Evans SG, Tutubalina OV, Drobyshev VN, Chernomorets SS, McDougall S, Petrakov DA, Hungr O (2009a) Catastrophic detachment and high-velocity long-runout flow of Kolka Glacier, Caucasus Mountains, Russia in 2002. Geomorphology 105:314–321

Evans SG, Bishop NF, Fidel Smoll L, Valderrama Murillo P, Delaney KB, Oliver-Smith A (2009b) A re-examination of the mechanism and human impact of catastrophic mass flows originating on Nevado Huascarán, Cordillera Blanca, Peru in 1962 and 1970. Eng Geol 108:96–118

Hewitt K (1988) Catastrophic landslide deposits in the Karakorum Himalaya. Science 242:64–67

Hewitt K (2002) Styles of rock avalanche depositional complexes conditioned by very rugged terrain, Karakoram Himalaya, Pakistan. In: Evans SG, DeGraff JV (eds) Catastrophic landslides: effects, occurrence, and mechanisms, vol XV. Reviews in Engineering Geology, Geological Society of America, Boulder, CO, pp 345–377

Huggel C (2008) Recent extreme slope failures in glacial environments: effects of thermal perturbation. Quatern Sci Rev. doi:10.1016/j.quascirev.2008.06.007

Jibson RW, Harp EL, Schulz W, Keefer DK (2006) Large rock avalanches triggered by the M 7.9 Denali fault, Alaska, earthquake of 3 November 2002. Eng Geol 83:144–160

Kaab A, Wessels R, Haeberli W, Huggel C, Kargel JS, Khalisa SJS (2003) Rapid ASTER imaging facilitates timely assessment of glacier hazards and disasters. EOS 84(13):117–124

Kelly M (1980) A prehistoric catastrophic rock avalanche at Holsteinsborg, West Greenland. Bull Geol Soc Denmark 28:73–79

McColl ST (2012) Paraglacial rock-slope stability. Geomorphology 153–154:1–16

McSaveney MJ (1975) Sherman Glacier rock avalanche of 1964: the emplacement and subsequent effects on the glacier beneath it. PhD thesis, Ohio State University, p 426

McSaveney MJ (1978) Sherman Glacier rock avalanche, Alaska, U.S.A. In: Voight B (ed) Rockslides and avalanches, vol 1, Elsevier Scientific Publishing Co., Amsterdam, pp 197–258

McSaveney MJ, Downes G (2002) Application of landslide seismology to some New Zealand rock avalanches. In: Rybar J, Stembek J, Wagner P (eds) Landslides. Balkema, pp 649–654

Nikonov AA, Vakov AV, Veselov IA (1983) Seismotectonics and earthquakes of the convergence zone of the Pamirs and Tien Shan. Moscow, Nauka Publishers, p 240 (in Russian)

Petrakov DA, Chernomorets SS, Evans SG, Tutubalina OV (2008) Catastrophic glacial multi-phase mass movements: a special type of glacial hazard. Adv Geosci 14:211–218

Reznichenko NV (2012) Rock avalanches on glaciers: processes and implications. PhD Thesis, University of Canterbury, p 288

Schulz WH, Harp EL, Jibson RW (2008) Characteristics of large rock avalanches triggered by the November 3, 2002 Denali fault earthquake, Alaska, USA. In: Chen Z, Zhang J, Li Z, Wu F, Ho K (eds) Landslides and engineered slopes, from the past to the future, vol 2, pp 1447–1453

Shugar DH, Clague JJ (2011) The sedimentology and geomorphology of rock avalanche deposits on glaciers. Sedimentology 58(7):1762–1783

Slope Instability Phenomenon in the Permafrost Region Along the Qinghai–Tibetan Highway, China

Hong Wang, Xianli Xing, Tonglu Li, Zhou Qin and Junhai Yang

Abstract The area of permafrost occupies 150 $\times$ 10^4 km^2 on the Tibetan Plateau. Slope stability in permafrost regions is one of serous geological problems in the construction of the Qinghai–Tibetan Highway, which has been claimed to be an environment harmony project. Based on the field investigation, it is found that the main types of slope failure in the permafrost regions include slope collapse, slope creeping, surface vegetation creeping, debris flow and thaw-slumping. Among which, the thaw-slumping is the most hazardous one to the environment, vegetation and the engineering. The slumping may attribute to engineering excavation, which can disturb the thermal balance of the slope soil and cause thawing. As the slope soil thawing, the strength decreases in a large extent or even lost mostly, then the slope may fail in a very low slope angle. The countermeasures for the thermal thawing slides should maintain the frozen state of the soil for keeping from thawing, using methods such as covering with coarse material which can prevent heat absorption and be good for heat release.

Keywords Slope stability · Permafrost · Tibetan Plateau · Failure mechanism · Embankment

1 Introduction

For construction of traffic lines and oil pipelines in high latitude permafrost region, research on permafrost was firstly performed in the developed countries such as Canada and United States. In 1974, McRoberts and Morgenstern (1974) divided

H. Wang · X. Xing · T. Li (✉)
Department of Geological Engineering, Chang'an University, Xi'an, Shaanxi 710054, China
e-mail: dcdgx08@chd.edu.cn

Z. Qin · J. Yang
First Highway Consultants Co. Ltd, Xi'an, Shaanxi 710054, China

W. Shan et al. (eds.), *Landslides in Cold Regions in the Context of Climate Change*, Environmental Science and Engineering, DOI: 10.1007/978-3-319-00867-7_2,

slope instability of permafrost into three types: debris flow, landslide and collapse. For stability assessment of permafrost slope, three methods have been put forward at present, namely, the effective stress method proposed by Weeks (1969); the total stress method by Hutchinson (1974) and the method based on the effective stress and melting-consolidation theory by McRoberts and Morgenstern (1974). The three methods all established the calculation model on the shallow plane infinite slope and Mohr-Coulomb criterion, although their mechanisms are different. Another important feature of permafrost slope is creep deformation. With trees-rings, Wu (1984) estimated that one of the permafrost slopes in Alaska has been creeping in the past 80 years. Through laboratory tests, McRobert proved that creep of frozen soil can occur at very low stress levels (McRoberts 1978), and a long-term creep potential would cause a large-scale deformation and instability of the slope.

The area of permafrost occupies 150×10^4 km^2 on the Qinghai–Tibet Plateau (QTP). In the early time, human influence in this region is relatively weak. However, since the 1950s, with the sequential constructing of Qinghai–Tibet highway (QTH), Yunnan–Tibet highway (YTH), the Qinghai–Tibet railway (QTR), and South-to-North Water Transfer Project, disturbance of geological environment in the permafrost region inevitably lead to instability of the slopes. Slope stability is one of the key problems faced in the engineering construction. However, the research on slope stability of permafrost is still insufficient in China. The research is carried out combining with the construction of QTR and QTH. The permafrost on QTP, belongs to the plateau permafrost, is different from that on the other parts of the world which belongs to high altitude permafrost. Based on temperature environment, Lin et al. (2011) divided instable permafrost slope on QTP into the two types of frozen slope and thawing slope. The change in temperature will lead to deformation and instability of slopes, even though permafrost is general a solid material with higher strength. The frozen slope often has two types of failure modes. One is rock or soil falls, mainly occurs in rocky slopes with fractures and the soil slopes with rich ice, which may suffer from frequently frozen-heaving cycles. Since it is the most common failure type in natural and excavation slopes, passive or active protective measures have to be taken. Another type is creeping. The existence of ice in permafrost makes its creep character much more complex than that of normal soil and the creeping occurs even at very low stress levels, the creeping can happen both in steep-slope and moderate-slope, so it is widespread on QTP. Creeping changes with seasons, and the results of field test in the Fenghuo mountain region of QTP show that creep mainly occurs in winter and summer, creep strain decreases with the increase of the depth, but increases with ground temperature at the same depth (Wang and French 1995). The inverse displacement along the slope in winter implies the action of frost-heave. Failure of the frozen slopes generally occurs naturally and has less influence on the engineering. The thawing slope has three types of failure models: thaw slumping, mudflow terrace and vegetation creeping. In permafrost region, thaw slumping is widespread. Due to rise of air temperature, surface frozen soil thaws, soil with high content of ice changes into mixture of hard rock block and flowing slurry, which

has quite low shear strength or even lose the strength. Thaw slumping has a very shallow sliding plane which roughly paralleling to the slope surface, and could occur on very gentle slopes. In the permafrost region of QTP, thaw slumping is likely to happen on the slopes with the gradient of higher than 3°. The failure has a retrogressive extension to backward and sideward and the failed land surface is hard to recover. Mudflow terrace is a ladder-like landform caused by sliding of thawed soil. A unique case was found in a wide valley with gradient of about 10° in the Fenghuo mountain. There are ten steps with width of 5–10 m each and well vegetation cover. Mud flow terrace is thought to be formed as the thawed soil slides down on the slope surface, the vegetation underneath may check the movement and company drainage and consolidation. At this period, the soil sliding down behind overlays on the former sliding mass to form a step with gentle surface. The same process may occur in a valley to form number of steps. Vegetation creep is an especial landform. The vegetation on the slope surface slides down in variety size of pieces to form the scale-like landscape. It occurs as the slope gradient higher than 15° and has less impact on the engineering, usually results in vegetation degradation and soil erosion, as well as the ecological crisis.

From the above mentioned, it is clear that thaw slumping is the worst of all the slope failures to engineering, but it is also induced by engineering.

2 Engineering Induced Thaw Slumping and the Forming Conditions

With construction of roads and railways on QTP since last century, the engineering disturbances caused thawing of frozen soil, and consequently thaw slumping and other slope failure occurred. The Qinghai–Tibet Highway (QTH) starts from Xining city, Qinghai province in the North–East, terminates to Lhasa city, Tibet in the South–West, with the total length of 1,936 km. QTH is a second degree road and mostly runs aside QTR line. QTH was started to construct in 1950 and put onto working in 1954. It was improved for times in the history. The last portion from Gelmud to Lhasa with the length of 1,140 km mostly lies on the permafrost region of high altitude over 4,500 m.

The thaw slumping caused by construction of QTH mainly locate in the Hohxil hill region (K3014–3019), Beiluhe Basin (K3030–3060), and southern slope of the Fenghuoshan mountain (K3070–3080) (Fig. 1). The total length is about 45 km.

The thaw slumping near the milepost K3035 was caused by an accidental removal of soil during road reconstruction in the years between 1990 and 1992. Outcropped ground surface formed after earth borrowing. In summer, thawing of ground ice on the pit wall led to collapse of the upper part of the soil, which caused slumping of the soil for the first time. Afterward, it started to develop outward year by year and now formed a slumping with the length of 103 m East–Westward, the width of about 72 m North–Southward, the thickness of 1.5–2.0 m and the size of

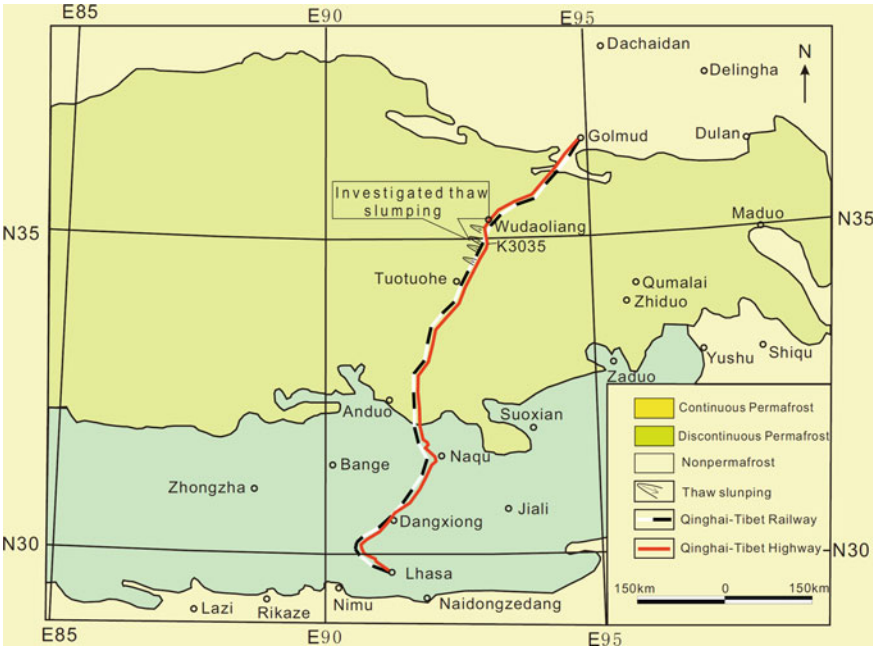

Fig. 1 Distribution of the permafrost and the thaw slumping on QTP

about 10,000 m^3 (Fig. 2). The slumping is located between Wudaoliang and the Tuotuo River, 40 km north of Fenghuo Mountain and at the altitude of 4,578 m. The slumping occurred on a gentle slope with the gradient of about 7°. We will take this case for further analysis on thaw slumping.

The area belongs to a dry-cold climate with thin air density and low air barometric. The four seasons here are not distinct and the annual freezing time lasts for seven to eight months. It freezes from September to next April,with the annual average temperature is −5.2 °C, extreme maximum temperature 23.2 °C and extreme minimum temperature −37.7 °C. It has the average annual rainfall of

Fig. 2 Thaw slumping near milepost K3035 of QTH

291 mm and the average evaporation of 1,317 mm. The annual mean ground temperature monitored is −1.75 °C, so it belongs to permafrost area of low temperature.

Boreholes and shafts revealed that the formations here are the upper Neocene lacustrine sediment and Holocene alluvial deposits. The strata from the surface is composed of 0.00 ~ 1.10 m reddish-brown sand, wet, loose, and locally intercalated with reddish-brown silty clay (w_p = 11.4–16.8 %, w_L = 18.9–26.9 %); 1.10–1.30 m, gray loose silt and fine sand; 1.30–2.00 m, red silty clay (w_p = 14.6 %, w_L = 25.5 %), with 20 cm ice block inclusions at the base; 2.00–4.00 m, thick ice bed with smooth surface; 4.00 ~ 11.80 m, highly weathered reddish-brown mudstone freezing all year; 11.8–13.3 m, gray sandstone, hard, with tiny fracture ice locally; under 13.3 m, argillaceous sandstone. According to the ice content and structure characteristics, the frozen soil from top to base is divided into the following three layers: 0.0–2.0 m, seasonal thawing layer; 2.0–4.0 m, soil containing ice; under 4.0 m, massive cryostructures. The upper boundary of the permafrost is about 2.0 m in depth, that is the upper surface of the thick ice bed.

3 Monitoring of the Thawed Soil Thickness

Two thermometer boreholes, A and B, were drilled on the K3035 slumping. Hole A is located behind the head scarp of the slumping, in which 5 temperature probes were installed in the distance of 0.5 m each other; Hole B is located in the upper of the slumping mass, also 5 probes set as Hole A. Positions of monitoring boreholes in plane and profile were shown in Figs. 3 and 4. Monitoring data applied here are from 16 August 2002 to 2005, which lasts for three climatic years.

Hole A represents the natural slope outside the K3035 slumping. Ground temperature at depth of 0.5, 1.0, 1.5, 2.0 and 2.5 m in the monitoring period is shown in Fig. 5 and the frozen depth in Fig. 6 respectively. First, it can be seen that soil temperature changes annually and there is a freezing period and a thawing period each year. The thawing period at the depth of 0.5 m lasts from early April to the beginning of December, and the freezing period lasts from early December to early April next year. With increase of the depth, the thawing period is shortened and delays in some extent. Figure 6 shows that the maximum thawing depth monitored is 2.2 m, generally appears in the mid-September and approximately the same in the three thawing periods. So, the upper boundary of the permafrost is 2.2 m.

The ground temperature at the depth of 0.5, 1.0, 1.5, 2.0 and 2.5 m monitored in Hole B is shown in Fig. 7 and the frozen depth in Fig. 6. Similar to Hole A, the soil temperature changes annually and the thawing period at the depth of 0.5 m is almost the same as that of Hole A. The thawing period is shortened with the increase of depth and also delays clearly. It can be seen from Fig. 6 that maximum thawing depth is relatively shallow, which is 1.5 m, and also the same in the three

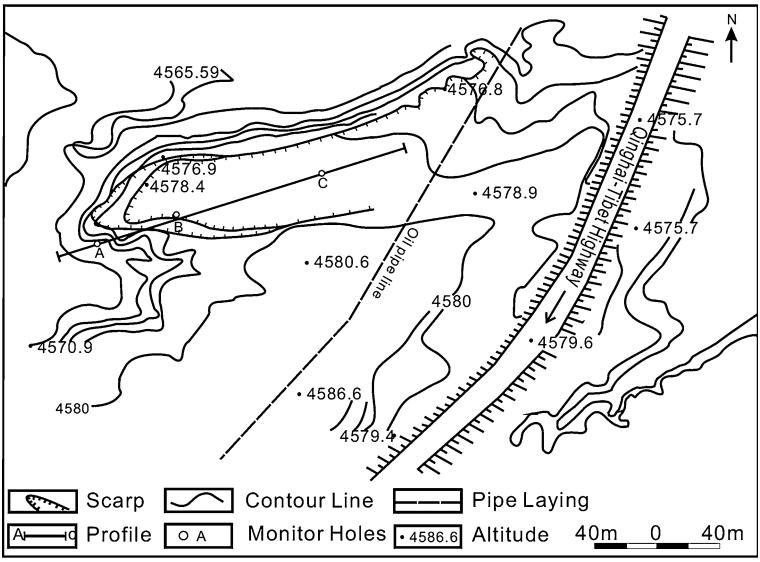

Fig. 3 Relief map and range of K3035 thaw slumping

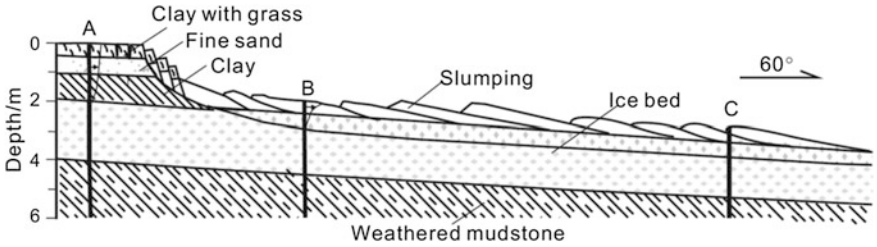

Fig. 4 Profile of the K3035 thaw slumping

is thawing periods. It shows that thaw slumping has changed the hydrothermal condition, and the annual maximum thawing depth is shallower than that in Hole A, so the upper boundary of the permafrost has redistributed in the slumping area.

In addition, Geokon-603 inclinometers were set in boreholes A, B and C. Of which, Hole C is located near the toe of the slumping mass as shown in Fig. 1. The monitoring started from 9 August 2002 to 16 April 2003, which had experienced a thawing period and a freezing one. Figure 8 shows the cumulative deformation of Holes A and C in the 250 days monitoring and that in Hole B in 15-day before 25 August, because the monitoring was stopped in Hole B at the date due to damage of the tube by extensive deformation. It can be seen that the maximum accumulative displacement at Hole A is 3.7 mm and that at Hole C is 10.9 mm. Even though Hole A is out of the boundary of the slumping, it still has slow displacement, but much smaller than that at Holes C, which indicates that the slumping

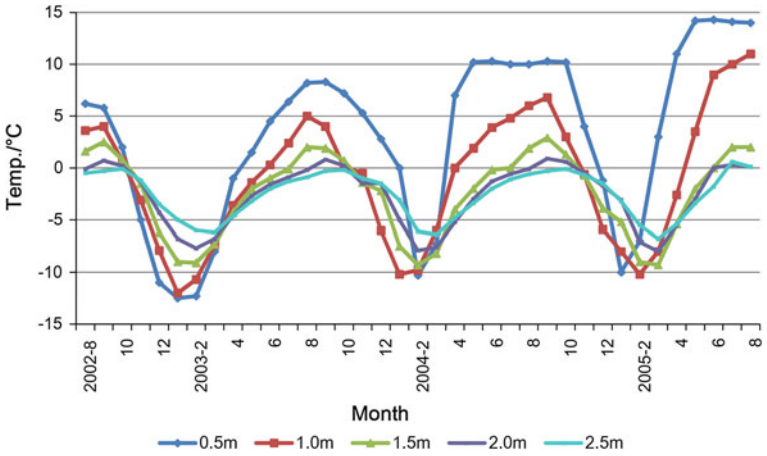

Fig. 5 Ground temperature changes at different depth versus time monitored in Hole *A*

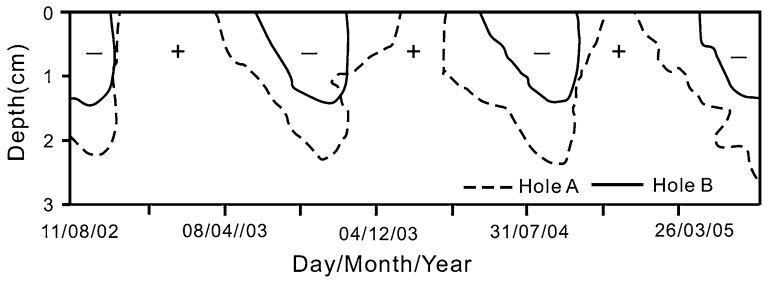

Fig. 6 The freezing depth monitored at Holes *A* and *B*

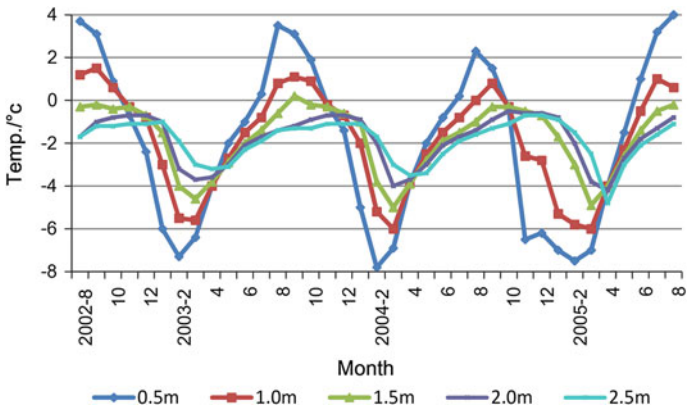

Fig. 7 Ground temperature changes at different depth versus time monitored in Hole *B*

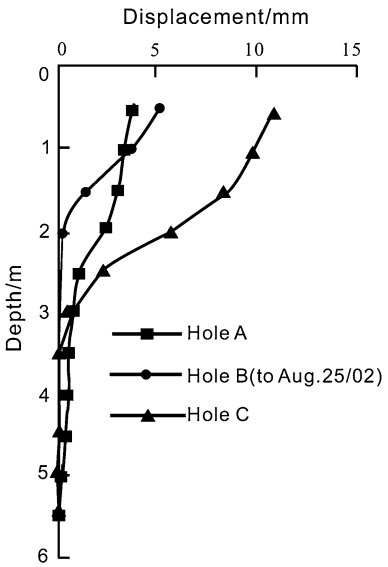

Fig. 8 Displacements versus depth monitored in the Holes *A*, *B* and *C* (8 Aug 2002 to 16 Apr 2003)

tends to develop backward. The maximum accumulative displacement at Hole B reached to 5 mm in 15 days reflects that displacement at the back of the slumping mass is larger than that in the front. Reclined fold and imbricate structure on the slope surface can also prove the movement feature.

Examining the displacement vertically, it is found that the deformation character of thaw slumping is different from that of general landslide. General landslide moves as blocks and has an obvious sliding surface. While the thaw slumping deforms transitionally, it means that, displacement changes from maximum to diminished from the surface to the bottom, which should be associated with the thermal gradient under the surface. With decreasing of temperature, viscous force of the sliding mass in plastic or flow state is enhanced and the strength of solid frozen bed is much higher, the displacement would be restricted in degrees with depth. There is no deformation under 2 m out of the slumping reflecting by the curve of Hole A, and the thickness of thawing soil observed at that point is 2.2 m, they basically agrees with each other. Obviously the deformation extended deeper on the slumping mass as seeing the curves of Holes B and C, but mainly concentrated in the depth of 0–2 m and diminished under 4.5 m. The ground temperature in Hole B shows that the thickness of the thawing soil is only 1.5 m, but the deformation zone extends below 1.5 m. It indicates that there is deformation in the frozen soil lying underneath the thawing layer. The curves of ground temperature at the depth of 1.5 m and 2.0 m in holes A and B are shown in Fig. 9. It can be seen that although the thickness of thawing soil at hole B is decreased, the ground temperature is increased. The lowest temperature of them has the difference over 4 °C. It indicates that the frozen soil in high temperature creeps too, so the effect on sliding mass has extended to the soil under the thawing layer. On the

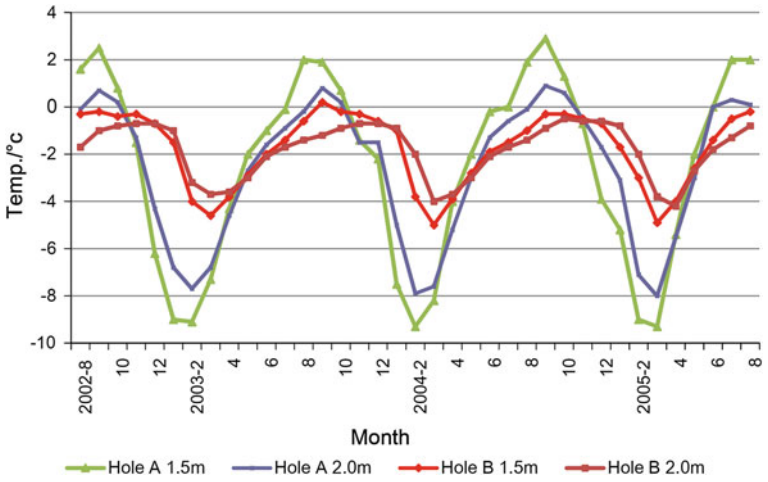

Fig. 9 Ground temperature versus month at depth of 1.5 and 2.0 m in Holes *A* and *B*

whole, deformation of the soil mainly occurred in the upper 2 m, above the surface of the thick ground ice, therefore, the thickness of thaw slumping is relatively less, but the influence area is large. It keeps on developing.

4 The Method for Thaw Slumping Stability Assessment

From the above analysis, thaw slumping has the features of thin thickness and broad area. The K3035 thaw slumping covers 7,200 m^2 of ground surface, but has the thickness of only 1.5–2.0 m, so the infinite slope model is suitable for its stability assessment as shown in Fig. 10. The model has the follow assumptions:

1. The sliding surface is a plane which parallels to the slope surface, so the thickness of the sliding mass is identical everywhere;
2. The thickness of the sliding mass is far more less than the length of the sliding mass;
3. The sides of the sliding mass extends infinitely, so the side effect is not considered;
4. The seepage flow direction is parallel downward to the sliding plane.

The shearing stress of the soil may be given by

$$\tau_f = c' + \sigma' \tan \phi' \tag{1}$$

To determine the factor of safety against failure along the plane *AB*, consider the slope element abcd. The forces that act on the vertical faces ab and cd are equal and opposite. The total weight of the slope element of unit length is

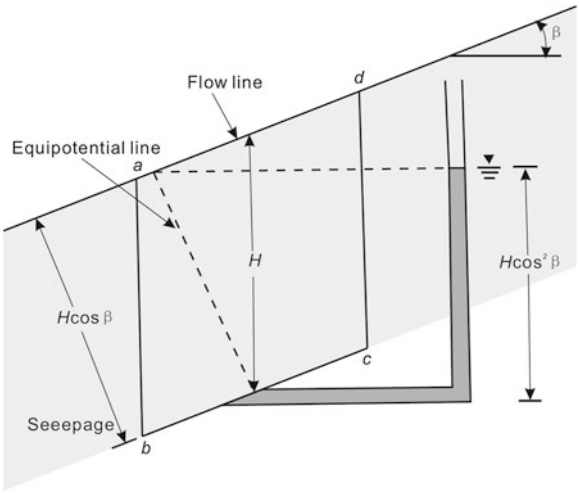

Fig. 10 Analysis model of infinite slope

$$W = \gamma_{sat} LH$$

The components of force acting on *the base bc of the element abcd in* the directions normal and parallel to plane ab are

$$N_r = \gamma_{sat} LH \cos\beta$$

$$T_r = \gamma_{sat} LH \sin\beta$$

The total normal stress and shear stress at the base of the element are:

$$\sigma = \frac{N_r}{L/\cos\beta} = \gamma_{sat} H \cos^2\beta \tag{2}$$

$$\tau = \frac{T_r}{L/\cos\beta} = \gamma_{sat} LH \cos\beta \sin\beta \tag{3}$$

Generally, the factor of safety is defined as

$$F_s = \frac{\tau_f}{\tau} \tag{4}$$

where F_s is factor of safety with respect to strength; τ_f is average shear strength of the soil; τ is average shear stress developed along the potential failure surface. From Eqs. (1) and (4), we get

$$\tau = \frac{\tau_f}{F_s} = \frac{c'}{F_s} + (\sigma - u)\frac{tg\varphi'}{F_s} \tag{5}$$

From Fig. 9, the pore water pressure can be deduced as

$$u = \gamma_w H \cos^2 \beta \tag{6}$$

Substituting σ in Eq. (2), τ in Eq. (3) and u in Eq. (6) into Eq. (5), we have

$$\gamma_{sat} LH \cos \beta \sin \beta = \frac{c'}{F_s} + (\gamma_{sat} H \cos^2 \beta - \gamma_w H \cos^2 \beta) \frac{tg\varphi'}{F_s}$$

The factor of safety with respect to strength can be deduced from the above equation as

$$F_s = \frac{c'}{\gamma_{sat} H \cos^2 \beta tg\beta} + \frac{\gamma'}{\gamma_{sat}} \frac{tg\varphi'}{tg\beta} \tag{7}$$

where γ' is effective unite weight.

As motioned above, during the warm seasons, the depth of the thawed soil on the ground can reach to 1.5–2.0 m and the soil is completely saturated. In addition, the surface of the frozen ice under the soil could be the sliding surface.

By direct shearing CD tests for six groups of the remolded silty clay sampling from the sliding plane K3035 slumping, its friction angle φ' is about 14° ~ 15° under the water content of liquid limit, while the cohesion c' is nearly zero, the saturated unit weight γ_{sat} of the soil is measured as 1.80 g/cm^3. As the slope gradient β is 7°, the safety factor Fs can be easily calculated from Eq. (7). It is between 0.90 and 0.97. Apparently, the sliding mass of the thaw-slumping is not stable in warm time. However, the stability is variable with seasonal thawing and frozen cycle, so it developed year by year.

5 The Forming Mechanism and the Mitigation Measure for Thaw-Slumping

Thaw-slumping is often initially triggered under disturbance of permafrost by engineering excavation, and then enlarges in the retrogressive process. A new cutting would damage the vegetation and disturb the thick ice bed underneath. The uncovered ground and the scarp may adsorb more solar radiation, then resulting in ice-rich permafrost thawing and part of the ice bed melting. Because the thick ice bed is impermeable, the thawed ice-rich permafrost could be extra-saturated and become liquid state, so it may flow down on the smooth ice surface. That is why the thaw-slumping may occur on a very gentle slope. The thaw slumping is commonly caused by slope toe disturbance. Once it is formed, slumping process would develop year by year, both laterally and backward.

From the experiences construction of QTH in decades, the conventional mitigation measures, such as retaining wall, stabilizing piles and frameworks are not effective for thaw-slumping control. The basic concept for mitigation of this special problem is to protect the permafrost, i.e., to reduce absorption and increase release of the solar radiation. Therefore, for those slopes already with thaw-

slumping have occurred, coarse grain material like sand or rock blocks are applied to cover the boundary of the slumping for keeping it in frozen state and block it from developing outward. The coarse material can obstruct the solar radiation to the permafrost, as well as release more heat out by the cold air flow through the porous. The rock blocks have been successfully used in the railway embankment to protect the permafrost in the foundation. For the slopes with slumping traces, it is important to fill and compact the fissures on the ground as early as possible, to make the ground recover to the original form and keep the surface sooth, as well as plant vegetation. For the slopes without slumping but within 500 m from the highway, it should be strictly prohibited to take soil material and vegetation should be planted to protect the slopes. Vegetation can absorb some solar energy and the roots can also stabilize the ground surface.

6 Conclusions

Construction of the QTH has caused some disturbance and damage to the permafrost environment. Thaw-slumping is one of the typical geological hazards induced by the engineering, which is characterized by the thin thickness, broad area, gentle sliding plane, saturated sliding mass, flow movement. Investigation for the K3035 thaw-slumping suggests that a little disturbance of the permafrost slope may induce a retrogressive slumping with long time activation, which may develop year by year. It is known that the QTP has a very sensitive and fragile environment because of the high elevations, insufficient oxygen, cold air and sparse vegetation. It is very difficult to recover the destructed environment. In engineering construction, protection of the environment is a severe challenge in the permafrost area.

References

Hutchinson JN (1974) Periglacial solifluction: an approximate mechanism for clay soil. Geotchnique 24:438–443

Lin ZJ, Niu FJ, Luo J, Lu JH, Liu H (2011) Changes in permafrost environments caused by construction and maintenance of Qinghai—Tibet Highway. J Central South Univ Technol 18:1454–1464

McRoberts EC (1978) Slope stability in cold regions. Geotechnical engineering for cold regions. MaGraw-Hill Book Company, New York, pp 363–404

McRoberts EC, Morgenstern NR (1974) The stability of thawing slopes. Can Geotech J 11:447–469

Wang B, French HM (1995) In situ creep of frozen soil. Tibet Plateau, China. Can Geotech J 23:545–552

Weeks AG (1969) The stability of natural slopes in southeast England as affected by periglacial activity. Q J Eng Geol 2:49–63

Wu TH (1984) Soil movement on permafrost slopes near Fairbanks, Alaska. Can Geotech J 21:699–709

Occurrence Mechanism and Movement Characteristics of Landslides in Bei'an to Heihe Expressway Area in China Under the Climate Change

Wei Shan, Hua Jiang, Zhaoguang Hu, Chunjiao Wang, Ying Guo and Chengcheng Zhang

Abstract In recent years, landslide occurrence is increasing in the section of Sunwu County to Xigang Town where the intersection of the Bei'an to Heihe Expressway and the northwest section of Lesser Khingan Mountain, China, is located. These landslides threat the stability of sub-grade and operation safety. The shape and movement characteristics of these landslides have significant difference with those in other areas. Based on the data of annual average temperature from 1954 to 2011 in Sunwu County, which was published by "China National Science and Technology Infrastructure Platform", and the data of cumulative monthly average air temperature, ground temperature, precipitation and maximum frozen soil thickness from 1971 to 2000 in Sunwu County, authors analyzed the relationship between the annual average temperature change and permafrost distribution. Based on the geological data, ground temperature, moisture, and landslide deformation monitoring data from 2009 to 2012 of the K178+530 and K177+550 cross section of the Bei'an to Heihe Expressway which pass through the northwest section of Lesser Khingan Mountain, authors comparatively analyzed the landslide formation mechanism and motion characteristics in the Bei'an to Heihe Expressway area combining with the temperature and atmospheric precipitation data of Sun Wu weather station in related time. The study results show that the annual average temperature in Sunwu region shows a clear upward trend in the past 50 years. After 1995, the annual average temperature in the region rises to 0 °C, and permafrost degradation process is accelerated. Landslides occurrence in this road area is the result of the combined effects of atmospheric precipitation, melting permafrost seepage water and geological condition. Sliding process of the landslides in this region is controlled by seasonal temperature change, water

W. Shan (✉) · H. Jiang · Z. Hu · C. Wang · Y. Guo · C. Zhang
Northeast Forestry University, Harbin 150040, China
e-mail: shanwei456@163.com

H. Jiang
Heilongjiang Institute of Technology, Harbin 150090, China

W. Shan et al. (eds.), *Landslides in Cold Regions in the Context of Climate Change*, Environmental Science and Engineering, DOI: 10.1007/978-3-319-00867-7_3,

content change. It is also related to geological condition with low angle, intermittent and creeping characteristics.

Keywords Climate change · Permafrost · Creeping · Landslide · Expressway

1 Introduction

Permafrost is widely distributed around north of 47° N in the Northeast China. In recent years, affected by climate change, south boundary of permafrost distributed in high latitude of the Northeast China has moved to north gradually. Permafrost near the southern boundary is distributed in the form of island. Degradation process of the permafrost is accelerating.

Climate change and its impact are the global research hotspots. The fourth assessment report of IPCC (Solomon 2007) pointed out that the global average surface temperature has increased. The global surface temperature showed a consistent warming trend. In addition, warming rate in nearly 50 years is almost two times in recent 100 years. Numerous studies show that climate change in China is consistent with the global climate change general trend (Chen et al. 2004; Lin et al. 1995; Shi et al. 1995; Zuo et al. 2004; Ren et al. 2005; Ding et al. 2006; Wang et al. 1998; Wang 1994). Warming rate in China is about 0.25 °C/10a in the past 54 years, which is much higher than the global or hemispherical average temperature increase rate over the same period. Moreover, the northeast China is one of the most significant temperature increasing areas (Chen et al. 2004; Zuo et al. 2004; He et al. 2013).

In recent years, the climate change causing permafrost degradation and influencing ecological environment has become a research hotspot.

Permafrost is the result of lithosphere and atmosphere energy exchange, which is an important part of the earth's cryosphere system. The presence, distribution, moisture, temperature, nature and state of permafrost are affected by many factors, and have showed distinct spatio-temporal variations. In the global and continental scale, permafrost is controlled by the climate latitude zonality law (Guo et al. 1998; Zhou et al. 2000). In the regional scale, the effect of altitude and longitude is distinct. In the local scale, various factors affecting the water and heat balance (such as snow, vegetation, gradient, exposure, lithology and water), the distribution and other characteristics of permafrost is strengthening (Cheng and Zhao 2000; Tutubalina and Rees 2001; Cheng 2003; Jin et al. 2008; Lv et al. 2008).

The Northeast China is the only high latitude permafrost region of China, also is China's second largest permafrost region. In the north Greater and Lesser Khingan Mountain, forests and snow have a very important impact on the temperature change and freeze-thawing process of the underlying seasonal frozen soil and permafrost. Snow, vegetation, water, topography, atmospheric inversion and other local factors significantly cause temperature displacement in the Greater and

Lesser Khingan Mountain in the Northeast China and Baikal region in Russia. Thus, Khingan-Baikal type permafrost is very different from the permafrost in polar and high altitude region (He et al. 2013). The northeast area is the cradle of cryopedology in China and one of the early study most intensive areas. However, during the thirty years period after the rising of the study on global climate change, in this area, we only can find the study on permafrost degradation affecting engineering structure in airport, road and pipeline. There is hardly any systematic study on climate change influence on permafrost change in northeast high latitude permafrost regions (Wei et al. 2010; Chang et al. 2013).

Landslide is a natural geological phenomenon in mountain area. Its occurrence mechanism and evolution is closely related to the geological condition and environmental factors, controlled by the factors of geological force, lithology and landform, and affected by environmental changes in land cover, rainfall and human activity. The characteristic of the temporal and spatial distribution is uncertain, abiogenetic, continuous and irreversible. Landslide is caused by geological environmental condition change, which also violently changes the geological environmental condition. Because of the complicated occurrence mechanism and evolution of landslides and the importance of landslide influencing on human survival and activities condition, people pay more and more attention on the research on landslide, and has get many valuable research results. However, in permafrost region, study on the occurrence mechanism, movement characteristics and disaster-causing mechanism of the landslides which are caused by permafrost melting aroused by climate change, extreme climate phenomena and geological condition of landslide is basically blank.

Taken the Bei'an to Heihe Expressway in China which pass through the Lesser Khingan Mountain area as study area, and the K177+550 and K178+530 landslide as study object, the formation mechanism and movement characteristic of the landslides were studied based on the weather monitoring data of the Sunwu County meteorological station, landslide section geological surveying and monitoring data.

2 The Study Area Natural Condition

The study area is located in the northwest section of the Lesser Khingan Mountain. The geographical position is N49°27′–N49°45′ and E127°12′–E127°33′. The elevation is from 210 to 330 m, and the average elevation is 285 m. Landform in study area is undulating terrain, and slope is quite steep in some areas. Slope surface is covered by flourished vegetation. The relative elevation difference is about 120 m.

The study area is is located in the Wuyun-Jieya new rift zone. The north side is Handaqi virgation and the south side is Shuhe upwarping zone. The existence and activity of the Heilongjiang fracture control and influence the tectonic activity of this area, especially the occurrence, development and evolution of tectonic

activities since the Yanshan movement, which form beach area and hilly topography.

The stratum substrate is volcanic rock of upper Jurassic Shenshu formation and lower Cretaceous Guanghua formation and granite of late Indosinian. The covering layer is the river and lake facies deposition of upper Cretaceous Nenjiang formation and Tertiary Pliocene Sunwu formation. The new tectonic movement in this area is mainly vertical movements of the fault blocks. The new rift zone decrease firstly and then increase. The Tertiary Pliocene Sunwu formation which is mainly consist of coarse sand or sand conglomerate overlaps the top of mountain and hilly. Rock with poor cementation shows a loose state. Mudstone, silty mudstone, tonhaltig fine sandstone and fine sandstone of the upper Cretaceous Nenjiang formation exposed in the lower part of the mountains or hills. Rock is with poor cementation, and its weathering zone is quite thick. The rock near ground surface is completely weathered River alluvium and stack layers of Quaternary period are distributed in the low-lying valley beach (Fig. 1).

There are many ancient landslides developed in the exposed area of the covering layer of new rift zone. Many landslides are distributed along both sides of the ridges or hills top. Somewhere, obvious stepped geomorphology can be found, which is caused by continuous sliding of landslides. Ridge part is relatively stable. Cracks caused by frost heaving were widely developed in exposed area of the upper Cretaceous mudstone. Island-shape permafrost distribution can be found in this region.

The study area is belong to continental monsoon climate. Winter is long, while spring, summer and autumn are short, cold and moist. Four seasons change obviously in this area. Spring get warm quickly, windy and dry weather. Summer is controlled by the southeast monsoon resulting in more easterly and southerly wind, mild and rainy. Weather become cool fastly in autumn. Harm often caused by early frost. Winter is affected by Siberia and Mongolia high pressure resulting in more west-northerly and northerly wind, cold and dry weather. The annual average temperature is −2 to 1 °C. Annual extreme maximum temperature is 38.6 °C. Annual extreme minimum temperature is −48.1 °C. The accumulated temperature is greater than or equal to 10 °C is 1,600–1,800 °C. The annual frost-free period is 80–120 d. The first frost is in late August to early September, and the last frost is in late May to early June. The annual average wind speed is 2.7–4.0 m/s. The average annual precipitation is 530–552 mm, sometimes reaches 800 mm per year. Rainfall concentrate in July to September of the summer, account for about 61–67 % of annual total precipitation. The first snow is in the middle of October, and the end snow is in late March to early April. Generally, the annual evaporation capacity is more than 1,000 mm, sometimes is 850 mm per year. The annual average sunshine is 2,500 h, changing from 2,200 h to 2,800 h. The annual total radiation amount average value is 1,148 kcal/cm^2. Standard seasonal frost depth is 2.3–2.5 m, maximum seasonal frozen depth is 2.85 m. Figure 2 the 30 years accumulative total month average air temperature, ground temperature (40 cm under the ground), precipitation, maximum frozen soil thickness curve from 1971 to 2000 in the Sunwu County meteorological station.

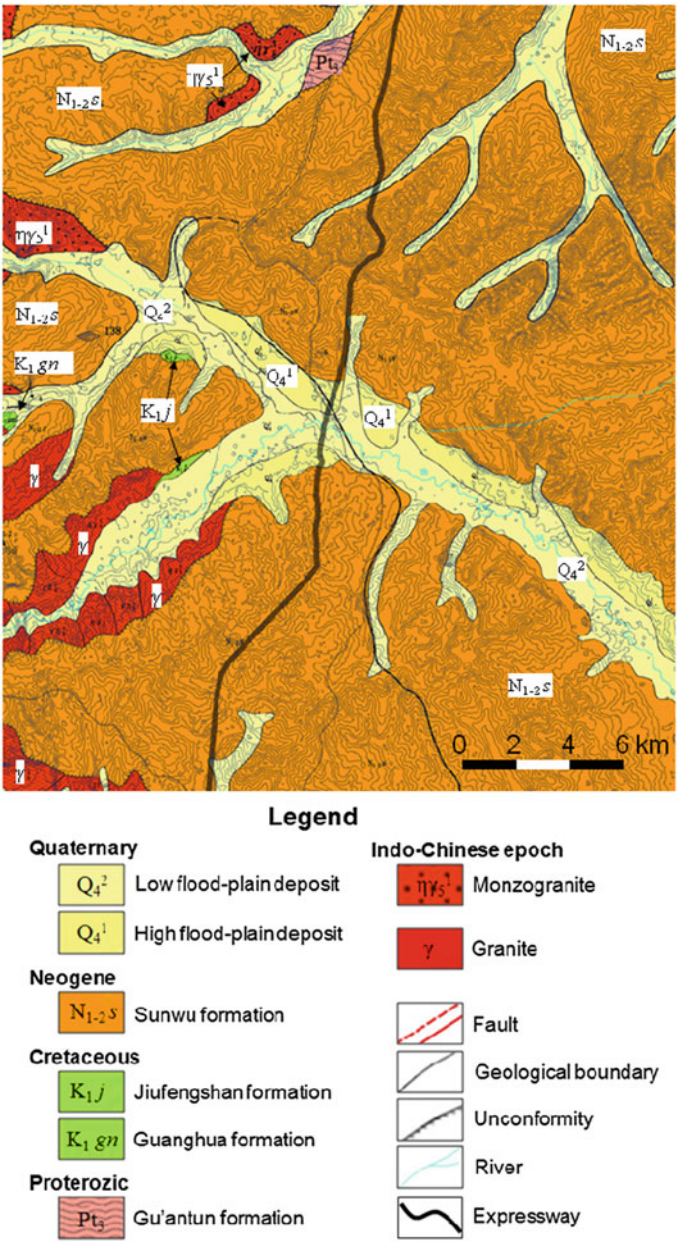

Fig. 1 Geological map of study area (scale: 1:200,000, 1996.01)

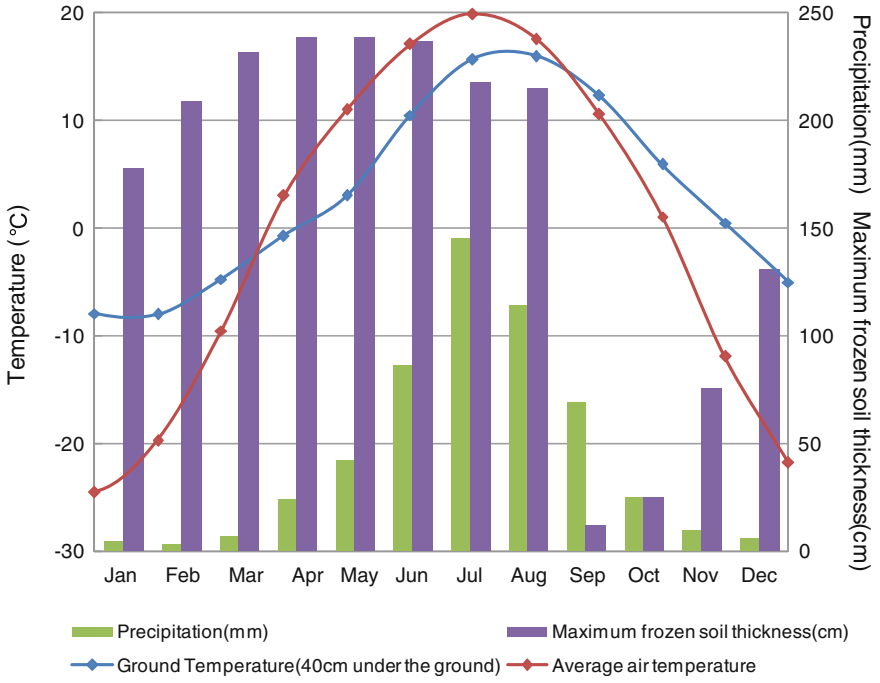

Fig. 2 Monthly average temperature/soil temperature in the depth of 40 cm/precipitation/maximum frozen depth (1971–2000, Sunwu)

3 Climate Change and Permafrost Degradation

The north area of Northeast China is located in the southern margin of Eurasia permafrost zone. The Greater and Lesser Khingan Mountain distribute along the north east, north west direction in the plane. The Nenjiang River Valley insert into the middle, the east and west is high, and middle is low. The climate is affected by inland and ocean high and low preaaure and monsoon alternated influence. Due to the Siberia and Mongolia high pressure in winter, climate is cold and inversion layer is widely distributed. Due to the Pacific high pressure in summer, the southeast monsoon enhance, warm air from south intersecting cold air from north in this area form rainy weather. The asymmetry of mountain distribution, slope direction and hilly area, wide and stable existence of inversion layer in winter have an important impact on the permafrost distribution rule, permafrost development and change process, and permafrost region features. However, the covering layer which is composed of forest, shrub, grass and moss plays an important role on the development and protection of permafrost. Due to the inversion phenomenon, loose covering layer thickness difference, vegetation, slope direction, surface water, geological structure and other natural factors, permafrost distribution and

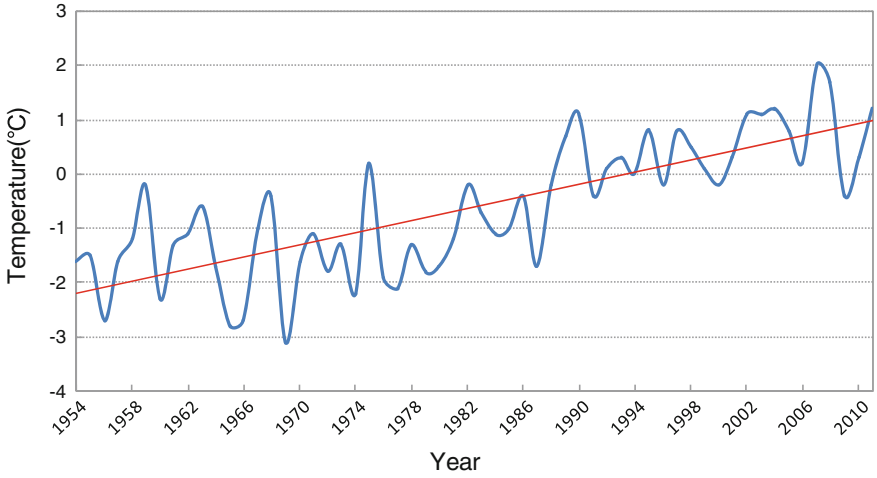

Fig. 3 Annual average temperature curve (1954–2011, Sunwu)

development degree of different geomorphological position in this region is obviously different.

"Khingan-Baikal type" permafrost was mainly distributed in high latitude permafrost region of China northeast. Its main distribution characteristics are that permafrost well develop in the relatively low-lying areas and with bigger thickness. The degradation process is that degradation firstly happened on sunny slope and then on shady slope; firstly happened on high altitude and then on low altitude; firstly happened on mountain and then on valley.

In the past 100 years, the global climate system has changed. From 1906 to 2005, global surface temperature has risen 0.74 °C. In China, the most significant temperature rising region is north China, east Inner Mongolia and northeast China in past 50 years. The highest heating rate reaches 0.8 °C/10a. Our study area is located in the Sun Wu-Heihe district which is one of the highest heating rate areas in nearly 50 years. According to the meteorological data of the Sun Wu weather station from 1954 to 2011, annual average temperature in Sun Wu rise from −1.6 °C in 1954 to 1.2 °C in 2011. Its ascensional range reaches 2.8 °C (Fig. 3).

In this study, the effect of climate change is not only reflected in the annual average temperature rising, but also in extreme maximum and minimum temperature changing. According to monthly extreme maximum temperature, minimum temperature, average air temperature data of the Sunwu weather station from 1954 to 2011, authors drew the trend distribution chart of monthly extreme maximum temperature, extreme minimum temperature and average air temperature (Fig. 4). The figure shows that each monthly extreme maximum temperature, extreme minimum temperature and average temperature is generally upward trend in this area from 1954 to 2011. The rise of extreme minimum temperature is fastest, except for September. The increase of extreme minimum temperature is

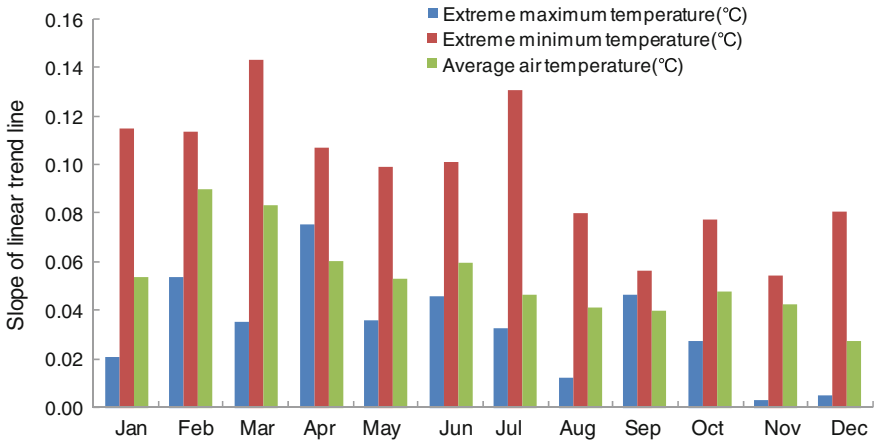

Fig. 4 Varies radio of monthly temperature (1954–2011, Sunwu))

two times than the extreme maximum temperature. From Fig. 2, we can find that September has the largest seasonal frozen soil thawing depth in this region. From another point of view, it demonstrates the relationship between permafrost degradation, distribution and climate change.

In the past 10 years, due to the climate and environment change, the occurrence condition of high latitude permafrost areas in the Northeast China becomes more vulnerable. Permafrost degradation process is accelerated. It mainly register as that the south boundary of permafrost moves to north gradually. The permafrost thickness becomes thinner and permafrost temperature is rising. Investigation data shows that number of the permafrost section of the Bei'an to Heihe Expressway reduced from 17 sections in 2000 to 5 sections in 2009. The length of permafrost section was decreased. Thickness of permafrost became thinner. In the road area passing Lesser Khingan Mountain, occurrence of small scale landslide was increased significantly.

4 Permafrost Degradation and Landslide Formation Mechanism

In the study area, 80 % surface is covered by larch, oak, poplar, linden, birch, coniferous and broad-leaved mixed forest. Slope angle is from 10 to 35°. Slope creeping platform is developed in this area (Fig. 5). The geological condition is very unstable. Carex tato, fish-scale turf, drunkard forest, sabre trees and other permafrost geomorphic features are distributed on the platform (Figs. 6 and 7).

Figure 5 is the satellite photo of study area on June 15, 2004 which is intercepted from Google earth. There are local surface folds and multi-level platform

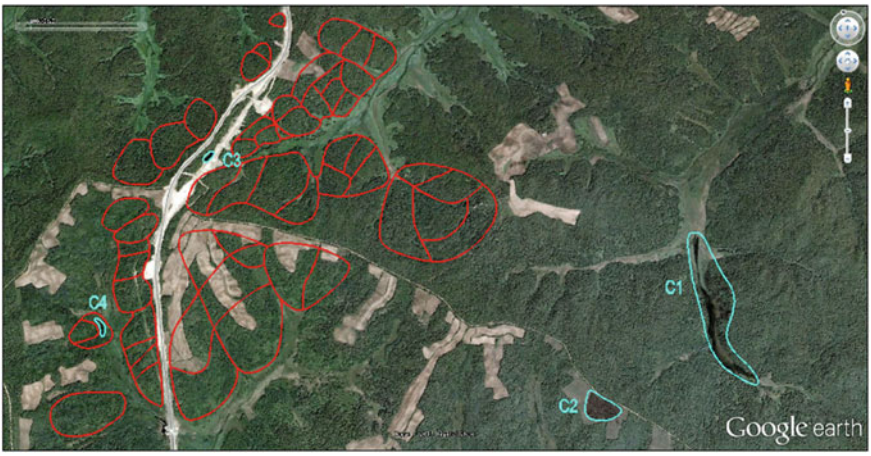

Fig. 5 Creeping platform and the distribution of melting permafrost in study area

Fig. 6 Physiognomy of Creeping platform in study area (taken on May 17, 2010)

distributed in the area. In the photo, the red line marked part is unstable region of the geological condition judged from geomorphology. The blue line marked part is the exposed region of the water from permafrost thawing on ground surface. C1 is the permafrost melting area of west-direction slope. And melt water flow into the seasonal river. C2 is the permafrost melting area of surface shallow of cultivated land. C3 is the exposed area of permafrost melting water along ridge. On the right side of C3, it is the abandoned road caused by the landslide occurred during the construction of subgrade in 2000. On the left side of C3, it is the section of highway relocation along ridge. C4 is the exposed area of permafrost melting water at the front of the second-creeping platform of landslide.

Fig. 7 Shallow ice covered by surface sedge in study area (taken on May 17, 2010)

Based on the Landsat ETM+ images on May 3, 2011 and October 10, 2011, thermal infrared band data were extracted. Through data fusion, thermal infrared band data were overlaid on the satellite photo of study area on June 15, 2004 which is intercepted from Google earth. As shown in Fig. 8, we can get the high upper limit permafrost distribution map in study area. It is consistent with the survey results. The inversion results show that permafrost distribution has obvious "Khingan-Baikal type" permafrost characteristics in study area. So the multi-level platform in the study area is the result of permafrost successive degrading and surface creeping. With the climate change process evolution, low-lying areas and

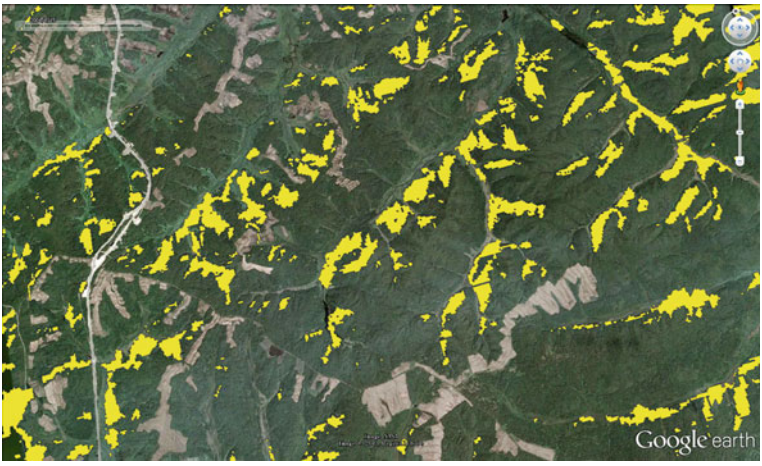

Fig. 8 The permafrost distribution map of high upper limit. (Based on Landsat ETM+ images)

deep permafrost will gradually degrade And surface creeping will further develop Then it will lead to incease of the potential energy platform creeping and landslide risk.

5 Lesser Khingan Mountain Northwest Section Landslide Moving Characteristics

In this study area, the comprehensive effect of geological condition, seasonal freezing and thawing, snow melt, atmospheric precipitation, permafrost degradation under the influence of climate change and other factors is the main reason resulting in shallow layer creeping and successive accumulation, and occurrence of landslides.

Through geological investigating, engineering survey, topographic measure and composite mapping, we can get the geological map of study area K177+400-K179+220 section (Fig. 9). From Fig. 9, we can find that surface covering layer in road area is the river and lake facies deposition of upper Cretaceous Nenjiang formation and Tertiary Pliocene Sunwu formation. The Tertiary Pliocene Sunwu formation which is mainly consist of coarse sand or sand conglomerate overlaps the top of mountain and hilly. Rock with poor cementation shows a loose state.

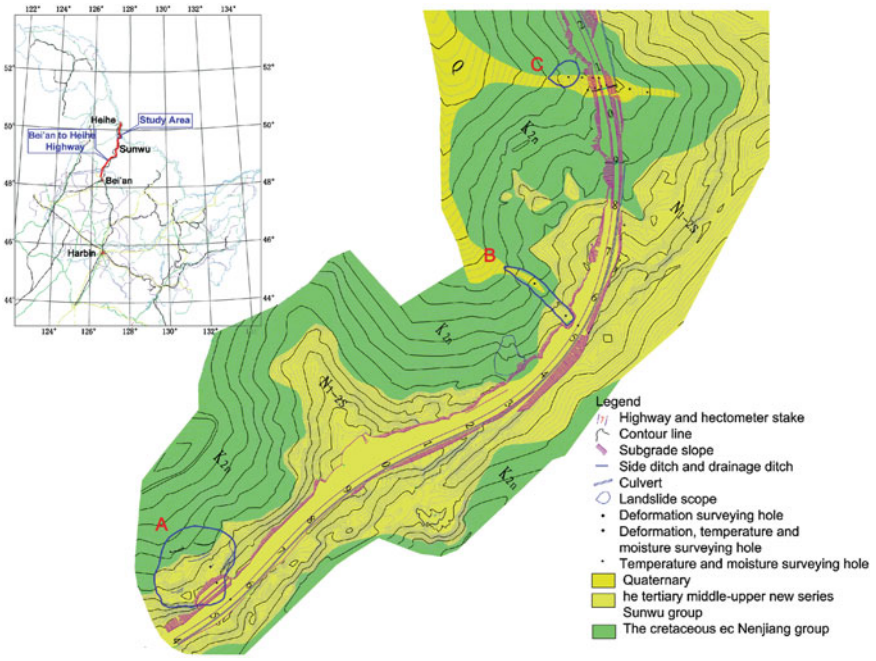

Fig. 9 Geological map of the section K177+400-K179+220

The upper Cretaceous Nenjiang formation exposed in the lower part of the mountains or hills. The lithology is mudstone, silty mudstone, tonhaltig fine sandstone and fine sandstone. Rock is with weak cementation and its weathering zone is quite thick. The rock near ground surface is completely weathered. In the higher ground, the water from snowmelt in spring and rainfall in summer and autumn rapidly infiltrates from loose sandstone to low permeability coefficient mudstone top. The water blocked run-off along the relatively dense rock top, gradually form scouring surface. The mudstone below the scouring surface soaked by water. Its shear strength decrease rapidly and form potential sliding surface finally. During heavy rainfall, seepage water is supplied from higher ground. Scouring surface reaches the upper limit of permafrost and induces permafrost melting. The rock and soil above the scouring surface will creep along the potential sliding surface under the action of gravity, until establish new stress balance. The creeping process is controlled by the water supply. The surface water supply of study area mainly comes from rainfall and snow melting. The strong rainfall mainly concentrates in July and August. So the surface creeping have intermittent and periodic characteristics, and creeping velocity is related to the slope, landform and rainfall intensity. The direct result of the surface creeping is slope platform developed, periodically and persistently develop. When the potential energy is accumulated to a certain extent, it will cause a landslide. If the sliding zone reaches the upper limit of permafrost, it will lead to permafrost melting quickly. Landslide process will be further accelerated. The risk and the damage will become bigger.

Figure 10 is the geological profile and diagram of monitoring equipment arrangement of K177+550 section of A landslide as shown in Fig. 9. Figure 11 is the geological profile and diagram of monitoring equipment arrangement of K178+530 section of B landslide as shown in Fig. 9. The common geological characteristic of two profiles is that the Nenjiang formation mudstone slope

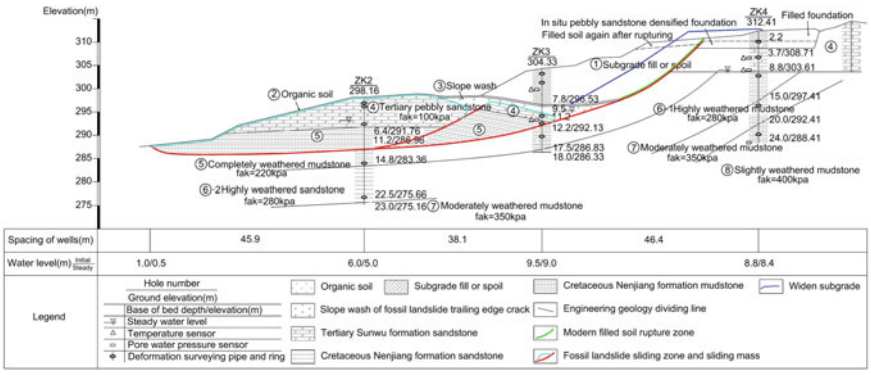

Fig. 10 Landslide geological profile and arrangement diagram of monitoring equipment (K177+550 section)

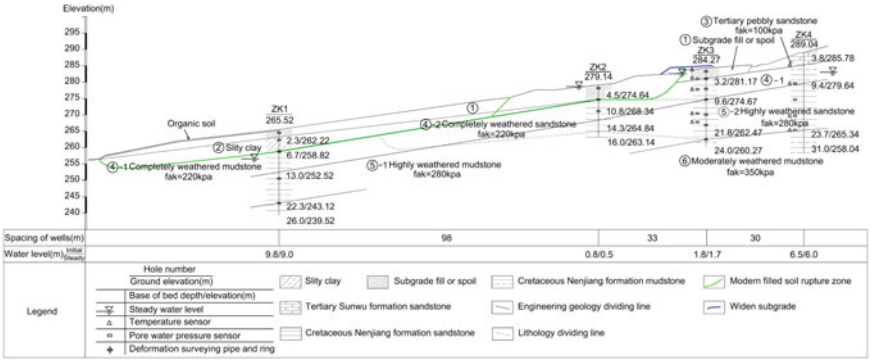

Fig. 11 Landslide geological profile and arrangement diagram of monitoring equipment (K178+530 section)

stratum is covered by Sunwu formation sandstone, building wasters of subgrade and so on, which conforms to the favorite structure for landslide.

Figure 12 is the atmospheric precipitation histogram during monitoring period obtained from Sunwu County Meteorological Station, and ground temperature with different depths, pore water pressure and time history curve the displacement of A and B landslides. From Fig. 2, we can find that landslide movement is closely associated with the ground temperature, precipitation and pore water pressure. During the thawing period in spring, with the complete melt of snow and soil, the pore water pressure began to rise, and landslide appeared creeping. In summer, pore water pressure increased rapidly to a peak caused by heavy rainfall, and movement speed landslide got increased. In autumn, with ground temperature reducing and precipitation decreasing, the pore water pressure dropped down. And the speed of landslide movement slowed down, then gradually stop sliding.

6 Conclusions

1. With climate change process accelerating, in the high latitude permafrost region of China northeast temperature rising speed is accelerated. The surface absorption of heat is obviously decreased in this article's study area which is located in the south boundary of high latitude permafrost region. Permafrost degradation process is accelerated.
2. With the permafrost degradation, the geomorphology of study area changes year by year. Occurrence of landslide increases in some area is affected by the geological condition.
3. Landslide movement in the study area have obvious seasonal characteristics. Its moving process is closely related to soil freezing and thawing condition,

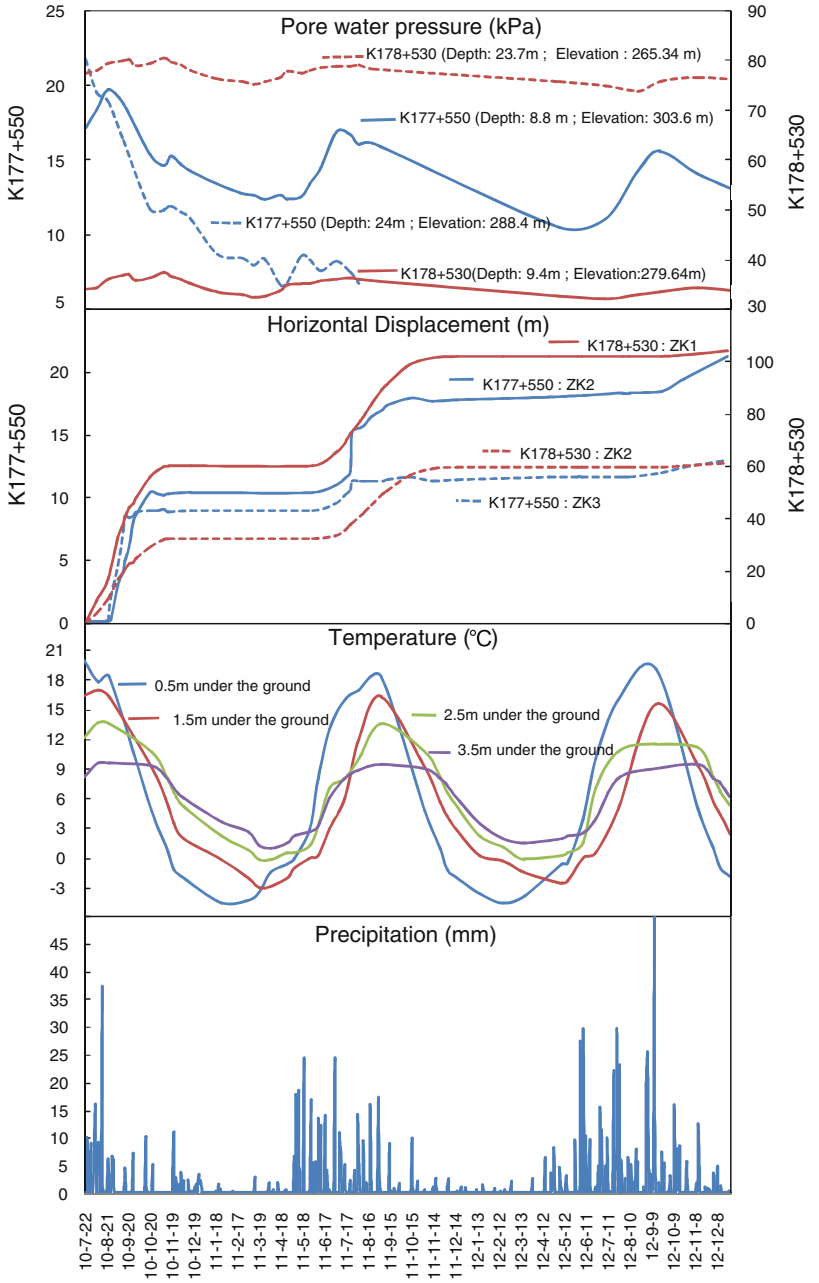

Fig. 12 Precipitation, soil temperature at different depths, pore water pressure, and landslide displacement curves of monitoring points (*A*, *B*)

precipitation and soil pore water pressure. Due to rock and soil sliding, geologic force is unleashed. Pore water pressure peak value reduces year by year, and sliding speed and range of landslide decrease year by year.

References

Chang XL, Jin HJ, He RX (2013) Review of permafrost monitoring in the northern Da Hinggan Mountains, Northeast China. J Glaciol Geocryology 35(1):93–100

Chen LX, Zhou XJ, Li WL, Luo YF, Zhu WQ (2004) Characteristics of the climate change and its formation mechanism in China in last 80 years. Acta Meteorol Sinica 62(5):634–646

Cheng GD (2003) The effects of local factors on permafrost distribution and its revealing of Qinghai-Tibetan Railroad design. Sci China Ser D 33(6):602–607

Cheng GD, Zhao L (2000) The problems association with permafrost in the development of the Qinghai-Xizang Plateau. Quat Sci 20(6):521–531

Ding YH, Ren GY, Shi GY, Gong P, Zheng XH, Zhai PM, Zhang DE, Zhao ZC, Wang SW, Wang HJ, Luo Y, Chen DL, Gao XJ, Dai XS (2006) China's national assessment report of climate change (I): climate change in China and the future trend. Adv Clim Change Res 2(1):3–8

Guo DX, Liu TL, Zhang WX (1998) Permafrost Institute, Siberian Branch. USSR Academy of Sciences. General Geocryology. Science Press, Beijing, pp 46–287

He W, Bu RC, Xiong ZP, Hu YM (2013) Characteristics of temperature and precipitation in Northeastern China from 1961 to. Acta Ecol Sinica 33(2):519–531

Jin HJ, Sun LP, Wang SL (2008) Dual influence of local environmental variables on ground temperatures on the Interior-Eastern Qinghai-Tibet Plateau (I): vegetation and snow cover. J Glaciol Geocryology 30(4):535–545

Lin XC, Yu SQ, Tang GL (1995) Series of average air temperature over China for the last 100-years period. Sci Atospherica Sinica 19(5):525–534

Lv LZ, Jin HJ, Wang SL (2008) Dual influence of local environmental variables on ground temperatures on the Interior-Eastern Qinghai-Tibet Plateau (II): Sand-layer and surface water bodies. J Glaciol Geocryology 30(4):546–555

Ren GY, Guo J, Xu MZ, Chu ZY, Zhang L, Zou XK, Li QX, Liu XN (2005) Climate changes of China's mainland over the past half century. Acta Meteorol Sinica 63(6):942–956

Shi N, Chen JQ, Tu QP (1995) 4-phase climate change features in the last 100 years over China. Acta Meteorol Sinica 53(4):431–439

Solomon S (2007) Climate Change 2007: the scientific basis/Contribution of Working Group I to the Forth Assessment Report of the Intergovernmental Panel on Climate Change. Cambridge University Press, Cambridge

Tutubalina OV, Rees WG (2001) Vegetation degradation in a permafrost region as seen from space: Noril'sk(1961–1999). Cold Reg Sci Technol 32(2–3):191–203

Wang SW (1994) Diagnostic studies on the climate change and variability for the period of 1880–1990. Acta Meteorol Sinica 52(3):261–273

Wang SW, Ye JL, Gong DY, Zhu JH, Yao TD (1998) Construction of mean annual temperature series for the last one hundred years in China. Q J Appl Meteorol 9(4):392–401

Wei Z, Jin HJ, Zhang JM (2010) Prediction of permafrost changes in Northeastern China under a changing climate. Sci China Earth Sci. doi:10.1007/s11430-010-4109-6

Zhou YW, Guo DX, Qiu GQ (2000) Geocryology in China. Science Press, Beijing, pp 171–423

Zuo HC, Lü SH, Hu YQ (2004) Variations trend of yearly mean air temperature and precipitation in China in the last 50 years. Plateau Meteorol 23(2):238–244

Part II
Forming Mechanism of Landslide in Cold Region

Forming Mechanism of Landslides in the Seasonal Frozen Loess Region in China

Tonglu Li, Ping Li and Hong Wang

Abstract In the area of Northern China, the landslides and other geological disasters frequently occur in the two seasons of autumn and early spring. Those occurred in the autumn are definitely induced by rainfalls; but in the early spring it is supposed to be induced by the freeze-thaw processes. This chapter introduces the fundamental characters and failure mechanism of the landslides related to freeze-thaw process. Monitoring of the ground temperature and the pore-water pressure at the landslide located at the side of the Heifangtai loess platform, Gansu province suggested freezing can build an underground water reservoir at the deep position within the slope in frozen season. Later, thawing water can be released out in warmer season. Consequently, it produces a high pore-water pressure in winter as well as a high water gradient in spring. Both the static high pore-water pressure in winter and the high water gradient in spring can decrease the slope stability and trigger landslide.

Keywords Loess landslide · Failure mechanism · Freezing · Thawing · Seasonal frozen loess

1 Introduction

A series of large landslides occurred one after another since the 1980s in the Loess Plateau in Northwestern China where the seasonal frozen area is. A large amount of losses and number of casualties was caused by landslides such as Saleshan, Longxi, Tianshui and Huangci landslides. Investigation suggests that huge landslides in Northwestern China not only concentrate in rainy season, but also in chilly freeze-thaw seasons. Table 1 shows some of the huge landslides occurred in freeze-thaw seasons in Northwestern China (Wu 1996). Generally speaking,

T. Li (✉) · P. Li · H. Wang
Department of Geological Engineering, Chang'an University, Xi'an 710054 Shaanxi, China
e-mail: dcdgx08@chd.edu.cn

W. Shan et al. (eds.), *Landslides in Cold Regions in the Context of Climate Change*, Environmental Science and Engineering, DOI: 10.1007/978-3-319-00867-7_4,

rainfall is the chief reason for most landslides, but in Gansu, Qinghai provinces and some other areas of the Western Loess Plateau, the situation is different. It has arid climate and less precipitation. The moisture content of natural loess is often less than 10 %. Therefore, those landslides occurred in freeze-thaw seasons are not merely related to the rise of groundwater table recharged by rainfall and irrigation, but closely related to seasonal freeze and thaw process. Freezing occurs in October to November and thawing in the following February to March in Northern China. The lowest air temperature can reach −20 °C or below, and the largest frozen depth varies from 1.0 to 2.5 m in those area.

Seasonal freezing and thawing includes two opposite processes of freezing and thawing, they have different mechanism and influence on triggering slope deformation and failure. Freezing can prevent groundwater discharging in loess, resulting in accumulation of groundwater in slope, which is called as Frozen Water Barred Effect (Wu 1997). The effect may cause a rise of static pore-water pressure, coincidently decreasing the slope stability. Inversely, thawing may suddenly release the enclosed water as it is warming, which will produce a high water gradient and also trigger landslides. The slope stability may be improved by draining in summer. However, the actions repeats year by year, finally can make the slope conditions worse and worse.

2 The Landslides at the Side of the Heifangtai Loess Platform Triggered by Seasonal Freeze-thaw Action

Here we take the landslides occurred at the side of the Heifangtai loess platform, Gansu Province as an example, to illustrate the forming mechanism of landslides triggered by seasonal freeze-thaw action. The Heifangtai platform is located in the town of Yanguoxia, Yongjing County, Gansu Province. It is situated on the left bank of the Yellow River and the convergence of the Yellow River and the Huangshui River. The platform was formed by Quaternary eolian loess deposit on the IV terrace of the Yellow River. Its north boundary is a gully with the depth of 30–110 m and the gradient of 13°–40°. The east and the south boundary is next to the II terrace of the Yellow River. The slope of the platform side has the height of 60–131 m and the gradient of 20°–50°. The steep and high slope at the side of the Heifangtai platform prefers to occurrence of landslides as shown in Fig. 1. The top of the platform is 1.7 km long at East-West, 1.3 km wide at south-north, and has the total area of 13.7 km^2. It used to be an arid platform without resident. In early 1960s, due to construction of the Liujiaxia, Yanguoxia and Bapanshan reservoirs, people lived in the reservoirs were immigrated onto the platform. To exploit the barren land for immigrant living, the Yellow River pumping irrigation project was begun to be built since 1966. Now there are four villages with 848 households and 4,028 people resettled on the platform. From July 1966 to June 1969, three high-lift pumping station were put into use, which has the total water supply of

Table 1 Some huge landslides occurred in freeze-thaw seasons in Northwestern China

Landslide name	Day/Month/Year	Volume($\times 10^4$ m^3)	Sliding mass	Grounder water condition	Lowest temp/°C
Saleshan, Gansu	07/03/1983	3,100	Loess + Mudstone	Vein-like groundwater with the flow less than 0.1 L/s was developed in conglomerates that interbedded in mudstone	−27.8
New-Saleshan, Gansu	26/03/1986	250	Loess + Mudstone	Vein-like groundwater with the flow less than 0.1 L/s was developed in conglomerates at shear outlet	−27.8
Qieshan, Gansu	01/11/1983	150	Loess	Abundant groundwater was developed in loess, with springs in the lower ditch	−19.9
Jiaojia, Gansu	05/03/1989	20	Loess	Groundwater was developed in the lower loess, and discharged in the form of spring	−23.1
Huangci, Gansu	30/01/1995	360	Loess + Sandy mudstone	Groundwater was developed in loess, and discharged linearly along the sliding surface above mudstone	−23.1
Chana, Qinghai	07/02/1943	16,000	Red clay + Sandy soil	Small amounts of groundwater appeared in the sandstone near the front of sliding surface	−28.9
Longxi, Qinghai	25/01/1986	150	Red clay + Sandy clay	Small amount of groundwater appeared in the sandstone near the front of sliding surface	−28.9
Huangnan, Qinghai	21/11/1984	200	Loess + Mudstone	Less groundwater	−22.9

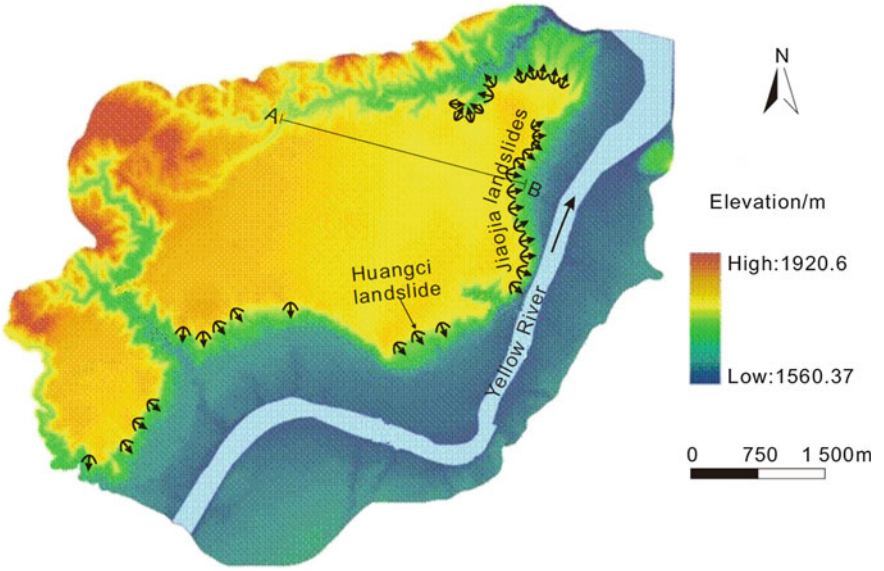

Fig. 1 DEM diagram and the landslides in the Heifangtai platform

2.115 m^3/s for 11,340 acres of farmland irrigation. Until April 2012, there are 11 trunk conduits with total length of 11.5 km and 48 branch ones with total length of 28.3 km on the platform. From 1981 to 1989, the average annual irrigation amount was 7.22 million m^3, averagely 598 m^3 per acre. From 1990 to 1999, the average annual irrigation amount was 5.76 million m^3, averagely 425 m^3 per acre. In recent years, the average annual irrigation amount keeps in 5.91 million m^3.

Since irrigating on the top of the platform, landslides began to occur at the side of the Heifangtai platform frequently. The landslides had caused more than 400 million of economic loss and 38 causalities, injured more than 100 people, destroyed about 500 acres of farmland, cut the roads leading to Yanguoxia Chemical Plant and Yanguoxia Power Plant for several times. 3,000 acres of arable land were abandoned in the margin of the platform. According to our investigation in August 2010, 37 landslides at the side of the Heifangtai platform were confirmed. The real number of landslide events is more than this number because at the same place may have several times of slope failure.

The Heifangtai platform is composed of Aeolian loess deposit, and alluvium of the Yellow River terrace and bedrock from top to bottom (Fig. 2). Aeolian loess (Q_3^{eol}) has grayish yellow color, loose texture and uniform structure, with macro porous, silt component and well vertical joints. It is easy to disintegrate in water. The loess bed is 21 $\sim$ 50 m thick and lays on the alluvium bed of the IV terrace of the Yellow River. The upper alluvium bed (Q_2^{al}) is of the 0.3–2.0 m thick of lamina light brown silty clay with horizontal bedding and interbedded with yellowish fine sand. The lower is pebbles which consists of quartzite, granite and metamorphic rocks, round to sub-round, well sorting, with the grain size of 3–10 cm, filled with

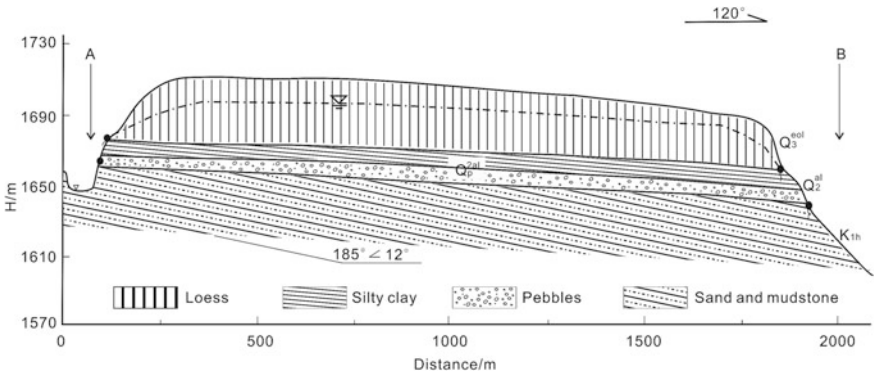

Fig. 2 Geological profile of the Heifangtai platform (line *AB* is shown in Fig. 1)

silt, no cementation. It is 2–5 m thick and outcrops along the side of the platform. The bedrock is Cretaceous interbedded sand-mudstone (K_1^{hk}) consisting of thick-bedded brown sandstone and fine bedded mudstone, commonly having 0.5 ~ 1.0 cm thick gypsum intercalations, with the attitude of 185° < 12°. The bedrock outcrops about 70 m thick on the lower of the side slopes.

The hydrogeological condition was entirely changed by the long-term and massive irrigation. Perched water table was formed in the loess bed over the whole area. Before irrigation, phreatic water was distributed discontinuously. The bedrock base dips from the west to east in the platform, so at the west side almost had no groundwater before, and at the east side only had a very thin groundwater. Since the extensive irrigation started in 1968, perched water table was formed on the relative impermeable alluvial silty clay and the water level increases at the rate of 0.27 m/year. The water level at the center of the platform has risen by 20 m high. Figure 3 shows that, on the upper of the side slope, groundwater has been leaking along the top of the silty clay bed. Undoubtedly, continuous rising of the groundwater level with irrigation was the main cause of landslides at the side of the Heifangtai platform. However, the landslides occurred at the side of the Heifangtai platform with clear time records are counted by month as shown in Fig. 4, it suggests that March and July are two with peak numbers (Wang and Yao 2008). The peak in July is closely related to the irrigation in May, while the peak in March was apparently related to freeze-thaw process.

3 The Mechanism of the Landslide Triggered by Seasonal Freeze-thaw Action

According to the material of sliding mass, the landslides at the side of the Heifangtai platform can be generally divided into two types: one is loess-mudstone landslides, which mainly occurred in Huangci village in the southwest side, and

Fig. 3 Groundwater flow along the top of silty clay on the upper slope

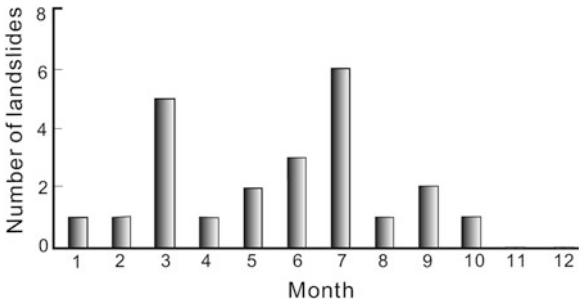

Fig. 4 Relation between the number of landslides and months on the side of the Heifangtai loess platform

the other type is loess landslides, which principally occurred in Jiaojia village in the northeast side.

Huangci landslide is a typical loess-mudstone landslide. The first sliding of the landslide occurred on 30 January 1995, which is the largest one at the side of the Heifangtai platform, with the volume of about 3.6 million m^3 and the height difference is 120 m from the top to the bottom of the slope, as shown in Fig. 5. It is basically a bedding-sliding slide because the most sliding surface is on the bedding of the mudstones. Before failure, a row of springs flowed out from the rock cracks with the water flow about 0.1 L/s each at the toe of the slope and also there was a large area of wetland nearby, so it is considered that the perched water in the loess layer may leak into the lower mudstone along the open crack or bedding of the rock. Figure 6 shows the geological section before sliding. The local residents found that the slope had apparently deformed in the spring of 1994. It was believed

Fig. 5 The Huangci landslide at the south side of the Heifangtai platform

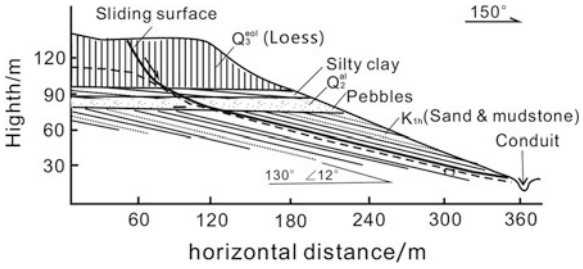

Fig. 6 Geological section of the Huangci landslide before failure

that freezing in winter barred the water flowing out and accumulating in the slope, thawing in spring led the inner water discharge quickly, which resulted in a continuous rising and suddenly lowing of the groundwater. The slope deformation mainly occurs in the spring of water drainage. Eventually, sliding happened in the winter of 1995. The Huangci landslide slipped again on 14 May 2006. The first sliding lasted 90 min, fortunately, there were no casualties, but massive property damage was caused.

Duo to the sliding surface is in mudstone, saturated mudstone often presents the constitution of ideal elastic-plasticity or hardening which has no strength reduction with strain, so the landslide had a very slow movement.

Loess landslide occurred in the loess bed lying on the alluvial silty clay. A thick perched water was generated on the top of alluvial clay because of relative impermeability. The Heifangtai platform tilts from South–West to North–East,

Fig. 7 The Jiaojia Landslide group (the location is shown in Fig. 1)

groundwater flows to North–East and spills along the top of the silty clay on the northeast side of the platform near Jiaojia village, so a series of landslides were triggered and distributes side-by-side as shown in Fig. 7. The earliest case occurred on 15 March 1989, which is located to the south of Jiaojia village and next to the bank of the Yellow River. There were 60,000 m^3 sliding mass slipped into the Yellow River, and the water was pushed onto the opposite bank and inundated 1.6 acres farmland. Another loess landslide with volume of 400,000 m^3 occurred along the slope behind the Silicon–Carbide Factory to the south of Jiaojia village on 12 March 1999. The sliding mass moved for 500 m in 30 s. In recent years, landslides often occurred in this area. A length of only 3 km slope of platform has 15 loess landslides distributed. Loess landslides show the characters of high shear outlet and quick sliding speed. The height of the shear outlet related to the toe of the slope is 60–80 m. As the landslide started to slip, the loose saturated loess in the base changed from solid to fluid rapidly, and then flowed down on the slope. It can be classified as rapid flow slide. Figure 8 shows the geological section of the Jiaojia loess landslide.

From more than 30-years record of the landslides on the side of the Heifangtai platform, it is found that the landslides occurred in the winter and the early spring were more than those in the other seasons. However, it is not the irrigation time, so

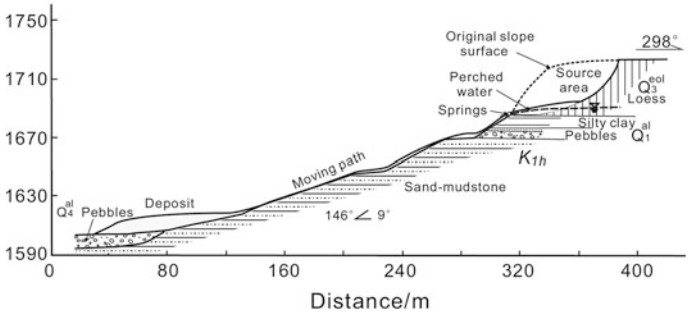

Fig. 8 Geological section of the Jiaojia loess landslide

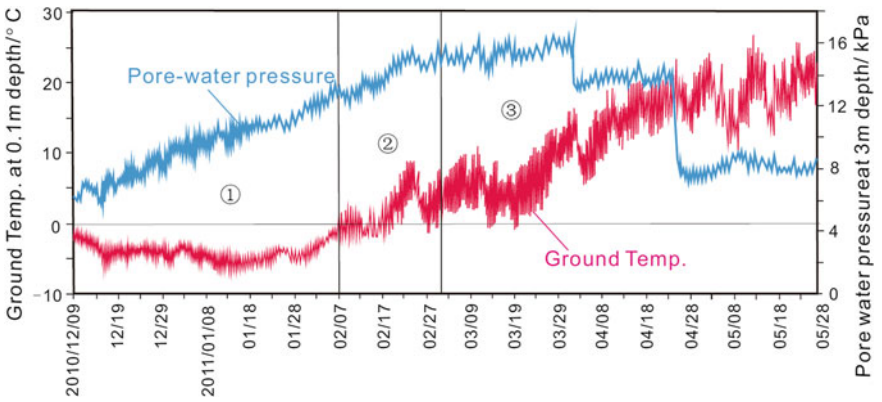

Fig. 9 Pore water pressure and ground temperature variation with time in JH9 landslide

the reason might attribute to freeze-thaw action. In order to obtain the data of ground temperature and pore-water pressure, monitoring devices were buried in the front of a largest landslide in Jiaojia village by the Xi'an Center of China Geological Survey. Figure 9 shows the data of ground temperature at the depth of 10 cm and pore water pressure at the depth of 3 m in the period from 9 December 2010 to 26 May 2011. From the results, the freeze-thaw process can be divided into three episodes, namely freezing, freezing-thawing and thawing. Freezing episode begins at the end of November and ends in the beginning of the next February, and the ground temperature is below 0 °C. Therefore, the groundwater drainage paths were closed, which resulted in a continuous rising of pore-water pressure in the slope. Freezing-thawing period begins in early February and ends in early March. Temperature fluctuates day and night, which may result in alternative freezing and thawing between day and night. However, the groundwater drainage paths were still blocked, so pore-water pressure can increase steadily. The thawing period starts from early March to the end of April, spring water begin to discharge as normal, and the pore water pressure does not rise any more.

The above monitoring results show that groundwater level in the slope could increase because the frozen water blocked the water drainage outlet. The range of water lifting on the slope could be 2 m in one frozen season, then it is estimated that the affected horizontal distance might be more than 30 m according to the loess permeability. The rise of groundwater level could lead to the rise of static pore water pressure and reduce soil strength. For investigating the loess strength under increasing of pore water pressure, intact loess samples near shear outlet the monitored landslide were taken. The specimens were saturated in laboratory and consolidated under definite confining pressure and axial pressure. Then, pore water pressure was increased by exerting counter pressure to make the specimen fail. The results are expressed as stress path in Fig. 10. Effective cohesion and internal friction angle may be calculated through parameters of K_f line. The effective cohesion was near to 0 and the internal friction angle was 30.1°. Gradients of the

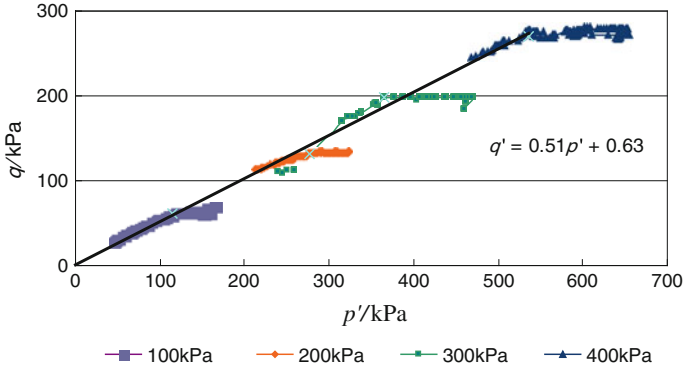

Fig. 10 Stress path of triaxial CU shear test under the conditions of giving confining axial pressure and by increasing pore-water pressure

loess slopes at the side of the Heifangtai platform were generally 30°–35°. It may be concluded that increase of groundwater level and pore water pressure by freezing caused that loess cohesion almost lost and the effective internal friction angle is even below the slope gradient, so the slope failure could be occurred naturally.

Once the landslide occurred, loess in the disturbed shear zone converted into flow state immediately because of its loose structure, and then rapid mud flow along the slope surface was generated. It can be measured that loess moisture content is greater than its liquid limit. Even during the thawing period, high hydraulic gradient would be generated due to the sudden release of groundwater, which was also unfavorable to slope stability.

4 Conclusions

There is a high incidence of landslides in freeze-thaw seasons in the loess region of the Northwestern China; seasonal freeze-thaw effect is a dominant factor for triggering this type of landslides. Landslides on the side of the Heifangtai platform, Gansu province, are the most typical cases triggering by freeze-thaw action. According to investigation, monitoring and triaxial test for the landslide in this area, it can be concluded that groundwater discharge outlet was barred by freezing action, which resulted in accumulation of groundwater within the slope, then increased pore water pressure and reduced soil strength consequently caused the slope failure. High hydraulic gradient may be generated by the sudden release of groundwater due to thawing, slope stability also can be reduced and fail eventually.

References

Wang NQ, Yao Y (2008) Characteristics and mechanism of landslides in loess during freezing and thawing periods in seasonally frozen ground regions. J Disaster Prev Mitig Eng 28(2):163–166

Wu WJ (1996) Seasonal freeze-thaw action and the entire deformation failure of slope. Chin J Geol Hazard Control 7(4):59–64(in Chinese)

Wu WJ (1997) Slide accelerated by water entrapment due to seasonal freezing. J Glaciol Geocryol 19(4):359–365 (in Chinese)

Investigation and Mechanism Clarification of the 2011.1.5 Atom-en Landslide in Kashima Area, Matsue City

Kenji Hatanaka, Yasuhiro Mitani, Austin Okeke, Yohei Kuwada and Fawu Wang

Abstract After a heavy snowfall between Dec 28, 2010 and Jan 4, 2011, a landslide occurred on a cut slope at the rear mountain edge of Atom-en, Kashima area, Matsue city on 5 January 2011. The aim of this study is to clarify the mechanism of the landslide. Three main works were carried out. Field survey was conducted to observe the structure of the landslide and measure the in situ shear strength of the soil on the sliding surface. Laboratory test was conducted to obtain soil strength properties such as permeability and shear strength. Finally, back analysis using Janbu's method was conducted to obtain the shear resistance of the sliding mass in the lower part of the slope, and to evaluate the effect of rise in groundwater level, while Flac3^{D} software program was used to clarify the deformation process of the landslide. The investigation and analysis indicated that the slope behind Atom-en has complex geologic structure, composed of completely weathered tuff and shale. The unfavorable geological structure and condition were the inherent factors that contributed to the landslide occurrence, while snow melting was the main triggering factor.

1 Introduction

High cases of debris flows, landslides, slope failures and other forms of mass movements are continuously recorded in Shimane prefecture due to severe impact of heavy rainfall events. Shimane prefecture is the second highest disaster-prone prefecture and has recorded more than 20,000 cases. As the number continues to increase, little effort is being made to mitigate and reduce imminent geodisasters.

K. Hatanaka · Y. Mitani · A. Okeke · Y. Kuwada · F. Wang (✉)
Research Center on Natural Disaster Reduction, Shimane University,
1060 Nishikawatsu-cho, Matsue 690-8504, Japan
e-mail: wangfw@riko.shimane-u.ac.jp

W. Shan et al. (eds.), *Landslides in Cold Regions in the Context of Climate Change*, Environmental Science and Engineering, DOI: 10.1007/978-3-319-00867-7_5,

Presently, statistical data shows that geotechnical remediation and countermeasure application to areas prone to geodisaster are only 17 % for Shimane prefecture.

This chapter concentrates on the January 2011 Atom-en landslide in Matsue city, Shimane prefecture, southwest Japan (Fig. 1). Geotechnical remediation works have been done on the sites before the event occurred. The Atom-en landslide occurred on a protected slope, therefore, a need for effective geotechnical remediation works on the slopes. In Atom-en, incessant rainfall was preceded by the landslide event, indicating that high precipitation was a major triggering factor for the slope failure. The high precipitation observed before the landslide occurred can be attributed to the reduction of shear resistance due to increase in pore water pressure within the relatively weathered tuff layer, as could be observed from similar landslide events around the area. This study concentrates on a landslide that occurred at Atom-en in Kashima area, Matsue city on January 2011. From disaster prevention viewpoint, the area is important because there are many public facilities around the area, and is designated as evacuation center in case of an emergency event.

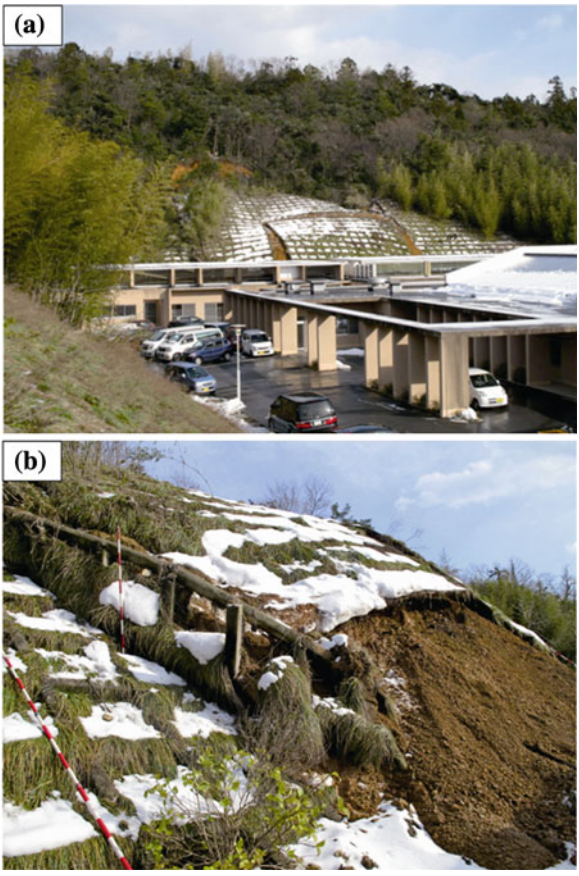

Fig. 1 **a** Front view of atom-en landslide. **b** Head scarp

The main triggering factor of this landslide was snowfall. Therefore, in reaction to landslide by snowfall, the term "snow melting landslide" is used. Relationship between snow and landslide has been studied in the past. Shiraishi (1988) studied generation mechanism of snow melting landslides. Matsuura (1998) reported that snow melt is one of the major triggering factors of landslides. Also, on the basis of study of snow melting prediction in existence and snow accumulation load, Matsuura (1998) reported problems in prediction of landslide occurrence due to snow melting. From observational result of landslide displacement amount, Sato et al. (2004) has studied motion characteristic of landslide in snow season.

However, there are few study examples about landslide due to snow melting in Shimane Prefecture. Therefore, to prevent landslide due to snow melting and to go ahead with suitable disaster prevention work, significance of this study is high.

Under the above study background, in this study, the field survey was conducted to observe the structure of the landslide, laboratory test was conducted to get the soil index properties; back analysis using Janbu's method was conducted to obtain the strength properties of the sliding mass in the lower part, and finite differences program Flac3^{D} analysis was carried out to clarify the deformation process in the landslide. This study purpose is to clarify the mechanism of the landslide due to melting snow.

2 Topography and Geological Summary in Study Field

2.1 Topography Summary

The study area is located in Kitakoubu Kashima area, mid-northern part of Shimane Peninsula (Fig. 2), about 6 km northwest of Matsue city. Bordering the study area in the eastern and northern axes are Mt. Ohira and Mt. Kitayama with slope heights of 503 and 200 m respectively.

Atom-en in Kashima area is surrounded by low relief mountain terrain with slope heights ranging between 100 and 170 m, with relative elevation difference of less than 150 m and slope gradient that is comparatively gentle.

These main valley and ridge lines in the mountain area extend in east–west, north-east or south-east axes extending in orthogonal direction. Structural features of the area include asymmetrical folds, chains of valleys and hills of high slope concavity due to regional fault (Fig. 3).

2.2 Geological Summary

The geology of the study area is underlain by the Josoji Formation which is composed of rhyolite lava, pyroclastic deposits, shale, and siltstone-shale interbed. In the northern part of the study area, mudstone is primary distributed, with

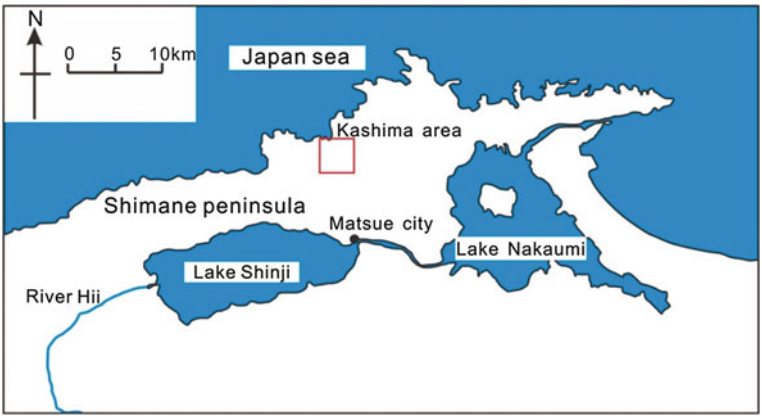

Fig. 2 Location map of the study object area

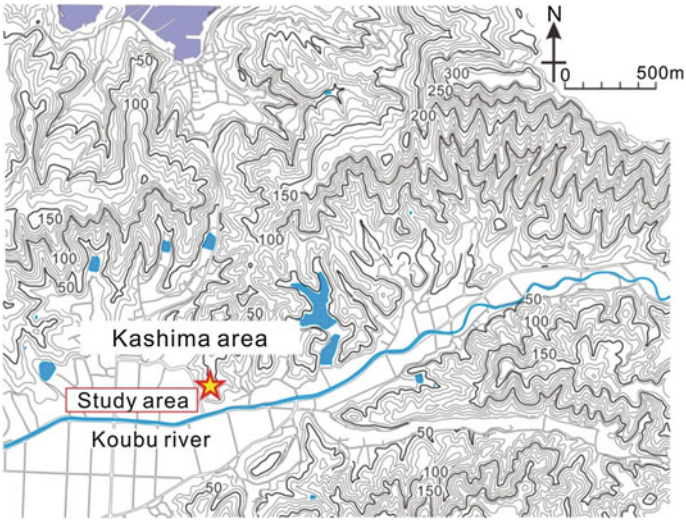

Fig. 3 Topographic map of the study area

alternating layers of mudstone and tuff (Fig. 4). On the other hand, volcanic tuff is primary distributed in the southern part of the study area. Field survey was conducted in order to delineate structural boundaries and geotechnical properties of outcrops studied in the area. This chapter shows photo of typical outcrop and describes the conditions.

Figure 5a shows collapsed section of the slope which is composed of tuff derived from the Josoji Formation. Figure 5b is magnified view of Fig. 5a, which shows weathering condition due to rainfall and chemicals. Almost all the tuff

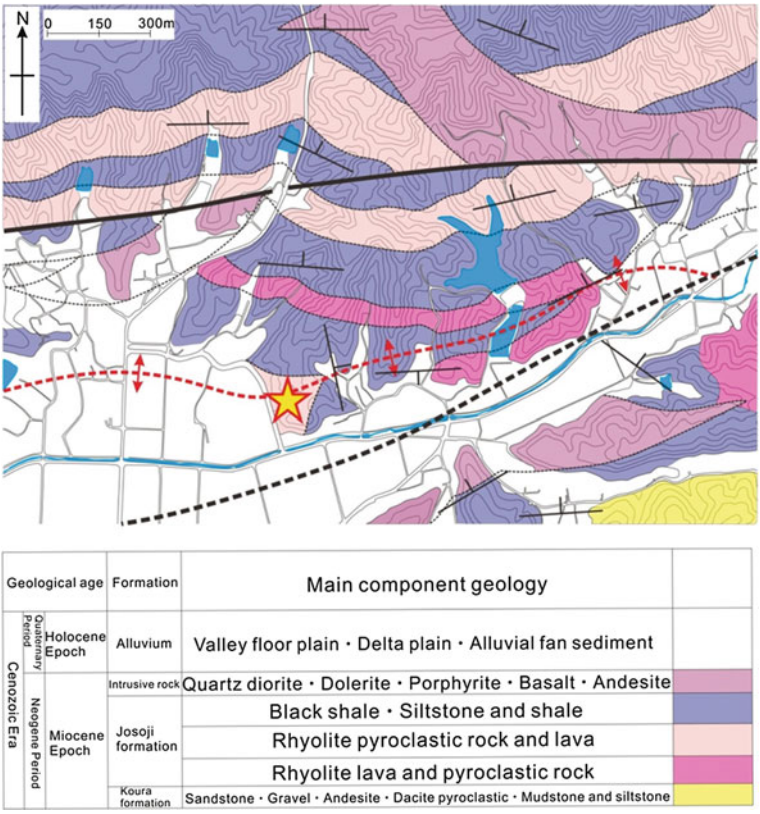

Fig. 4 Geologic map of the study area (Kano and Yoshida 1985)

layers within the study area are weathered; it is presumed that the prime factor that led to the failure of the slope is the relatively steep nature of the slope.

Figure 5c–f shows mudstone in the Josoji Formation which has been weathered mainly by slaking. In Fig. 5e and f, mudstone outcrop exists near the road at height and width of 3 and 5 m, respectively.

2.3 Meteorological Summary

AMEDAS in Kashima area Matsue city monitored rainfall of 76 mm on December 31, maximum rainfall per hour were up to 8.5 mm (Fig. 6). However, AMEDAS in Kashima area Matsue city did not monitor snowfall. To estimate snowfall in Kashima area, rainfall data and snowfall in Matsue city collected from meteorological weather station was utilized. Rainfall in Matsue city on December 31 is 57.5 mm, with maximum rainfall per hour averaging 9.0 mm. The snowfall in

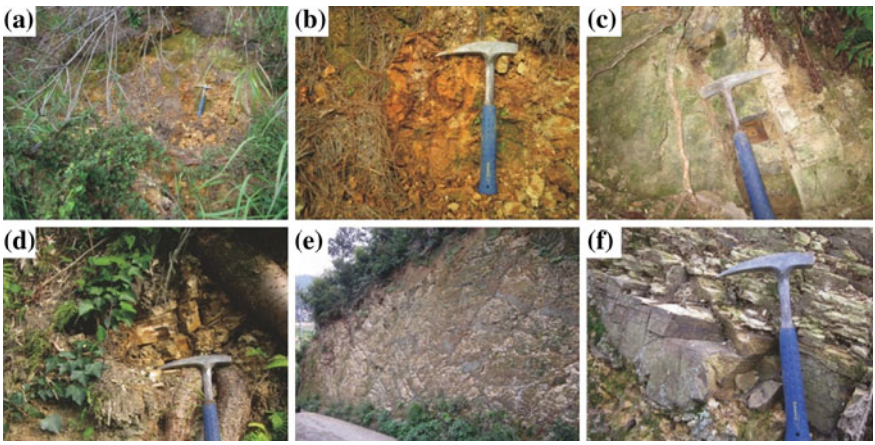

Fig. 5 Lithofacies in the vicinity of study area. (**a**, **b**: Weathered (oxidized) tuff layer showing irregular streaks of *brown* and *red* colors, **c**, **d**, **e**, **f**: Slaking on the mudstone layer)

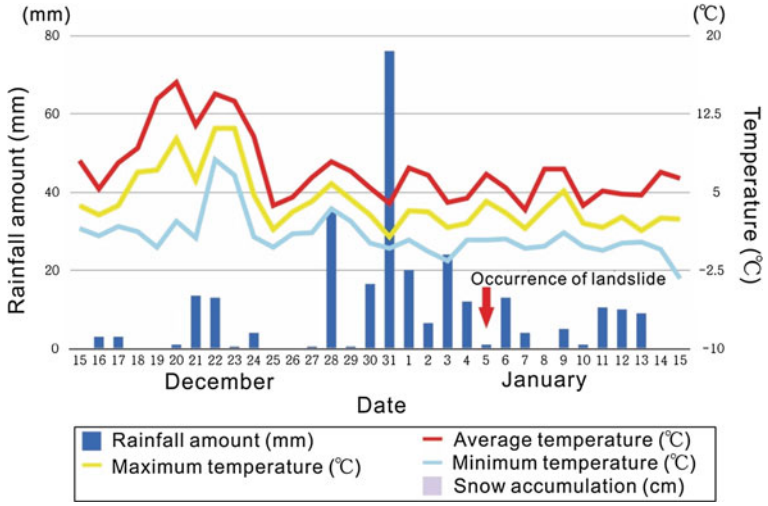

Fig. 6 Graph of rainfall amount and snow accumulation in Kashima area

Matsue on December 31 recorded 52 cm, with maximum snowfall averaging 51 cm (Fig. 7). Compared with Kashima area and Matsue city, Kashima area has a lot of rainfall than Matsue city. Therefore, it is presumed that snow depth in Kashima area is deeper than 51 cm.

Also, temperature changes are as important as snowfall. Figure 6 shows that day below zero just before occurring landslide is few. That is, the supplied amount of snowmelt water increased into the ground. And, weight of deposited snow is

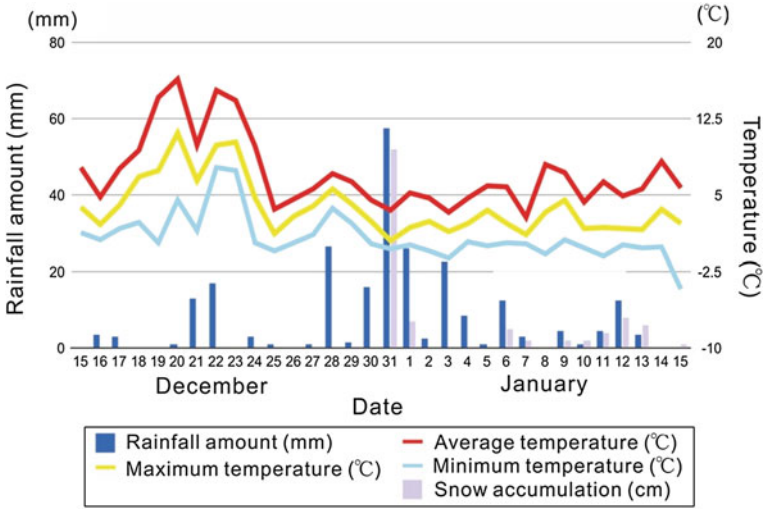

Fig. 7 Graph of rainfall amount and snow accumulation in Matsue city

important, too. However, it is difficult to evaluate them because survey and observation relevant to weight of deposited snow were not conducted.

3 Field Investigation

Field investigation was conducted using many geotechnical tools. Laser distance meter was used to delineate boundaries and dimensions of the landslide. Analysis of the data shows that the width and length of the landslide is 30 and 40 m respectively, having slip height of 40 m after traveling some distances to the southwest (Figs. 8 and 9). The sliding surface was found on the main scrap (Fig. 10), with structural attitude of N30° ∼ 40°W30° ∼ 40°SW. Permeability of the soil layer at the head scarp is high due to the relative dominance of plant roots and loose colluvial cover at the top of the slope. In contrast, the lower part of the soil units are underlain by rhyolitic tuff. Contact spring was observed between the upper and lower part of the relatively weathered soil layer showing thin beds of mottled clay of few centimeters. The attitude of the bedding plane on the upper part of the slope, between the volcanic tuff and the shale unit trends N48°W34°SW, thus indicating that the slip surface of the landslide is located within the bedding plane. On the other hand, it was observed that the shale layer on the lower part of the slope has been moderately to highly weathered owing to the observed difference in color and stratification. The slope movement was temporarily stabilized by an original slope protection barrier constructed near the toe of the slope which was not affected during the slope movement, but suffered only slight fractures due to the impact of the slope materials on the concrete abutment.

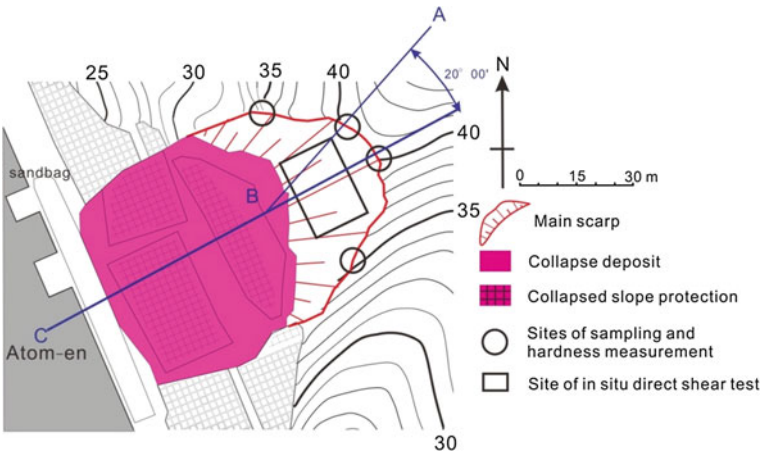

Fig. 8 Base map of the study area showing the landslide geometry. (provided by Fujii consulting & associates)

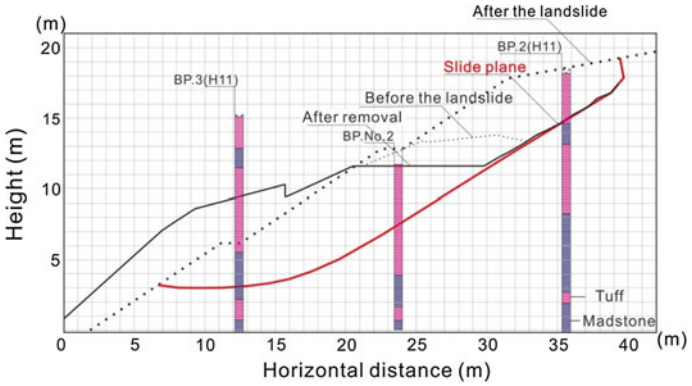

Fig. 9 Cross-section diagram of landslide. (provided by Fujii consulting & associates)

The main triggering factor of this landslide was contributed by the effect of high concavity of the slope structure which was formed by gradual slope debuttressing and weathering of the soil cover by rainfall, which is enhanced by the influx of water from melting snow that inadvertently increased pore water pressure and reduced shear resistance.

Also, strength properties of the soil at the head scarp were carried out using soil hardness tester. This survey was carried out in two consecutive times at location 4 on the head scarp. The survey results are shown in Fig. 11. With few exceptions, results obtained from the investigation show that the overall hardness of the slope mass decreases with increase in depth.

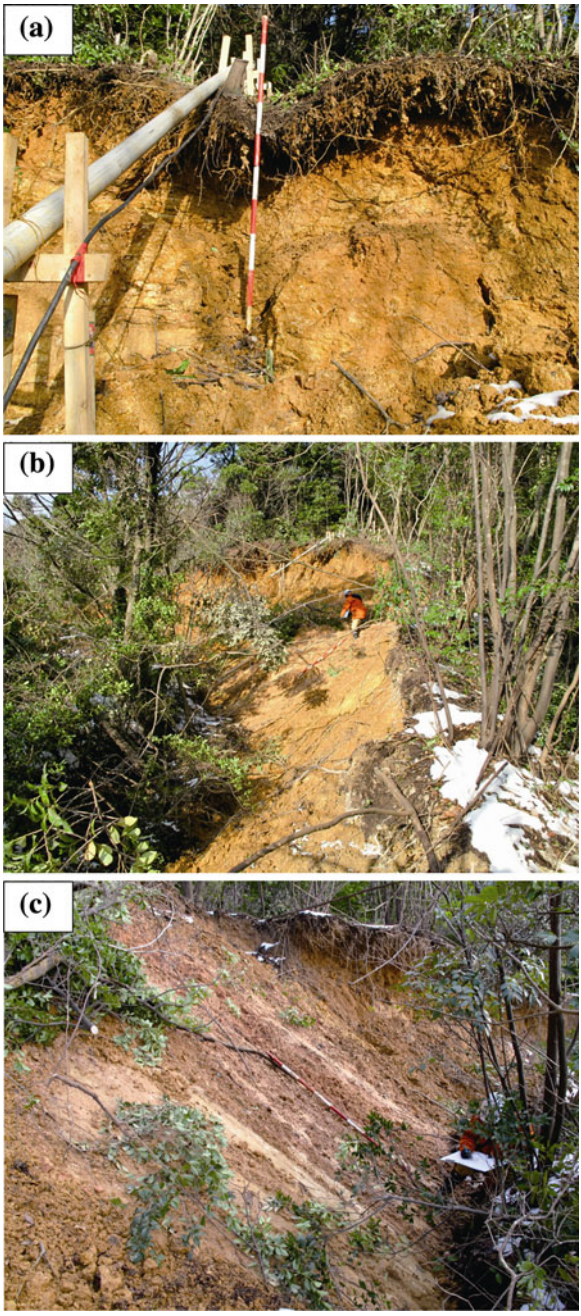

Fig. 10 Photo showing some sections of the landslide. (**a** Head scarp. **b** *Left* flank. **c** Sliding surface)

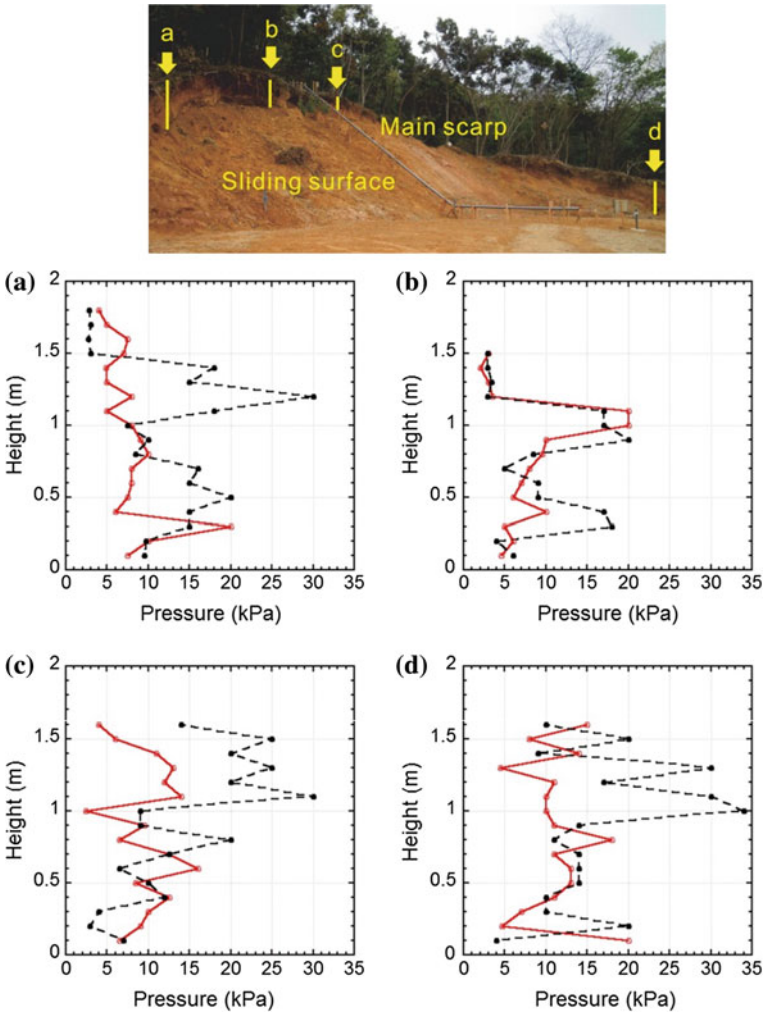

Fig. 11 Result of soil hardness measurement on the head scarp

4 Laboratory Test

After the heavy rainfall events on May 10th and 11th 2011, sampling was conducted at 7 sites on the head scarp and at another location on the sliding surface. Precautions were taken during the sampling to ensure that the samples collected are almost similar to the original physical properties of the slope mass after the landslide event. Laboratory tests (soil water content, dry and wet density tests, particle size analysis, direct shear test and permeability tests), were carried out to

Table 1 Result of laboratory test

Sampling point	Sample number	Wet density (kg/m^3)	Dry density (kg/m^3)	Soil particle density (kg/m^3)	Water content (%)	Void ratio	Degree of saturation (%)
Scarp	HS-1	1,721	1,250	2,686	37.3	1.149	88.2
Scarp	HS-2	1,808	1,377	2,713	31.3	0.970	87.5
Scarp	HS-3	1,643	1,108	2,708	48.3	1.444	90.5
Scarp	HS-4	1,713	1,277	2,506	34.2	0.962	89.0
Scarp	HS-5	1,774	1,445	2,607	22.8	0.804	73.8
Scarp	HS-6	1,702	1,227	2,815	38.7	1.294	84.2
Scarp	HS-7	1,721	1,254	2,642	37.9	1.107	90.5
Sliding surface	SLS-1	1,727	1,281	2,673	35.5	1.087	87.3

determine the conditions of the soil in the field. The results of the tests are summarized in Table 1.

The result of water content test varies between 30 and 40 %, while result of soil density test varies between 2,500 and 2,800 kg/m^3. Wet density test on the soil was conducted using a sampler. The result of the test varies between 1,700 and 1,800 kg/m^3.

For direct shear test, a constant pressure test was conducted. The consolidation process lasted longer than or equal to 24 h. The test was carried out with a shear velocity of 1.19 mm/min under three (3) confining (normal) stress of 30, 60, 90 kPa. Result obtained from the tests show that the soil cohesion is 12.2 kPa while the internal frictional angle is 25.3°. Also, constant-head permeability test was conducted. The result obtained shows that coefficient of permeability is 2.2×10^{-2} m/s.

5 Analysis Using Janbu's Method and Flac3D

5.1 Back Analysis Using Janbu Method

At the initial stage, no in situ or laboratory tests were conducted on soil material at the lower part of the slope toe. The internal friction angle of the sliding surface at the lower part of the slope was gotten using Back analysis method.

a. Model construction

The topography of the slope before the landslide and configuration of the sliding surface were extracted from the cross section (Fig. 9). The collapsed landslide mass was cut into 11 slices as shown Fig. 12 following Janbu's method. This study assumed that piezometric head before the landslide was high even though it was not monitored (Fig. 13).

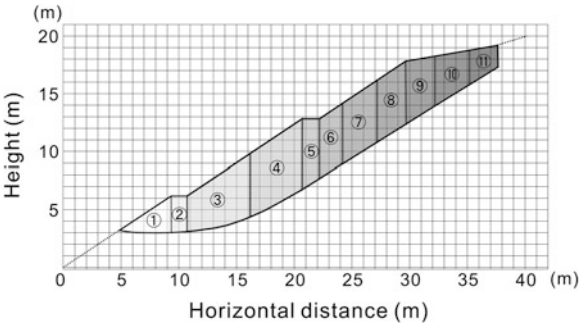

Fig. 12 Slice split of model for back analysis

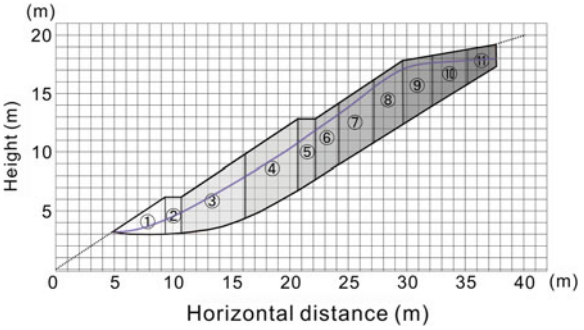

Fig. 13 Slice split of model when groundwater is high

b. Setup of parameter

The parameter is calculated for Back analysis with regards to the sliced slope mass, (Table 2). Each parameter is defined as shown in Fig. 14. The factor of safety is less than 1.00 when the failure occurred. Therefore, the factor of safety is assumed to be 0.98.

Acceleration due to gravity	$g = 9.8\ (m/s^2)$
Wet density	$\rho_t = 1,727\ (kg/m^3)$ (from result of laboratory test)
Density of water	$\rho_w = 1,000\ (kg/m^3)$ (from result of laboratory test)
Void ratio	$e = 1.087$ (from result of laboratory test)
Saturated density	$\rho_{sat} = \frac{\rho_s + e\rho_w}{1+e}$
Wet unit weight	$\gamma_w = \rho_w \cdot g$
Saturated unit weight	$\gamma_{sat} = \rho_{sat} \cdot g$
Water unit weight	$\gamma_t = \rho_w \cdot g$
θ_i (°)	Compute from model coordinate
Δx_i (m)	Read from model coordinate
l_i (m)	$l_i = \frac{\Delta x_i}{\cos\theta_i}$
h_{1i} (m)	Compute from model coordinate
h_{2i} (m)	Compute from model coordinate
h_i	$h_i = h_{1i} + h_{2i}$

Table 2 Values of inverse analysis tan $\varphi'_{1\sim3}$

Slice	θ_i (°)	Δx (m)	h_1 (m)	h_2 (m)	c'i (kPa)
1	−6	4	1.25	0.75	3
2	2	1.5	1.5	1.5	3
3	18	5.5	1.5	3	5
4	31	4.5	1.75	4	12.2
5	31	1.5	1.5	4	12.2
6	31	2	0.75	4.5	12.2
7	31	3	1	4.5	12.2
8	31	2.5	0.5	5	12.2
9	31	2.5	0.5	4.25	12.2
10	31	3	2	1.5	12.2
11	31	3	1	1.5	12.2

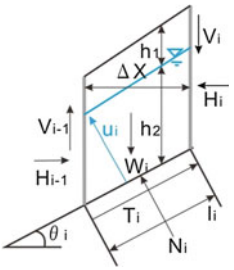

Fig. 14 Definition of physical properties values for back analysis

W_1 $W_1 = h_{1i} \cdot \Delta x_i \cdot \gamma_t$
W_2 $W_2 = h_{2i} \cdot \Delta x_i \cdot \gamma_{sat}$
W_i $W_i = W_1 + W_2$
u_i $u_i = h_2 \cdot \gamma_w \cdot \cos^2 \theta_i$
c_i $c_1 \sim c_3 = h_i$, $c_4 \sim c_{11} = 12$ (kPa) (from result of laboratory test)
φ'_i $\varphi'_{4\sim11} = 25$ (°)

c. Back analysis

First, unknown $\varphi_{1\sim3}$ is assumed as an arbitrary angle. And, m_{ai} is calculated using the following formula.

$$m_{ai} = \cos\theta_i + \left(\frac{1}{Fs}\right) \sin\theta_i \cdot \tan\varphi_{1\sim3}. \quad (1)$$

Substitute in the following formula using m_{ai}. To get internal friction angle $\varphi_{1\sim3}$ of slice 1 to 3, the following formula is used.

$$F_s = \frac{\sum \frac{1}{m_{ai} \cdot \cos\theta_i} \left\{c'_i \cdot l_i \cdot \cos\theta_i + (W_i - u_i \cdot l_i \cdot \cos\theta_i) \tan\varphi'_i\right\}}{\sum W_i \cdot \tan\theta_i} \quad (2)$$

This becomes,

$$\tan \varphi_i' = \frac{(F_s \cdot \sum W_i \cdot \tan \theta_i) - \sum \frac{1}{m_{ai} \cdot \cos \theta_i} \cdot (c_i' \cdot l_i \cdot \cos \theta_i)}{\sum \frac{1}{m_{ai} \cdot \cos \theta_i} \cdot (W_i - u_i \cdot l_i \cdot \cos \theta_i)} \quad (3)$$

The computational method was used to solve the difference between the calculated value and the assumed value. The calculation is repeated until the difference is relatively close to zero.

Table 2 shows values of data used in the back analysis, each value is gotten from the model and each parameter is calculated using the above definition. Internal friction angles $\varphi'_{1\sim3}$ of slice 1 to 3 were presumed to be 20° before conducting the calculation. The result shows that the calculated value φ_i' is approximately 26°—showing a difference of 6°. Initial presumed values $\varphi'_{1\sim3}$ were changed from 20° to 26°as the calculation is conducted again. The calculated value φ_i' became approximately 26°, showing no difference. Therefore, the final calculated internal friction angle $\varphi'_{1\sim3}$ of slice 1 to 3 is 26°. In order to verify the validity of this result, the presumed value of the factor of safety (Fs) in previous analysis was set as unknown. The factor of safety is solved using the formula in Eq. (2). The result shows that the factor of safety is approximately 0.943 which corresponds to the initial computation.

5.2 Analysis of the Influence of Groundwater Level Using Janbu's Method

Janbu's method was used to carry out slope stability analysis with low groundwater level in order to evaluate the influence of groundwater level on the slope as shown in Fig. 15. The calculation was made using different slope parameters shown in Table 3. The internal friction angle of the slope toe, $\varphi'_{1\sim3}$ were assumed to be 26°. After calculating each parameter, safety factor is solved using Eq. (2). The result obtained shows that the factor of safety is 1.193. This indicates that groundwater level contributed to the instability of the slope.

5.3 Analysis of Slope in the Field Using Flac3D Program

This study analyzed the model in the case of high groundwater level and the model in the case of low groundwater level using Flac3D program. Figure 16 shows constructed slope model based on Fig. 9. This model was built using ANSYS and Auto CAD. The lithologies are made up of light-brown shale layer and dark-brown tuff unit. Figure 17a shows that distribution of pore water pressure when groundwater level is low. Figure 17b shows the distribution of pore water pressure

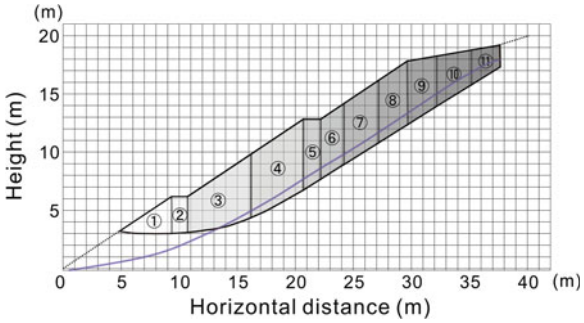

Fig. 15 Slice split of model when groundwater is low

Table 3 Dataset used in the analysis of the effect of groundwater level

Slice	θ_i (°)	Δx (m)	h_1 (m)	h_2 (m)	c'i (kPa)
1	−6	4	2	0	3
2	2	1.5	3	0	3
3	18	5.5	4.5	0	5
4	31	4.5	4.75	1	12.2
5	31	1.5	4.5	1	12.2
6	31	2	4.25	1	12.2
7	31	3	4.5	1	12.2
8	31	2.5	4.5	1	12.2
9	31	2.5	3.75	1	12.2
10	31	3	2.5	1	12.2
11	31	3	1.5	1	12.2

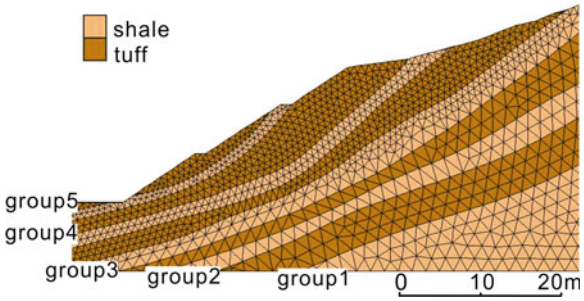

Fig. 16 Finite element model of the cross section using ANSYS, Auto CAD

when groundwater level is high. The parameters for the analysis are shown in Table 4. The parameters of the surface layer were set using the geological survey report carried out by Wesco. Result of analysis shows that the basic strength properties of the slope mass increases with depth.

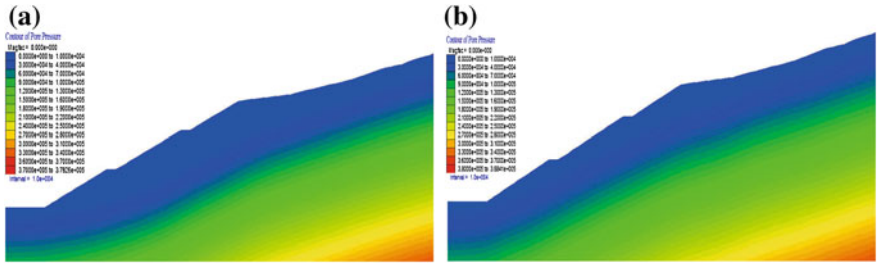

Fig. 17 **a** Pore water pressure distribution at low groundwater level. **b** Pore water pressure distribution at high groundwater level

Table 4 Dataset used in Flac^{3D} analysis

	Shale 1	Tuff 1	Shale 2	Tuff 2	Shale 3	Tuff 3	Shale 4	Tuff 4	Shale 5	Tuff 5
Density (kg/m^3)	2,160	2,160	2,000	2,000	1,980	1,980	1,840	1,840	1,730	1,620
Cohesion (KPa)	25	25	20	20	15	15	10	10	5	5
Friction angle (°)	24	30	23	26	22	24	21	21	20	20

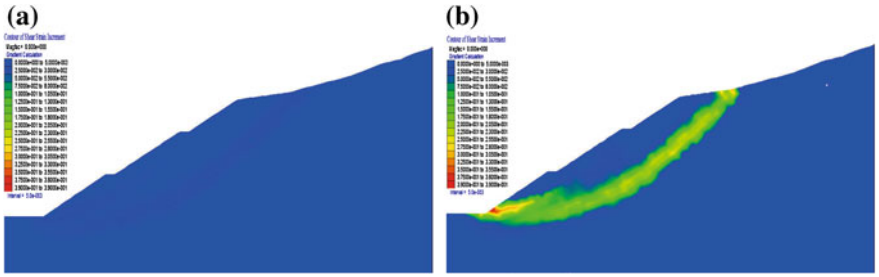

Fig. 18 **a** Shear stress distribution at low groundwater level. **b** Shear stress distribution at high groundwater level

Figure 18 shows cross section of the slope model under the influence of groundwater. The model shows that the zone of shear strength decrease did not appear when the groundwater level is low. On the other hand, zone of shear strength decrease appears as the groundwater level increase within the slope. The zone of shear strength decrease observed on the slope mass widens and forms the sliding surface.

Figure 19a shows displacement when groundwater level is low while Fig. 19b shows displacement when groundwater level is high. The results show that at low

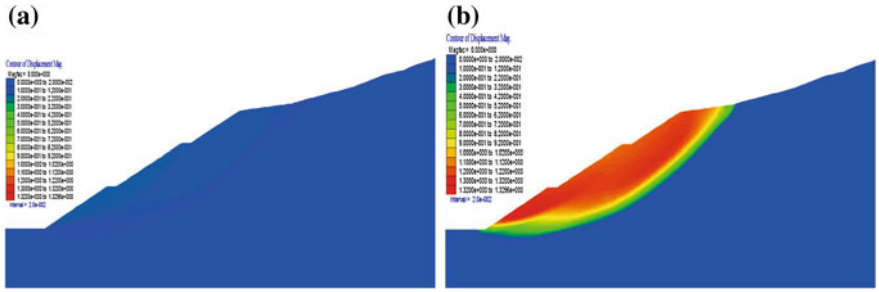

Fig. 19 **a** Displacement when groundwater level is low. **b** Displacement when groundwater level is high

groundwater level, displacement on slope is negligible or zero, while at high water table, displacement is high due to loss of shear strength, as the sliding zone develops within the weak layers.

6 Conclusions

1. Atom-en landslide occurred due to the combined effect of incessant rainfall, snowmelt and steep nature of the slope.
2. The landslide occurred from a height of 40 m, width of 30 m and length of 40 m and traveled in the southwest direction.
3. Result obtained from field investigation shows that the landslide occurred within the volcanic tuff layer that is underlain by weathered mudstone as the bedding plane became the sliding surface on upper part of slope.
4. Result obtained from in situ shear test shows that cohesion is 5 kPa while internal frictional angle ranges from 30 to 40°.
5. Result obtained from laboratory tests show that cohesion is 12 kPa while internal frictional angle is 25°.
6. Result of back analysis using Janbu's method shows that the internal friction angle of the lower part of the slope is 26°. Equally, evaluation of the effect due to groundwater using the same method shows that the slope was destabilized due to rise in groundwater level.
7. Analysis of the slope using Flac^{3D} program showed that the occurrence of the landslide is due to rise in groundwater level by infiltration from snowmelt. In the upper part of the slope, shear failure occurred along bedding plane, while shear failure occurred within the soft layer at the lower part of the slope.

References

Kano K, Yoshida F (1985) Geology of Sakaiminato area. Geological map with a scale of 1 to 50,000. Geol Surv Japan:57

Matsuura S (1998) Difficulties in predicting snow-induced landslides. J Japan Landslide Soc 34(4):39–46

Sato H, Shiraishi S, Ito T (2004) The behavior of the tertiary landslides through the snowy period in Niigata prefecture, central Japan. J Japan Landslide Soc 41(1):37–42

Shiraishi K (1988) Occurrence factor of landslide in snow season. In: Proceedings of the 16th symposium handout in the Japan landslide society, Niigata Branch, pp. 30–40

Bedding Landslide Formation Mechanism and Traits in Lesser Khingan Mountain

Hua Jiang, Wei Shan and Zhaoguang Hu

Abstract In China's Heilongjiang Province, Bei'an to Heihe expressway utilizes the original second-class highway to widen and expand for freeway. Subgrade of some sections located at the tailing edge of the landslide, influenced by landform, geological condition and climatic factors are in unstable states, thus poses great difficulty in widening and expansion programs. In the process of this study, the authors identified the space form of the landslide; analyzed the failure mechanism of the landslide; evaluated the stability condition and the development tendency of the landslide; and determined the prevention and treatment measures. This study concentrated on the K178+530 section landslide located on Bei'an to Heihe freeway, and employed field survey, topographic mapping, geological drilling, laboratory tests, numerical simulation, field monitoring and theoretical analysis methods to carry out integrated study of the failure mechanism of the landslide. Study results show that the K178+530 landslide belongs to translational landslide, rupture surface is located at the bottom of sub-grade spoil and silty clay; during survey, the landslide is in the limit equilibrium state, directly affects the stability of sub-grade slope; atmospheric precipitation, snowmelt water and seasonally frozen soil thawing water provide a continued water source for landslide, surface water and ground water supply the Quaternary pore water by infiltration and lateral runoff through surface cracks and shallow high permeability rock and soil, low permeability rock and soil under the loose overburden form aquiclude, rock and soil of the aquiclude are saturated to be soften form rupture surface; the landslide have seasonal, gradual, low angle characteristics.

Keywords Freeway · Translational landslide · Formation mechanism · Stability

H. Jiang · W. Shan (✉) · Z. Hu
Northeast Forestry University, Hexing Road 26, Harbin 150040, China
e-mail: shanwei456@163.com

W. Shan et al. (eds.), *Landslides in Cold Regions in the Context of Climate Change*, Environmental Science and Engineering, DOI: 10.1007/978-3-319-00867-7_6,

1 Introduction

Landslide is a natural phenomenon that, rock and soil on the slope, affected by river scour, groundwater activity, earthquake, artificial cutting slope and other factors, under the action of gravity, slide down along a weak plane or zone (Kong et al. 2008; Qiao 2002). High grade highway constructed in mountain area, due to its special geology, geomorphology, hydrology and climatic condition, often trigger landslides (Sun et al. 2008). Landslides often disrupt traffics, affect inter-city and local transport systems, cause river-blockage and create dams, destroy highways, cause socio-economic loss by destroying factories and urban and rural municipalities in mountain areas (Zhu et al. 2007; Li et al. 2011).

Bei'an to Heihe highway utilizes the original second-class highway to widen and expand for freeway in Heilongjiang province of China. During the first-stage of the construction process, landslides were triggered on many section sub-grade and slopes of the K159+000-K184+000 section which traverses the Lesser Khingan Mountains. In the most serious K176+500-K179+300 section, the sub-grade lost stability due to landslides after construction, were forced to change the route to build (Shan et al. 2012). Design stage investigation results show that some sections are located on active landslide material (see Fig. 1), affected by landform, topography, rainfall, freeze–thaw and other factors, foundations are in unstable state, bring enormous difficulties to widening and expanding implementation (Jiang et al. 2012).

Therefore, need comprehensively analyze the mechanism, scale and hazard of landslide; accurately reflect the characteristics, occurrence and development law of

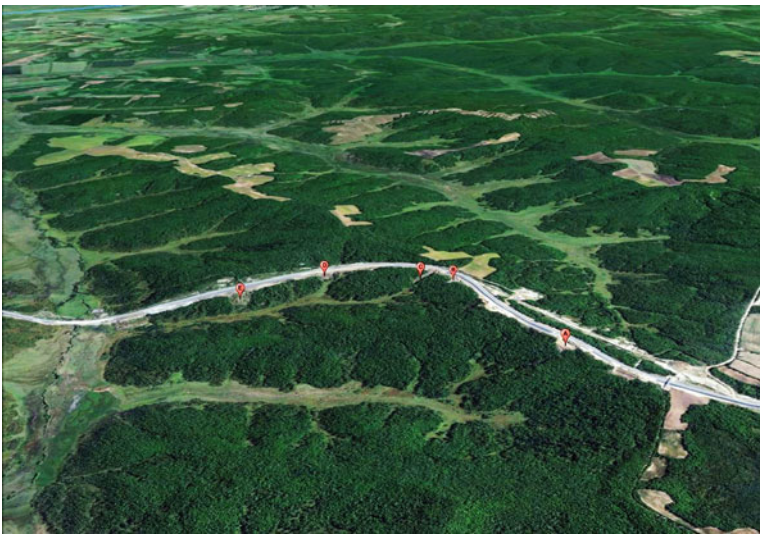

Fig. 1 Aerial view of Bei'an to Heihe freeway landslide section

landslide, so that can employ effective prevention and remediation measures in the freeway construction period (Long et al. 2010). This article took the Bei'an to Heihe freeway K178+530 section landslide as the research object, employed field survey, topographic mapping, geological drilling, indoor tests, numerical simulation, field monitoring and theoretical analysis methods to carry an integrated study on the formation mechanism of the landslide.

2 Natural Geographic Condition of Study Area

The study area is located in China's Lesser Khingan Mountain island permafrost region. The climate of the area belongs to continental monsoon climate which records high temperatures in spring seasons and high amount of precipitation and humidity in summer; autumn and winter seasons are relatively cold and last until late-February or mid-March. Annual average temperature is about −0.6 °C while lowest average temperature is about −48.1 °C. Also, the highest average temperature is 35.2 °C with short frost free period of 90 to 125 days. Average annual precipitation hover around 530 and 552 mm, with July to September (summer) high rainfall records accounting for about 61–67 % of annual total precipitation. The ground surface of the area can form seasonal frozen soil, the time of ground reaching maximum frozen depth is the late of May, and the maximum seasonal freezing depth ranges from 2.26 to 2.67 m. Many island permafrost are distributed in the area.

The research area has a hilly topography with small relative height difference, and part of slope is steep. The tectonic is in the Wuyun-Jieya new rift zone, the south is Shuhe upwarping zone and the north is Handaqi virgation. Surface exposed stratum: the upper Cretaceous Nenjiang Formation exposed in the lower part of the mountains or hills, the acreage is larger, is comprised of river and lake facies clastic deposition, lithology is mudstone, silty mudstone, tonhaltig fine sandstone and fine sandstone, rock is bedded, weak cementation and anti-weathering ability, weathering depth is large, near surface portion substantially weathered, both water containing and water proof, unconformably overlaps on the upper Jurassic Shenshu Formation and lower Cretaceous Guanghua Formation volcanic and late Indosinian granite; Tertiary Pliocene series Sunwu Formation, exposed in the upper part of the mountains or hills, is comprised of river and lake facies clastic sediments. The lithology is mainly composed of loose and friable uncemented pebbly sandstone, unconformably overlaps on the upper Cretaceous Nenjiang formation; Quaternary Holocene series recent river alluvium and stack layers dispersed in low-lying valley beaches, is comprised of surface detrital material, clay, gravel sand and mud soil. This unit is stratified, weakly cemented with strong resistance to weathering, weathering depth is larger, near surface portion substantially weathered. According to the aquiferous medium, supply and drainage conditions, groundwater is divided into Cretaceous pore water, Tertiary pore water and Quaternary pore water three kinds.

3 Field Survey

We carried out geological survey and topographic mapping work in the study area, found five landslides distributed in the study section, this article aimed at the K178+530 landslide, as show in the Fig. 1 "C" area.

The landslide is located in the valley. The flat shape of landslide body presents a tongue (see Fig. 2), its acreage is about 7,000 m^2, the distance from toe to rear edge is about 200 m, the elevation of toe is 254 m, and the elevation of rear edge is 285 m. There are conspicuous arc dislocation and ponding on the tailing edge of the landslide, upheaval on the front of the landslide and cracks on the surface of the landslide body (see Fig. 3).

4 Geological Exploration

The geologic condition of the landslide was studied by arranging four drill holes and six resistivity measurement lines as shown in Fig. 2. The geologic profile of the landslide was drawn using data obtained from drilling and resistivity surveys (Fig. 4). Displacement monitoring equipments, temperature and pore water pressure sensors were installed in the drill holes.

Stratigraphic profiling shows that the region is underlain by Quaternary loose sediments, Tertiary pebbly sandstone, Cretaceous mudstone and sandstone. The sub-grade material is generally yellow, loose, soft and plastic, composed mainly of Tertiary pebbly sandstone, Cretaceous mudstone and sandstone. Silty clay: yellow,

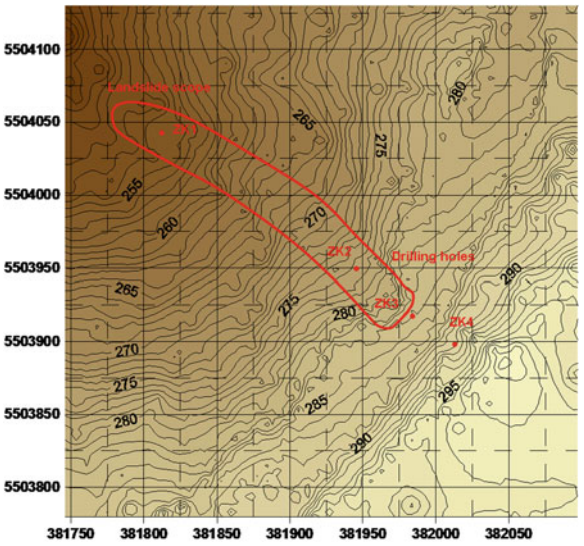

Fig. 2 Topography of the K178+530 landslide region

Fig. 3 Landform characteristics of the K178+[1]530 landslide

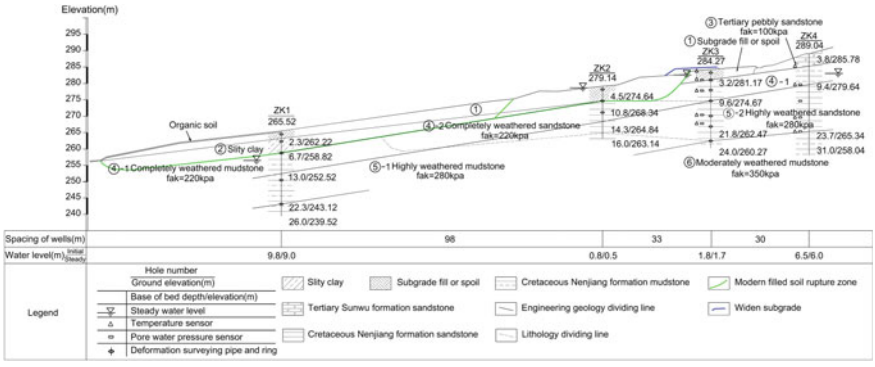

Fig. 4 K178+530 landslide engineering geological profile

soft plastic, high constrictive and strong frost heaving soil. Sub-grade filling: loose Tertiary pebbly sandstone consolidated in situ, permeability, weak frost heaving soil. Tertiary pebbly sandstone: Yellow, slightly wet, no cementation, good gradation, strong permeability, and weak frost heaving soil. Mudstone: gray black, weak cementation, argillaceous structure, layered structure, dried broken into

small pieces, easy to be softened by water. Sandstone: yellow, weak cementation, fine sand structure, layered structure, easy to be disintegrated by water.

The surficial layer of the landslide is comprised of poorly consolidated Tertiary pebbly sandstone and sub-grade spoil of high void ratio. The surface of the sub-grade spoil is covered with irregular cracks and discontinuities filled with run-off water. The sub-grade spoil and silty clay are underlain by relatively weathered mudstone and sandstone. Through indoor test, permeability coefficient of sub-grade spoil is 6.19×10^{-8} cm/s, silty clay is 3.84×10^{-8} cm/s, Tertiary pebbly sandstone is 4.11×10^{-4} cm/s, completely weathered mudstone is 6.34×10^{-6} cm/s, and completely weathered sandstone is 2.12×10^{-7} cm/s. There are many cracks on the slope surface and the permeability coefficient of the upstream pebbly sandstone is larger, the permeability coefficient of the sub-grade spoil and silty clay is smaller, when the water penetrates downward and accumulates at the bottom of sub-grade spoil and silty clay, the water content of it increased gradually, shear strength decreases significantly. This judgment, the landslide belongs to translational landslide; rupture surface is located at the bottom of sub-grade spoil and silty clay.

5 Landslide Stability Numerical Simulation

Limit equilibrium method is the most advanced method in landslide stability study. The limit equilibrium method is characterized in that only considers static equilibrium condition and soil Mohr–Coulomb failure criterion, need assume rupture surface during calculating. Compared with limit equilibrium, finite element method namely considers the soil static equilibrium, also meets the strain compatibility and stress strain constitutive relation, can serve as a more rigorous theoretical system for slope stability analysis, it needn't assume the shape and position of rupture surface, determines the stability of landslide through stress and strain analysis.

Based on geological survey and indoor test results, employed the finite element method to simulate the safety factor of K178+530 landslide. Rock and soil finite element calculation parameters are shown in Table 1.

During surveying, the sub-grade spoil water content is 37.1 % and saturation is 0.953, silty clay water content is 28.7 % and saturation is 0.925, the slope safety factor is 1.02, the landslide total deformation before damage is shown in Fig. 5, and the landslide equivalent plastic strain cloud map before damage is shown in Fig. 6. The landslide is in the limit equilibrium state, when the surface soil saturated with water or abandon soil loading or filling sub-grade, the landslide will slide, and directly affect the stability of sub-grade slope.

Table 1 Physical and mechanical parameters of K178+530 landslide calculation model

Rock and soil name	Unit weight (g/cm^3)	Cohesion (kPa)	Friction angle (degree)	Modulus of elasticity (MPa)	Poisson's ratio
Sub-grade spoil	1.87	13	1.5	0.63	0.47
Silty clay	1.91	14.2	7.2	2.2	0.43
Pebbly sandstone	1.98	5.9	31	28	0.22
Completely weathered mudstone and sandstone	1.76	23.4	11	58	0.35
Highly weathered mudstone and sandstone	1.83	35.6	13	75	0.33
Moderately weathered mudstone	1.89	48.3	17	90	0.30

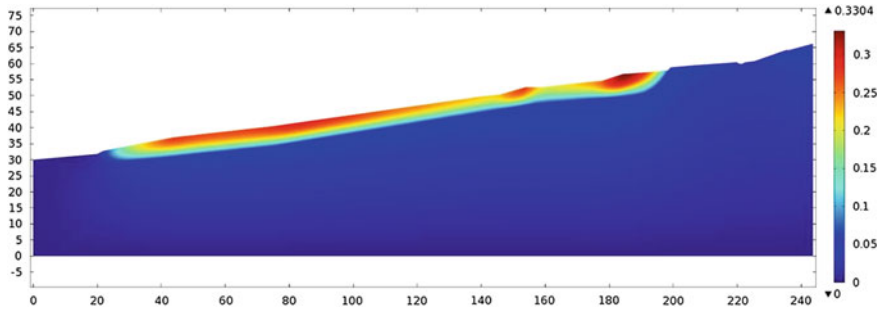

Fig. 5 K178+530 landslide total deformation cloud map before damage

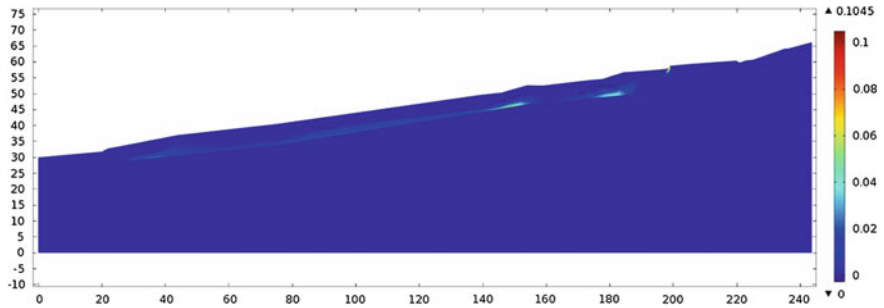

Fig. 6 K178+530 landslide equivalent plastic strain cloud map before damage

6 Field Monitoring

Monitoring data were collected after field survey. The data shows that ZK1 and ZK2 deformation monitoring pipes installed in the landslide material were sheared to depths of 6.5 and 4.2 m, respectively. Dislocation on the landslide trailing edge increased, striation appeared on the both sides of landslide, cracks on the landslide body increased. Based on these data and phenomena, judged that the slope occurred slide. At that same time, employed GPS to monitor the tube nozzle moving data (see Fig. 7), and paid attention to the pore water pressure data (see Fig. 8), ground temperature data (see Fig. 9) and deformation data of ZK3, the vertical and horizontal displacement of ZK3 were very small.

The landslide began to slide in the rainy season as pore water pressure in the soil increased and reached a steady state in winter; the maximum horizontal displacement recorded are 32.2 and 60.0 m. The landslide failure is mainly influenced by precipitation. The landslide slid again in the spring melts period of the following year, the seasonal frozen soil layer of the area was completely melted at that time, pore water pressure increased rapidly, and the maximum horizontal displacement recorded are 50.8 and 91.5 m. The slope movement is mainly influenced by melting of frozen soil and snowmelt.

7 Failure Mechanism of the Landslide

The failure mechanism of the landslide is mainly affected by the landform, climate and underground water, geologic condition and other inherent factors.

Topographic condition: topography of landslide is upper steep and lower gentle, around high and intermediate low (see Fig. 10), is avail for surface water and

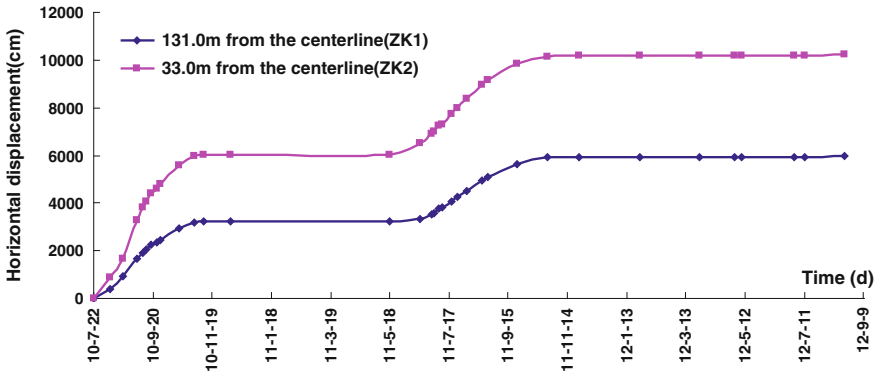

Fig. 7 Curve of nozzle horizontal displacement changes with time

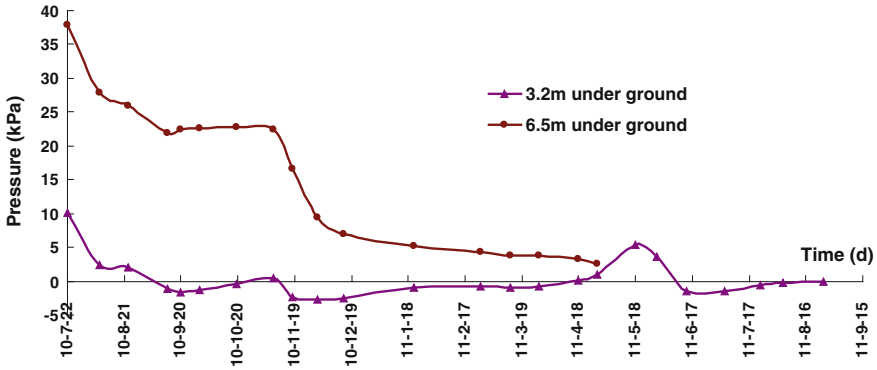

Fig. 8 Curve of ZK3 pore water pressure changes with time

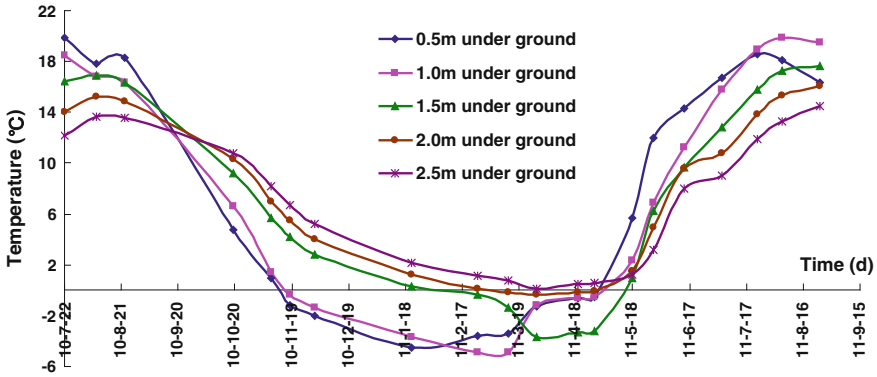

Fig. 9 Curve of ZK3 ground temperature changes with time

ground water to assemble in landslide; the rupture surface is so gentle to retain water for a long time.

The effect of climate and water: atmospheric precipitation, snowmelt water and seasonally frozen soil thawing water constantly supply the Quaternary pore water. Under the action of water, unit weight of the sliding mass increases and shear strength of the rupture zone decreases.

Geological condition: surface cracks and shallow high permeability rock and soil provide infiltration and lateral runoff channel for surface water and groundwater; dense sub-grade spoil and silty clay form aquiclude, sub-grade spoil and silty clay of the aquiclude are influenced by the Quaternary pore water to be saturated, shear strength decrease dramatically and form rupture surface.

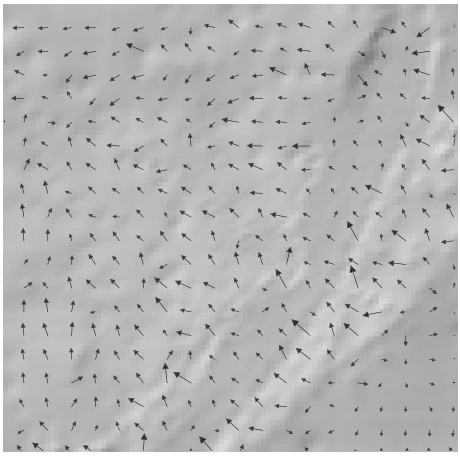

Fig. 10 Landform vector graph of landslide region

8 Conclusions

This chapter employed geological survey, topographic mapping, geological drilling, geophysical exploration, indoor tests, numerical simulation, field monitoring and theoretical analysis methods to carry an integrated study on the failure mechanism of the Bei'an to Heihe freeway K178+530 landslide and arrived at the following conclusions:

The K178+530 landslide is a translational landslide with rupture surface located at the bottom of slope composed of sub-grade material and silty clay.

Preliminary survey shows that the stability of the sub-grade slope is being affected because the landslide is in limit equilibrium state.

Seasonal precipitation, snowmelt water and seasonally-frozen soil thawing water provide continuous source of underground water for the landslide; surface water and ground water supply the Quaternary pore water by infiltration and lateral runoff through surface cracks and shallow high permeability rock and soil; low permeability rock and soil under the loose overburden form aquiclude, rock and soil of the aquiclude are saturated to be soften form rupture surface.

Due to the special climate, landform and geological condition, the landslide has seasonal, gradual, low angle characteristics.

Acknowledgments This work was financially supported by the key science and technology project of Heilongjiang Communications Department "Study on Sub-grade Stability Controlling Technology of Freeway Expansion Project Permafrost Melt and Landslides Sections" (2011318223630).

References

Jiang H, Shan W (2012) Formation mechanism and stability analysis of Bei'an-Heihe expressway expansion project K178+530 landslide. Adv Mater Res 368–373:953–958

Kong FL, Chen C, Sun GJ (2008) Application of multi-electrodes electrical method to landslide investigation in Qingjiang Shuibuya reservoir. Chin J Eng Geophys 5(2):201–204

Li DQ, Han WX, Pang MK (2011) Seepage analysis of landslide under condition of water level falling in three Gorges reservoir. Water Resour Power 29(1):85–88

Long JH, Guo WB, Li P (2010) Creep property of soil in sliding zone of loess landslide. Chin J Geotechn Eng 32(7):1023–1028

Qiao JP (2002) Structure and shape of landslide. Chin J Rock Mech Eng 21(9):1355–1358

Shan W, Jiang H, Cui GH (2012) Formation mechanism and characteristics of the Bei'an to Heihe expressway K177 landslide. Adv Mater Res 422:663–668

Sun QH, Xu HW, Zhang YQ (2008) Application of high density resistivity method in highway road landslide prediction. J Guizhou Univ Technol 37(6):101–105

Zhu YS, Li HJ, Cao NE (2007) Finite element method research on road slide stability analysis. J Highw Transp Res Dev 24(4):39–42

Part III
Impact of Landslide on Environment and Facilities

The Impact of Freeze–thaw on the Stability of Soil Cut Slope in High-latitude Frozen Regions

Ying Guo, Wei Shan, Hua Jiang, Yuying Sun and Chengcheng Zhang

Abstract It has been widely reported that variations in soil moisture content is one of the factors that contribute to landslide occurrence in cut slopes. The effect of freeze–thaw cycles on the stability of seasonally-frozen cut slope along Fangzheng-Harbin expressway was studied. A comprehensive study on the silty clay material of the cut slope was carried out by combining results obtained from field monitoring tests, laboratory experiments and numerical simulations. Also, the variation of soil moisture content with subsurface temperature and the impact of soil moisture content on the physical and mechanical index properties of the soil were studied. Results obtained from finite element analysis shows that soil moisture content contribute to instability of the cut slope especially in spring periods of snow melt. Field monitoring result indicates that during the process of soil freezing, moisture content of the soil decreases to the freezing front, and forms ice segregates in some parts of the frozen area. In spring, when snow melts and temperature increases to 0 °C, increase in temperature stops temporarily, and soil moisture rises slowly. After a period of time, the soil moisture curve rises rapidly, followed by the rapid rising in soil temperature. This phenomenon is due to the absorption of heat by the frozen layer due to ice melting process. Triaxial test results show that when the soil moisture content is less than optimum moisture, soil cohesion increases with increase in moisture, while when the soil water content is higher than the optimum water content, soil cohesion decreases with increase in moisture. The peak value of soil cohesion is near the optimum water content. The internal friction angle of the soil decreases with increasing moisture content. Soil cohesion decreases with increasing freeze–thaw cycles. The internal friction angle of the soil increases after the first freeze–thaw cycle, but it decreases in later freeze–thaw cycles. Finite element analysis results show that factor of

Y. Guo · W. Shan (✉) · H. Jiang · Y. Sun
Northeast Forestry University, 150040 Harbin, China
e-mail: shanwei456@163.com

H. Jiang · Y. Sun · C. Zhang
Heilongjiang Institute of Technology, 150090 Harbin, China

W. Shan et al. (eds.), *Landslides in Cold Regions in the Context of Climate Change*, Environmental Science and Engineering, DOI: 10.1007/978-3-319-00867-7_7,

safety of the slope decreases with increase in soil moisture. Results obtained from physical and mechanical parameters of the cut slope material in K560+700 section is in critical unstable state. This is validated by comparing the physical and mechanical parameters from another shrub slope in K563+870 section which is in a more stable state. This simulation result is consistent with the actual situation. It follows that moisture content in the soil mass accumulates to frozen areas in the freezing process, and rapid increase of the soil moisture in shallow layer of the slope during the thawing period is the main reason for the instability of cut slope.

Keywords Highway · Cut slope · Silty clay · Freeze–thaw · Moisture changes

1 Introduction

In high-latitude frozen regions of northeast China, landslides are often triggered by soil cut slopes (Wu et al. 2006; Liu and Wang 2006). The reason is mostly due to seasonal freeze–thaw cycles. In winter periods, atmospheric temperature falls below 0 °C, which results to the accumulation of ice in the shallow layer of the slope. The association and arrangement of soil particles is changed by frost heaving, and the mechanical properties of soil materials are also affected (Shan et al. 2009). In spring when the rate of snow melting is high, frozen layers in the shallow part of the slope thaws. During the time of thawing water infiltrating downward, they was hampered by frozen layer or dense soil with low permeability below it, results in the water content increasing rapidly in the interface between thawed layer and impermeable layer, and reaching saturation or super saturation state, then the effective stress of the soil in the cut slope reduced. Gradually, in the shallow layer of the slope, slip band formed along the interface between thawed layer and the impermeable layer, and then the partial or whole of the shallow layer of the slope slide down along the slip band due to gravity (Niu et al. 2004).

The study of the stability of permafrost slopes appeared earlier (Tarr 1897; McRoberts and Morgenstern 1974; Clark 1988; Zhou and Guo 1982), but mainly is in permafrost plateau (Zhu et al. 1996; Wang and French 1995; Niu and Cheng 2002; Li and Zhao 2002). There are differences between the instability in seasonal frozen region and the instability in permafrost. In seasonal frozen regions, there is a larger change in temperature and repeated freezing-thawing cycles, and has obvious seasonal characteristics.

Relying on the highway expansion project from Jiamusi to Harbin of Tongsan Highway, the study area is located on the side of widening from K560+090 to K565+690. The terrain graph fluctuation of study area is bigger, the soil of it is sandy clay, its natural density is 1.8–2.1 g/cm^3, the average height of the cut slope is 5 ~ 15 m, and the average ratio of the slope is 1.5–1.75.

Through on-site investigation, monitoring soil moisture, ground temperature in shallow layer of the slope, and indoor test of soil physical and mechanical index properties, the soil physical and mechanical nature varying with soil moisture and freeze–thaw cycles was studied. Through calculation and analysis, the impact of soil moisture on slope stability during freeze–thaw process was analyzed.

2 The Monitoring of the Temperature and Moisture of the Soil Body of Cut Slope

According to meteorological data of Heilongjiang Province (China), within the depth of 20 cm below the surface of study area, the negative temperature of the soil emerges is in early November each year, and transforms to positive temperature till to the end of March in the next year; The maximum freezing depth is about 1.9 m. From on-site investigation, depth of the sliding surface of the cut slope landslide is about 1–1.5 m, and its thickness is 10–25 cm.

In order to understand the relationship between the atmospheric temperature, soil temperature and moisture in the slope, we selected K560+700 section as monitoring section, in different place of the monitoring section (top -slope, slope toe), and installed temperature and moisture sensors in different depths (0.6, 1.4, 2.2 m), from January 2009 to June 2010. We regularly monitored the temperature and moisture in different depths of the soil body. Figures 1, 2 and 3 shows the temperature and moisture curve of K560+700 section in three different depths of 0.6, 1.4, 2.2 m.

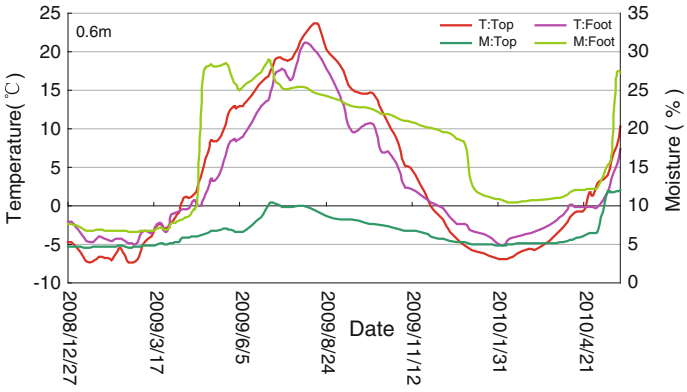

Fig. 1 The temperature and moisture curve of soil body in the depth of 0.6 m in K560+700 section

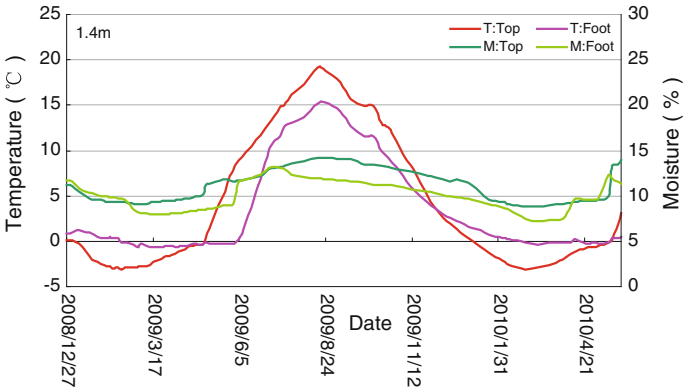

Fig. 2 The temperature and moisture curve of soil body in the depth of 1.4 m in K560+700 section

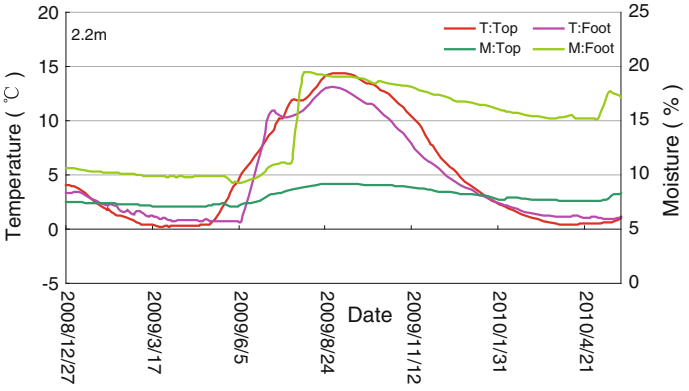

Fig. 3 The temperature and moisture curve of soil body in the depth of 2.2 m in K560+700 section

2.1 The Variation of Soil Temperature of the Cut Slope

It could be seen from Figs. 1–3 that, many factors could affect the soil temperature, such as solar radiation, atmospheric temperature, air flowing, soil moisture, heat conduction and so on. Among them, for the deeper soil layer, heat conduction is key influencing factors. From the curve, the data of temperature could be got and shown in Table 1.

It could be seen from the comprehensive analysis that: For the variation amplitude of soil body temperature, which in top-slope is bigger than that in foot-slope. For the time of beginning thawing, which in top-slope is earlier than that in

Table 1 Max. and min. temperature of soil body in the cut slope

Location	Top-slop			Slope toe		
Depth	0.6 m	1.4 m	2.2 m	0.6 m	1.4 m	2.2 m
Max Tem. (°C)	23.7	19.1	14.4	21.0	15.3	13.0
(Date)	(09.8.16)	(09.8.16)	(09.09.06)	(09.8.03)	(09.8.24)	(09.8.24)
Min Tem. (°C)	−7.8	−3.7	0.2	−5.4	−0.7	0.7
(Date)	(10.02.04)	(09.02.27)	(09.03.23)	(10.02.04)	(09.03.23)	(09.04.29)
Variation amplitude of Tem. (°C)	31.5	22.8	14.2	26.4	16.0	12.3

foot-slope. For the duration time of lower temperature, deeper soil body is longer than shallow soil body.

2.2 The Variation of Soil Temperature and Moisture of the Cut Slope

It also could be seen from Fig. 3 that, the factors affecting the soil moisture could include precipitation, overland runoff, evapo-transpiration, and infiltration, the state of freeze or thaw and moisture migration and so on. Among them, for shallow layer of the slope, such as precipitation, overland runoff, evapo-transpiration, infiltration have more influence on the soil moisture. With the depth of soil layer become deeper, such as the state of freeze or thaw, moisture migration and infiltration would be main impact factor of soil moisture.

It should be noted that: the data in the monitoring curve is the value of water mass fraction, which is the conversion value coming from dielectric constant measured by moisture sensor. When the soil come into the frozen state, part of the water in the soil became into ice (segregate) (as shown in Fig. 4), so the moisture measured is conversion moisture of the mixture of ice and water. When the soil is in the non-frozen state, the moisture measured is actual soil moisture.

It could be known from the note above that, when the actual soil moisture is bigger, the change of moisture curve will be more apparent. This conclusion could be proved by the moisture curve of slope toe in Fig. 1.

Combining with the soil temperature cycle, the freeze–thaw process of the soil could be divided into five stages: Non-frozen, Early-freezing, Frozen, Early-thawing, and Ongoing-thawing. The soil temperature and moisture in five stages will be analyzed followed.

Soil moisture migration in stage of early-freezing. The stage of early-freezing refers to the period that is from soil temperature coming into 0 °C to soil temperature keeping a certain stable negative temperature. It could be found from Fig. 1 that: in this period, in 0.6 m depth, there are slight drops both in moisture curve and in temperature curve. The reason for it is: During freezing process, especially the soil temperature was close to 0 °C, the temperature of soil particle

Fig. 4 Segregation-ice caused by the migration of water in the pit

decreased firstly, because of solids and gases having different thermal conductivity, so the soil particle absorbed the heat of pore water and pore air among them by conduction, which made those three medium come into heat balance. This heat balance would keep a period of time, until the pore water near the soil particle crystallized by releasing the heat of hydration. From then on, this heat balance would be broken again and soil temperature decreased continually. The sign of this process was moisture curve measured having a drop, but the drop in different depth wasn't alike.

Moisture and temperature in stable frozen stage. In stable frozen period, especially in Early-Freezing stage just finishing, with a further decline in soil temperature, the soil moisture curve decreased further, but slightly. This is because small amount of unfrozen water near the freezing front migrated to the freezing front. With having a relatively stable negative temperature in soil temperature, the soil moisture also have stable state for some time. This is because the stable temperature field could made temporary balance between frozen water and unfrozen water.

Moisture and temperature in stage of early-thawing. The stage of Early-thawing refers to the period that soil negative temperature rise from the lowest negative temperature to −0.3 °C. During this period, with the stable ascent of soil temperature, at the beginning, soil moisture curve uplift slowly even had uplift step. Then the soil moisture kept constant, even the soil temperature still be rising. This is because the crystallization in soil voids began to thawing. Because crystallization thawing need enough hydration heat, so the soil moisture would be constant until the energy gathering from soil particle was bigger than the heat of hydration. This process is the energy reserves for the next stage of Ongoing-thawing.

Moisture and temperature in ongoing-thawing stage. The ongoing-thawing stage refers to the period that the soil temperature rises from −0.3 to 0 °C. During this period in frozen soil layer, the temperature rose from −0.3 to 0 °C and

lingered near 0 °C. But the soil moisture had a steep uplift at a certain moment. After steep uplift of soil moisture, soil temperature rapidly rose to 5–10 °C. Next, soil moisture became rising slowly again, then soil temperature also rose slowly. At same time, in non-frozen soil layer, the soil temperature maintained at a certain lower temperature, but the soil moisture had a slight declined in short time just before the steep uplift of soil moisture in frozen soil, after that soil moisture rose again. The reasons for this phenomenon are: The crystallization in soil voids thawed completely that lead to the steep uplift of soil moisture. The heat of hydration the crystallization needed came from two directions, one is upper soil body supplied by solar radiation, and another is below soil body provided by non-frozen soil. So, during the accumulating period of hydration heat energy, the soil temperature both in frozen soil and in non-frozen soil remained relatively constant. At same time, because there was an ice thawing layer over the non-frozen soil body, which made the moisture in non-frozen soil migrating to the interface of ice thawing, so the soil moisture in non-frozen soil had a slight declined. When the crystallization in soil voids thawed completely, and interface of ice thawing disappears, the upper soil moisture permeates into the non-frozen soil layer, the soil moisture of non-frozen rose rapidly again.

Moisture and temperature in non-frozen stage. The stage of non-frozen refers to the period which the soil temperature is in positive value. In this period of time, the soil temperature varies with air temperature, the soil moisture is mainly affected by rainfall, evapo-transpiration and penetration.

Taking the data of July 2 as the example, and conduct analyzing as follow:

On June 5th, at depth of 0.6 m, the soil moisture at the slope toe was 25.03 and 6.58 % at the top of the slope. Until July 2nd, their soil moisture both reached the maximum value within one month. The increase of moisture at the top of the slope and the slope toe were 3.76 and 3.96 %, respectively. According to meteorological data in this period, there was more concentrated rainfall. So it could be concluded that at depth of 0.6 m, the soil moisture is largely affected by rainfall, but the soil moisture in different part of the slope is very different, the original soil moisture at the slope toe is much higher than values obtain at the slope top.

At depth of 1.4 m, when it came into non-freeze period in May, the soil moisture both in foot and top of the slope rose slowly at the beginning, but the time of peak soil moisture value was very different: In slope toe, soil moisture reached peak value 13.13 % on July 12th, then dropped quickly, till July 23rd, it declined 0.94 % in 11 days; In top-slope, the time of moisture peak value was on August 14th, which was one month later than its in slope toe, and the moisture dropped slowly after peak value. So it could be known that, in the depth of 1.4 m, the rate of water permeation is faster, which means the soil body here have high permeability, or there is cracks channel in somewhere of the soil body.

At depth of 2.2 m, the soil moisture at the slope toe and top slope were very different: The moisture in the slope toe rose sharply after July 23rd, from July 23rd to August 3rd, the moisture increased from 11.15 to 19. 23 %, the rising amount was up to 8.08 %, These occurred precisely after the sharp drop of soil moisture in 1.4 m depth. It could be known from that, in 2.2 m depth, there were lots of water

permeating from the upper layer, and gathered here, that means it is cracks in upper layer but isn't high permeability soil there. Through on-site investigation, this guess was in line with the scene facts. In contrast with slope toe, in top-slope, from May 30th to August 24th, the moisture increased from 7.05 to 9.17 %, the rising amount merely is 2.12 %. Through on-site investigation, there were not any cracks in soil body.

3 The Impact of Freeze–thaw on Shear Strength of Slope Soil

In order to understand the impact of freeze–thaw cycles, soil moisture and soil dry density on the shear strength of soil slope, basic geotechnical soil index property analysis was carried out on silty clay from cut slope, the data is shown in Table 2.

Triaxial test was conducted under various test conditions. Specific programs is as followed, dry density is 1.615 g/cm^3, moisture is 9, 14, 19, 22 %, and freeze–thaw cycles is non, one, and five. The test results are shown in Figs. 5 and 6.

Table 2 Basic physical properties indicators of silty clay

Liquid limit (%)	Plastic limit (%)	Plasticity index (%)	Maximum dry density (g/cm^3)	Optimum water content (%)
32.5	18.7	13.8	1.90	13

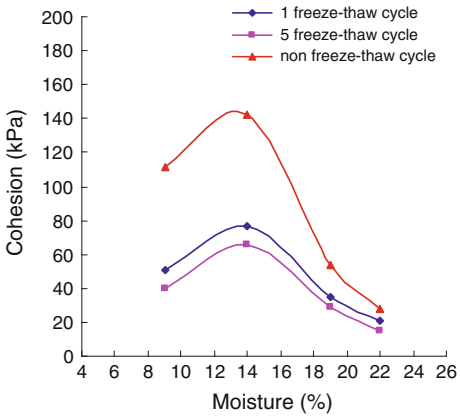

Fig. 5 The relationship curve between soil cohesion and soil moisture before and after Frozen–thaw with dry density 1.615 g/cm^3

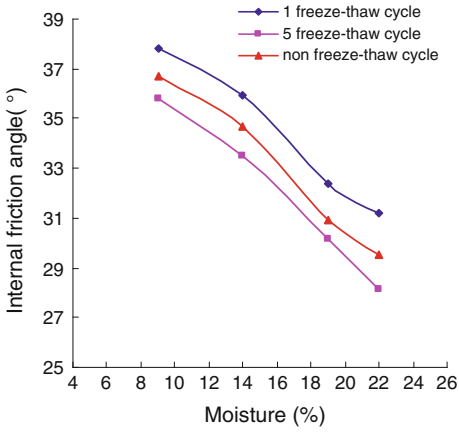

Fig. 6 The relationship curve between soil internal friction angle and soil moisture before and after frozen-thaw with dry density 1.615 g/cm^3

3.1 The Impact of Freeze–thaw Cycles and Soil Moisture on Soil Cohesion

Remoulded soil samples with dry density of 1.615 g/cm^3 were used to conduct triaxial tests under different freeze–thaw cycles. Figure 5 shows the relationship between soil moisture and soil cohesion. It could be seen that when soil moisture is close to optimum value, soil cohesion reaches its peak. Soil cohesion decreases gradually with increasing freeze–thaw cycles. When the soil moisture is at optimum value, soil samples undergo one and five freeze–thaw cycles as soil cohesion reduces to 81.62 and 118.8 kPa, accounting for percent strength loss of 51.85 and 75.45 % respectively.

3.2 The Impact of Freeze–thaw Cycles and Soil Moisture on Soil Friction Angle

Triaxial tests were conducted on remoulded soil samples of dry density, 1.615 g/cm^3 considering different freeze–thaw cycles. Figure 6 shows the relationship between soil moisture and soil friction angle. It could be observed that soil friction angle decreases as soil moisture increases. After freeze–thaw cycle, soil friction angle decreases; the higher the soil moisture content, the lower the soil friction angle. The plot shows that soil moisture increased from 9 to 22 %, after freeze–thaw cycles, soil friction angle reduce 6.42, 15.86, 21.51 % respectively.

Soil cohesion reduced gradually with the increasing of freeze–thaw cycles. Soil friction angle increased after the first freeze–thaw cycle, and then decreased gradually in later freeze–thaw cycles.

4 Stability Analysis of the Impact of Soil Moisture on the Cut Slope

Using the software of finite element analysis—COMSOL, and the physical and mechanical parameters from indoor test in K560+700 section, and adopting the method of strength reduction, the deformation of monitoring section was simulated in the context of variety soil moisture. Combined with the actual situation of K560+700 section, considering the influence of freeze–thaw and rainfall, the soil body in the cut slope was divided into four layers. The soil unit for simulating is triangle, and the finite element mesh is shown in Fig. 7.

Figures 8 and 9 are total displacement nephogram of K560+700 section, the soil moisture data in Fig. 8 is the actual moisture measured from K560+700 section (planted with turf), the soil moisture data in Fig. 9 is the data from K563+870 section (planted with shrub). It could be seen from them that from April 26 to May 5 2009, the maximum displacement in the shrub-covered slope caused by moisture is 7.132×10^{-2}cm, but under the same conditions, the maximum displacement in the slope covered with turf is 4.46 cm, which is 62.54 times higher than that of shrub-covered slope. This shows that shrubs have better reinforcement effect on cut slope.

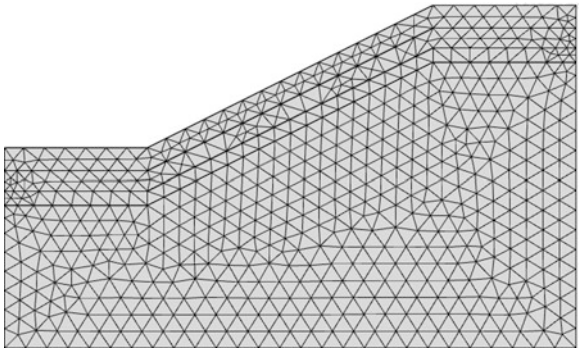

Fig. 7 Grid of finite element calculation in K560+885 section

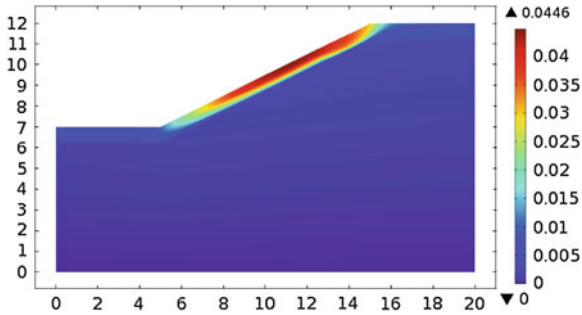

Fig. 8 Total displacement caused by different moisture (turf slope)

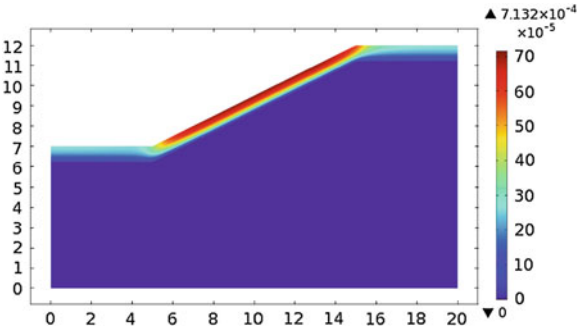

Fig. 9 Total displacement caused by different moisture (shrub slope)

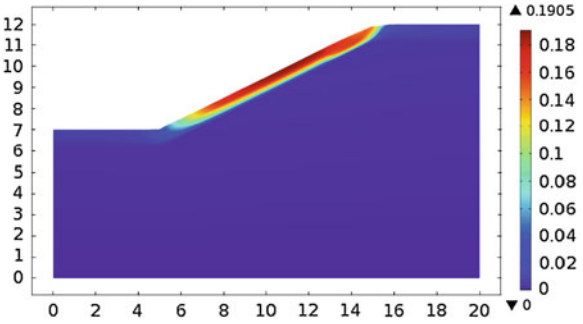

Fig. 10 Total displacement after strength reduction (before destruction)

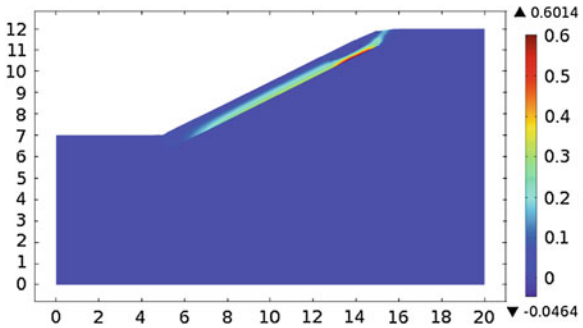

Fig. 11 Equivalent plastic strain after strength reduction (before destruction)

Safety factor of two slopes is: The turf slope is 1.069, the shrub slope is 4.720. The reinforced mechanisms and mechanical effects of shrub reinforcing the slope will be stated in another chapter.

Using the method of strength reduction, Fig. 10 is the total displacement of K560+700 section, it indicated that the maximum displacement before the slope failure occurred in the middle of the slope, and the maximum displacement of slope surface is 19.05 cm. Figure 11 is the plastic strain before the slope failure, and it indicated that the maximum plastic displacement before the slope failure

Fig. 12 The creep deformation of the slope bottom (K560+700 section)

Fig. 13 The crack in the middle of the slope (K560+700 section)

occurred in the top of the slope, the depth of it is 80 cm. These calculated results are consistent with the actual scene (see Figs. 12, 13).

5 Conclusions

1. The result of on-site monitoring shows that: In stage of early-freezing, when the soil temperature is about 0 °C, the pore water between the soil particles crystallizes because the soil particles absorb the heat from pore water. At the same time, unfrozen water migrates to the freezing front, which makes uneven

distribution of water in the soil body. With the freezing of the pore water, the soil moisture drops abruptly; In stable frozen stage, frozen water and unfrozen water reaches the equilibrium state, so the soil moisture is also in steady state because of little influence of soil temperature. In stage of early-thawing, although the soil temperature curve increased from the negative temperature, the soil moisture only had slightly rising, because the frozen soil began to melt slowly now, but the thawing water was small amount, and migrated rapidly, so moisture curve changed little; In stage of ongoing-thawing, soil temperature lingered at 0 °C, the frozen water among soil particle thawed by absorbing the heat of hydration, so the soil moisture rose steeply to a stable value. When the frozen water melted completely, the soil temperature also had its inflection point; the value rose from 0 °C to a stable value, and then entered into non-freeze period. So, the characteristics of temperature and moisture in soil cut slope, determines the landslide risk during the thawing season.

2. The results of indoor test show that soil cohesion decreases with increasing moisture. The peak value of soil cohesion is near the optimum water content. The internal friction angle of soil decreases with increasing moisture. Soil cohesion decreases with increasing freeze–thaw cycles. The internal friction angle of soil increases after the first freeze–thaw cycle, but it decreases in later freeze–thaw cycles.
3. The result of finite element analysis shows that safety factor of cut slope decreased as soil moisture increases. If adopting effective methods to decrease the moisture in slope body, the risk of instability in cut slope caused by freeze–thaw will be reduced significantly.

Acknowledgments The authors would like to thank the financial supports provided by the research project of Heilongjiang provincial Science and Technology Department (GZ07 C401), and the Key project of Heilongjiang provincial Transportation Department "Highway Slope Stability and Greening by Vegetation in Cold Regions".

References

Clark MJ (1988) Advance in periglacial geomorphology. John Wiley & Sons Ltd, New York, pp 325–359

Li YC, Zhao KN (2002) The analysis of landslide in k2023 of QING-Zang highway. J Geol Hazards Environ Preserv 13(4):33–35 (in Chinese)

Liu HJ, Wang PX (2006) Stability analysis of loss of stability caused by freeze and melt of earthen side slopes of highways. J Harbin Inst Technol 38(5):764–766 (in Chinese)

McRoberts EC, Morgenstern NR (1974) The stability of thawing slopes. Can Geotech J 11:447–469

Niu FJ, Cheng GD (2002) Study on instability of slopes in permafrost regions of Qinghai-Tibet high plateau. In: Proceedings of the 5th international symposium on permafrost engineering, Yakutsk: Permafrost Inst. SB RAS Press, pp 192–197

Niu FJ, Cheng GD, Lai YM (2004) Instability study on thaw slumping in permafrost regions of Qinghai-Tibet plateau. Chin J Geotech Eng 26(3):402–406 (in Chinese)
Shan W, Guo Y, Liu HJ (2009) Effect of freeze-thaw on strength and microstructure of silty clay. J Harbin Inst Technol 16:207–211 (in Chinese)
Tarr RS (1897) Rapidity of weathering and stream erosion in the arctic latitudes. Am Geol 19:131–136
Wang BL, French HM (1995) In situ creep of frozen soil. Fenghuo Shan, Tibet plateau, China. Can Geotech J 32(3):545–552
Wu H, Gao W, Wang GF (2006) Cause and control of soil-cutting's sliding collapse in frigid zone. J Nat Disasters 15(3):66–70 (in Chinese)
Zhou YW, Guo DX (1982) Principal characteristics of permafrost in China. J Glaciol Geocryology 4(1):1–19 (in Chinese)
Zhu C, Zhang JX, Cheng P (1996) Rock glaciers in the central Tianshan mountain China. Permafrost Periglac Process 7:69–78 (in Chinese)

Effect of Solar Energy Absorption in the Embankment of the Qinghai-Tibet Railway in the Permafrost Region

Lijuan Huang, Ziran Zhang, Tonglu Li, Boyuan Gu and Junhai Yang

Abstract The in situ observation of the ground temperature was conducted in the embankment of Qinghai-Tibetan Railway on the Beiluhe field site. The results suggest that the mean annual ground temperature in the depth of 0.5 m on south side is 3 °C higher than that on the north side. The difference becomes prominent in winter time and less in warmer season, which is because the south side of the embankment slope faces to the sun and can receive more solar energy while the north lies back to the sun and receive less. However, the thermal difference on the two sides may result in an asymmetric thermal field in the embankment and even in the foundation soil. So the possible un-even traverse settlement should be concerned for the trail stability.

Keywords Embankment · Temperature · Solar energy · Slope · Railway · Permafrost

1 Introduction

The Qinghai-Tibet Railway (QTR) starts from Xining city, Qinghai province in the north-east, terminates to Lhasa city, Tibet in the south-west, with the total length of 1,956 km. QTR was constructed in two periods. A length of the beginning 814 km from Xining to Gelmud had been put into operation since 1984. The end

Z. Zhang · T. Li (✉)
Department of Geological Engineering, Chang'an University, Xi'an 710054, China
e-mail: dcdgx08@chd.edu.cn

L. Huang
School of Geological Science & Environmental Engineering, Southwest Jiaotong University, Chengdu 611756, China
e-mail: 370179972@qq.com

B. Gu · J. Yang
First Highway Consultants Co. Ltd, Xi'an 710054, China

W. Shan et al. (eds.), *Landslides in Cold Regions in the Context of Climate Change*, Environmental Science and Engineering, DOI: 10.1007/978-3-319-00867-7_8,

1,142 km from Gelmud to Lhasa was begun to build in June, 2001 and put onto working in July, 2006. QTR has 960 km running above the altitude of 4,000 m, and 550 km on the permafrost region as shown in Fig. 1. QRT reaches to the highest altitude of 5,072 m as going over the Tanggula Mountain, it is the highest railway in the world.

As the railway passes through the permafrost region, stability of the embankment constructed on the permafrost is the most concerned problem because uneven deformation may be caused by un-equivalent absorption of the solar radiation. The ground temperature on a certain depth are generally controlled by the solar radiation the ground receives and the heat exchange between ground surface and atmosphere, as well as the heat flow form in the soil. Although the soil heat flow varies with the soil types and the position, it usually keeps constant in a certain period, so the ground received radiation and the ground-atmosphere heat exchange may be the key factors affecting the ground temperature. It is known that the global warming has begun to degrade the permafrost. Actually, the engineering construction in permafrost region has far more severe influence in permafrost than the climate warming does (Instanes 2003).

In the permafrost region of the Qinghai-Tibet Plateau, the first well-known engineering is the Qinghai-Tibetan Highway (QTH) constructed in 1950s, which had encountered plenty of serious embankment deformations as crossing permafrost region. It has been observed in the highway embankment that the settlement

Fig. 1 Position of the QTR and distribution of the permafrost

on the south side is usually more than that on the north side, which indicated that the permafrost on the south side is more possible thawing than that on the north side. It is not difficult to understand that in north hemisphere, the slopes faced to south may receive more solar radiation than those faced to north.

QTR, a state key project, encounters the same problem. However, the railway has more strict limitation for the embankment deformation, so some in situ monitoring sites were established on the line of permafrost to observe the embankment stability and to ensure the railway working normally. The main monitoring items include temperature and settlement of the embankment and the underlying soil. In this paper, only the temperature field of embankment is analyzed.

2 The Site Condition for Temperature Monitoring

The observation site was set on the milepost of DK1139+618, in the south of Beiluhe basin, where is a diluvial alpine plain with the altitude of 4,639 m above sea level. The embankment has the height of ranging from 2. 5 to 4. 5 m and was filled with gravel. The ratio of surface vegetation coverage there is less than 20 %. A drilling hole revealed that the soil underground consists of diluvial clay inter-bedded by silty sand on the upper 4 m and mud-sandstone underneath. The upper bound of the permafrost depth is about 2.5 m and a thick ice bed entombed underneath. The mean annual temperature on ground surface ranges from −0.28 to −0.69 °C. The frozen soil belongs to instable to extreme-instable permafrost.

The railway extends in the direction of SE130 °C on the monitoring site, so generally south-west embankment slope faces to the sun while the north-east side stands with back to the sunshine. The ground temperatures were monitored on the depth of 0.5 m under the embankment surface in the profiles of milepost DK1139+670. The apparatus used were thermal-susceptible resistance sensors and Fluke IV multi-meters with a 0.1Ω precision, and entombed in the south side, north side and the top surface respectively. The monitoring began on 1 June 2002, half a year after the embankment being completed, and ended on 29 August 2003. The frequency of data collection is once ten days.

3 The Temperature Differences in the Embankment

The average ground temperatures in each month within the monitoring period were counted. Figure 2 shows the monthly temperature change on the two sides and the top of the embankment. First, it is obvious that the three sites have the same periods of annual cycle change, but keep differences all the year. The ground temperature on the north slope is always the lowest and that on the south slope highest, while that on the top surface is moderate in the same month. The extent of

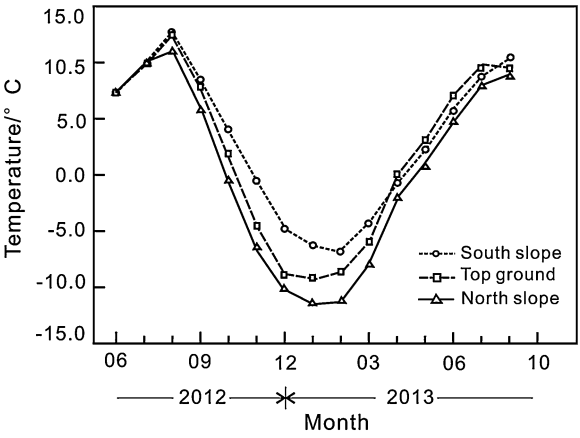

Fig. 2 Ground temperatures at the depth of 0.5 m under embankment surface

the temperature difference among the three points also changes annually. The big difference occurs in winter time during the last November to next February, while in the warmer seasons during May to September, the difference becomes less.

Further statistics of the monitoring data from September 2002 to August, 2003, a complete climatic year, are shown in Table 1. It shows that the temperature on the three points has no obvious difference when the air temperature get to highest, the ground temperature on the south slope is only 1.76 °C higher than that on north slope. While in the time of the air temperature at the lowest, the difference becomes enlarged. The ground temperature on the south slope is 4. 9 °C higher than that the on north slope and 2. 70 °C than that on the top surface. Accordingly, the freezing index on the north slope is over two times as large as that on the south slope, but the thawing index is only three fourth of the south slope. In Table 1, the freezing index is defined as the accumulation of the negative temperature of the monitoring period, coincidently, the thawing index as the accumulation of the positive temperature of the period. The mean annual temperature on the north slope and the top surface is negative, while that on the south slope is positive. The difference of mean annual temperature reaches to 3.2 °C between the north and the south. The monitoring data indicate that the embankment is not equivalent in solar energy absorption that the south side has the advantage to receive more radiation. The higher ground temperature on the south slope of the railway embankment has the potential effect on degradation of the permafrost under the railway foundation.

To reveal the influence of the railway construction on the solar energy adsorption, the air temperature and the natural ground temperature at 0.5 m depth recorded by the local weather station nearby were also obtained and counted in Table 1. Comparing the ground temperature of the natural ground and those monitoring in the embankment, all the highest values in the embankment are higher than that of the natural ground; while the lowest values on the top ground and the north slope of the embankment are lower than that on the south slope of the embankment and higher than that on nature ground. The annual ranges of ground

Table 1 Statistical result of annual temperature indices from Sep. 2002 to Aug. 2003

	South slope	Top ground	North slop	Air Temp.	Natural ground
Highest temperature/°C	11. 3	10.4	9.5	6.2	7.9
Lowest temperature/°C	−6.7	−9.4	−11.6	−13.2	−8.0
Annual range/°C	18.0	19.7	21.1	19.4	15.9
Freezing index/°C. day	−676.3	−1140.1	−1493.3	−1950.9	−943.3
Thawing index/°C. day	1,325.6	1,289.2	986.1	551.3	791.6
Mean annual temperature/°C	1.8	0.43	−1.4	−3.8	−0.42

temperatures in the embankment are all larger than that of the nature ground, close to that of air temperature. The thawing indices in the embankment are larger than that of the nature ground, while the freezing indices on the top ground and the north slope of the embankment are larger than that on south slope and is less than that of the nature ground.

The ratio between freezing (thawing) index of ground temperature on the depth of 0.5 m and corresponding freezing (thawing) index of air temperature is defined as freezing (thawing) factor n of ground temperature. (Karunaratne and Burn 2003; Riseborough 2003). The n values of the factors in the embankment and the nature ground are shown as a column diagram in Fig. 3. Generally the positive freezing factor n is correlated to the ground heat release; meanwhile, the positive thawing factor n is correlated to the solar energy absorption. It can be seen that the freezing factor on the south slope is the lowest, while thawing factor is the highest, so the south slope prevails on solar energy absorption. The freezing factor on the north slope is highest, while the thawing factor is lower than that on the top ground and the south slope, and a little higher than that of the nature ground, so the north slope is also in exothermic state relative to the natural ground.

The south slope has the thawing factor closing to the factor on the top ground, so the higher ground temperature on the south slope may attribute to that less energy is released out in winter. Accordingly, the lower ground temperature on the north slope may attribute to that less solar energy is absorbed in summer.

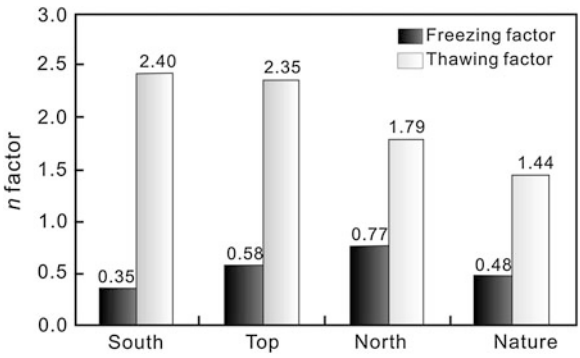

Fig. 3 Temperature factors n at the depth of 0.5 m in embankment and the nature ground

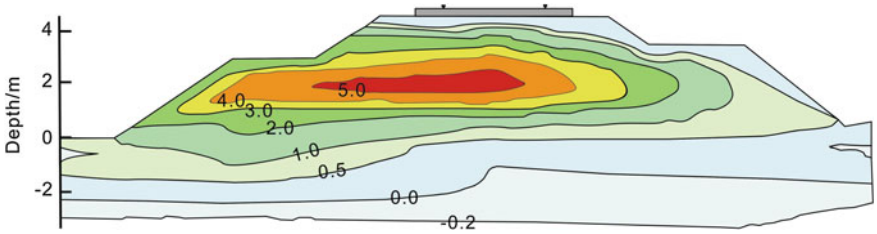

Fig. 4 The temperature field of the monitoring profile in Oct. 19, 2002 (The unit Centigrade)

4 An Asymmetric Thermal Field in the Embankment

The ground temperatures monitored above are all on the depth of 0.5 m under the surface of the embankment, which may reflects the inhomogeneous temperature field underground. When effect of the solar energy absorbed by the ground surface get to the permafrost under embankment, it would lead to thaw the permafrost and consequently possible induce an uneven settlement of the railway foundation.

To investigate the temperature field in the whole embankment, a row of drilling holes were conducted on the monitoring profile on Oct.19, 2002 to measuring the temperature on different depth. The results were drawn in isotherms as shown in Fig. 4. Of which, the 0 °C isotherm is considered as the upper boundary of the frozen soil (permafrost). It shows that the temperature field in the embankment is remarkable asymmetry. The temperature on the south side is higher than that on the north side; meanwhile, the upper boundary of the permafrost on the south side is about 0.5 m shallower than that on the north side.

From the monitoring results, it is clear that construction of the railway has changed the temperature field underneath. The asymmetry of temperature field in the soil beds underlying is not very obvious at present. Therefore, the tendency will be worse. When the thawing depth moves down to the upper boundary of the permafrost, the induced uneven deformation of the embankment would threat the safety of the running train, so it has to be pay more attention all the time.

5 Conclusions

The monitoring results show that the annual ranges of ground temperatures in the embankment are all higher than that on the nature ground, which reflects that construction of the railway changes the condition of solar energy adsorption and makes the ground temperature fluctuate more violent.

The mean annual ground temperature on the south slope has over 3 °C higher than that on the north slope and an inhomogeneous temperature field has been produced in the railway embankment because the south slope of the embankment can receive more and release less radiation in winter. The asymmetry of the

temperature field in the embankment and the foundation may lead to uneven settlement of embankment and become a potential threat to the railway safety. Because the temperature changes slowly, even the problem does not reveal in a short period, however, for the longtime being, it has to be paid attention.

References

Instanes A (2003) Climate change and possible impact on Arctic infrastructure. In: Proceedings of the 8th International Conference on Permafrost, Zurich, Switzerland, vol 1, pp 461–466

Karunaratne KC, Burn CR (2003) Freezing n-factors in discontinuous permafrost terrain, Takhini River, Yokon-Territory, Canada. In: Proceedings of the 8th International Conference on Permafrost, vol 1, pp 519–524

Riseborough DW (2003) Thawing and freezing indices in the active layer. In: Proceedings of the 8th International Conference on Permafrost, vol 2, pp 953–958

Geochemistry of Plant-Soil-Permafrost System on Landslide-Affected Slopes, Yamal, Russia as an Indicator of Landslide Age

Nataliya Ukraintseva, Marina Leibman, Irina Streletskaya and Tatiana Mikhaylova

Abstract Cryogenic landslides on saline marine sediments are widely distributed in Typical tundra bioclimatic subzone of the Yamal Peninsula. Interrelation between the height and productivity of the willow tundra, and activation of cryogenic processes are discussed. It is supposed that high willow canopies are the indicators of ancient landslide activities and may serve as fundamental guide for mapping of landslides in the region. Various procedures are proposed to evaluate the relative age of the landslides. They include, study of the succession of vegetation cover, ash content in each vegetation group, groundwater and sediment chemistry on the landslide-affected slopes. It is shown that the landslide process causes desalinization of marine sediments and enriches the active layer with salts. This is an important peculiarity of cryogenic landslides in the region with saline permafrost distribution.

Keywords Cryogenic landslides · Age assessment · Soil and plant geochemistry · Willow shrubs

1 Introduction

Cryogenic landslides are widespread on the Yamal and Gydan Peninsulas, on the Taimyr coast of Yenisei Gulf (from Dixon to Cape Shaitansky), as well as on the islands of the Canadian arctic archipelago (Geertsema and Pojar 2007; Romanenko 1993; Harry and Dallimore 1989; Lewkowicz 1990; Matsuda et al. 1988 etc.).

N. Ukraintseva (✉) · M. Leibman · T. Mikhaylova
Earth Cryosphere Institute SB RAS, Malygina Road 86, Tyumen 625026, Russia
e-mail: ukraintseva@mail.ru

I. Streletskaya
Geographical Department of Moscow State University, Moscow 119991, Russia

W. Shan et al. (eds.), *Landslides in Cold Regions in the Context of Climate Change*, Environmental Science and Engineering, DOI: 10.1007/978-3-319-00867-7_9,

Landslides of permafrost zone (active-layer detachment slides after French 1976; Lewkowicz 1990 etc.) are known to move over an active layer base. The permafrost table serves as a landslide shear surface. Landslides are widely distributed in Typical tundra bioclimatic subzone of the Yamal Peninsula, in the northern part of west Siberian Lowlands. They actively change the primary surface of ancient marine plains and terraces. Landslide activation took place in the late 80s, while the main event occurred in 1989 (Leibman 1995; Poznanin 2001; Leibman and Egorov 1996 etc.).

Specific features of the Yamal landslides are connected with permafrost deposits underlying active layer, which have marine origin and due to the influence of the relatively cold climate (no thaw in the Holocene optimum) preserved their high soluble-salt concentration (Dubikov et al. 1996; Brushkov 1998, 2007). Exposure of the frozen saline marine sediments due to landslide disturbance leads to desalinization of these sediments and enrichment of the active layer with ions. In addition to mechanical dislocation of the active-layer deposits by landslides, lateral redistribution of elements within the active layer is observed (Harry and Dallimore 1989; Matsuda et al. 1988; Dubikov 2002; Lewkowicz 1990; Leibman 1995; Leibman and Streletskaya 1997; Ukraintseva 1997, 2008; Ukraintseva et al. 2000, 2003; Streletsky et al. 2003).

Since the 1980s, new knowledge has been obtained in connection with cryogenic landslides of the Yamal peninsula. It was noted that abnormally high willows of up to 1–1.5 m tall, characterize landslide-affected areas in Typical tundra bioclimatic subzone of the west Siberian Lowland. The area of high-willow tundra coincides with the limits of distribution of saline marine deposits near the surface. In the southern tundra subzone, south of these limits where permafrost degraded in the Holocene optimum and temporarily thawed saline deposits were washed out and desalinized (Dubikov et al. 1996), willows were replaced by low dwarf birch/moss communities on the stabilized landslide slopes (Ukraintseva 1997, 2011).

Cryogenic landslides are cyclic in time—various parts of the landslide-affected slopes are periodically involved in movements after a certain period of recovery (Leibman and Streletskaya 1997; Leibman et al. 2003, 2012). As a result of this process, landforms consist of stable surfaces and landslide-affected slopes of various age comprising different landforms: A—hilltops and convex stable slopes not affected by landslides; B—concave shear surfaces of landslides, C—convex hummocky landslide bodies; D—depressions (lake and stream valleys) which serve as local base level. The landslide age, defined by direct observation, analysis of multi-temporal images, and radiocarbon dating of buried organic matter, varies from less than 100 to more than 2000 years (Leibman et al. 2003). Three age generations of landslides were subdivided for this study: 1, young, occurred between 1989 and 1991, directly observed, 2—old (under 300 years old, detected using air-borne data), and 3—ancient (300 to more than 2000 years) (Ukraintseva et al. 2003; Ukraintseva 2008; Leibman et al. 2003, 2012). Method of landscape indication was applied to initially assess relative ages of landslides (young, old and ancient) in each landscape.

Cycles of landslide activation are important to understand in terms of climate change and active development of the Tundra zone. Technogenic disturbances in turn, cause the activation of landslide process (Leibman and Streletskaya 1997). Thus, the study of landscape-geochemical indicators of the landslide-affected surfaces and their relative age is an important and timely task. This paper presents: (1) the vegetation recovery stages on the landslide-affected slopes, (2) assessment of the high willow shrubs appearance in the key area, (3) spatial redistribution of the water-soluble salts in the active layer deposits and groundwater within different landforms, (4) chemical composition of plants and surface deposits.

This research is based on data obtained from the central Yamal field since 1988.

2 Study Area and Methods

The research area is located in the Typical tundra bioclimatic subzone of the Central Yamal peninsula, in the vicinity of Bovanenkovsky gas field and the research station (Vaskiny Dachi), bordered by rivers Mordy-Yakha in the west and Se-Yakha the north. Central Yamal Peninsula (Fig. 1) is comprised of a highly dissected plain in the Typical tundra bioclimatic subzone (bioclimatic subzone D, after Walker et al. 2009, 2012), with continuous permafrost, rather thick (0.8–1.2 m) active layer in sandy and clayey deposits, often saline due to marine origin. In the area of the Bovanenkovsky gas field, landscapes of the Upper Pleistocene marine plain, terraces and flood-plain of Naduj-Yakha, Se-Yakha and Mordy-Yakha rivers were observed. Typical tundra moss-lichen-grass-undershrub

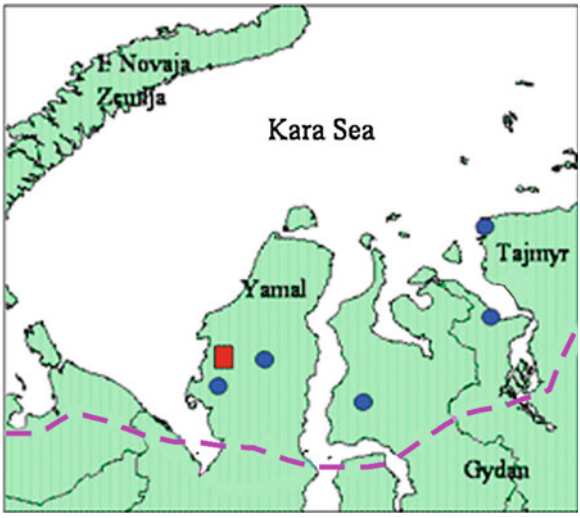

Fig. 1 Location map. Research polygon "Vaskiny Dachi" is marked by a *red square*. *Blue circles* mark sites of landslide observations. *Dashed red line* is the southern limit of the frozen saline marine deposits (after Dubikov 2002)

Table 1 Sampling scope for chemical analyses in active-layer deposits, ground water and vegetation canopy at Vaskiny Dachi Research polygon

Chemical analyses	Number of samples		
	Active layer deposits and soils	Ground water	Vegetation
Semi-quantitative spectral analysis	235	–	240
X-ray fluorescent analysis	110	_	128
Conventional ion analysis of water-soluble salts	228	67	_

vegetation here is complicated by vast areas of high willow shrubs, not found elsewhere at the same latitude and bioclimatic subzone.

The complex field study covered active-layer, upper permafrost and organic covers. Sampled were vegetation, active-layer and permafrost deposits, and groundwater at selected 80 points of the 10 cross-sections along the landslide-affected slopes. Detailed leveling of the relief, thaw depth measurements, soils profile description, as well as species composition and coverage of vegetation canopy were carried out along cross-sections. Aboveground total phytomass was collected at various layers: shrubs from a site 3 × 3 m, herb and moss layers from a site 0.5 × 0.5 m. Weight of the samples in air-dry state was expressed in g/m^2. Geochemical features were studied along 10 transects of total length of 6 km. The data are grouped according to landslide element and age. Separately presented are various media: groundwater, active-layer deposits, and upper permafrost.

The technique of laboratory analysis of samples has been described earlier (Ukraintseva et al. 2003). The main ionic concentrations of the groundwater and water extraction out of the sediments were determined by standard chemical methods at the Dokuchaev Soil Institute in Moscow (analysts RV Grishina and NS Nikitina). Accuracy of laboratory analysis did not exceed 5 %. Semi-quantitative spectral analysis of homogenized sediments and ashes of plants were carried out. Large number of samples (Table 1) allows to make an assessment of average concentration of trace elements. Chemical analyses of air-dried and homogenized plants and sediments were carried out using X-ray flourescence spectrometer ORTEC-TEFA (analysts SE Sorokin and AT Savichev, Dokuchaev Soil Institute, Moscow).

3 Results and Discussion

Authors assume that high willow canopies are indicators of ancient landslide activities. Various procedures are proposed to evaluate the relative ages of the landslides. Suggested are various methods of estimating the relative ages of cryogenic landslides:

- Study of stages of vegetation recovery on revegetating shear surfaces of landslides;
- Measurement of aboveground phytomass and its structure on landforms of different ages;
- Determination of grain-size composition of the active-layer deposits for different landforms;
- Analysis of soluble-salt concentration in groundwater and water extraction from active-layer deposits;
- Analysis of trace-element concentrations in the active-layer deposits and plants;
- Ash content in plants in each vegetation layer: shrub, grass, and moss;
- Study of Nenets toponyms distribution on the large to medium scale topographic maps.

3.1 Vegetation Recovery Stages on the Landslide-Affected Slopes

Anomaly of high willow distribution on the Yamal Peninsula and other areas of the arctic plains has been documented by past researchers (Danilov 1958; Andreev 1970; Bazilevich 1993; McKendrick 1987; Sturm et al. 2001; Pospelova and Pospelov 2000; Warren Wilson 1957 etc.). However, authors did not link them to geochemical features of the active layer caused by landslide activities. Willow shrubs were associated with climate change, warming and "greening", or an early stage of serial changes in vegetation, which colonize bare surfaces formed due to natural and/or anthropogenic processes (Walker 1987; Walker et al. 2011, 2012; Forbs et al. 2010; Pajunen 2009; Epstein et al. 2009; Jumponen et al. 1998; Sturm et al. 2001; Bret-Harte et al. 2008). Numerous studies concentrated on geochemistry of the tundra shrub (Manakov 1968; Meltser and Moskovchenko 1997; Tentyukov 1998 etc.) with no mention of slope processes as controls. The predominance of high willow shrubs (*Salix glauca*) on landslide-affected slopes was noticed by Matsuda et al. 1988; Rebristaya et al. 1995; Ukraintseva 1997; Ukraintseva et al. 2000; Ermokhina and Myalo 2012.

Our study shows that the dominating communities on the hilltops and stable slopes (A3) are the undershrub/grass/moss and moss/lichen tundra (Table 2). These are the background communities for Typical tundra bioclimatic subzone. After 10–15 years since the landslide event, the *first stage* is considered when bare patches alternate with pioneer herbages, such as *Puccinellia sibirica, Poa alpigena subsp. alpigena, Deshampsia sp., Phippsia concinna, Tripleurospermum Hookerii* etc., on young surfaces (B1, Table 2, Fig. 2a). The second stage comprises of colonization by meadow sedge/grass communities (*Calamagrostis sp., Poa alpigena subsp. colpodea, Carex concolor, Nardosmia frigida, Equisetum arvense subsp. boreale, Polemonium acutiflorum, Ranunculus borealis* etc.) with active willow restoration, as observed on old shear surfaces (B2, see Table 2, Fig. 2b).

Table 2 Vegetation as an indicator of morphological elements and relative age of landslides

Morphological elements of the landslide-affected slopes	A3	B1	C1	B2	C2	B3	C3
Height above sea level, m	47–52.7	33–49.5	26–48	26–47	24–42	27–39	24–36
Slope gradient, degree	0	5–10	1–8	3–8	3–5	3–5	2–7
Shrub coverage, %	5–20	0	50–70	10–40	50–70	20–50	80–90
Shrub height, cm	15–30	0	50–80	30–50	100–130	100–150	150–170
Salix glauca coverage	1*	–	3	2	3	2	3
Betula nana coverage	3		3		1		
Undershrub-Herbs coverage, %	60–70	15–70	40–60	50–80	50–60	85	50–70
Poa arctica	1	1					
Vaccinium vitis-idaea subsp. minus	3						
Carex arctisibirica	2						
Calamagrostis groenlandica	1						
Rubus chamaemorus	1						
Puccinellia sibirica		3					
Tripleurospermum Hookerii		1–2					
Deshampsia sp.		1					
Phippsia concinna		1–3					
Alopecurus prateum		1					
Calamagrostis sp.		1		2	3		1
Festuca rubra subsp. arctica		1	1	2	1		
Poa alpigena subsp. alpigena		3	1	2		2	
Calamagrostis Holmii		1	3	2		2	
Equisetum arvense subsp. boreale			3	2	2–3	1–2	2–3
Polemonium acutiflorum			1–2	1–2	2	2	1–2
Ranunculus borealis			1–2	1	1	1	1
Nardosmia frigida	1		2	1	1–2		1
Carex concolor	1		1–2	2	1–2	3	1–2
Polygonum viviparum				1	1	1	
Poa alpigena subsp. colpodea				2	1–3	3	1
Parnassia palustris		1		3	1		
Moss coverage, %	90–100	0	40–70	30–80	70–80	50–80	50–100
Lichen coverage, %	5–10	0	3–5	0	0	0	0
Drepanocladus uncinnatus	1		1–3	3	3	3	3
Mnium sp.			2	1–3	3	3	3
Hylocomium splendens	1		1–3	1	1	1–2	3
Ptilidium siliare	1	1		1	1	1–2	
Aulacomnium turgidum	1		3		1		3
Dicranum elongatum	3		2	2			
Polytrichum juniperinum	3		1–3				
Cetraria cucullata	2		2				
Cladonia rangiferina	3						
Cladonia sp.	1						

*Abundance of species according to Braun-Blanquet system: 1—few, 2—moderate, 3—plenty (Rabotnov 1978)

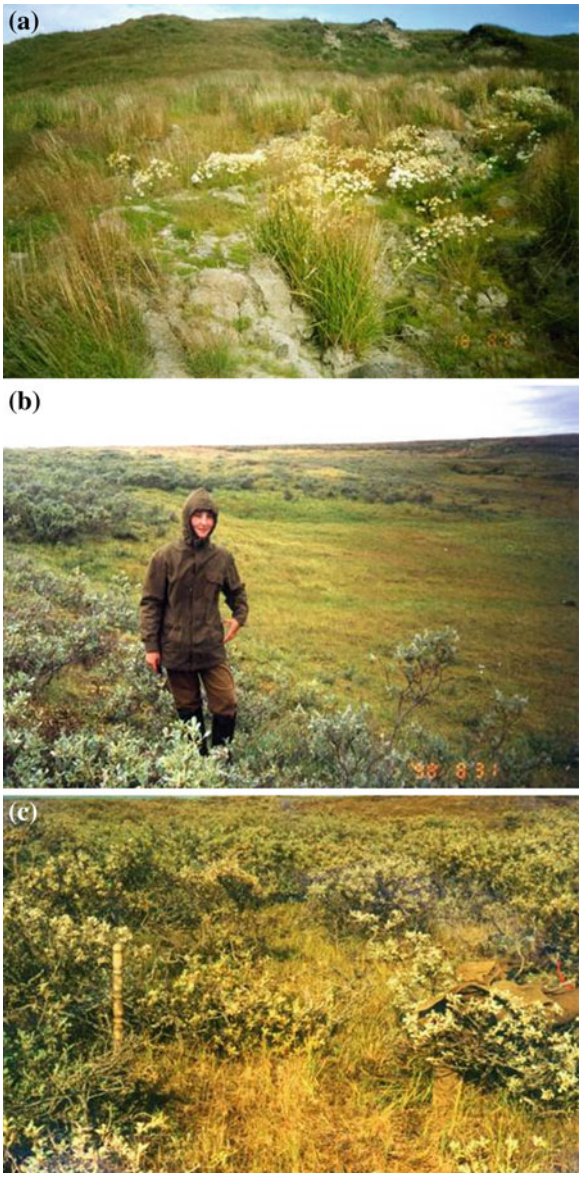

Fig. 2 Landslide shear surfaces of various age: **a** young, **b** old, **c** ancient

The third, final stage comprises of colonization by the high willow/meadow communities (B3—Fig. 2c).

The young landslide bodies (C1—Fig. 3a) are dominated by low shrubs (willow, dwarf-birch), with gradual loss of the moss cover and slow revegetation of *Calamagrostis sp., Poa alpigena subsp. alpigena, Equisetum arvense subsp. boreale, Polemonium acutiflorum, Ranunculus borealis* and cotton-grass. On the

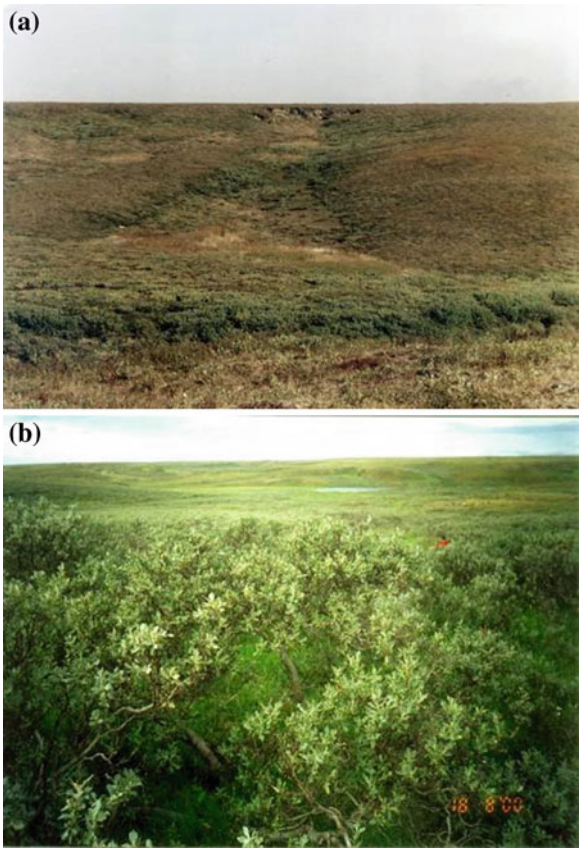

Fig. 3 Landslide bodies of various age: **a** young, **b** ancient

older bodies (C2), high willow/meadow communities with mosses replace C1-type. Dense willow canopy covering moss/herbaceous communities dominate on ancient landslide bodies (C3—Fig. 3b).

According to the structure of the phytomass, landslide-affected slopes differ distinctly from background surfaces (A3). On A3, moss coverage is 100 %, and willows cover less than 10–15 % of the area. On the landslide-affected slopes, the willow quota increased up to 50–80 %, and less than 40–80 % is covered by mosses (Uraintseva and Leibman 2000; Ukraintseva 2011). The total aboveground phytomass on ancient landslides (B3, C3) on average is about 1,600 g/m^2 compared to 850-1200 g/m^2 of A3 (Fig. 4). The values on stable surfaces are within the range obtained from the Yamal transect by the LCLUC-Yamal project: between 440 and 1100 g/m^2 for hilltops of this region (Epstein et al. 2009). One can see substantial difference between phytomass on hilltops and phytomass on landslide slopes in our study.

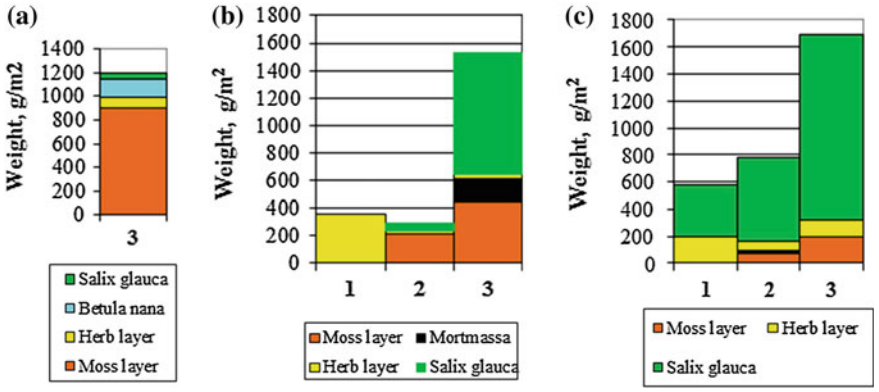

Fig. 4 Total aboveground phytomass of vegetation cover at 'background' surfaces (**a**) and young (1), old (2) and ancient (3) landslide-affected slopes: shear surfaces (**b**) and landslide bodies (**c**), mean values

3.2 Grain Size Composition

The grain-size composition in the active-layer on A3 (the oldest surface) appeared to be rather uniform. The silt fraction, composed mainly of coarse silt particles, makes up to 40–60 % of the samples (Fig. 5). The proportion of the fine and small-grain sand fraction is slightly less and reaches 30–50 %. The clay fraction does not exceed 10 %. Grain size distribution within the active-layer section is rather even and the upper horizons are close in grain size composition to the lower ones contacting permafrost (Ukraintseva and Leibman 2007).

The young landslide shear surfaces are however completely different in grain size composition and are characterized by the domination of clay particles (40–60 %) and high lateral differentiation between the shear surfaces (B1) that are more clayey as compared to the relatively silty landslide bodies (C1) (Fig. 5).

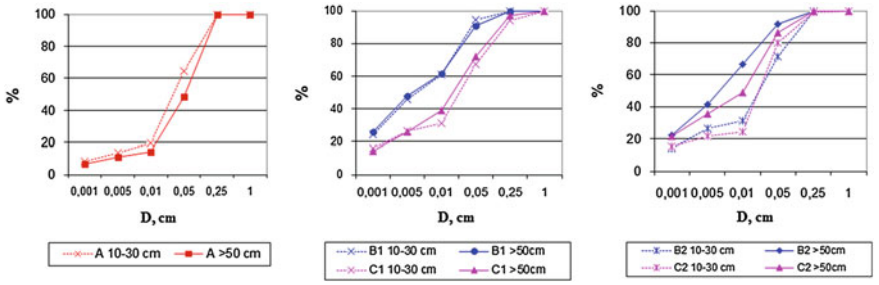

Fig. 5 Generalized grain-size composition at the landslide affected *slopes*: *D* a particle diameter; *A* an undisturbed surface; *B*1 a shear surface and *C*1 a landslide body, both at a young landslides; *B*2 the shear surface and *C*2 the landslide body, both at an old landslides. *Dotted line* is for the upper 20-cm *horizon*, and *solid line* outlines the *horizon* below 50 cm

Maximum heterogeneity in grain size composition both laterally and vertically is found on the ancient slopes that underwent repeated landsliding resulting in superposition and mixing of clay (shear surface) and sand (landslide body) units (Fig. 5).

3.3 Chemical Composition of Groundwater and Water Extracted from the Active-Layer Deposits

Analyzed are water-soluble salts (ions) in the active-layer deposits. Average values are presented in Tables 3 and 4.

Water-soluble salts are more mobile and move both in the vertical and lateral directions. These salts are also most approachable for plants, forming growing substrate for plant roots. Table 3 shows three main parameters that characterize the hydrology of the active layer. These parameters are: concentration of water-soluble salts (% in solution), concentration of Cl-ion in the solution (10^{-3} %), and "marine index" equal to the proportion of cations Na+K/Ca+Mg (after Dubikov 2002). Cl-ion and "marine index" are indicators of marine origin of deposits.

As seen in Table 3, young shear surfaces (B1), are characterized by maximum values of all the parameters which are 5–10 times higher than the respective parameters on the stable surfaces (A3). The same trends are observed on the landslide bodies: maximum values are on young landslide bodies (B1) reducing in the sequence old (B2) > ancient (B3) landslide bodies. At the same time, parameters on the landslide bodies are only slightly higher compared to the stable surfaces and substantially lower than the shear surfaces of the same age (Table 3).

The young landslides are much more saline compared to the background surfaces, because the landslides remove washed out active-layer deposits and expose saline marine permafrost. On the young shear surfaces, salinity and marine index values are 5–8 times higher when compared to stable slopes and hilltops, and Cl-ion concentration is 25 times higher (Table 3). Salinity and Cl-ion concentration are gradually reduced from old to ancient landslides, but remain higher than

Table 3 Geochemistry of the active-layer deposits at the landslide-affected slopes

Element of slope	Number of samples	Salinity (D_{sal}), %		Cl, 10^{-3} %		(Na + K)/(Ca + Mg)	
		Mean	StDev	Mean	StDev	Mean	StDev
A3	45	0.039	0.065	3.23	3.84	0.61	1.10
B1	41	0.242	0.196	84.22	75.1	5.52	4.62
B2	21	0.118	0.121	48.48	68.5	1.17	0.99
B3	23	0.070	0.093	33.27	29	0.89	0.88
C1	22	0.046	0.053	8.43	12.8	1.27	1.47
C2	24	0.039	0.034	8.87	7.57	1.11	1.08
C3	48	0.034	0.044	3.8	5.1	0.98	1.15

Table 4 Geochemistry of the ground water at the landslide-affected slopes

Element of slope	Number of samples	Salinity (Dsal), %		Cl, 10^{-2} %		pH	
		Mean	StDev	Mean	StDev	Mean	StDev
A3	10	0.09	0.07	1.40	1.09	6.95	0.88
B1	9	3.54	4.56	127.05	187.09	8.58	0.21
B2	8	2.52	2.41	151.30	151.52	7.99	0.88
B3	10	0.71	1.45	30.60	63.89	7.67	0.76
C1	7	1.15	2.02	36.42	68.50	7.41	0.34
C2	12	0.45	0.42	10.41	12.71	8.26	0.94
C3	11	0.15	0.18	8.38	16.87	7.52	0.84

background parameters. On ancient shear surfaces, salinity of soil and sediment is only 0.07 % (Table 3).

High values of the "marine index" and Cl-ion in water extractions of the young shear surfaces (B1) prove marine origin of landslide slope deposits.

Groundwater of the landslide slopes is highly heterogeneous in both ionic structure and concentration (Table 4). A3 are characterized by low concentration of water-soluble salts (0.05–0.1 g/l, averaging 0.09 g/l) and dominated by Ca^{2+}, Mg^{2+} and $SO_4{}^{2-}$. Shear surface desalinization starts after permafrost deposits of marine origin gets involved in seasonal thaw. First most mobile Cl^- and Na^+ move into the groundwater. Their high concentration indicates recent landslide event.

Ionic concentration on the young shear surfaces on average exceeds 3 g/l (reaching maximum of 10 g/l and even more, being 100 times higher than the background salinity), and abruptly reduces to about 0.7 g/l on the ancient shear surfaces. Ionic concentration within ancient shear surfaces is heterogeneous ranging between 0.3 and 0.5 g/l, and 4–5 g/l. This indicates that the area of salt accumulation and salt washout exists simultaneously in groundwater on ancient landslides depending on surface topography. Ionic structure changes from Cl-$HCO_3{}^-$ to $HCO_3{}^-$. Na^+ domination is replaced by Ca^{2+} and Mg^{2+} ions.

3.4 Gross Concentration of Trace Elements in Active-Layer Deposits

According to semi-quantitative spectral analyses of 40 chemical elements on 235 samples in the study area, most common are: strontium, barium, titanium, manganese, chromium, vanadium, nickel, cobalt, copper, silver, zinc, lead, molybdenum, phosphorus, and boron. These elements are found in all collected samples; their relative abundance varies markedly over the landforms. Age differences are visible on the shear surfaces of the landslides. The bodies of the landslides in their trace-element composition are similar to the hilltops and stable slopes (A3); their geochemical evolution in time depends on location on the slope which controls inflow of matter in the respective locations.

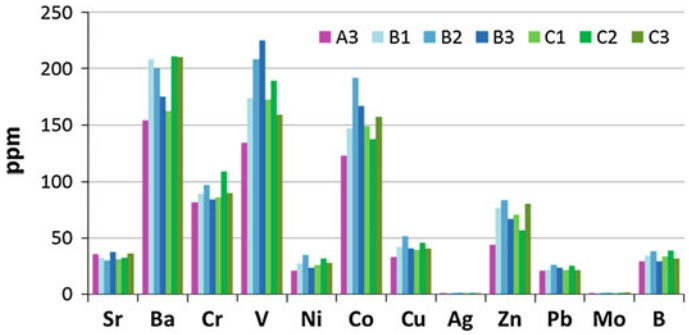

Fig. 6 Trace elements in the active layer deposits (average values for different landforms on landslide-affected *slopes*)

Four elements which are most significant are: barium, vanadium, cobalt and zinc (Fig. 6). Their concentrations on landslide slopes are 1.2–1.5 times higher than values obtained from stable surfaces. Barium concentration is the highest on the young landslide shear surfaces (B1) and gradually decreased towards the old (B2) and ancient (B3) shear surfaces. Vanadium, however, increased significantly from B1 to B3. The maximum concentration of cobalt and zinc, as well as chromium, nickel, copper and boron are typical for B2, while both B1 and B3 show lower concentrations. Obviously, these differences are related to the mobility of elements. Most mobile in active-layer deposits is barium, which is being gradually washed out of marine sediments. Vanadium is the most inert; its relative abundance increases with time due to reduction in the proportion of more mobile elements. The remaining trace elements are intermediate in abundance, in the beginning their percentage proportion increases, and then, on the old shear surfaces, where element migration is reduced and may even be the inflow of matter, their share gets significantly reduced.

On geochemical spectra (Fig. 7), Clark concentration (CC) of key trace elements in the active layer deposits is shown. Comparison of geochemical spectra for stable landforms and for landslide slopes of various age shows that concentration of most trace elements is close to Clark values in sedimentary rocks (Voitkevich et al. 1990).

In stable areas, active layer deposits are depleted of strontium, barium, nickel, zinc and molybdenum (CC = 0,01 ÷ 0,4). Phosphorus and boron concentration slightly exceeds their Clark in sedimentary rocks.

On the shear surfaces and landslide bodies, concentration of vanadium, cobalt, copper, zinc, nickel, boron increased over background stable slopes (Fig. 7), and approached Clark of sedimentary rocks.

Thus, increase in the concentrations of some trace elements on the shear surfaces of landslides is induced by the chemical composition of the original marine substrate. In stable areas concentration of trace elements decreased with time

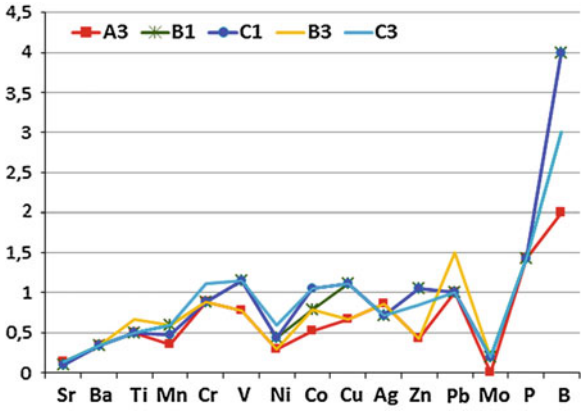

Fig. 7 Clark concentration (CC) of key microelements in the active layer deposits (geochemical spectra)

through numerous cycles of freeze–thaw (frost weathering) and groundwater action in the warm seasons.

3.5 Gross Concentration of Trace Elements in Plants

The concentration of trace elements varies not only by groups of plants, but also by landforms on landslide slopes, as well as by landslide age. Most trace elements (except strontium, zinc, and boron), are most actively accumulated in mosses (Fig. 8). Moss layer forms the base of plant communities in typical tundra subzone and dominates on the watersheds, covering more than 60 % of the phytomass (Fig. 4, Table 2). However, the landslide completely disturbs moss cover on the shear surface and it withers and degrades on landslide bodies. Saline ground water with pH of 7–8.5 prevents remediation of moss, which prefers acidic media with pH of 5.5–6. Only on old landslides new moss cover appears, which thickness does not exceed 0,5–1 cm, moss cushion often is absent (Table 2). The chemical composition of mosses shows uncomfortable conditions for their growth on landslide slopes (Fig. 8).

Despite the richness of trace element composition in the active layer deposits of the landslide shear surfaces, the oppressed mosses accumulate trace elements in much smaller concentrations. For most trace elements: Ni, Co, Cu, Zn, Pb, Mo, maximum concentrations are characteristic of watershed stable surfaces and only sometimes of the ancient landslides.

In the willow branches concentration of trace elements is most sustained in space on the slopes of the same age. This once again proves that the willow serves as a clear *aedificator* of plant communities occupying most comfortable ecological niches on landslide slopes. Willows, though having less total concentration of trace elements compared to mosses, show high concentration of zinc, strontium and boron (Fig. 9). Strontium (which can replace calcium) helps build a large willow

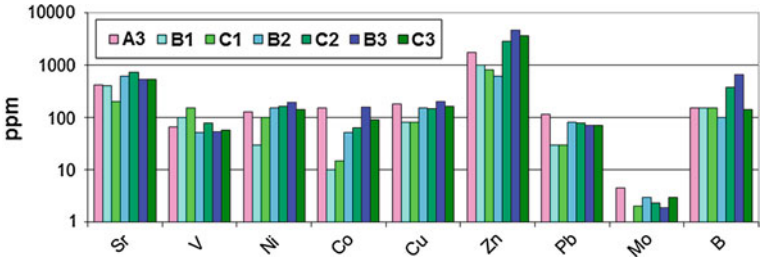

Fig. 8 Average trace-element concentration in mosses

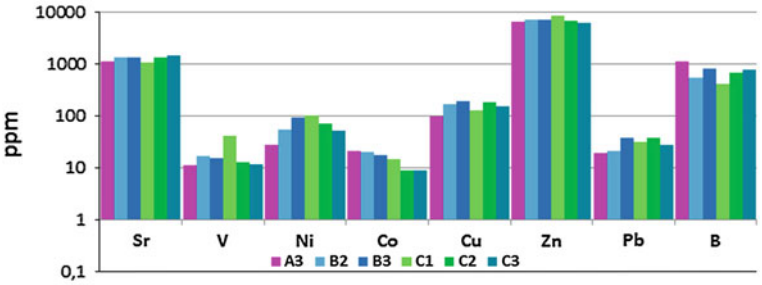

Fig. 9 Average trace-element concentration in willow leaves

"skeleton": the trunk and branches; zinc increases frost-resistance of willows, allowing it to create stable groups in the typical tundra subzone (Rebristaya et al. 1995; Ukraintseva 1997; Meltzer and Moskovchenko 1997; Tentyukov 1998).

Of greatest interest to recognize landsliding is copper and nickel concentration in the branches of *Salix glauca*. It significantly increases on landslide slopes (B1-3 and C1-3) compared to the background (A3). In addition, the nickel concentration on the shear surfaces is higher than on landslide bodies of the same age.

Trace elements and ash content in the willows vary depending on the shrub location on landslide shear surfaces and landslide bodies. Concentration of some elements decreases and of others increases with time in the direction from younger to older surfaces (Table 5). Ash content successively decrease from younger to older surfaces, and is much higher on landslide slopes compared to background surfaces, especially in grasses and willow leaves (Fig. 10). This allows using trace-element concentration and ash content as indicators of landslide's relative age.

Concentration of all trace elements in the willow leaves is significantly lower than in the branches (Ukraintseva and Leibman 2000). This can be explained by the method of semi-quantitative spectral analysis. Trace elements were determined in the plant ash in relation to ash content. Due to the high ash content in the leaves (5–8 %), in contrast to the branches and trunks, where the ash content does not exceed 1.5–2.5 % (see Fig. 10), total concentration of trace elements in the leaves is maximum.

Table 5 Trace elements in willow branches as the indicators of landslide age

Type of slopes	Trace elements
B+*	V, Co, Cr, Ni, Sr, Cu**
B−	Ba, Zn, (B)
C+	Ba, Sr, Co, Zn
C−	V(B)

+ concentration of trace elements increases with age, – concentration of trace elements decreases with age; ** informative ability decreases from left to right, poor-informative elements are parenthesized

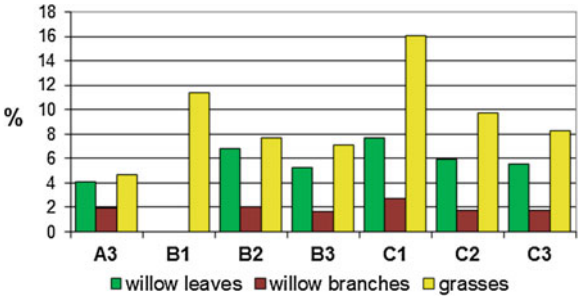

Fig. 10 Average ash content in plants

X-ray fluorescence quantitative analysis was used to determine trace element concentration in the air-dried plants. This test shows that trace element concentration in the leaves is higher than in other parts of the willow (Fig. 11).

The use of X-ray fluorescence analysis allowed the determination of not only the trace elements, but also macroelements in the willow leaves (Fig. 12). The characteristic trend observed is significant increase in calcium, magnesium and chloride concentrations on landslide slopes compared to stable areas. But even in the dwarf willow-herb-shrub-lichen-moss communities on hilltops dwarf willows accumulate much more macroelements than mosses (Fig. 12).

Grasses show noticeably less concentration of most trace elements compared to the willow leaves and branches (Fig. 13). They are sensitive to the particular manifestation of slope processes. After the landslide event, *Gramineae* creates

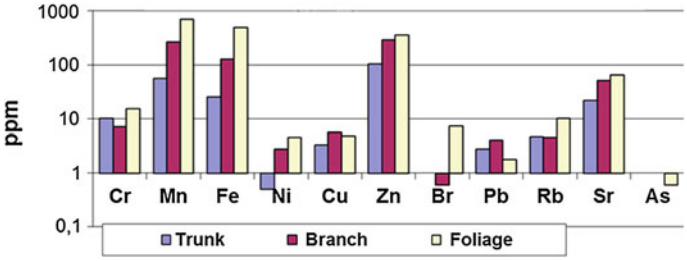

Fig. 11 Average trace-element concentration in various parts of willow shrub

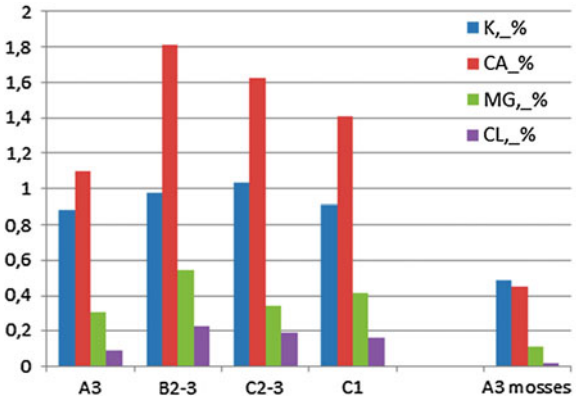

Fig. 12 Macroelements in willow leaves

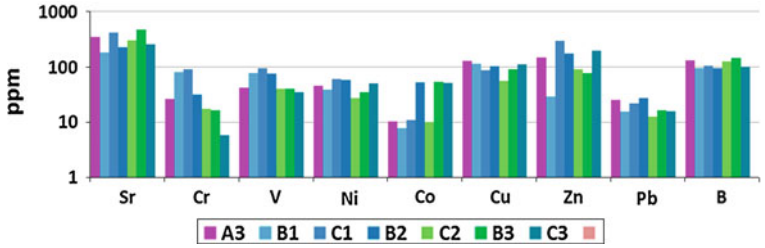

Fig. 13 Average trace-element concentration in grasses

pioneer groups on the exposed shear surfaces, tolerates high salinity of soil water (halophytes are marked among *Gramineae,* Rebristaya et al. 1995). On old landslides, grasses predominate in the understory of willow shrub communities, only on ancient landslides gradually giving way to mosses (Figs. 8, 13, Table 2, Ukraintseva et al. 2000, 2003; Ukraintseva 2011).

3.6 Lateral Changes in Biogeochemical Features of Landslide Slopes

Lateral changes in ionic concentration in groundwater and water extraction from active-layer deposits as well as macro-elements in plants are being studied in a key landslide-affected slope.

Two transects crossing ancient (Transect 1) and young (Transect 2) landslides are presented as an example of downslope distribution of geochemical features. Transect 1 cross a series of landslides of various ages, estimated approximately by

landform expressiveness and degree of revegetation. It starts from the hilltop edge (48.5 m asl) and ends at the base level in the lake depression (21.5 m asl). This transect, 850 m long crosses alternation of concave and convex surfaces of various sizes comprising of shear surfaces and landslide bodies respectively.

In general, ionic concentration is laterally variable with maximum value at the shear surfaces (Fig. 14). Ionic concentration on the hilltop is much lower than values obtained on ancient landslide-affected slope.

Concentration of the main ions in the water extraction from the active-layer deposits at depths of 0.4–0.5 m is highly variable and substantially depends on slope morphology (Fig. 14c). Higher concentrations are noted for Na^+ and Cl^- ions.

Chemical composition of the active-layer ground water within this transect is also heterogeneous. Water samples taken within a period of 2–3 days during the same weather conditions showed concentration within a wide range between 0.05 and 2 g/l. Distribution of ions downslope is shown in Fig. 14d. The highest concentrations (5–30 times higher than that of background values), were observed on concave shear surfaces. Important to note is that the groundwater is of Chloride-Sodium composition similar to that of the substrate. Active-layer groundwater on the ancient shear surfaces show higher concentration of ions compared to landslide bodies of the same age.

In contrast with the deposits and groundwater, ages of the shear surfaces are remarkably evident on the vegetation, with high values of Mg^{2+} and Cl^- ions in the leaves of the willow plants and understory vegetation. Their concentration is much higher on the old landslide (B2-C2) than on the ancient landslide (B3-C3) (Fig. 14a, b).

Transect 2 crosses young landslide starting from stable convex slope (A3) through the shear surface and the landslide body, and ends at the local base level (lake depression). Concentration of water-soluble salts in the active-layer deposits of the shear surface is 10–30 times higher than that obtained from the stable surface (Fig. 15c). In a landslide body, concentration of ions is substantially lower compared to the shear surface, but yet is 2–3 times higher than ionic concentration on stable surfaces. In general, Mg and Cl in willow leaves and grasses show noticeable rise on the young landslide. Cl shows greater contrast when taken in grasses, while Mg is a better indicator of age in willow leaves (Fig. 15a, b).

Additional feature of the transect is deformation of the permafrost table. Various landforms of the landslide-affected slopes control vertical dynamics of the permafrost table.

A3 slopes have stable position of permafrost table (maximum depth on average about 80 cm). The shear surfaces are characterized by the removal of mature sediment and soil (Fig. 14e). Permafrost table follows the newly formed shear surface shape by thawing of upper permafrost (***lowering*** of permafrost table). Landslide bodies override each other in the zone of accumulation, buried layers refreeze, thus, active layer thickness remained the same (observed is relative ***rise*** of permafrost table, Fig. 14e). The thickness of the refrozen deposits may reach 5 m and more (Ukraintseva and Streletskaya 1999).

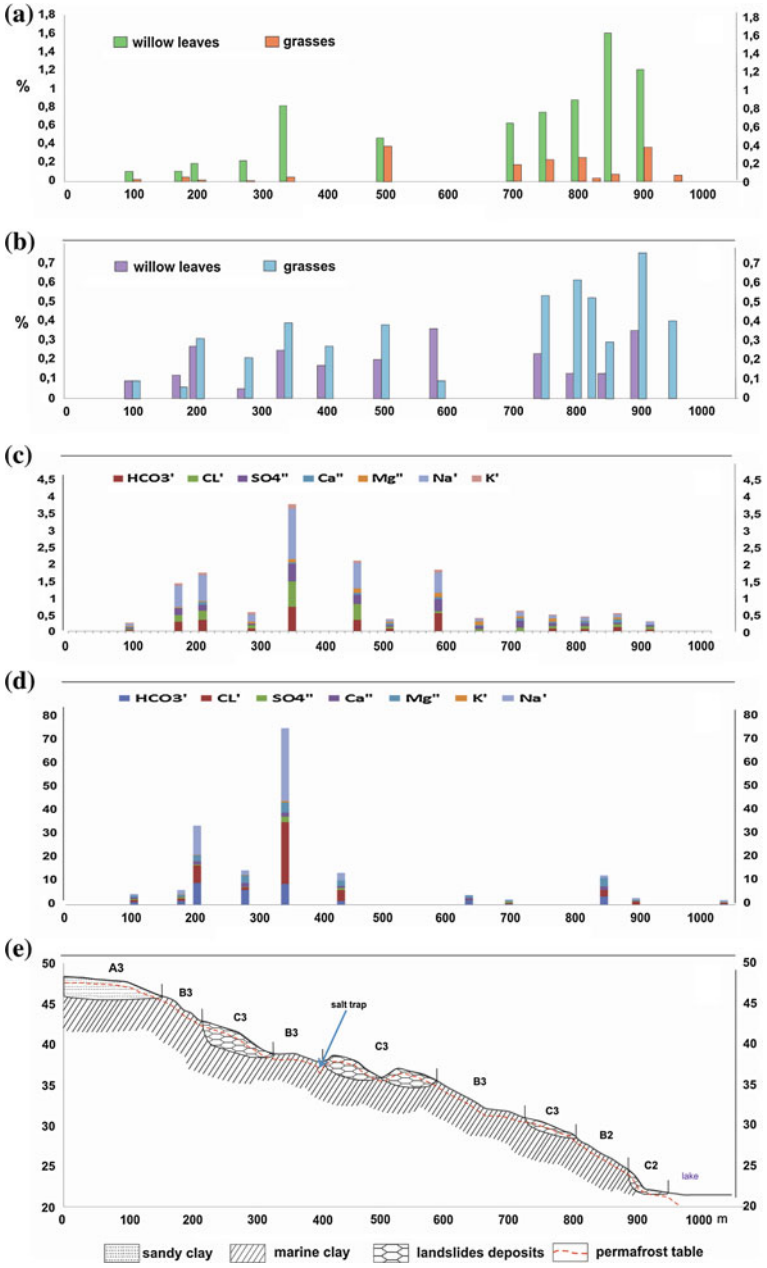

Fig. 14 An ancient landslide slope (Transect 1), lateral variability of: Mg (**a**) and Cl (**b**) concentrations in willow leaves and grasses; water-soluble salt composition in active-layer sediment (**c**) and ground water (**d**). A3 permafrost table, marked by a red square, is stable, B2-3 permafrost table is sinking, C2-3 permafrost table is rising, "salt trap"—highly saline lenses of ground water

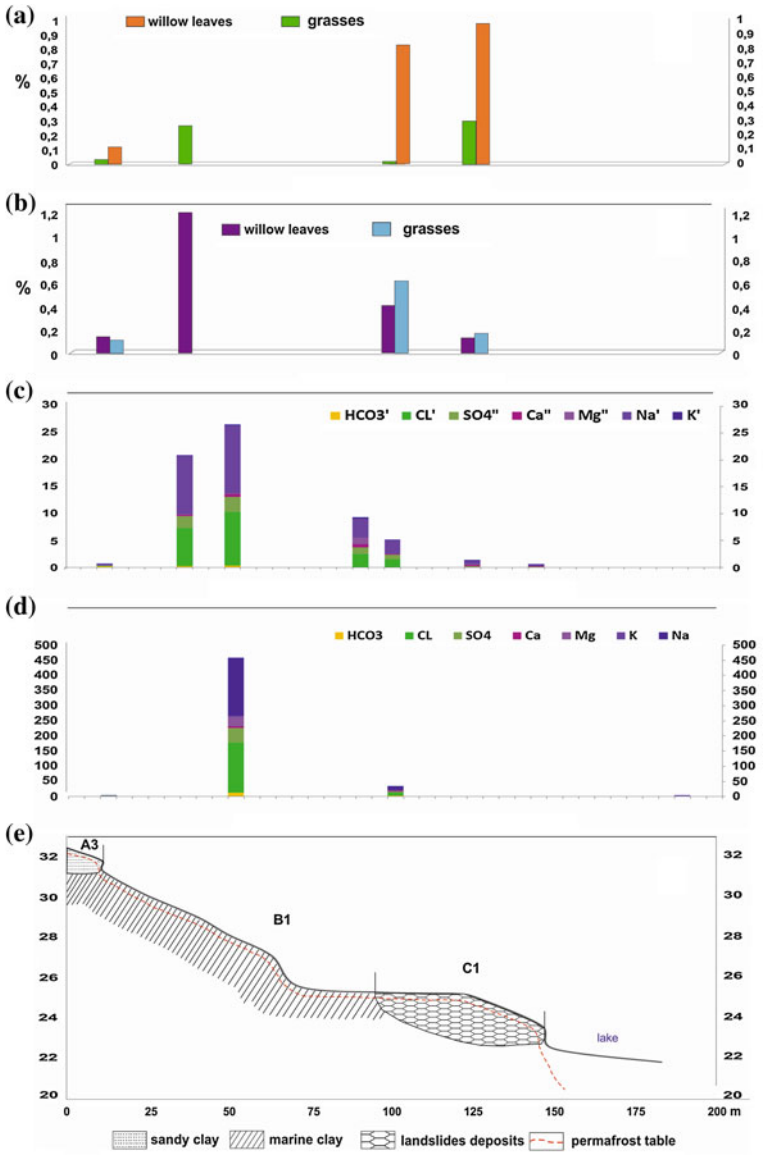

Fig. 15 A young landslide slope (Transect 2), lateral variability of: Mg (**a**) and Cl (**b**) concentrations in willow leaves and grasses; water-soluble salt composition in active-layer sediment (**c**) and ground water (**d**)

Saline ground water accumulates in local depressions of the permafrost table, and formed highly saline lenses of groundwater (salt traps).

Lenses of highly saline groundwater were also found 50–70 km away of the key area at Bolshaya Ledyanaya Gryada (north of confluence of Mordy-Yakha and Se-Yakha rivers), and on the eastern coast of lake Khalev-To (Dubikov 2002). These salt traps are an important feature of cryogenic landslide region with saline permafrost distribution.

The domination of Na^+ and Cl^- ions in chemical composition of the groundwater and superficial sediments, proves marine origin of the native deposits and recent inflow of water-soluble salts in the active-layer deposits, as these ions are very mobile and normally, their concentrations decrease in time (Streletsky et al. 2003). Cl and Mg in plants are indicators of both morphology and age of landslides.

3.7 Willow Tundra in Nenets Toponymics

How long tall willows have been growing in typical tundra subzone? The answer to this question will determine the duration of landslide activation period in the region. We attempted to solve this problem by studying the toponymics of the Nenets using topographic maps of medium to large scale.

The main toponymic feature of the Nenets people living in the far north, in severe climatic condition, is the deep knowledge and understanding of their environment. To survive in tundra, every Nenets observes seasonal rhythms of the surrounding environment and is able to predict sharp changes in weather by monitoring the behavior of animals or state of the surrounding vegetation.

It has been reported (Ukraintseva 2008) that the Nenets toponymics representing vegetation are strictly linked to the bioclimatic subzones (CAVM Team 2003). Frequently used terms for the arctic tundra are *pyasyada* (bald), *tarts*ya (nude). In typical tundra toponyms *nero, nerka, neruta, neromo* (willow shrub, willow canopy) are very common. *Pae*, *payu* correspond to alder shrubs. The northern limit of these names in the Yamal Peninsula is the Yuribei river. The authors observed the most northern alder shrubs in the Yuribei valley using air surveillance.

Toponymic boundaries in general show outlines of natural subzones only slightly displaced to the north (Fig. 16).

Willows North of Yuribei river willows replace alders, which are linked to the river valleys. Thus willows can be indicators of ancient landslide activity as well as serve as basis for landslide activity mapping (Ukraintseva 2008). Nenets toponyms existed for a long period of time before they appeared on topographic maps. This is an indicator of the existence of high willow shrublands in the Typical tundra bioclimatic subzone for centuries and invariably supports the results of radiocarbon dating of landslide activities which lasted for more than 2000 years (Leibman et al. 2003, 2007).

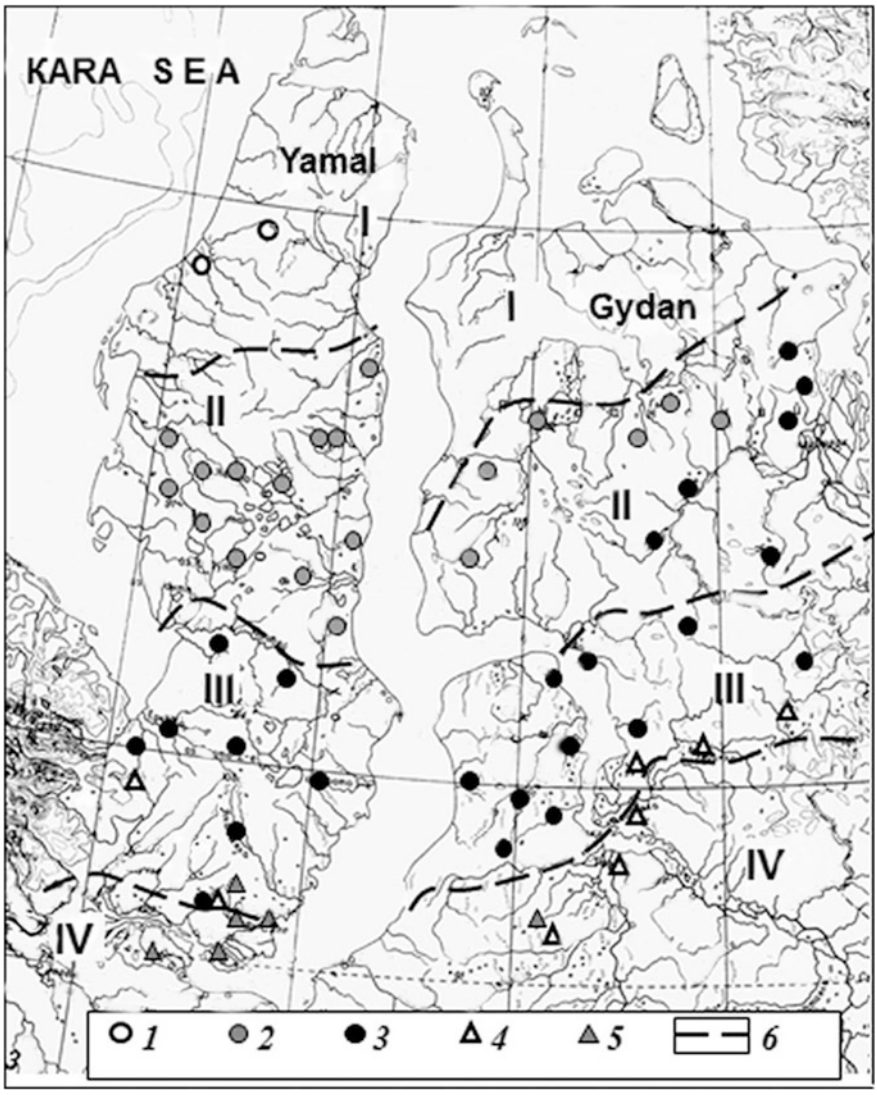

Fig. 16 Nenets toponymics (denominations) on the West-Siberian topographical map: 1 *pyasyada, tartsya (*nude); 2 nero,*nerka, neruta* (willow shrub, willow canopy, *Salix sp.*); 3 *pae, paya* (alder shrub, *Alnus fruticosa*); 4 *kharv* (larch, *Larix sibirica*); 5 *khadita* (fir, *Picea obovata*); 6 limits of subzones. *Zone and subzone: I* arctic tundra; *II* typical (subarctic) tundra; *III* southern (low) tundra; *IV* forest-tundra

4 Conclusions

Various data obtained from field investigation confirms the relationship of height and productivity of willow shrubs with the activation of cryogenic processes in regions with widely distributed saline deposits of marine origin. We observed that azonic high-willow canopy is an indicator of ancient landslide activity, and areas of its distribution can be used as a basis for mapping of landslides on aerial and satellite images.

The landforms of the stable areas and landslide-affected slopes (shear surfaces and landslide bodies) can serve as indicators of permafrost table position, heterogeneity of grain-size distribution and salinity of the surface sediments.

This study offers a variety of methods for estimating the relative ages of landslides, from which the following conclusions were drawn:

Landslide-affected slopes are very different, depending solely on the structure of the phytomass on stable slope surfaces. On landslide slopes, willows cover more than 70 % of the slope while the background is dominated by moss (60–70 %). Bulk phytomass on ancient landslides (an average of about 1,600 g/m^2) is much higher than on stable surfaces (an average of about 850 g/m^2).

The chemical composition of sediments and plants within cryogenic landslides, which develops in saline permafrost, changes dramatically depending on the age of the landslide.

The two most important parameters needed in the estimation of landslide ages are: groundwater salinity and active-layer deposits, as well as ash content of the vegetation. They are significantly different on landslides when compared to background. Trace elements (Zn, B, Co, Sr, Cu, Mn) concentration in the vegetation of landslide slopes is subject to changes with time (age of a landslide). At the same time, concentration of trace elements in active-layer deposits is rather homogeneous on various landforms and unlikely to be used to determine the relative age of the landslide.

Macro-element concentrations (Cl, Mg, Ca) of plants is determined by the duration of their existence in the pre-disturbed landslide surface, and can be used to determine the relative age of the landslide. Concentration of chemical elements can either increase with age, or decrease. This is obviously due to the mobility of elements and speed of its migration in the active layer.

Acknowledgments This study was supported by grants 11-05-00544-a, 11-05-10084-k, 10-05-10027-k from the Russian Foundation for Basic Research; Grant SS 5582.2012.5 from the President of the Russian Federation for Science Schools. It was carried out as part of integration programs of the Presidium of the Siberian Branch RAS, as well as international projects RISES, TSP and CALM. The authors would like to express their gratitude to NN Smetanin and KA Ermokhina for their assistance in the field and contributions in data processing, and also to SE Sorokin and RV Grishina for performing various chemical tests.

References

Andreev VN (1970) Some geographical laws in distribution of aboveground phytomass in tundra zone in connection with progress to the north of tree-shrubs vegetation. In: Biological basis of nature usage in the North. Komi Publisher, Syktyvkar, pp 6–13 (in Russian)

Basilevich NI (1993) Biological efficiency of ecosystems of Northern Eurasia. Nauka Publisher, Moscow, p 293 (in Russian)

Bret-Harte MS, Mack MC, Goldsmith GR, Sloan DB, DeMarco J, Shaver GR, Ray PM, Biesinger Z, Chapin FS (2008) Plant functional types do not predict biomass responses to removal and fertilization in Alaskan tussock tundra. J Ecol 96:713–726

Brushkov AV (1998) Salt frozen deposits of the Arctic coast, their origin and characteristics. MSU Publisher, Moscow, p 330 (In Russian)

Brushkov AV (2007) Saline permafrost in the Arctic coast: origin and properties. In: Melnikov VP (ed) Problems of construction upon saline permafrost soils. Epokha, Moscow, pp 4–33 (in Russian)

CAVM Team (2003) Circumpolar Arctic Vegetation Map. Scale 1:7,500,000. Conservation of Arctic Flora and Fauna (CAFF) Map No. 1, U.S. Fish and Wildlife Service, Anchorage, Alaska

Danilov DN (1958) Productivity of dwarf birch and willows in east part of Bolshezemelskaya tundra. Bot J 43(3):388–393 (in Russian)

Dubikov GI (2002) Composition and cryogenic structure of permafrost in West Siberia. GEOS Publisher, Moscow (In Russian)

Dubikov GI, Ivanova NV, Streletskaya ID (1996) Salinity of frozen ground and cryopegs. Engineering-geological monitoring of Yamal gas fields. Vol Ï: Geocryological conditions of development of Bovanenkovo deposit. IPOS Publisher, Tyumen, pp 27–37 (in Russian)

Epstein HE, Walker DA, Raynolds MK, Kelley AM, Jia GJ, Ping CL, Michaelson GJ, Liebman MO, Kaarlejärvi E, Khumotov AV, Kuss HP, Moskalenko NG, Orekhov P, Matyshak G, Forbes BC, Yu, Q (2009) Vegetation biomass, leaf area index, and NDVI patterns and relationships along two latitudinal transects in arctic tundra. Abstract GC31A-0697, presented at AGU Fall Meeting. San Francisco, Dec pp 14–18. 90:GC31A-0697

Ermokhina KA, Myalo EG (2012) Phytoindicators of landslide disturbances in the Central Yamal. Proccedings of the tenth international conference on permafrost, In: The Northen Publisher (ed), Salekhard, vol 2, pp 531–536

Forbes BC, Fauria MM, Zetterberg P (2010) Russian Arctic warming and 'greening' are closely tracked by tundra shrub willows. Global Change Biology pp 1542–1554

French HM (1976) The periglacial environment. Longman, London, p 309

Geertsema M, Pojar JJ (2007) Influence of landslides on biophysical diversity—A perspective from British Columbia. Geomorphology 89(1):55–69

Harry DG, Dallimore SR (1989) Permafrost, ground ice and global change in the Beaufort Sea Coastlands. GEOS, Moscow 3:48–53

Jumponen A, Mattson K, Trappe JM, Ohtonen R (1998) Effects of Established Willows on Primary Succession on Lyman Glacier Forefront, North Cascade Range, Washington / U.S.A.: Evidence for Simultaneous Canopy Inhibition and Soil Facilitation. Arct Alp Res 30(1):31–39

Leibman MO (1995) Preliminary results of cryogenic landslides study on Yamal Peninsula, Russia. Permafrost Periglac Process 6:259–264

Leibman MO, Egorov IP (1996) Climatic and environmental controls of cryogenic landslides, Yamal, Russia. Landslides. Balkema Publishers, Rotterdam, pp 1941–1946

Leibman MO, Kizyakov AI (2007) Cryogenic Landslides of the Yamal and Yugorsky Peninsulas. Earth Cryosphere Institute SB RAS, Moscow-Tyumen, p 206 (in Russian)

Leibman MO, Streletskaya ID (1997) Land-slide induced changes in the chemical composition of active layer soils and surface-water run-off, Yamal Peninsula, Russia. In: Proceedings of the international symposium on physics, chemistry, and ecology of seasonally frozen soils, Fairbanks, pp 120–126

Leibman MO, Kizyakov AI, Sulerzhitsky LD, Zaretskaya NE (2003) Dynamics of the landslide slopes and mechanism of their development on Yamal peninsula Russia Permafrost. In: Phillips M, Springman SM, Arenson LU (eds) Proceedings of the 8th international conference on permafrost. Zurich 21–25 July 2003. Balkema, Lisse, pp 651–656

Leibman MO, Gubarkov AA, Khomutov AV (2012) Research station Vaskiny Dachi. Excursion guidebook. In: Tenth International Conference on Permafrost. Salekhard, Russia, June 25-29, 2012. Tyumen, Pechatnik, 50

Lewkowicz AG (1990) Morphology, frequency and magnitude of active-layer detachment slides, Fosheim Peninsula, Ellesmere Island N W T. In: Burgess MM, Harry DG, Sego DC (eds) In: Proceedings of the 5th Canadian Permafrost Conference. Quebec, Canada, June 1990, Laval University, Quebec, Collection Nordicana, vol 54, pp 111–118

Manakov KN (1968) Circulation of ashy elements and nitrogen in shrub tundra of northeast of the Kola peninsula. Pedology 1:80–92 (in Russian)

Matsuda K et al (1988) Observations of geomorphic and vegetational changes caused by thermal erosion of an involuted Hill in Tuktoyaktuk, N.W.T., Canada. In: Characteristic of the massive ground ice body in the Western Canadian Arctic related to paleoclimatology. Inst Low Temp Sci, Hokkaido University, 1984–1985

McKendrick JayD (1987) Plant succession on disturbed sites, North Slope, Alaska, U.S.A. Arctic and Alpine Research 19 (4):554–565

Meltser LI, Moskovchenko DV (1997) Modeling of stability of cryogenic landscapes, north of Western Siberia. Results of basic research of Earth cryosphere in Arctic and Subarctic. Nauka Publisher, Novosibirsk, pp 79–84 (in Russian)

Pajunen M (2009) Environmental and biotic determinants of growth and height of arctic willow shrubs along a latitudinal gradient. Arct Antarct Alp Res 41(4):478–485

Pospelova EB, Pospelov IN (2000) Relic high shrub communities near the northern border (the central part of Byrranga mountains, Taymyr Peninsula). Novosti Akademii nauk, seriya geographicheskaya 4:92–97

Poznanin VL (2001) Morphology, the mechanism of formation and dynamics active-layer detachments on the central Yamal. In: Problems of environment and natural resources, Moscow VINITI vol 2, pp 78–92

Rabothov TA (1978) Phytosociology. MSU, Moscow (In Russian)

Rebristaya OV, Khitun OV, Chernyadyeva IV, Leibman MO (1995) Dynamics of vegetation on the cryogenic landslides at the central part of Yamal Peninsula. Bot J 80(4):31–48 (In Russian)

Romanenko FA (1993) Distribution and dynamics of earth flows at one of the sites in central Yamal. Engineering geography, engineering-geomorphological aspects. In: Abstracts of Inter-state conference in Vologda 13–17 Sep 1993. Vologda, 1:7–9 (In Russian)

Streletsky DA, Streletskaya ID, Rogov VV, Leibman MO (2003) Redistribution of ions within the active layer and upper permafrost, Yamal, Russia. In: Phillips M, Springman SM, Arenson LU (eds) Permafrost: Proceedings of the 8th international conference on Permafrost. A.A. Balkema Publishers, Zurich, vol 2, pp 1117–1122

Sturm M, Racine C, Tape K (2001) Increasing shrub abundance in the Arctic. Nature 411:546–547

Tentyukov MP (1998) Geochemistry of landscapes of Central Yamal. Ekaterinburg. p 101 (in Russian)

Ukraintseva NG (1997) Willows tundra of Yamal as the indicator of salinity of superficial sediments. In: Results of basic research of Earth cryosphere in Arctic and Subarctic. Nauka Publisher, Novosibirsk, pp 182–187 (in Russian)

Ukraintseva NG (2008) Vegetation response to landslide spreading and climate change in the West Siberian tundra. In: University of Alaska Fairbanks. Proceedings of the ninth international conference on Permafrost, University of Alaska Fairbanks, vol 2, pp 1793–1798

Ukraintseva NG (2011) The tall willows at Yamal peninsula: the causes of widespread, community structure, and the methods of the biomass. In: Komarov Botanical Institute RAS

(BIN RAS). Proceedings of the conference "National geobotany: milestones and prospects", St. Petersburg, vol 2, pp 261–264 (in Russian)
Ukraintseva NG, Leibman MO (2000) Productivity of willow-shrub tundra in connection with landslide activity. In: 30th Arctic Workshop, March 15–19 2000, INSTAAR, University of Colorado, Boulder, CO USA, pp 150–152
Ukraintseva NG, Leibman MO (2007) Cryogenic landslides (active-layer detachments) and fertility of tundra soils on Yamal Peninsula, Russia. In: Conference CD: Proceedings of the First North American Landslide Conference Vail, Colorado, pp 1605–1615
Ukraintseva NG, Streletskaya ID (1999) Landscape indication of surface soil on West Yamal landslide slopes. In: Dyakonov KN, Mamai II (eds) Lomonosov Moscow State university landscape school: traditions, achievements, future. RUSAKI, Moscow, pp 120–129 (In Russian)
Ukraintseva NG, Streletskaya ID, Ermokhina KA, Yermakov S Yu (2003) Geochemical properties of plant-soil-permafrost system at landslide slopes, Yamal, Russia. In: Phillips M, Springman SM, Arenson LU (eds) A.A. Balkema Publ Permafrost. Proceedings of the 8th International Conference on Permafrost, Zurich, vol 2, pp 1149–1154
Vojtkevich GV et al. (1990) Handbook on Geochemistry. Nedra Publisher, Moscow p 480
Walker DA (1987) Height and growth rings of *Salix lanata ssp.richardsonii* along the coastal temperature gradient of northern Alaska. Can J Bot 65:988–993
Walker DA, Leibman MO, Epstein HE, Forbes BC, Bhatt US, Raynolds MK, Comiso J, Gubarkov AA, Khomutov AV, Jia GJ, Kaarlejärvi E, Kaplan JO, Kumpula T, Kuss HP, Matyshak G, Moskalenko NG, Orechov P, Romanovsky VE, Ukraintseva NG, Yu Q (2009) Spatial and temporal patterns of greenness on the Yamal Peninsula, Russia: interactions of ecological and social factors affecting the Arctic normalized difference vegetation index. Environ Res Lett 4:16 doi:10.1088/1748-9326/4/4/045004
Walker DA, Forbes BC, Leibman MO, Epstein HE, Bhatt US, Comiso JC, Drozdov DS, Gubarkov AA, Jia GJ, Karlejaärvi E, Kaplan JO, Khumutov AV, Kofinas GP, Kumpula T, Kuss P, Moskalenko NG, Raynolds MK, Romanovsky VE, Stammler F, Yu Q. (2011) Cumulative effects of rapid land-cover and land-use changes on the Yamal Peninsula, Russia. Gutman G, Reissel A (eds) Eurasian Arctic Land Cover and Land Use in a Changing Climate. Springer. New York, vol 4, pp 206–236 doi:10.1007/978-90-481-9118-5_9
Walker DA, Bhatt US, Epstein HE, Bieniek PA, Comiso JC, Frost GV, Pinzon J, Raynolds MK, Tucker CJ (2012) Changing Arctic tundra vegetation biomass and greenness. in State of the Climate in 2011. Bull Am Meteorol Soc 93(7):138–139
Warren Wilson J (1957) Arctic plant growth. Adv Sci 13(53):383–388

Cryogenic Landslides at Dam Abutments

Ninel Krivonogova and Stanislav Panov

Abstract The Svetlinskaya HPP is located on the Vilyui River in the north-eastern part of Russia, in the zone of continuous permafrost. The hydroelectric complex includes two earth and rockfill dams and run-of-river hydraulic power plant. The steep left bank is represented by permanently frozen rock with marks of ancient preglacial landslides. Inevitable melting of this rock massif after filling of the reservoir can trigger potentially dangerous landslide processes. This paper describes engineering measures aimed at reducing dangerous impacts of these processes on operational safety of the Svetlinskaya HPP hydroelectric complex.

Keywords Permafrost · Thaw process · Landslide · Hydraulic structure · Dam · Grout curtain · Frozen curtain

1 Introduction

Dam construction in permafrost zone is complicated significantly by almost inevitable thaw processes developing after reservoir infilling. They lead in particular to activation of old landslides on the valley slopes that are dormant while rock massif remains in frozen state, but can become quite unstable when affected by relatively warm seeping water. Special measures undertaken to ensure slope stability at dam abutments are described by example of the Svetlinskaya dam on the Vilyui River in Yakutia.

N. Krivonogova (✉) · S. Panov
JSC Vedeneyev VNIIG, Gzhatskaya St., 21, 195220 St. Petersburg, Russia
e-mail: KrivonogovaNF@vniig.ru

W. Shan et al. (eds.), *Landslides in Cold Regions in the Context of Climate Change*, Environmental Science and Engineering, DOI: 10.1007/978-3-319-00867-7_10,

2 Main Parameters of the Svetlinskaya HPP

The Svetlinskaya dam is part of hydroelectric power chain on the Vilyui River in Yakutia and is located 100 km downstream from the power site of the Vilyui HPP-1-2. The main structures of the Svetlinskaya HPP comprise of run-of-river power house, combined with the operational spillway, and embankment earth-and-rock-fill dams. The total length of the front is 570, 152 m of which is power house and, 292 and 126 m are the right- and left-banks of the dams, respectively (Fig. 1).

The concrete power house has four hydraulic units with total power output of 400 MW, combined with 16 sluice spillway ports, sufficient to pass maximum operational discharge. Loamy core serves as an anti-seepage element of embankment dams, retaining prisms are made of rock fill. The core width is from 3.5 to 16.5 m with additional widening by the foundation.

The dam crest is at 184 m a.s.l. and foundation stands at 123 m a.s.l., while the maximum height of the embankment dams is about 60 m. The maximum operating level (MOL) of the reservoir is 183.0 m a.s.l., standard design level (SDL)—181 m a.s.l., top of head storage (THS)—179.0 m a.s.l. Maximal river level downstream is 163.6 m a.s.l., minimal—150.5 m a.s.l. Maximum head on the structure is 32.5 m.

3 Engineering-Geocryological Conditions

Svetlinskaya HPP was constructed in the region with harsh continental climate with average annual air temperature of about −8 °C. Winter and summer temperature conditions of the area averages +35 °C and −60 °C, respectively.

Geocryological engineering conditions of the dam site are complicated (Fig. 2). The watershed area and upper parts of the slopes (above SDL) are composed of dolerites while major parts of the slopes and valley beds are composed of carbonate-clayey unit represented by alternation of marl, limestone, dolomite, with sparse sandstone beds.

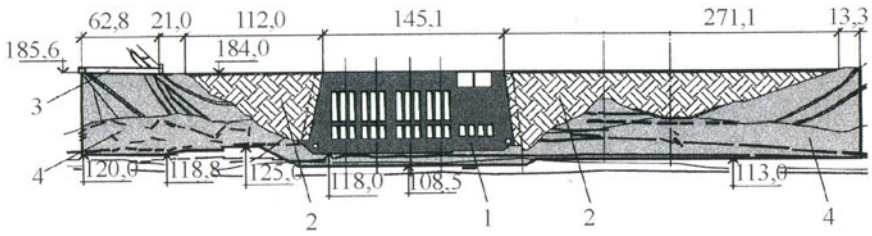

Fig. 1 Longitudinal section of structures of the Svetlinskaya HPP head front. 1—power house combined with the spillway; 2—earth-and-rock-fill dams; 3—grouting galleries; 4—grout curtain

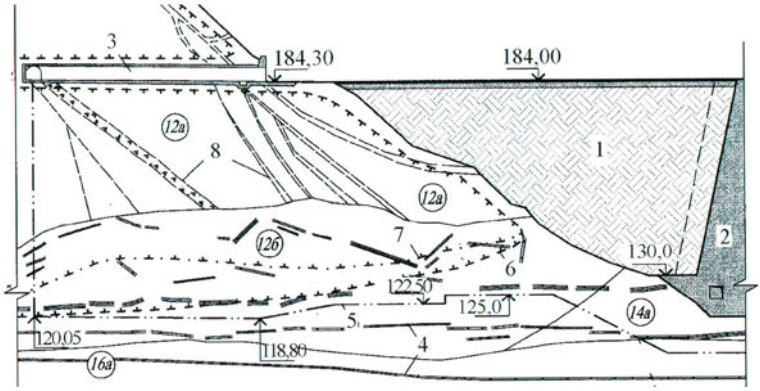

Fig. 2 Engineering-geological section along the axis of left-bank earth-and-rock-fill dam (ERD). 1—left-bank ERD in full profile; 2—concrete power house; 3—grouting gallery No 1; 4—layers of dolomite and limestone; 5—lower boundary of the grout curtain; 6—permafrost boundary before it electric thawing; 7—boundary of the plastic-frozen rocks zone with ice; 8—large zones of sliding and crushing; Engineering-geological units: 12a—landslide deposits; 126—dislocated rocks of the Verkholensk suite; 14a—rubble and gruss of clayey marl and siltstone with loam and rare interbeds of limestone and dolomite debris; 16a—marl with rare interbeds of limestone, dolomite and siltstone, with negative temperature and cryopegs

The dam is located in an area of powerful solid permafrost with two-level structure. Thickness of the upper part of the permafrost zone is composed of frozen rock with temperature of about −1 to 3 °C in the left-bank massif and −4 to −7 °C in the right-bank massif changes from 50 to 100 m on the bed and slopes of the valley and up to 200–300 m on the watershed. Below are rocks with pores and cracks filled with salt water with negative temperature (cryopegs). Talik exists under the river-bed where there is increased mineralization of groundwater with increase in depth (from fresh water to salt brine with negative temperature at definite depth). Peculiarities of interaction of salt sub-permafrost and fresh waters of super-permafrost underflow talik and seasonally-thawed layer caused active chemical transformation of marlaceous rocks along the valley contour, in the result of that the rocks (in valley slopes at depths of 20–25 m, and under the river-bed—at depths of 35–40 m) are transformed into loam and sandy silty gravel, characterized by low strength parameters. This fact defined basically the insert depth and design features of concrete structures of the hydraulic structure.

The physical state and structure of rocks on these valley slopes are extremely complex. In the upper zones, the rocks are present as landslide deposits—large-sized blocks and heterogeneously-sized angular boulders (from tens of centimetres to tens of meters in size) of differently oriented marly rocks. Matrix is represented by sandy-silty loam. Pores and fissures are filled, besides loamy aggregates, with ice of different origin. Ice content is irregular and changes within 5–50 % in rock blocks of different volume. Steep open fissures and partially filled fissures of 0.3–0.5 m wide traversing the blocks and inter-block space can be found too.

Landslide bodies are separated from each other by sliding surfaces and sliding zones of several meters thick. Material composing the sliding zones are grinded to sandy-loam-loamy, rubbly-gruss material with interstices, ice pockets and veins up to 2 m thick.

Multiple decompaction cracks, inheriting stratification cracks, and joint present in landslide bodies. According to the tunnel documentation, the crack voidage coefficient differs from 1.5 to 4 %, while at the reference sites this value ranges from 0.3 to 25 %.

In the left slope of the valley, the specific group of fissures is the contemporary cracks of slope unloading. They stretch sub-parallel to the valley slope of Vilyui River by azimuth of 50–70°. Though being oriented consistently they could be discontinuous, en-echelon shingling and interconnected. Before the left-bank slope excavation these cracks did not outcrop because they were overlapped by scree cover of 1–5 m thick. These cracks extend up to 165 m a.s.l.

Flank release fractures in the valley slopes are basically characterized by steep angles (80–90°), dip direction towards the excavation and significant length up to hundreds meters. Cracks opening is 0.1–0.2 m in average, though wider fissures were recorded at some sites (tunnel 1004, fracture No 57–0.8 m wide, fracture 206–0.5 m wide). Fissures are mostly filled with ice, rarely with sublimation ice. In some cases cracks are open or filled with solifluction material (loam, debris) (Fedoseev et al. 2009).

Presence of large partially open fissures, sub-parallel to the valley slope, determines high permeability of the left-bank landslide deposits. According to calculations performed in Lenhydro project Institute and in Moscow University of Construction and Architecture, the seepage coefficient in frozen massif is estimated as 10 m/day on an average, after thawing, 50–350 m/day, and more than 1000 at large tension cracks.

Bottom and toe part of the slopes are composed of Cambrian sedimentary rocks which are made up of clayey marl with thin interlayers of dolomite and limestone sandwiched between siltstone and moderately indurated mudstone. The rocks show sub-horizontal bedding with saline content of 1–7 %, containing moderate amount of gypsum. In frozen bank massifs rocks are characterized by bedded-cracked cryogenic texture and ice content of 5 %. Permeability of rocks in thawed state and in the zone of sub-permafrost waters with negative temperature is given in Table 1 (Ziskovich and Krivonogova 1986).

The dam foundation is composed of the Verkholensk and the Ilginsk suites of Upper Cambrian rocks, affected mainly by processes of weathering, and landslide formations overlapped by outwash-solifluction and outwash-colluvial sediments.

Verkholensk suite is composed of clay and carbonate siltstone with marl, limestone and dolomite interbeds. The rocks are stratified and strongly deformed, with medium to weak strength. Due to the influence of landslide activity, the rocks were folded into flat, more rarely narrow micro-folds. Rocks along the crest lines were crushed into rubble with 10–30 % of loamy matrix. Above 105–107 m a.s.l. rocks are unloaded.

Table 1 Hydraulic conductivities of thawed soils and the soils located in the zone of subpermafrost waters with negative temperature (according to JSC "Lenhydroproject" data)

EGE	Name of soil	Soil state	Hydraulic conductivity,m/day
13 and 13a	Calcinated and dolomite loam with 30–40 % of crushed rock with layers of relatively undisturbed weak marl	Thawed	1.00
14a	Crushed rock and gravel of weak clay marl, siltstone with loam—to 30–40 %, with layers of relatively undisturbed weak marl	Thawed	1.00
16b	Clay marls with layers of limestone, dolomite, semi-rock marl, weak in top part	Thawed	0.15
Layer No1	Limestone-dolomite layer with average thickness to 1.5 m	Thawed	50.00
Layer No2	Limestone-dolomite layer with average thickness to 0.5 m	Thawed	15.00
Layer No3	Limestone-dolomite layer with average thickness to 0.4 m	Thawed	1.00
13	Calcinated and dolomite loam with 30–40 % of crushed rock with layers of relatively undisturbed weak marl	Frozen	5.00 (after thawing)
14	Crushed rock and gravel of weak clay marls, siltstone with 30–40 % of loams with layers of relatively undisturbed weak marl	Frozen	5.00 (after thawing)

The amount of gypsum in the rocks ranges from 1 to 1.5 %. The rocks are frozen showing cryogenic texture—cracked-bedded. Visual ice content is up to 5 %.

The formations, similar by lithologic composition but without ice, with negative temperature and with cryopegs are classified as the engineering-geological unit (EGU) 16a (see Fig. 2). Rocks with similar composition and structure that form underflow talik were assigned to EGU 166.

Engineering-geological unit 14a, delineated in the near-riverbed part of the left-bank dam foundation is composed by eluvium of the Verkholensk suite—rubble and gruss soil with loamy matrix from 5 to 45 %. Rock fragments are represented by marl, weak and medium-strong mudstone. Thawed soil contain from 1 to 2 % of gypsum and from 0.3 to 6 % of water-soluble salts.

The above-mentioned unit is overlain by landslide deposits ascribed to EGU126. Sliding affected rocks of the Upper Cambrian Verkholensk suite landslide deposits are composed of rubble and loamy soils with blocks of intact marl, dolomite, siltstone and mudstone. The gypsum content is 1–3 %, while the content

of water-soluble salts ranges from 0.5 to 7 %. Thawed rocks and rocks with negative temperature, without ice, contain cryopegs. Cryogenic texture is ice-covered and incorrectly gridded. Visual ice content is 3–5 %.

The engineering-geological unit 126 is overlain by the engineering-geological unit 12a that consists of landslide deposits composed of siltstone, marl, limestone, sandstone, and mudstone blocks of the Upper Cambrian Iglinsk suite. The blocks are divided by fissures and sliding planes and crushed zones. The rocks are thawed. Cryogenic texture is cracked-vein, ice-covered, solid; visual ice content is up to 5 %. The cryogenic texture is basal in the zones of disturbances. Visual ice content is 15–20 %, in some places—to 50 %.

4 Engineering Measures Aimed to Provide the Left-Bank Slope Stability

The following measures were stipulated according to the original design to provide stability at the left-bank dam abutment during HPP operation:

- construction of deep grout curtain in the left-bank abutment from two grouting galleries pierced parallel to the dam axis;
- construction of impervious loamy facing at the upstream site of the left bank about 370 m long, conjugated with the dam core. It was protected by a surcharge layer of crushed rock from 1.0 to 3.0 m thick and with slope base 1:1.5.

According to in situ observation during the first years of Svetlinskaya HPP operation, it was asserted that the impervious materials in the dam body and its foundation are not impermeable enough to prevent thawing of the dam foundation and its left-bank abutment. The protective facing of the left bank slope suffered from weak damping settlements and horizontal displacements accompanied by formation and development of multiple cracks. It was also observed that there was intense seepage in the dam body that leads to progressive thawing of not only the dam foundation but also soils of the left-bank abutment massif (Fig. 3).

Further development of the above-mentioned processes might cause activation of old landslides in the left bank massif. By this reason, the dam itself and its bank abutment, including the following measures, were rehabilitated in 2012. The following measures were carried out:

- the existing waterproof facilities of the dam were supplemented with drill-concrete along the entire height of the dam with its embedded into foundation rock for 4–5 m below its surface. Slurry was is characterised by following parameters: borehole depth of 70 m; 158 boreholes with diameter of 1.2 m and 0.7 m spacing, drill footage of 10,664 running meters, volume of clay containing concrete—13,260 m^3;

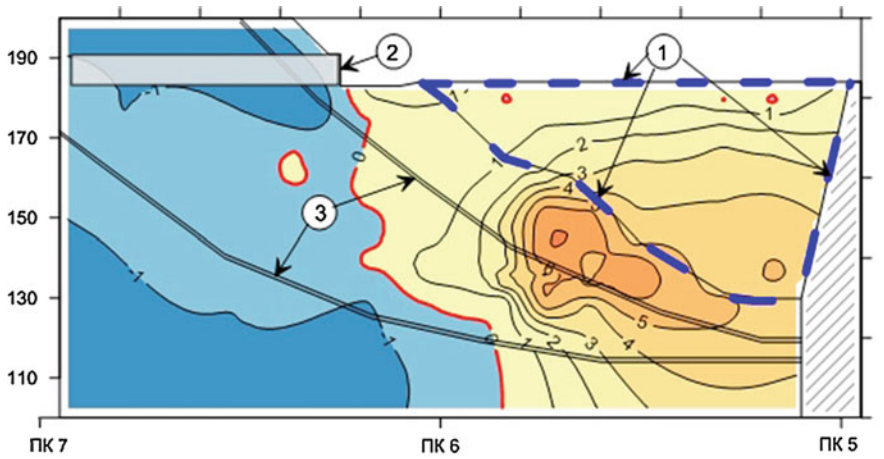

Fig. 3 Temperature distribution in the body and foundation of the left-bank dam after 5 years of its operation: 1—outline of the left-bank dam, 2—two cement-grout gallery in the massif of the slope abutment, 3—sliding surfaces of ancient landslides

- two-raw constantly acting 60 m deep frozen curtain aimed to protect abutment soils from thawing were installed in the left-bank abutment massif with drill footage of 6,271 running meters, and carbon dioxide used as a cooling agent.

According to in situ observations, the slurry wall decreased piezometric heads in the downstream end of the dam fill by 6 to 10 m that points to practically full stop of seepage in the dam body and its foundation. The results of seepage calculations, seepage and static stability of dam elements demonstrate that at the present time, the diagnostic parameters of these processes correspond to the design requirements.

The efficiency of frozen curtain will be estimated based on results of instrumented in situ observations for the thermal state of the massif of the left-bank abutment as well as for vertical and horizontal displacements of the slope surface.

5 Conclusions

It was found that the Svetlinskaya dam left-bank abutment's thermal state changes induced by reservoir filling can initiate activation of an ancient landslide body.

Engineering measures including installation of a slurry wall in the dam's body and a permanently active deep two-row frozen curtain in its abutment are supposed to reduce bypass seepage intensity and provide stability during the Svetlinskaya HPP operation.

References

Fedoseev VI, Shishov IN, Pekhtin VA, Krivonogova NF, Kagan AA (2009) Antiseepage curtains of hydroengineering structures on permafrost. In: Serov AA (ed) Design and construction experience. B.E. Vedeneev VNIIG Publishing House, St. Petersburg (in Russian)

Ziskovich VH, Krivonogova NF (1986) The influence of goecryological characteristics of construction site on design decisions for Viluiskaya HPP-III. Power Eng Constr 8:53–56 (in Russian)

Part IV
Research Methods for Landslide in Cold Region

Cryogenic Landslides in the West-Siberian Plain of Russia: Classification, Mechanisms, and Landforms

Marina Leibman, Artem Khomutov and Alexandr Kizyakov

Abstract Cryogenic landslides are the main relief-forming process on the Northern part of West Siberian Plain. This chapter discusses the theory of cryogenic landslides and suggests classification method based on mechanisms, specific landforms—manifestations of various landslide processes. The study is based on the long-term field observations at Research station "Vaskiny Dachi" in Central Yamal, as well as occasional observations in other areas. Two main types of cryogenic landslides were distinguished based on mechanism and mode of displacement. They are (1) earth/mud flows (retrogressive thaw slumps) and (2) translational landslides (active-layer detachments). The first type results from thawing of massive ground ice within permafrost layers, while the second type is caused by the thawing of ice lenses in the active-layer base (transient layer). Distinguished are specific landforms: (1) thermocirques, and (2) landslide cirques. Landslide cirques are considered to start at a subsequent stage of thermocirque after the massive ground ice layer is exhausted or buried by landslide masses. The thermocirque changes are noted within years and decades, while new landslides within landslide cirques are separated by several centuries. As landslide masses bury organic material of soil and vegetative canopy, it is possible to use radiocarbon dating method to know the age of the landslides. Shear surfaces of ancient landslides are overgrown by abnormally high willow shrubs which allow the use of dendrochronologic method in the analysis of landslide cirque development.

Keywords Cryogenic landslides · Thermocirques · Landslide cirques · Mechanisms of cryogenic landslides · Classification of cryogenic landslides · Ground ice

M. Leibman (✉) · A. Khomutov
Earth Cryosphere Institute SB RAS, 1230 Tyumen 625000, Russia
e-mail: moleibman@gmail.com

A. Kizyakov
Moscow State University, Faculty of Geography, Vorobievy Gory, Moscow 19991, Russia

W. Shan et al. (eds.), *Landslides in Cold Regions in the Context of Climate Change*, Environmental Science and Engineering, DOI: 10.1007/978-3-319-00867-7_11,

1 Introduction

In permafrost regions, the down-slope movement of seasonally thawed ground has been widely reported. One of the most complete reviews covers the period up to 1964 (Kaplina 1965). Later works by French (1976), Ananieva (1984), Lewkowicz (1988, 1990), French (2007) and others deal with the mechanisms of the movement in different environments and soil types. In Russia, detailed study was undertaken after the widespread landslide event in the northern part of West Siberia, especially on Yamal Peninsula in 1989 (Leibman 1994, 1995 a, b; Leibman et al. 1991, 1993b, 2000, 2003; Romanenko 1997; Ukraintseva et al. 1992; Voskresenskiy 1999). Triggering factors and mechanisms are analysed in (Leibman and Egorov 1996). General aspects of cryogenic landslide processes within the Arctic are discussed in (Bolikhovsky and Kuntsel 1990; Harris and Lewkowicz 2000; Kokelj and Lewkowicz 1998; Poznanin and Baranov 1999; Voskresenskiy 1999). The latest monograph reviewing previous knowledge and suggesting classifications and mechanisms based on extensive field study in the Kara sea region is published by Leibman and Kizyakov (2007).

Specific aspects related to strong impact of cryogenic landslides on all components of the geosystem like vegetation, soils, active layer, ground water, and ground temperature were analyzed in a number of Russian publications (Ermokhina 2009; Khomutov 2010, 2012; Leibman and Streletskaya 1997; Leibman et al. 1993a, 1997; Rebristaya et al. 1995; Ukraintseva and Leibman 2000, 2007; Ukraintseva et al. 2000, 2003).

Main topics of landslide study in the Arctic plains were (1) discovery, description and morphometric classification of the landslides; (2) mapping the landslide distribution at the study polygon about 90 km^2 in size; (3) determining the age of the landslides and cyclicity of their formation and classification of landslides according to their age; (4) suggesting mechanisms, forcing factors, triggers of landslide processes and classification of landslides by mechanism. This paper is largely on cryogenic classification of landslides, mechanisms of their activation, and landforms resulting from landslides of various mechanisms typical of the Arctic plains.

2 Key Site Characteristics

Vaskiny Dachi research polygon is located at the watershed of the Se-Yakha and Mordy-Yakha Rivers (Fig. 1), and comprises a number of highly-dissected alluvial-lacustrine-marine plains and terraces in which a number of hazardous processes operate, landslide process being mostly widespread. The deposits are sandy to clayey, most are saline within permafrost, and some are saline in the active layer. Massive ground ice including tabular ice and polygonal ice wedges, are found within the geological section. The hilltop periphery is occupied by

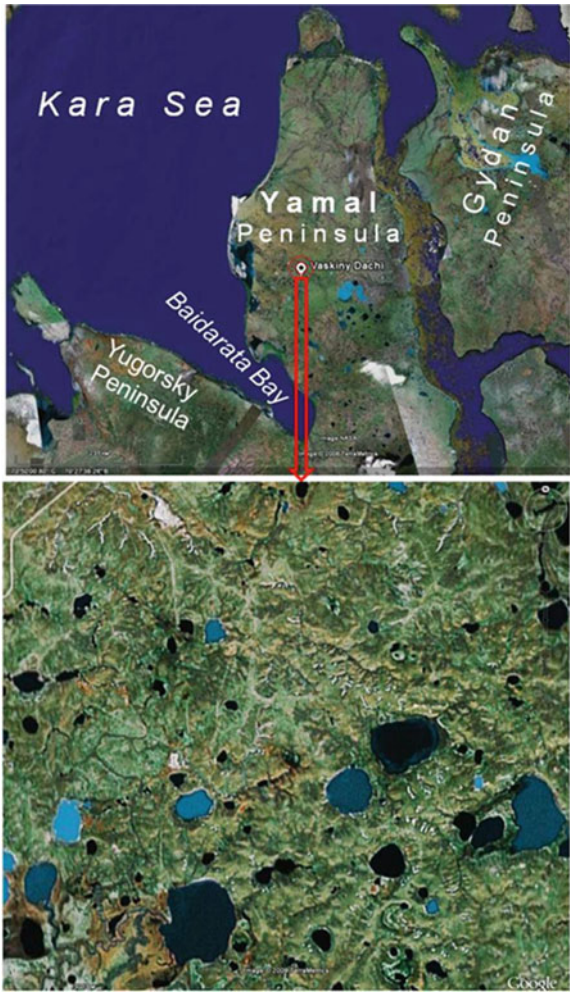

Fig. 1 Key site "Vaskiny Dachi", google view

windblown sand hollows, covering huge areas. Saddles between the hilltops are covered by polygonal peatlands. Maximum elevation averages 58 m above sea level while maximum depth of the dissected area averages 20–50 m.

Up to 60 % of the study area is covered by gentle slopes (gradient less than 7°); steep slopes (more than 7°) occupy about 10 % of the area and the rest 30 % being hilltops, river valleys and lake depressions.

The study area is characterized by continuous permafrost of 400 m thick, and even more. Average annual ground temperature at the depths of zero annual amplitude ranges between 0 and −9 °C.

Cryogenic processes observed in the area are connected to tabular ground ice found in geological sections at the depths of 1–25 m practically everywhere. Most widespread processes observed in the study area are landslide process of various

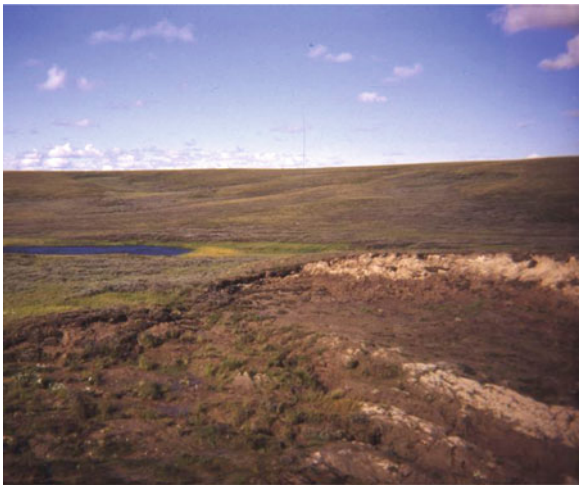

Fig. 2 Active-layer detachments (scarp and shear surface) at the research polygon "Vaskiny Dachi" on central Yamal

Fig. 3 Retrogressive thaw slumps which renovated thermocircue in 2010 (photo by A. Gubarkov), first discovered in 1993 (Leibman 1995)

types and thermo-erosion due to the effect of the prevailing slopes. Cryogenic landslides (active layer detachments) showed extremely wide activity in August 1989, up to 400 new landslides appeared in the area of 90 km^2 (Leibman and Kizyakov 2007, Fig. 2).

Last years, since 2006, due to warm summers several new exposures of tabular ground ice formed by landslide activity (retrogressive thaw slumps, Fig. 3).

3 Mechanisms and Classification of Cryogenic Landslides

Landslides in general are known to be triggered by high pore pressure due to water saturation (e.g. Schuster and Krizek 1978). In permafrost zones, water saturation is provided by atmospheric precipitation together with melting of ground ice in the

Table 1 Mechanisms and classification of cryogenic landslide process

Cryogenic translational landslides (active-layer detachments, block glides)	Cryogenic earth flows (mudflows, retrogressive thaw slumps)
Rather dry and dense sandy-silty active-layer deposits	Water-saturated viscoelastic or viscofluid silty-clayey active-layer deposits
Result of upward freezing of the active-layer and subsequent thaw of the ice at the active-layer base	Result of massive ice and/or ice-rich permafrost thaw
Inter-annual active-layer dynamics	Local lowering of permafrost table
Landslide body is a one piece or broken into several pieces block with well expressed vertical sidewalls along the perimeter	Landslide body is a spread flow with parabolic outlines, with floating pieces of turf (sod) overgrown by shrubs on top

active layer or/and upper permafrost. The shear surface coincides with the lithological boundary or with permafrost table depending on which is closer to the surface (Leibman et al. 2003).

The cause for a high pore pressure is, at the same time an indicator of landslide mechanism.

For the Arctic plains, such as the northern part of West Siberia, we subdivide two different mechanisms of landslide activity, two sets of initiating conditions, triggers, and landforms. The name of process in a reference to the mechanism of landslide process in Table 1 is translation of Russian terms (in the parenthesis are more or less equivalent terms used in the English cryogenic-landslide literature).

Cryogenic translational landslides **(CTL)** (Table 1, left column) results from rapid thaw of ice-saturated deposits at the active layer base (transient layer after Shur 1988). This assumption is proved by the following observations. Accumulation of segregation ice at the active-layer base and formation of the transient layer is due to active layer depth decrease in the course of several years of cooling as observed in Yamal from 1985 to 1988 (Leibman and Egorov 1996). Intensive heat influx in late summer and heavy rainfalls linked to this period both cause relatively rapid thaw of the ice layer at the active-layer base (about 17 cm during the period from July 15 to August 14 in 1989, about 75 % more rapid than in other years, Leibman and Egorov 1996), excess water accumulates in the active layer because of low permeability of the silty soils (first centimetres per day, Leibman et al. 1993b), and pore pressure rises dramatically (up to 100 cm rise of water level in piezometers installed on landslide-affected slopes). Gravity causes displacement of blocks, broken up by frost, desiccation, or edge cracks, "floating" on the layer with excess pore pressure (Leibman and Egorov 1996, Fig. 4).

Blocks preserve integrity due to structural bounds, formed by multiple freeze–thaw, drying-liquefaction and desiccation of the middle portion of the active layer by two-sided freeze back (Lewkowicz 1990; Leibman et al. 2003; Fig. 5).

Cryogenic earth/mud flows **CEF(viscoelastic)/CMF(viscofluid)** (Table 1, right column) result from thawing of massive ground ice. CEF/CMF are also referred to as retrogressive thaw slumps. This type of sliding mechanism is linked to areas where massive ground ice is close to the surface (Burn and

Fig. 4 Outflow of silt suspension in the cracks under the high pore pressure on gentle slope, research station Vaskiny Dachi, summer 2012

Fig. 5 CTL block, undisturbed structure, shrubs on top continue growing

Lewkowicz 1990) and is occasionally involved in seasonal thawing through natural or technogenic disturbance, or noticeable summer warming (Fig. 3). At the exposures, thawing ice causes failures of overlaying deposits liquefied by meltwater and produces mudflows with pieces of turf, floating ontop of the flow. When exposures are covered by talus, some parts of the meltwater are absorbed by the slope deposits and earth flows form (Leibman and Kizyakov 2007).

Different from the CTL, CEF/CMF can develop every year until massive ground ice is within the zone of seasonal thaw. CMF are formed during warm periods at the ice exposures while CEF form only during warm years, mainly at the end of the warm period under maximum thaw depth. Rain water is not as crucial for CEF/CMF development because massive ice melt-water provides enough moisture for embodiment of the landslide potential on slopes (Kizyakov 2005; Kizyakov et al. 2006).

Landslide-affected slopes present a specific set of morphological elements (Figs. 8, 9): hill tops and stable slopes not affected by landslides (background);

cirque-shaped depressions, landslide scarp and shear surface (denudation and transition zone); and deformed hillocks and terraces, landslide bodies (accumulation zone).

4 Landforms Produced by Landslide Process

On our opinion, modern landforms produced by landslide events are inheriting those resulting from past thermokarst events of climatic optimum of the Holocene. At that time tabular ground ice bodies were involved in permafrost degradation from the surface and formed deep lakes which are now found on Central Yamal. In the areas with water outflow slope depressions, thermocirques formed through retrogressive thaw slumps. These landforms are developing now but at a less scale inland, though more active at the sea coast (Kizyakov 2005; Khomutov and Leibman 2008, Fig. 6).

Evolution of thermocirques resulted to flattening of slopes, re-vegetation of former exposures and thus transformation of thermocirques into landslide cirques. The reason is exhausting or burying of near-surface layers of tabular ground ice, cooling of climate which causes formation of transient layer immediately beneath the modern active layer and finally replacement of CEF by CTL and formation of landslide cirques as shown on a sketch (Fig. 7).

To evaluate the potential for the activation of thermocirques, we introduce the concept of landform development phase. The *active phase* is characterized by a combination of climatic conditions over the years which favors CEF/CMF (warming and massive ice thaw, significant summer rainfall is a favorable factor as well). Passive phase coincides with the cold dry periods.

While stages of thermocirque development probably last for centuries, the phases are controlled by short-term climate variations and last for several years or decades.

The last stage of thermocirque development coincides with the first stage of landslide cirque. Further development of the latter is under the influence of climatic factors, as described above.

Fig. 6 CEF (1) and CMF (2) at the Kara sea coast

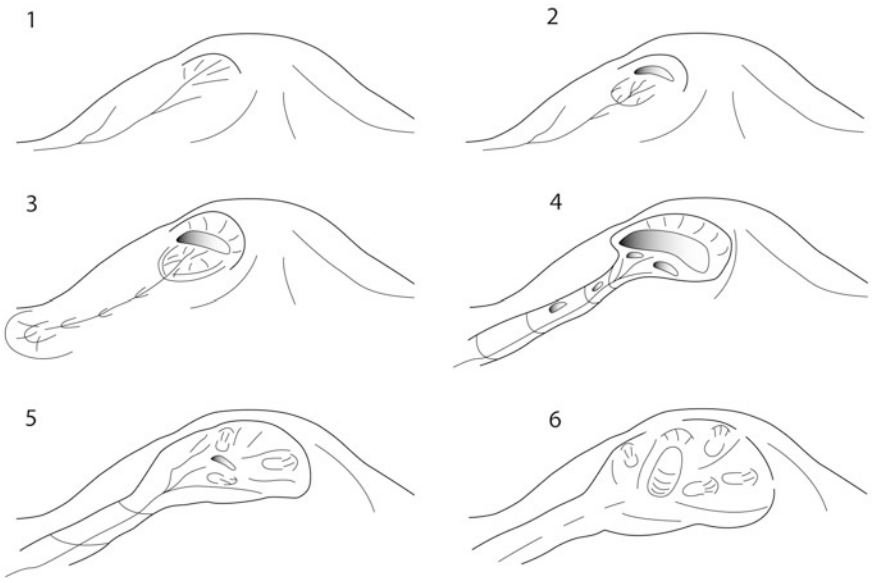

Fig. 7 Evolution of thermocirque into a landslide cirque: **1** initial lowering of the surface; **2** initial exposure of massive ground ice, CEF development; **3** expansion of landslide process, increase of the ice exposure area; **4** widening and deepening of concavities; **5** burial of concavities by landslide material during thaw of the main bulk of the massive ice; **6** extinction of termodenudation, development of CTL, complete thaw of the massive ice layer or its burial by landslide masses

Within a single CTL "sub-stages" of development can be subdivided into: (1) initial landslide event; (2) development of deep erosion troughs on the shear surface; (3) sedimentation and vegetation recovery in the rear of the landslide, flattening of the erosion troughs; (4) overgrowths on the shear surface, its leveling and wetting of the shear surface; and finally, (5) new landslide process. As follows from our observations in the key area "Vaskiny Dachi", the first two sub-stages last for more than 15 years but less than 50 years. Sub-stage 3 takes 200 years or more.

Landslide cirque is harder to interpret when new landslides are not in view. At Research Station Vaskiny Dachi, we observed modern landslides which occurred in 1989 and thus were able to distinguish these landforms of older age including the ancient ones (Fig. 8a–c).

5 Dating Cryogenic Landslide Events

The method used to determine the age of landslides of various generations is by dating the soil, turf, humus, wood, buried by landslides and exposed in trial pits and boreholes. The idea is to determine the time intervals between stages of landslide development. This time is required for the slope to attain a critical strain, and prepare for the next stage of activation.

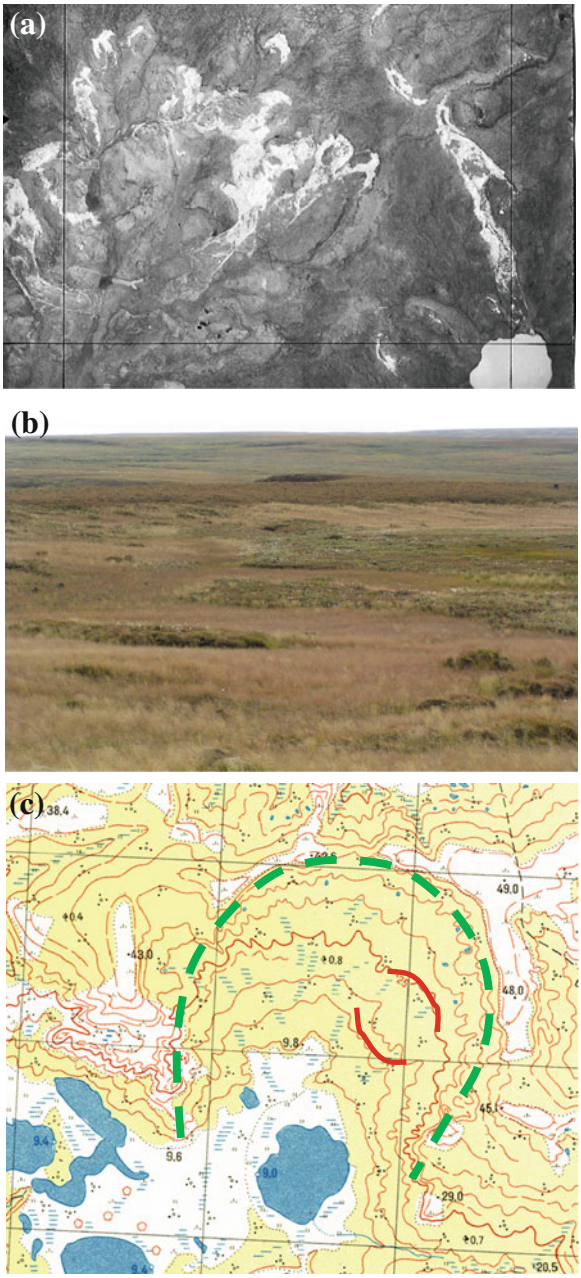

Fig. 8 Landslide-affected slopes on the photos and topographic maps at central Yamal: **a** landslide cirque on aerial image of 1991 showing bare shear surfaces of landslides after the 1989 event. The lightest photo-tone reflects dry clayey surface, *grayish* are crushed landslide bodies. **b** The same landslide cirque, photo of 2005, after 16 years of re-vegetation of shear surface. **c** A landslide cirque on a topographic map, outlined by *dashed green line*. Meandering isohypses with disagreement between convex portions (*curved down-slope*, accumulation zone) and concave portions (*curved upslope*, scarp and shear surface) as marked by *red lines* are indicators of ancient landslides

A case study at one of the landslide cirques (Fig. 9) was aimed at dating a series of landslides from modern to more than 2000 years old. Dating of each landslide event within one slope system shows the time needed for "preparation" of the

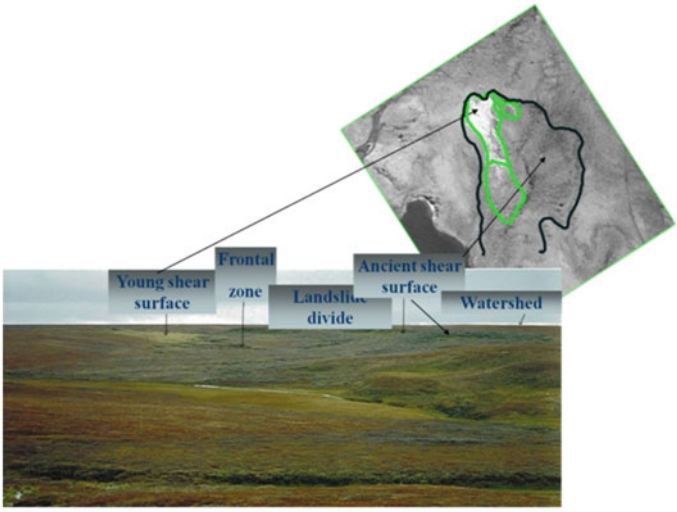

Fig. 9 Etalon landslide cirque, overview

slope for new active-layer detachment, depending on certain climatic conditions. The "preparation" period, is needed for: (a) formation of a transient layer at the active-layer/permafrost interface, at least one cold and wet summer preceding the next colder summer with less seasonal thaw, (b) re-vegetation and strengthening of the organic material which acts as a cementing material that holds the deposits together, resisting strain except along the shear zone, (c) levelling of erosion channels on the shear surface of the previous landslide, for better moisture saturation and high pore pressure.

5.1 Radiocarbon Dating

Buried by a landslide body turf-soil-vegetative layers are found in the profile (Fig. 10). Radiocarbon dating was undertaken to date ancient landslides with poorly expressed features. Analyzed were buried turf, humus, peat and willow branches, which were collected from several pits within an etalon landslide cirque (Fig. 9). Laboratory ^{14}C tests were performed at the Isotope geochemistry and geochronology laboratory of Geological Institute, Russian Academy of Sciences (GIN RAS), Moscow, by Sulerzhitsky and assisted by Kizyakov, Leibman and Zaretskaya (Table 2, Leibman et al. 2000, 2003; Leibman and Kizyakov 2007).

Turf collected in pit 22 (Fig. 11) from depth of 78–81 cm has a ^{14}C age of 2250 ± 100 yr BP (GIN-11300, Table 2). It is the most ancient date obtained at the studied landslide cirque. At the same pit, at 45–64 cm depths, the second horizon of buried soil showed an average ^{14}C age of 1880 ± 120 yr BP (GIN-11299, Table 2). Proximity of the age of this soil to the date obtained at pit 13

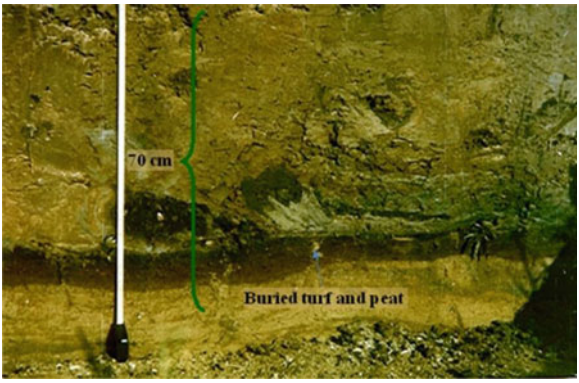

Fig. 10 Organic matter is represented by buried under a landslide body ground cover and peat

Table 2 Results of radiocarbon dating by GIN RAS in a landslide cirque (Fig. 11) (Leibman et al. 2003)

Pit #	Depth, cm	Material	14C age, years BP	Laboratory code
AK9	82–88	Peat	1,060 ± 70	GIN-10314
AK13	40–45	Peat	1,790 ± 140	GIN-10315
AK15	57–67	Peat	1,360 ± 40	GIN-10316
AK16	42–51	Peat	700 ± 40	GIN-10317
AK16	42–51	Wood	330 ± 40	GIN-11298
AK22	45–64	Humus	1,880 ± 120	GIN-11299
AK22	78–81	Humus	2,250 ± 100	GIN-11300
AK23	48–54	Humus	1,000 ± 60	GIN-11301
AK23	63–65	Humus	700 ± 40	GIN-11302

(Fig. 11, 1790 ± 140 yr BP, GIN-10315, Table 2) suggests that a single soil unit was buried by a landslide of the second generation.

During the third stage of the landslide cirque development, the landslide, defined by buried turf discovered at pit 15 (Fig. 11) at depth 60 cm, occurred at 1360 ± 40 yr BP (GIN-10316, Table 2). Two dates were obtained from pit 23 (Fig. 11). The age of the buried humus lenses at depth range of 48–54 cm is 1000 ± 60 yr BP (GIN-11301, Table 2), and the age of the discontinuous turf horizon at depth range of 63–65 cm is 700 ± 40 yr BP (GIN-11302, Table 2). Inversion of dates has been observed at this point where recent organic materials are overlain by ancient deposits. This is explained by a "caterpillar" effect in the frontal zone (Fig. 12). In the immediate proximity, at a depth of about 60 cm, there are soils with dates of 1 360 ± 40 and 700 ± 40 yr BP (Table 2, Fig. 11).

At the foot of the slope, the age of the buried turf was determined to be 700 ± 40 yr BP at pit 16 (GIN-10317). Buried willow branches were collected from the same horizon at the same location, and their age was found to be 330 ± 40 yr BP (GIN-11298).

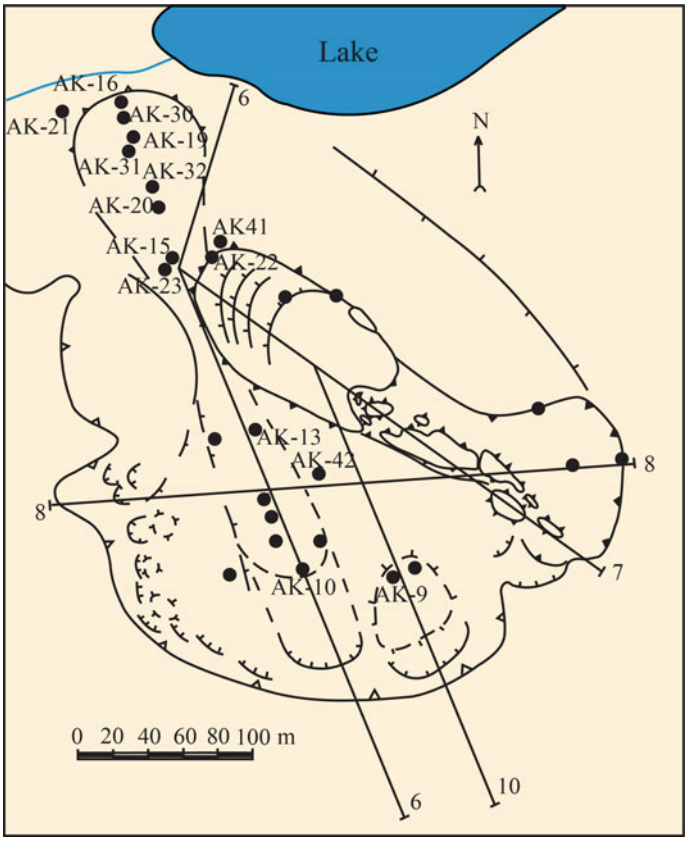

Fig. 11 Schematic map of etalon landslide cirque with radiocarbon dating, dendrochronology, soil and geochemical studies (after Kizyakov 2005)

Fig. 12 The zone in the circle (which is about 20 cm in diameter) is where older soil is resting on top of younger turf

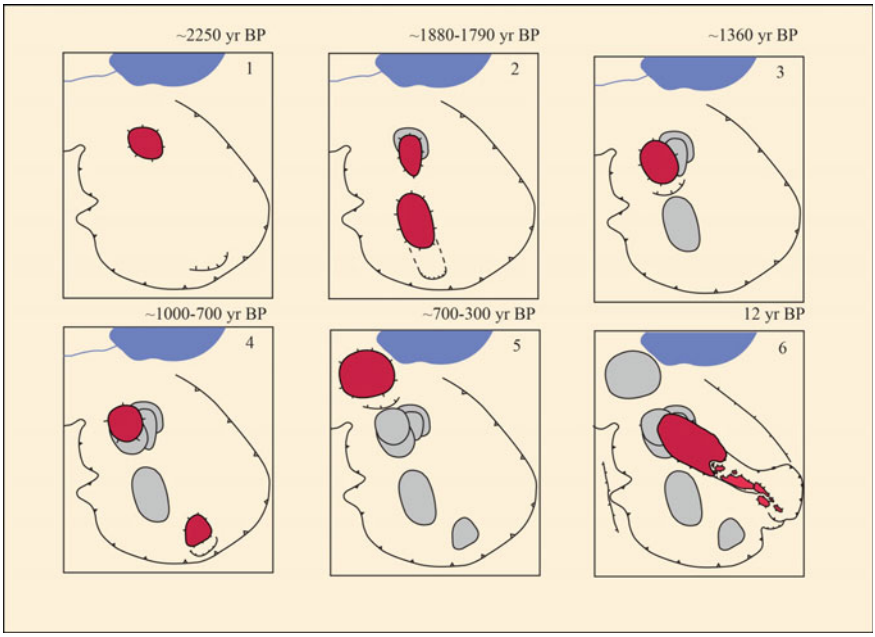

Fig. 13 Possible pattern of the landslide cirque development (after Kizyakov 2005)

This experiment showing the difference in soil-turf and wood dates from the same depth at pit 16 proves the suggestion that it takes at least 330 years for organic material to form in the climatic and landscape conditions of the study area (700 years of average turf age minus 330 years of branches age, and minus maximum 40 years of the willow life span). Finally, the last stage of landslide activity is represented by landslide of the sixth generation, which happened in 1989, and is dated by direct observation (Fig. 13).

5.2 Dendrochronology

It was established through radiocarbon dating that landslides could repeat in the same place after several centuries. Willow shrubs not older than 100 years (maximum 104 year old willow in the area was dated by Gorlanova (2002) (Leibman et al. 2003), therefore, they can't be used to determine the age of older landslides, but they can be used to estimate the impact of landslides from their growth pattern and thus find indication of landslide age between radiocarbon limit and earliest remote-sensing data available. This was determined by analysis of ring width in relation to summer temperature and position on the morphological element of landslide slopes.

The age of willow branch slices collected by the authors, was determined by Gorlanova of the Institute of Ecology of Plants and Animals, Ural Branch of the Russian Academy of Sciences according to the methods developed by (Shiyatov and Gorlanova 1986; Gorlanova 2002).

Study objects were willow shrubs Salix lanata L and S. glauca L, as well as Betula nana L. As root system of the shrubs in permafrost is close to the surface, active-layer detachments allow willows to continue growing in the new place, while detachment and change of the position affects annual rings width and shape.

Samples from recent landslides of known age due to direct observation and interpretation of remote-sensing data allow studying mechanisms of landslide impact on willow annual rings. Samples from ancient landslides can be interpreted using results obtained at the dated landslides (Gorlanova 2002; Leibman et al. 2000, 2003). Thus, the period of possible stresses to which a shrub within a landslide body or near the landslide shear surface was subject would not exceed 100 years, in most cases only 50–80 years. Sampling was undertaken along the transects starting from the stable surface of the hilltop down across the slope (shear surface and landslide body, its front swell), and ends at the undisturbed slope toe. Analyzed were cross-sections of the branches, subterranean stems and tillering nodes at the shrub base. Diagrams of annual growth were built, and cross-dating performed for samples from different parts of one shrub (Gorlanova 2002).

Actually dating young landslides by tree-rings was a pioneer study of Leibman et al. (2000, 2003) and Gorlanova (2002). Examined were 120 cross-sections of 55 willows and dwarf birch shrubs. It was found that ring pattern reflects both favourable and poor conditions for growth depending on the position against the morphological unit of the landslide as well as local features (cracks, folds, drainage or moisturizing). Criteria for landslide dating are shown in Table 3.

It follows from Table 3 that in the shrubs growing on the young landslides (that of 1989) there are sharp changes in the annual growth in the year of the landslide event and the next year, both positive and negative at various parts of the body. Yet it should be noted that landslide activation is linked to warmer and wetter summers which are also favourable for tree-ring growth. Diagram on Fig. 14 reflects the number of shrubs with well developed positive responses (increase in annual growth speed and formation of new sprouts) as well as negative responses (decrease in annual growth speed and mechanical injury of roots and branches). Correlation of the tree-ring growth curves with the normalized summer temperature as well as with the normalized summer precipitation, both equal to the relative difference between the annual and perennial average value during the period of weather observations (Leibman and Egorov 1996), shows the following. Both relatively high summer temperature as well as summer precipitation as a rule are favourable for annual growth speed as can be seen in 1953, 1981 and 1990 (Fig. 14). Yet, the highest number of samples with maximum and minimum growth speed does not correlate with, respectively, the highest and lowest summer temperature and precipitation. For example, many samples with the positive annual growth response belong to 1990, 1981, 1953 and 1970 (Fig. 14). Normalized summer temperature in the same sequence decreases and is less than

Table 3 Criteria for landslide dating by tree-ring method (after Gorlanova 2002)

Tree-ring pattern	Growth controls	Landslide element*	Years (number of samples if more than 1) with observed tree-ring pattern
1. Sharp decrease in annual growth speed and mechanical injury of roots and branches	Changes of soil, hydrology, and irradiation, deformation of a landslide body during movement down slope	A1	1970, 1980, 1988, 1989
		A2	1924, 1953 (2), 1954 (2), 1956, 1982, 1989, 1990 (4)
		B3	1957 (2), 1959, 1965, 1967, 1971 (2), 1977, 1978, 1980 (2), 1981, 1986 (2), 1989 (2), 1990
		C1	1989, 1990
		C3	1952, 1956, 1957 (2), 1964, 1975, 1976, 1977 (2), 1980 (2), 1986, 1987, 1988 (2), 1989 (2)
2. Sharp increase in annual growth speed and formation of new sprouts	Rootage of branches, improvement of soils and water-thermal regime	A1	1957, 1970, 1981
		A2	1922, 1987, 1990 (2)
		B3	1923, 1955, 1960, 1961, 1981 (2), 1990
		C1	1982, 1990
		C3	1925, 1927, 1929, 1953, 1954, 1955, 1956, 1957, 1972, 1981 (2), 1982, 1988, 1989, 1990
3. No response	No relation between the growth conditions and landslide	A1	No
		A2	5
		B3	2
		C1	No
		C3	4

**A1* Stable surface close to the landslide scarp; *A2* The same, far from the landslide scarp; *B3* Re-vegetated surface of the ancient landslide shear surface; *C1* A body of a young landslide; *C3* A body of an ancient landslide

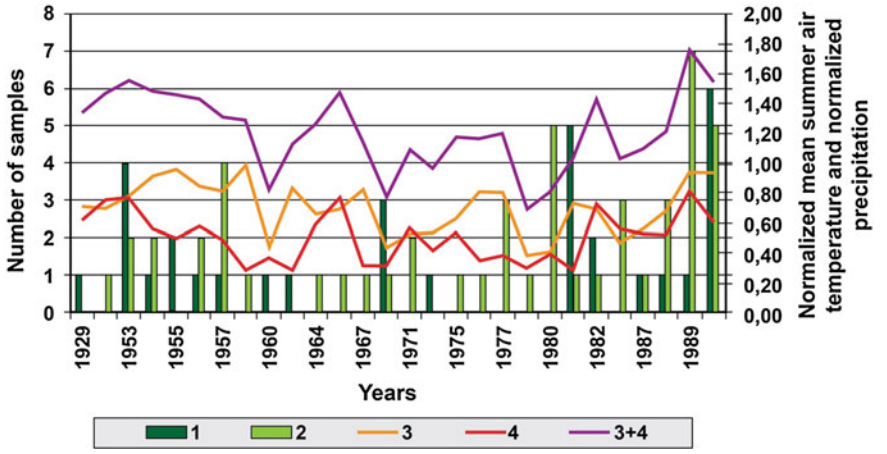

Fig. 14 Relation of tree-ring growth speed at the polygon "Vaskiny Dachi" to the normalized mean summer air temperature in 1929–1990 calculated from Marre-Sale weather station records (only for years with noticeable accretion): **1** samples with increasing accretion; **2** samples with decreasing accretion; **3** normalized to maximal for the period of records mean summer air temperature; **4** the same for summer precipitation; 3+4 warm-wet index

average values: 95, 74, 79 and 45 % of maximum. At the same time, precipitation in the same sequence change as follows: 60, 29, 77 and 32 %, which is much lower than average.

Normalized summer temperature and precipitation were also summarized to obtain "warm-wet" index which was the highest in 1989, the year of extremely high landslide process activity, as well as in 1982, 1965 and 1953. In 1953 there is a high positive response, probably due to just beneficial climate of the summer. There was practically neither positive nor negative response in 1965 and very little in 1982.

An essential number of samples with the negative growth speed is noted in 1989, 1990, 1980 and 1957. These years are characterized by the norm of summer temperature equal to 95, 95, 41, and 82 % respectively (for precipitation 82, 60, 39 and 49 %). Thus, close to maximum summer temperature in 1989–1990, also coinciding with high summer precipitation resulted in decrease of the ring growth speed instead of expected increase, which doubtlessly is a result of hazardous activation of landslide process in 1989.

The tree-ring growth speed analysis shows that in the landslide cirques under study in addition to the known landslide event of 1989 (with positive response in 1990) were earlier events in 1980 (with positive response in 1981). Possibly, the negative response of tree-ring growth speed in relatively warm 1957 was also connected to the landslide activation.

6 Conclusions

Cryogenic landslides are the main relief-forming processes on the Arctic plains of the northern part of West Siberia. Specific landforms of the Central Yamal Peninsula include concave slopes with mosaic vegetative cover represented by various pioneer to mature vegetative communities, patches of high willow shrubs, and heterogeneous mesorelief. These are shown to be landslide cirques formed by series of landslide events during the late Holocene. Buried organic material appears as a mixture of soil, humus, turf, and plant remnants buried by a landslide body and can be dated by radiocarbon test.

Cryogenic landslides are climate-related features, for this reason, they are utilized as indicators of past and modern climate fluctuations. The landslide activation is controlled first by increasing atmospheric precipitation, and second, rise in summer air temperature.

Two main types of landslide processes are subdivided according to the mechanism and geomorphic effect: (1) cryogenic translational slides (close term: active-layer detachments) which are caused by thawing of the ice-rich transient layer at the active-layer base triggered by heavy rain events supported by warm summer; (2) cryogenic earth/mud flows (close term: retrogressive thaw slumps) caused by melting of the massive ground ice of various origin enclosed in perennially frozen deposits and triggered by high summer temperature.

Main landforms resulting from multiple landslide events at the early stages of development are thermodenudation cirques, turning into landslide cirques at the later stages.

The time span separating landslide events ranges from 350 to 500 years. This time is needed for a slope to prepare for the next landslide session: to restore the vegetative cover, fill and flatten the thermoerosion gullies, and form an icy transient layer at the active-layer base. The closest feasible for landslide activation climatic situation (extreme precipitation and air temperature) causes the next landslide event on a “ready to fail” slope.

Research in key landslide cirque allocated 7 cycles of cryogenic landslide activities defined using the radiocarbon method of absolute dating, direct observation, and based on the assumptions on the duration of the cycle. Dates of landslide events in the key landslide cirque are approximately—250 BC, 210, 640, 1000, 1300, 1700 and 1989 AD. With an accuracy exceeding that of the accuracy of radiocarbon dating, these dates coincide with the years characterized by warm summers as determined using dendrochronologic analysis. Periods of activation are separated by periods of relative stability lasting 290–460 years needed to recover the stress state of slopes and terrain conditions favourable for landslide process of CTS type. These conditions include formation of dense vegetative canopy, cryogenically-transformed (loose at the top and bottom and compact in the middle) slope deposits, flattened concave surface without marked drainage pattern, then the slope is ready to respond to the proper climatic conditions, such as several years of cooling and reducing the active-layer depth (to form icy transient layer),

consequent warm summer (to thaw the transient layer), and high summer precipitation (to dramatically rise pore pressure within the active layer).

Ancient landslides with fully restored vegetation cover are probably at least 300 years old and some formed at least ~2000 years ago.

Concave landforms develop under the cryogenic landslides depending on climatic fluctuations through alternation of the active and passive phases. With these phases as a background, directional development of the original surface is noted into thermocirque and consequently into a landslide cirque.

Climate warming is followed by ground temperature rise and thus, the southern limits of CTL occurrence should probably move northward where conditions for the ice formation at the active-layer base still preserve. As to CEF/CMF, their northern limits probably shift further northward due to active-layer thickening towards the deep-seated massive ice bodies.

Prediction of the landslide activation due to climate change is a complicated multi-factor analysis and can't be reduced to the climate warming model.

Acknowledgments This study was supported by the Interdisciplinary Integration grants No. 122 and No. 144 of the SB RAS, and Science School Grant No. 5582.2012.5 to the Earth Cryosphere Institute SB RAS.

References

Ananieva GV (1984) Slope processes as indicators of cryogenic construction of permafrost on locations with massive ground ice distribution. In: Study and prediction of cryogenic physical-geological processes. VSEGINGEO Publisher, Moscow, pp 12–17 (in Russian)

Bolikhovsky VF, Kuntsel VV (1990) Development of landslides in permafrost of West Siberian tundra. Inzhenernaya Geologiya (Eng Geol) 1:65–70 (in Russian)

Burn CR, Lewkowicz A (1990) Retrogressive thaw slumps. Can Geogr 34(3):273–276

Ermokhina KA (2009) Phyto-indication of exogenous processes in the tundras of central Yamal. Candidate dissertation, Moscow University Press, Moscow, Russia, p 18 (in Russian)

French HM (1976) The periglacial environment. Longman, London, p 309

French HM (2007) The periglacial environment, 3rd edn. Wiley & Sons, New York, p 458

Gorlanova LA (2002) Methods of dendrochronologic dating of landslide events. Abstracts of international conference "Extremal cryospheric phenomena: fundamental and applied aspects". Pushchino, Russia, Scientific Council on Earth Cryology RAS, pp 148–149

Harris C, Lewkowicz AG (2000) An analysis of the stability of thawing slopes, Ellesmere Island, Nunavut, Canada. Can Geotech J 37(2):449–462

Kaplina TN (1965) Cryogenic slope processes. Nauka Publisher, Moscow, p 287 (in Russian)

Khomutov AV (2010) Relation of natural cryogenic processes to the dynamics of tundra landscapes, case study in subzone of typical tundra of the Kara region. Candidate dissertation, Earth Cryosphere Institute SB RAS, Tyumen, p 18 (in Russian)

Khomutov AV (2012) Assessment of landslide geohazards in typical tundra of central Yamal. In: Melnikov VP, Drozdov DS, Romanovsky VE (eds) Proceedings of the 10th international conference on permafrost. Salekhard, 24–29 June 2012, 2:157–162

Khomutov AV, Leibman MO (2008) Landscape factors of thermodenudation rate at the Yugorsky Peninsula coast. Kriosfera Zemli (The Earth Cryosphere) XII(4):24–35 (in Russian)

Kizyakov AI (2005) Dynamics of thermodenudation processes in the area of tabular ground ice distribution. Candidate dissertation, Moscow University Press, Moscow, p 26 (in Russian)
Kizyakov AI, Leibman MO, Perednya DD (2006) Destructive relief-forming cryogenic processes at the coasts of the Arctic plains with tabular ground ice. Kriosfera Zemli (The Earth Cryosphere) X(2):79–89 (in Russian)
Kokelj SV, Lewkowicz AG (1998) Long-term influence of active-layer detachment sliding on permafrost slope hydrology. Hot weather Creek Ellesmere Island Canada. In: Proceedings of the 7th international permafrost conference. Yellowknife, 23–27 June 1998, pp 583–589
Leibman MO (1994) Cryogenic landslides and their interaction with linear constructions on Yamal Peninsula Russia. In: Smith DW, Sego DC (eds) Proceedings of the 7th international cold regions engineering specialty conference. Edmonton, pp 865–869
Leibman MO (1995) Preliminary results of cryogenic landslides study on Yamal Peninsula Russia. Permafrost Periglac Process 6(3):259–264
Leibman MO (2004a) Mechanisms and stages of slope cryogenic process formation in the western sector of Russian Arctic In Relief forming processes: theory, practice, research methods. Materials of XXVIII Plenum of Geomorphic Commission. Novosibirsk, pp 160–162 (in Russian)
Leibman MO (2004b) Mechanisms of formation for cryogenic translational landslides and conditions for their indication by high willow shrubs in central Yamal. Transactions of the Moscow Center of Russian geographical society. Biogeography, 12 RASHN. Moscow, pp 89–94 (in Russian)
Leibman MO, Egorov IP (1996) Climatic and environmental controls of cryogenic landslides, Yamal, Russia. In: Senneset K (ed) Proceedings of the 7th international symposium on landslides. Balkema, Trondheim, 1941–1946
Leibman MO, Kizyakov AI (2007) Cryogenic landslides of the Yamal and Yugorsky Peninsulas. Earth Cryosphere Institute SB RAS, Moscow-Tyumen, p 206 (in Russian)
Leibman MO, Streletskaya ID (1997) Land-slide induced changes in the chemical composition of active layer soils and surface-water run-off Yamal Peninsula Russia. In: Iskandar IK, Wright EA, Radke JK, Sharratt BS, Groenevelt PH, Hinzman LD (eds) Proceedings of the international symposium on physics chemistry and ecology of seasonally frozen soils. Fairbanks. CRREL Special Report 97-10, CRREL, Hanover, 10–12 June 1997, pp 120–126
Leibman MO, Lakhtina OV, Miklyaev SM, Titova IR (1991) Pattern of relief-forming cryogenic process distribution at western Yamal Peninsula. In: Denudation in cryolithozone. Nauka Publisher, Moscow, pp 92–99 (in Russian)
Leibman MO, Rivkin FM, Streletskaya ID (1993a) Chemical and physical features of the active layer as related to landslides on Yamal Peninsula. In: Post-seminar proceedings. Joint Russian-American seminar on cryopedology and global change. Pushchino, pp 257–262
Leibman MO, Rivkin FM, Saveliev VS (1993b) Hydrogeological aspects of cryogenic slides on the Yamal Peninsula. In: Proceedings of the 7th international conference on permafrost. Beijing 5–9 July 1993, 1:380–382
Leibman MO, Streletskaya ID, Konyakhin MA (1997) Assessment of surface dynamics at Bovanenkovo gas field (Central Yamal Peninsula) during the period 1949 to 1990. Geomorfologiya (Geomorphol) 2:45–48 (in Russian)
Leibman MO, Archegova IB, Gorlanova LA, Kizyakov AI (2000) Stages of cryogenic landslides on Yugorsky and Yamal Peninsulas. Kriosfera Zemli (The Earth Cryosphere) IV(4):67–75 (in Russian)
Leibman MO, Kizyakov AI, Sulerzhitsky LD, Zaretskaya NE (2003) Dynamics of the landslide slopes and mechanism of their development on Yamal Peninsula Russia Permafrost. In: Phillips M, Springman SM, Arenson LU (eds) Proceedings of the 8th international conference on permafrost. Zurich, Balkema, Lisse, 21–25 July 2003. pp 651–656
Lewkowicz AG (1988) Slope processes. In: Clark MJ (ed) Advances in periglacial geomorphology. Wiley, New York, pp 325–368
Lewkowicz AG (1990) Morphology, frequency and magnitude of active-layer detachment slides, Fosheim Peninsula, Ellesmere Island N W T. In: Burgess MM, Harry DG, Sego DC (eds)

Proceedings of the 5th Canadian permafrost conference. Quebec, Canada, Laval University, Quebec, Collection Nordicana, June 1990, 54:111–118

Poznanin VL, Baranov AV (1999) Cryogenic slope processes. In: Erosion processes of Central Yamal. St-Petersburg, pp 119–132 (in Russian)

Rebristaya OV, Khitun OV, Chernyadieva IV, Leibman MO (1995) Dynamics of vegetation on cryogenic landslides in the central Yamal Peninsula. Botanicheskiy Zhurnal (Bot J) 80(4): 31–48 (in Russian)

Romanenko FA (1997) Formation of the lake basins on Siberian Arctic plains. Candidate dissertation, Moscow State University, Moscow, p 18 (in Russian)

Schuster RL, Krizek RJ (1978) Landslides: analysis and control. National Academy of Sciences, Washington, p 234

Shiyatov SG Gorlanova LA (1986) Pathologic structures in the timber of Siberian larch. In: Botanical research in the Urals (information materials). Sverdlovsk, p 71 (in Russian)

Shur YL (1988) Upper horizon of permafrost and thermokarst. Nauka Publisher, Siberian Branch, Novosibirsk, p 213

Ukraintseva NG, Leibman MO (2000) Productivity of willow-shrub tundra in connection with landslide activity. In: 30th Arctic workshop, INSTAAR. University of Colorado, Boulder CO USA, 15–19 March 2000, pp 150–152

Ukraintseva NG, Leibman MO (2007) The effect of cryogenic landslides (active-layer detachments) on fertility of tundra soils on Yamal Peninsula Russia. Conference presentations from the 1st North American Landslide conference Vail Colorado 3–8 June 2007. In: Schaefer, Schuster, Turner (eds) Landslides/slope instability AEG Special Publication, 23 Omnipress (Conference CDROM), pp 1605–1615

Ukraintseva NG, Shuvalova EM, Vasiliev AA (1992) Estimation of potential slope processes hazard within the territory of Bovanenkovo gas field. In: Methods of cryogenic processes study. VSEGINGEO Publisher, Moscow, pp 109–113 (in Russian)

Ukraintseva NG, Leibman MO, Sreletskaya ID (2000) Peculiarities of landslide process in saline frozen deposits of Central Yamal Russia. In: Bromhead E (ed) Proceedings of the 8th international symposium on landslides: landslides in research theory and practice. Cardiff UK 26–30 June 2000, Thomas Telford, London, 3:1495–1500

Ukraintseva NG, Streletskaya ID, Ermokhina KA, Yermakov SYu (2003) Geochemical properties of plant-soil-permafrost system at landslide slopes Yamal Russia. In: Phillips M, Springman SM, Arenson LU (eds) Proceedings of the 8th international conference on permafrost. Zurich, Switzerland, 21–25 July 2003, Balkema, Rotterdam, 2:1149–1154

Voskresenskiy KS (1999) Landslides-flows and thermokarst. In: Erosion processes of central Yamal. St-Petersburg, pp 33–139 (in Russian)

Based on the Drilling and High-density Resistivity Method to Research Landslide in the Permafrost Regions

Zhaoguang Hu, Wei Shan and Hua Jiang

Abstract In recent years, permafrost in north-eastern part of China is being severely degraded. Bei'an to Heihe expressway passed through the north-western part of the Lesser Khingan Range region. Stability of embankment in this region is being seriously affected landslide occurrence and the degradation of permafrosts. The expressway utilizes the original second-class highway to widen and expand, being restricted by the original location of the old road, some sections of new subgrade are located at the toe of the landslides. The formation and development of the landslide at K178+530 section of the expressway is mainly affected by the topography, engineering geology, hydrology and climatic influences. Topography, loose stratum, active groundwater, intense freeze–thaw erosion and human engineering activities are inherent conditions and contributing factors affecting the stability of the slope. In order to study and analyze the landslide, geological drilling exploration and high-density resistivity method were employed to understand the failure mechanism of the landslide along the expressway. The results show that high-density resistivity technology and drilling exploration gave similar result near the landslide sliding surface; there is a significant difference between inside and outside the landslide soil resistivity values. When the landslide had not yet formed, the landslide resistivity value had no obvious stratification, and had no saltation phenomenon of the resistivity. After the landslide began to move, the resistivity value at the sliding surface location showed significant stratification, and the resistivity values of its upper and lower location were obviously different.

Keywords Landslide · Formation mechanism · Drilling exploration · High-density resistivity method

Z. Hu · W. Shan (✉) · H. Jiang
Northeast Forestry University, Harbin 150040, China
e-mail: shanwei456@163.com

W. Shan et al. (eds.), *Landslides in Cold Regions in the Context of Climate Change*, Environmental Science and Engineering, DOI: 10.1007/978-3-319-00867-7_12,

1 Foreword

Landslide is a natural phenomenon that, rock and soil on the slope, affected by river scour, groundwater activity, earthquake, artificial cutting slope and other factors, under the action of gravity, slide down along a weak plane or zone (Gu et al. 2009; He et al. 1991). Landslides are often triggered on high grade highways constructed in mountainous areas, due the effect of geologic, geomorphologic, hydrologic and climatic conditions of the region (Hu et al. 2011). The occurrence of landslides often affect local and interstate traffic, disrupt movement of vehicles on highways; large-scale landslide block rivers, destroy highways and factories and cause huge economic loss on buildings and traffic facilities in mountain areas (Li et al. 2003; Liu et al. 2007; Hu and Wang 2010).

Only a few scientific literatures exist on landslides in cold regions of the Lesser Khingan range of Heilongjiang province. The study area is located in the high latitudes permafrost regions; ground slope in the landslide area is relatively low (Yang et al. 2010; Hu et al. 2005; Duan 1999). Landslides of this area have distinct failure mechanism and motion characteristics that are different from landslides of other areas.

This study employs drilling exploration and high-density resistivity methods to analyze and understand the failure mechanism of landslides in the area. The study area is located in K178+530 section of the Bei'an-Heihe expressway, in the Lesser Khingan range of the central region, in the high latitude permafrost degradation of China. We used drilling exploration to survey the geologic characteristics of the landslide, and used high-density resistivity method to detect the resistivity of the landslide. We also analyzed variations in geologic characteristics and the internal physical properties of the landslide materials.

2 General Situation of the Study Area

2.1 Geographical Conditions of the Study Area

Figure 1 shows topographic base map of the study area. It is located in the central region of the Lesser Khingan Range, in the high latitude permafrost degradation of China. The climate of the area belongs to continental monsoon, with warm spring, relatively humid and rainy summer periods, cold autumn and long winter periods. Average annual temperature is −0.6 °C, the lowest temperature is about −48.1 °C while the highest temperature is 35.2 °C; frost free period lasts for 90–125 days. Average annual precipitation ranges between 530 and 552 mm with peak rainfall period of July to September accounting for about 61 to 67 % of total annual precipitation. The ground surface of the area forms seasonal frozen soil. The time for the ground to reach maximum frozen depth is usually around May, and the maximum seasonal freezing depth ranges from 2.26 to 2.67 m (Fig. 2)

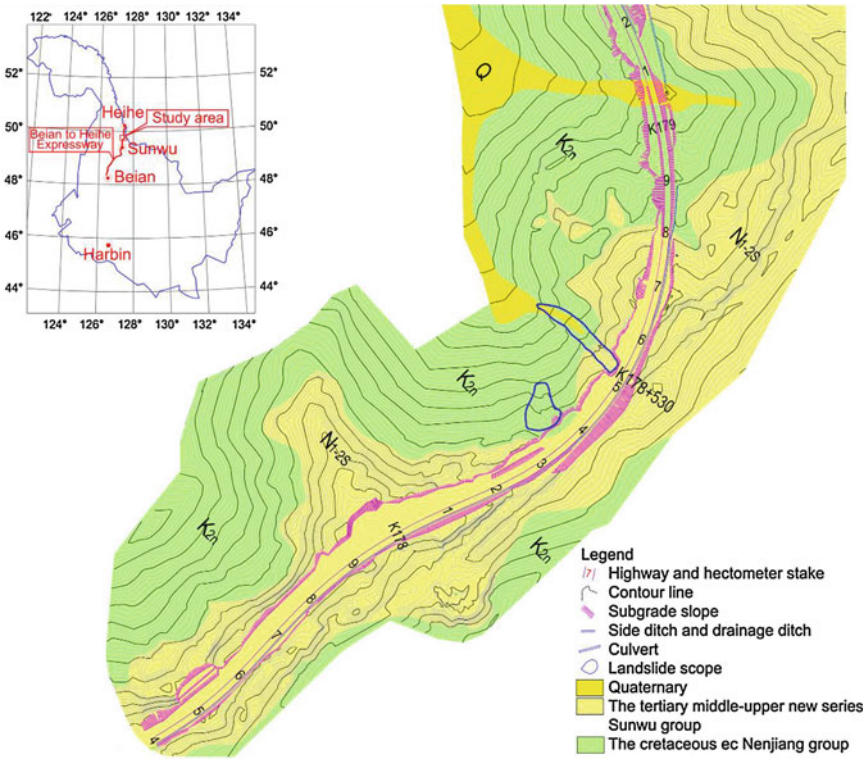

Fig. 1 K178+530 section geographical position

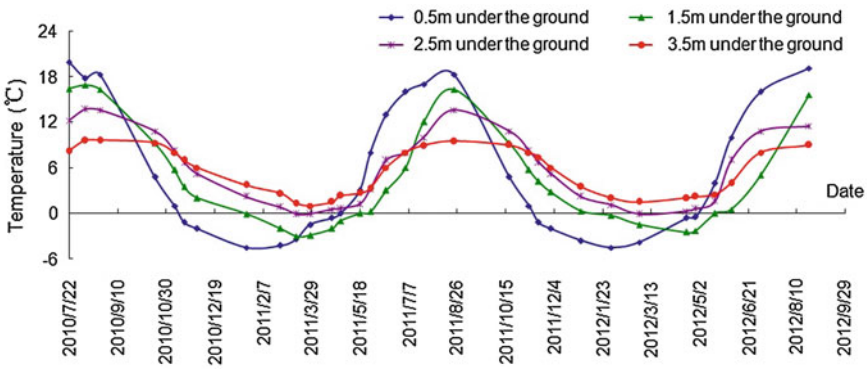

Fig. 2 The temperature curve of K178+530 section

K178+530 landslide is located on the left side of the highway embankment, as shown in Fig. 3. Relict soil material and sub-grade filling soil slide along the gully, The 178+530 landslide has a tongue-shaped structure, with average width of

Fig. 3 K178+530 landslide photo

20–30 m, covering an area of about 5,000 m^2. The landslide has total horizontal distance of about 200 m and maximum toe and rear edge elevation of approximately 254 m and 285 m, respectively.

2.2 Study Area Engineering Geological Conditions

Drilling exploration was carried out in the study area to understand the internal geotechnical condition of the landslide. Four exploratory holes were drilled in the area at depth range of 14–26 m; the drill holes arrangement are shown in Fig. 4.

The stratigraphic profile of the study area shows that the area is underlain by loose Quaternary sediments, Tertiary pebbly sandstone, and Cretaceous mudstone and sandstone. The geologic profile of the study area is shown Fig. 5. Subgrade soil: yellow and very wet, that is mainly loose hybrid material including Tertiary pebbly sandstone, Cretaceous mudstone and sandy mudstone, it is loose when dry, and soft plastic once saturated. Clay: yellow, soft and plasticity, dry strength and large toughness. Silty clay unit is located in the depth of 1.5–3.8 m on upper sector of landslide, and in the depth of 0–6.7 m on middle and lower sector of landslide, and there are more than one sand sandwich layers in silty clay layer, single-layer thickness is about 1–10 cm, which greatly increases the ability of water permeability. Tertiary pebbly sandstone: located in the depth of 3.8–4.5 m on the upper sector of the landslide, and its component including long stone and sand mineral, weathered, slightly wet, and minus cement with loose sand and good gradation, the ability of water permeability is very good. Weathered siltstone: yellow, located in the depth of 4.5–14.3 m in the upper section of the landslide. Sandy structure,

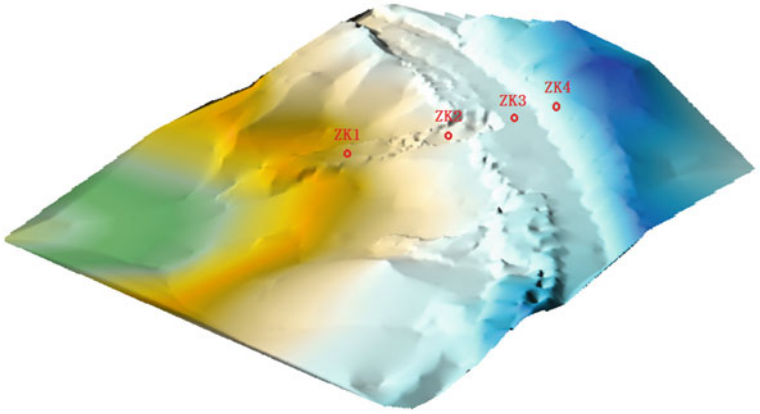

Fig. 4 Drilling holes arrangement of K178+530 section

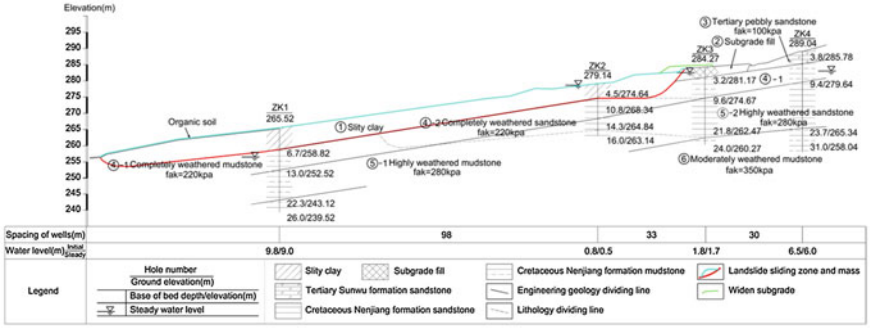

Fig. 5 Geological profile of K178+530 section

bedding construction of low permeability. Weathered mudstone: yellow or black-grey, muddy structure and layered structure, poor water resistance to soften, and low permeability. Strongly weathered mudstone: black-grey, muddy structure and layered structure,rocks in unconsolidated. Medium weathered mudstone: brown and black-grey muddy structure and layered structure.

2.3 Landslide Formation Mechanism

The formation and development of the K178+530 section landslide is mainly affected by topography, engineering geology, hydrology and climatic characteristics. Geographical controls, active groundwater, intense freeze–thaw erosion and human engineering activities are some of the inherent factors that contributed to the occurrence of the landslide (Li et al. 2002; Zhu et al. 2007).

The landslide is a superficial and translational landslide of high motion velocity common in permafrost regions. The landslide is usually triggered in spring season during snow melting and early rainy seasons. Tympanic cracks on the landslide are beneficial to permeate and stockpile. High permeable, surface soil grit layer and silty clay in weathered sand provides passage for water infiltration. The infiltration capacity in the lower mudstone and siltstone was very small, and formed water-resisting layer. Rainfall, snowmelt water, fissure water and thawed frozen soil which produced water were cut off by frozen soil and impervious layer in the process of infiltration. This is the main cause that triggers landslides in this area. In late July 2010, the landslide started to slide.

Freezing and thawing have far-reaching consequences on the landslide, exhibiting intermittent slide and bench slope, and there are drumlin fields on the landslide slope.

Slip surface of the upper section is located in the depth of 4.5 m, located at the interface of gravel sand and siltstone, the soil under sliding surface is siltstone of weak penetrating power. Slip surface of the middle and lower sectors is in the depth of 6.5 m, located at the interface of silty clay and mudstone, the soil under sliding surface is mudstone of weak penetrating power.

3 Based on High-Density Resistivity Method for Surveying Landslide

3.1 High-Density Resistivity Method Measuring Line Layout

During the application of high density resistivity method on K178+530 section, we used two-dimensional high-density resistivity method inversion software to inverse least square method. Inversion of the program used is based on least square method which is based on quasi-Newton algorithms for nonlinear optimization, and module width is set to one-second unit electrode spacing to improve monitoring precision. To ensure depth and accuracy, the unit electrode spacing is 3.0 m in the test while the sounding is about 30 m.

At the K178+530 landslide section, as the centre of the landslide, nine high density resistivity method survey lines were emplaced, as shown in Fig. 6.

Along the slope tendency laying a total of 5 survey lines, which was named as the longitudinal 1, 2, 3, 4 and 5 respectively, electrodes numbers arrangement as follows: from medial divider of road to leading-edge of landslide orientation layout 1–60 in turn. The position of longitudinal 1 and 5 survey lines are 5 m out of both sides of the landslide; Longitudinal 2 and 4 are on the landslide, at the distance of about 2.5 m from the edge of the landslide respectively. Longitudinal 3 is on the landslide, located in the middle of landslide. We laid 4 survey lines perpendicular the direction of landslide, which were named as the transverse 1, 2, 3 and 4. and the location are 30, 90, 110 and 140 m away from the trailing edges of

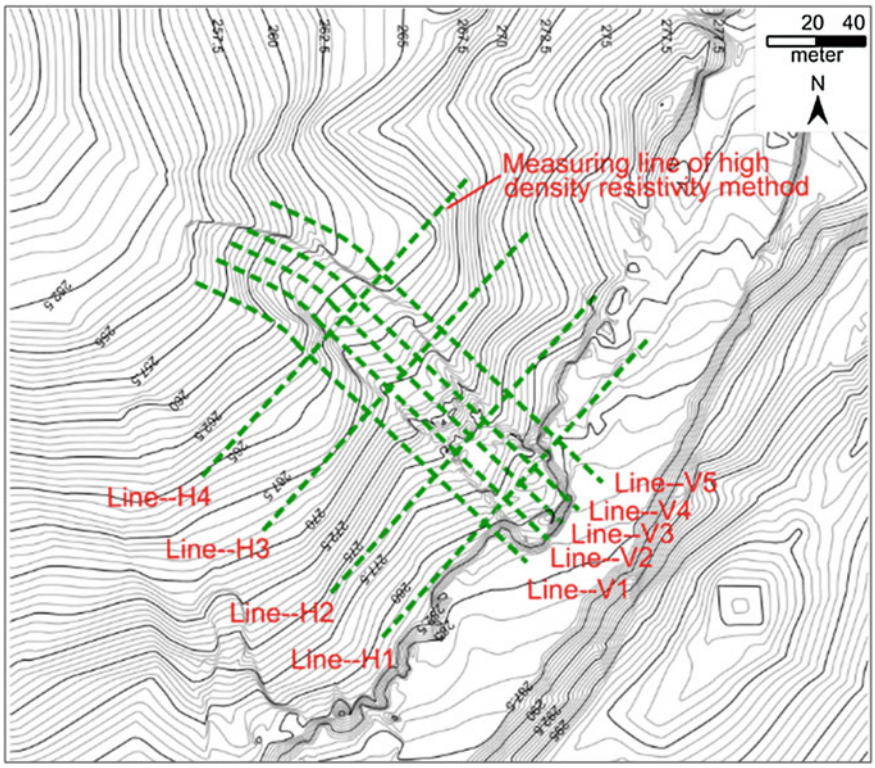

Fig. 6 The high density resistivity measuring line

landslide, electrode codes number 1–60 are decorated from left to right. During the test procedure, Winner arrangement method is all used. Five Detection times of each survey line, the date is June 1st, 2010, September 10th, 2010, November 1st, 2010, and June 10th, 2011, respectively.

3.2 Contrast Resistivity Value of Different Positions on the Landslide

Figure 7 showed the resistivity inversion images along the centre of landslide soil (measuring line V3). The measuring line is from the median strip going through the landslide rear edge, drilling ZK2 and drilling ZK1 location and stretching into 177 m along landslide to where is 32 m distance from the forefront of the landslide. The distance of the landslide back edge, drilling ZK2 and drilling ZK1 location from the first electrode respectively are 9, 42, and 96 m. From the figure, we can understand that the resistivity of landslide soil layered apparently.

Drilling 1 position is far from the first electrode 96 m. Depth 0–2.1 m is silty clay, which containing about 15 % of the organic matter as grass roots, and resistivity value is 20–67 Ω · m; Depth 2.1–6.7 meters is silty clay, there are weathered sand sandwich on the local scale, and resistivity value is 15–32 Ω · m; Depth 6.7–8.0 meters is mudstone, and its structure is pieces, and resistivity value is 46–54 Ω · m; Depth 8.0–26 m is gray mudstone, where is close to ground water level or below ground water level in the underground, and resistivity value smaller is 10–35 Ω · m. In 0–2.1 m depth is silty clay that contains a lot of grassroots, water down the plant roots to infiltrate is easy; Below 6.7 meters is mudstone, the permeability coefficient is small, water is difficult to infiltrate, forming water-resisting layer. Water is easy to gather in the top surface of mudstone layer, mudstone in water softening disintegration and easy to form the sliding surface. Due to the local weathered sand sandwich, the silty clay in 2.1–6.7 m depth can make water infiltrate easily. That site's resistivity value was as shown Figs. 7 and 8.

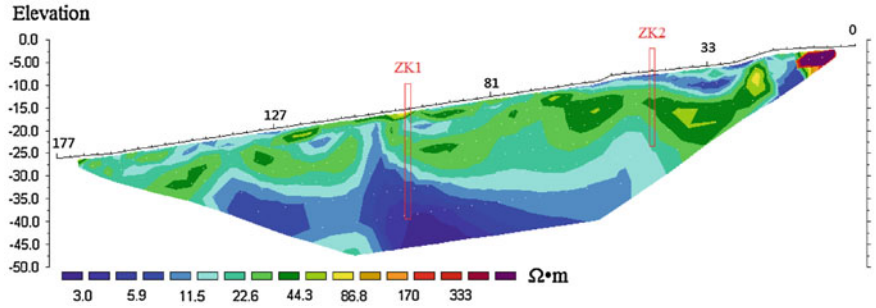

Fig. 7 The inversion images of landslide soil resistivity on September 10, 2010

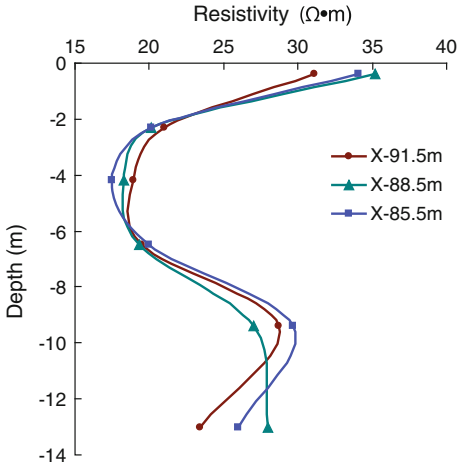

Fig. 8 Resistivity curve of drilling 1 position

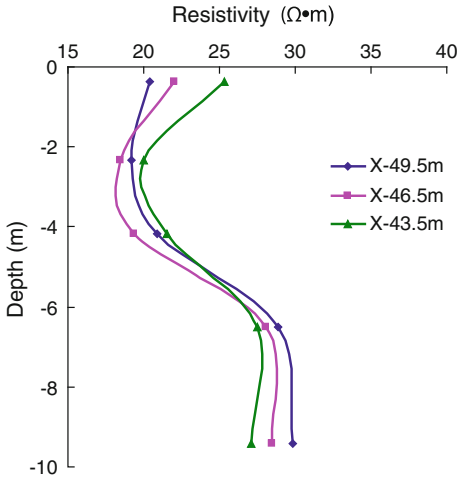

Fig. 9 Resistivity curve of drilling 2 position

Drilling 2 position distance the first electrode of 42 m, in 0–4.5 m depth, resistivity value was 10–27 Ω · m, the surface layer road building abandon soil give priority to silty clay (Depth 0 ~ 3.8 meters), resistivity value is 15–27 Ω · m, resistivity value of sand gravel (Depth 3.8–4.5 m) is 10–22 Ω · m. Depth 4.5–9.7 m is siltstone, and resistivity value is 25–54 Ω · m. Depth 9.7–14.6 meters is sandstone, and resistivity value is 21–43 Ω · m; In the 4.5 meters, the position of sand gravel and siltstone handover, the resistivity apparent stratification. Depth 0–4.5 m, the soil is good permeability, water infiltrates easily; Below 4.5 m is siltstone, particles smaller and seepage ability is poor, forming water-resisting layer. The soil infiltration to 4.5 m depth location is easy to gather and form the sliding surface. These resistivity values were shown as Figs. 7 and 9.

The resistivity value at the slip surface location showed significant stratification, and the resistivity values of its upper and lower were more obvious differences. According to the typical characteristic of the slip surface, we can infer the position of sliding surface as shown in Fig. 10.

According to the mutations and layering of resistivity value at landslide position, we concluded the transverse sliding surfaces position of landslide, as shown in Figs. 11 and 12, there were resistivity images of measuring line H1 and the measuring line H2 on September 10, 2010. The shape of Landslide was approximately circular arc or inverted trapezoidal. The place near the central position of landslide sliding surface was deepest. They were 4.5 and 6.5 m depth. The position both walls of landslide was the shallowest, about 1–1.5 m depth.

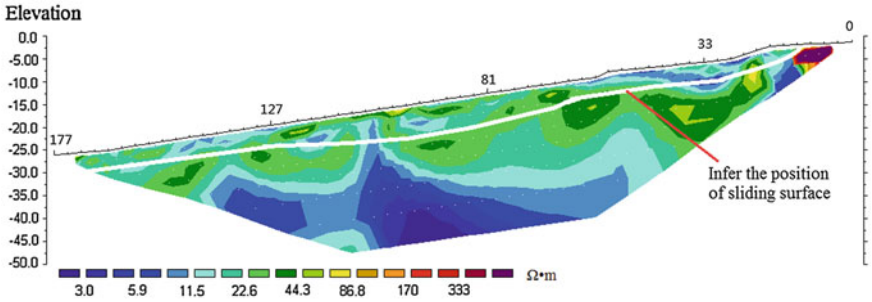

Fig. 10 Infer the position of sliding surface of Line-V_3

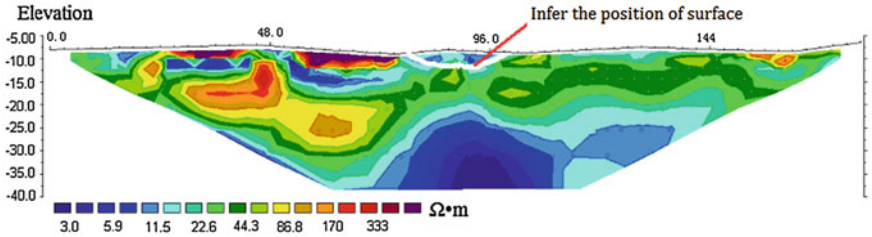

Fig. 11 Infer the position of sliding surface of Line-H_1

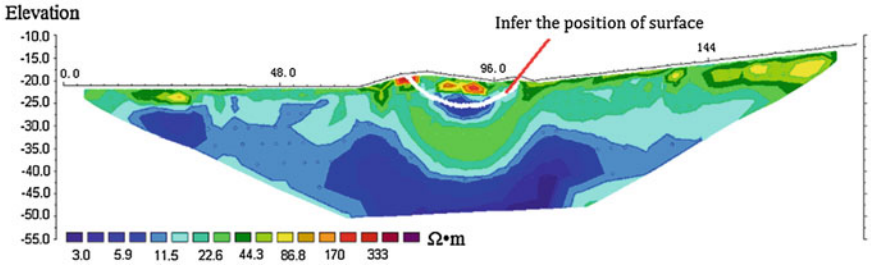

Fig. 12 Infer the position of sliding surface of Line-H_2

3.3 Contrast on Soil Resistivity Value in and out of the Landslide

From landslide rear edge 90 m position, perpendicular to the landslide line (the measuring line H2) as an example, we contrasted on soil resistivity value in and out of the landslide. Figure 13 was resistivity image of measuring line2 on November 1 2010. From the figure we could know that resistivity value image out

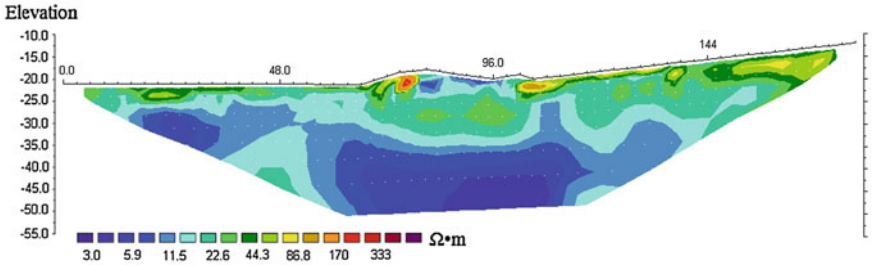

Fig. 13 The inversion images of landslide soil resistivity of Line-H_2 on November 1 2010

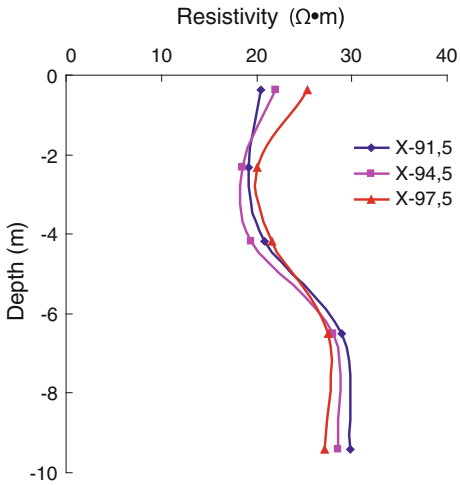

Fig. 14 Soil resistivity curve in landslide

of the landslide only appeared higher resistivity in the surface, resistivity basically presented decreasing along with the depth. The resistivity values in and out of landslide soil were obviously differences. There were mutations and layered resistivity values in sliding surface. These resistivity values in up and down position of soil layers have obvious difference.

Figure 14 was soil resistivity curve in landslide and Fig. 15 was soil resistivity curve out of landslide. Both resistivity value curve of difference characteristics showed that the resistivity in and out of landslide had obviously difference.

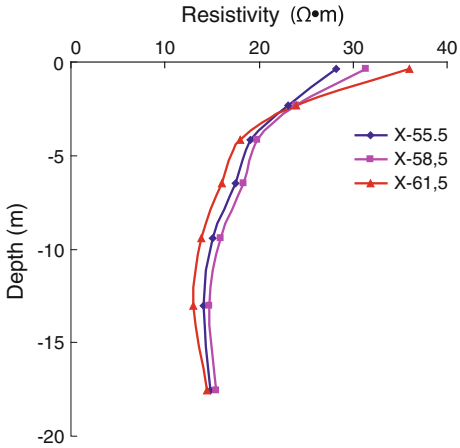

Fig. 15 Soil resistivity curve outside landslide

4 Conclusions

This paper combines drilling exploration and high density resistivity survey method to study the failure mechanism and geologic characteristics of the K178+530 landslide. Results and conclusions drawn from the investigations are summarized as follows:

1. The landslide is a superficial and translational landslide of high motion velocity, sometimes common in the permafrost region. Material of the sliding surface is composed of silty clay, which is loose and friable when dry, soft and plastic; snowmelt water, rainwater and fissure water act as lubricating agents for the landslide; irregular cracks and fractures on the slope enhances atmospheric precipitation pool in the landslide sediments. High permeability of the landslide materials provide easy infiltration of run-off water into the subsurface; mudstone and sandstone with low permeability form aquifuge while silty clay layer above the aquifuge influenced by infiltrated water are easily saturated, forming rupture surface. Freezing and thawing have far-reaching consequences on the landslide, exhibiting intermittent slide and bench slope, and there are drumlin structures on the landslide slope.
2. Resistivity values of the soil outside the landslide are high near the upper part of the subsurface and gradually decreases with increase in depth. In the landslide sliding surface location, resistivity rendering mutation hierarchies, it is much obvious different between upper and lower soil resistivity values change. According to the characteristics of this anomaly mutation, we can conduct the differential sliding surface position of feature flags in practice. Using the high-density resistivity method to survey the landslide and its surrounding, accurately to detect the landslide resistivity value at different locations, according to

characteristic of resistivity value, and combined with drilling results, to determine the position of sliding surface: at rear edge, the position of sliding surface was at the depth of 3.2 m apart from the ground; at 30 m apart from rear edge, sliding surface was at the depth of 4.5 meters; at the middle landslide, sliding surface was at the depth of 6.5 meters; near the landslide toe, sliding surface was at the depth of 4 m, at toe position, sliding surface was at the depth of 2.5 m.

3. The high-density resistivity technology and drilling exploration come to the same result at the position of the landslide sliding surface. It shows that high-density resistivity technology is a quick, economic and reliable test method for subsurface evaluation of landslides. It can quickly and correctly measure the depth and location of the sliding surface of landslides when high-density resistivity technology and the drilling exploration are used together, it can prove correctly reference to linear engineering positioning and the relevant project measure.

Acknowledgments This work was financially supported by Heilongjiang Communications Department project and subtopic of the western communication science and technology project "Study on Sub-grade Stability Controlling Technology of Expressway Expansion Project Permafrost Melt and Landslides Sections".

References

Duan YH (1999) Basic characters of geo-hazards and its development trend in China. Quat Sci 19(3):208–216

Gu TF, Wang JD, Lu X, Meng YL (2009) Characteristics and stability analysis of accumulations landslide No.3 in Tuoba of Southeast Tibet. J Nat Dis

He YX (1991) Application of D.C. Electric Sounding for the Permafrost Exploration along Xinjiang-Xizang Highway. J Glaciology Geocryology

Hu ZG, Shan W (2011) Application of geological drilling combined with high-density resistance in Island structure permafrost survey. The International Conference on Electronics, Communications and Control (ICECC2011)

Hu RL, Wang SS (2010) Main feature and identification method of sliding-surfaces in soil and rock slopes. J Eng Geol 18(1):35–40

Hu XW, Tang HM, Liu YR (2005) Verificatio verification of transfer coefficient method applied to landslide stability analysis by physical model test. Rock Soil Mech 26(1):63–66

Li YH, Zhang XY, Cui ZJ et al (2002) Periodic coupling of debris flow active periods and climate periods during Quaternary. Quat Sci 22(4):340–347

Li TL, Zhao JL, Li P (2003) Analysis on the characteristics and stability of the No. 2 Landslide of 102 Landslide Group on Sichuan-Tibet Highway. J Catastrophol

Liu LH, Zhu DY, Liu DF (2007) Discussion on multiple solutions of safety factor of a slope. Rock Soil Mech 28(8):1661–1664

Yang T, Zhou DP, Ma HM et al (2010) Point safety factor method for stability analysis of landslide. Rock Soil Mech 31(3):971–975

Zhu YS, Li HL, Cao NE et al (2007) Finite element method research on road slide stability analysis. J Highway Trans Res Develop 24(4):39–42

The Use of Radar Interferometry in Landslide Monitoring

Filippo Catani, Paolo Canuti and Nicola Casagli

Abstract This chapter presents some specific considerations on the use of SAR interferometry to landslide studies. Both space-borne and ground-based methods are briefly reviewed and main issues in the application of them discussed on the basis of real examples. The large literature on the subject seems to suggest that PSI techniques have a large field of possible applications ranging from landslide mapping to monitoring. Limitations are mainly linked to revising time, thus time resolution and can be overcome, for selected priority unstable slope, by the implementation of GB-InSAR early warning systems, where SAR methods must always be complemented by traditional (or new technology) in situ direct measurements, including underground tools such as inclinometers.

Keywords Landslide mapping · Landslide monitoring · Radar interferometry · Landslide hazard · Landslide early warning

1 Introduction

In the last 20 years, the use of remote sensing (RS) has been steadily increasing its range of application, accuracy and flexibility in all the different stages of landslide risk management, from landslide recognition and mapping to early warning and damage assessment (Canuti et al. 2007). The nowadays widely accepted importance of RS in this field, as well as in the wider field of natural hazards, is underlined by the increase in the number of specific research programmes that have been funding research in RS application to landslides in the last decade in particular. At the forefront of this strategic tool development and application is the

F. Catani · P. Canuti (✉) · N. Casagli
Department of Earth Sciences, University of Florence, via La Pira, 4 50121 Florence, Italy
e-mail: canuti37@gmail.com

F. Catani
e-mail: filippo.catani@unifi.it

W. Shan et al. (eds.), *Landslides in Cold Regions in the Context of Climate Change*, Environmental Science and Engineering, DOI: 10.1007/978-3-319-00867-7_13,

synthetic aperture radar interferometry (InSAR) in all its several different possible forms and implementations.

The relevance of InSAR is manifold and is based mainly on the capability of microwaves of working in all-weather conditions, providing high space resolution and offering high accuracy in the measurement of displacements (Canuti et al. 2007). Traditional InSAR processing for the detection of ground movements is based on differential InSAR (DInSAR) (Massonnet and Feigl 1998; Rosen et al. 2000). Several studies have shown the importance of using DInSAR in landslide related studies (Rott et al. 1999; Xia et al. 2004; Catani et al. 2005) but they also highlighted the presence of typical weaknesses of DInSAR analysis such as temporal decorrelation and atmospheric noise (Ferretti et al. 2001). Such drawbacks can be overcome by using multi-interferometry, in which a series of SAR images is used to build a statistically robust stack of interferogram couples instead of just one as in traditional DInSAR. Multi-interferometry is mainly referred to as Persistent Scatterers Interferometry (PSI) and has been proposed for the first time in the PSInSAR technique by Ferretti et al. (2000, 2001) and later improved by Colesanti et al. (2003). Several similar techniques have thence be produced such as the Stanford Method for Persistent Scatterers (StaMPS, Hooper et al. 2004, 2007), the small baseline approach called Coherent Pixel Technique (CPT, Mora et al. 2004; Lanari et al. 2004) or the Interferometric Point Target Analysis (IPTA, Strozzi et al. 2006). Other recent long-term approaches for PSI analysis are the Small Baseline Subset (SBAS, Berardino et al. 2002) and the Stable Point Network (SPN, Crosetto et al. 2008).

Satellite based techniques are thus demonstrably very useful especially in studying basin scale problems. When, instead, the focus is on slope scale and a more elevated accuracy is needed, as well as a higher temporal resolution, a ground-based approach is often more suitable. For this reason, the EU Joint Research Centre developed a ground-based InSAR capable of producing high resolution interferograms at very short time-intervals (GB-InSAR, Tarchi et al. 2003). This tool has been successfully used in many cases of landslide displacement monitoring (see e.g. Casagli et al. 2010). Each technique has its specific application field and many examples can be found in the literature reporting the use of PSI to mass movement detection, characterization, prediction and monitoring (Canuti et al. 2007; Casagli et al. 2010; Lu et al. 2012).

In this paper we briefly present and discuss the main characteristics and results of InSAR methods through examples related to single slope and basin scale analysis.

2 InSAR Methods Generalities

2.1 Satellite Radar Interferometry

Satellite based interferometry was born as a basic 2-image phase difference interferogram, produced using techniques generally referred to as DInSAR. For landslide mapping and monitoring, though, PSI techniques are more suitable, since a longer

time interval of monitoring is necessary and because of the localized, spatially uncorrelated nature of landslide events with respect to more spatially continuous processes or process-generated features such as subsidence and earthquakes.

The PSI approach, differently from traditional DInSAR, measures the displacement at specific ground targets with high accuracy. In case one of these targets belong to a mass movement in active state, then the PSI numerical information gives an accurate figure of the displacement occurred in the time span between the first and the last SAR image in the image stack. The PSI techniques are based on the use of SAR images generated by post-processing of radar satellites such as the ESA's ERS1, ERS2 and ENVISAT, the Canadian RADARSAT or the German–French DLR's TERRASAR-X. Recently, new higher resolution sensors are available on board of the Italian ASI COSMO constellation (4 satellites) which has a capability of producing high spatial resolution (1 m) images at a very short revisting time (up to 1 day). This leads to a potentially high capability of covering the Earth surface for landslide mapping and monitoring purposes over large areas (Fig. 1).

The PSI targets are stable radar benchmarks on the ground surface that are often represented by man-made structures such as buildings, roads, walls, bridges, dams and so on. Less frequently, PSI targets can be found on rock outcrops or bare soil surfaces. The presence of stable backscatterers on vegetated surfaces is almost always impeded by decorrelation effects. The accuracy in the definition of ground displacements is theoretically dependent on the radar wavelength which is used, being the PSI technique basically a phase difference computation. This would mean sub-millimeter accuracy using SAR images from ERS, ENVISAT and RADARSAT satellites, for example. Actually, though, practical accuracy is in the order of $\pm$ 2 mm/year due to the presence of noise and precision errors. For this reason (see Fig. 1 as an example) displacement velocities between -2 and +2 mm/year are considered as negligible and the relative target points deemed as stable.

When a long time series of images is available, it is also possible to furtherly elaborate the SAR image data stack to produce a displacement time series for the period covered by the SAR database used in the PSI advanced analysis (Fig. 2). This being the case, more information can be extracted of fundamental importance in landslide monitoring, such as period and magnitude of acceleration and deceleration episodes possibly connected to triggering events such as rainfall.

Even though PSI analysis is widely used in landslide studies since several years (see e.g. Farina et al. 2006), there are some open problems which will be discussed in the following sections of this chapter that are now being addressed by the scientific community and that must be taken into consideration to avoid misinterpretation or errors in the use of this technique.

2.2 Ground-Based Radar Interferometry

When wide-area analysis is not sufficient for providing the needed spatial and temporal resolution on the ground, the best alternative is the use of ground-based

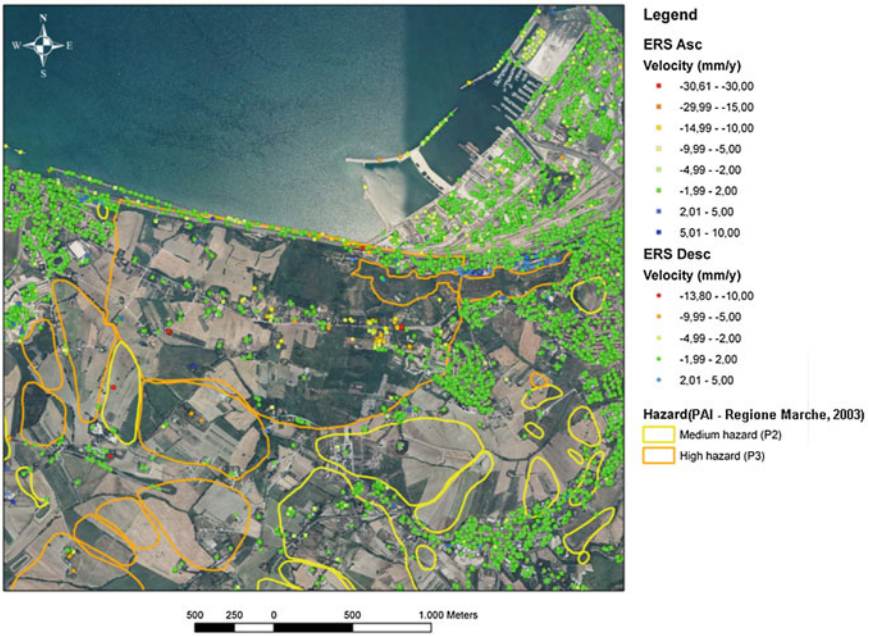

Fig. 1 Example of a typical PS-InSAR product, showing ERS satellite based displacement velocities along ascending (*Asc*) and descending (*desc*) orbits. Negative velocities depicts displacements away from the sensor (subsidence or landslides) whilst positive velocities movements towards the sensor (uplift or various origin)

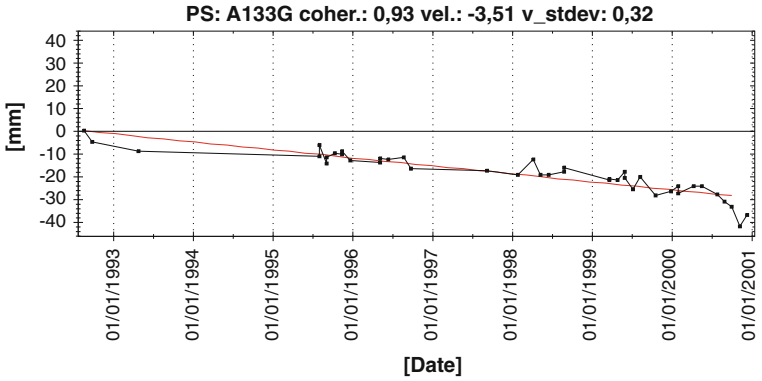

Fig. 2 A time series relative to the displacement registered by the PSI analysis at a given target point showing an average trend of downslope displacement and some acceleration events

interferometers (GB-InSAR). As already introduced, GB-InSAR, initially based on the development efforts carried out by the EC JRC (Tarchi et al. 2003) relies on a permanent, stable SAR installation on the ground surface, usually positioned in

Fig. 3 The Linear Synthetic Aperture (LiSA) radar designed by JRC in a typical installation setting on the field (image courtesy of EC-JRC and Ellegi srl LiSALab)

front of the slope under monitoring. Basically, the instrumentation is made up of a couple of radar antennas (one transmitting and one receiving) mounted on a sled which is automatically moved along a rail to produce the synthetic aperture needed to cover the area under monitoring (Fig. 3). In other cases, the antenna couple is fixed and does not rely on synthetic aperture whilst in some novel implementations the moving sled and the rail are avoided and substituted by an array of small radar antennas.

In any case, the most distinctive characteristics of such instruments with respect to satellite based SARs are: the capability of very high spatial resolution due to the proximity between radar and target (usual working distances range from a few hundreds of meters to more than 2 km); the equally high temporal resolution (due to the fast image acquisition rate with respect to satellites) and the flexibility in the definition of the working parameters, which allow for a fine tailoring of GB-InSAR instrumentation to specific monitoring purposes.

In particular, the spatial resolution is mainly dependent on the wavelength used (typically in the K radar band), the distance to the target and the complexity of the hillslope topography. Possible operative ground resolution ranges from 10^{-1} to 10^{1} meters depending on such factors and on the needs of the monitoring system. A second important feature of GB-InSAR systems is their ability to produce SAR images in a few minutes, thus allowing for the detection of displacements too fast for the capability of space-borne sensors. A comparison between the time resolution of satellite and ground-based SAR in the detection of landslides shows that the available radar satellites have repeat time in the order of about 35 days for ERS and ENVISAT (meaning a maximum detectable velocity—MDV—of about 0.5 m/year), 24 days for RADARSAT 1 and 2 (with a MDV around 0.75 m/year), 11 days for TERRASAR-X (MDV $\approx$ 1.0 m/y) and 4 days for the COSMO SkyMed constellation (with a best space-borne MDV of about 2.5 m/year). On the other hand, a GB-InSAR can produce several interferograms every hour, thus

increasing the MDV to values in the order of 10^3 m/year. This extends the capability of InSAR systems beyond the usual limit of very slow movements (according to the classification of Cruden and Varnes 1996), typical of space-borne sensors, towards moderate and rapid movements. It is clear, however, how this much higher capability is obtained at the expense of flexibility and coverage. GB-InSAR are clearly the best solution for the monitoring of a single, well defined unstable slope. The typical result of each repeat pass scan of the GB-InSAR apparatus is an interferogram depicting a continuous displacement field at the chosen spatial resolution. The ensamble of several interferograms collected consecutively in time can be used to monitor specific targets, to average velocities in order to reduce local noise or to understand the behaviour of complex landslides (Fig. 4).

The GB-InSAR measurement suffer the same drawback of satellite-based systems in vegetated areas. Despite the much higher time resolution of the method, the interferogram is always affected by decorrelation where pseudo-random local

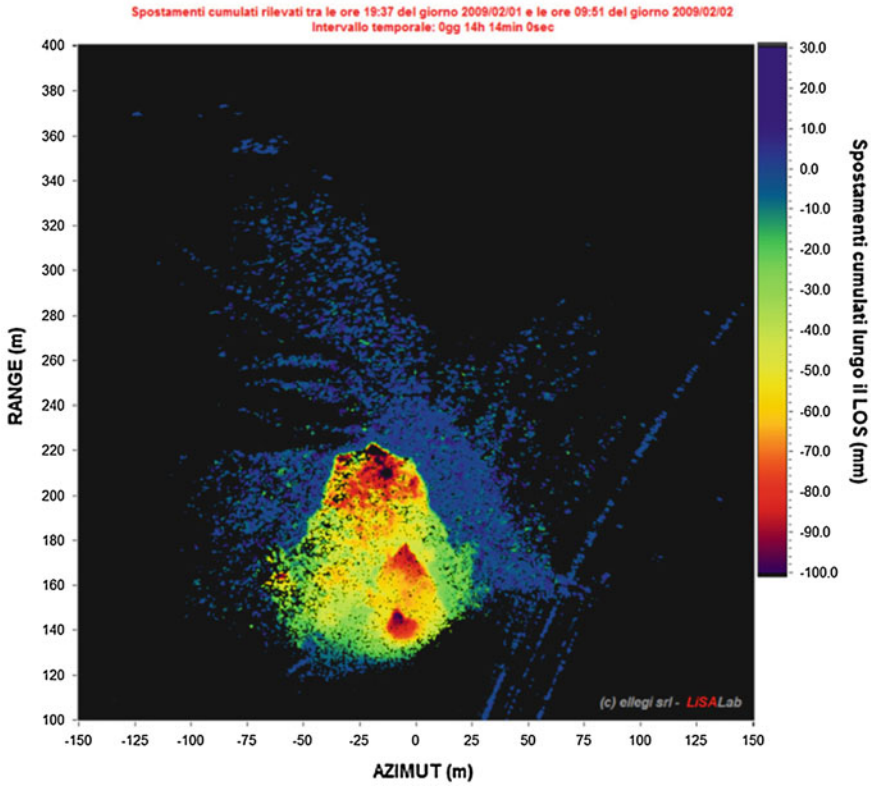

Fig. 4 Example of a typical GB-InSAR interferogram related to an unstable slope. The interferogram cumulates displacements over about 14 h. Different parts of the landslide are clearly visible as having local independent behaviour (image courtesy of Ellegi srl LiSALab)

displacements occur in presence of trees, bushes, small plants and even grass (see black masked out areas in Fig. 4).

3 InSAR Applications and Recent Issues

3.1 Satellite PSI Analysis: Open Issues

Despite the many applications potentially useful for landslide studies, the PSI-like techniques still cannot be used alone. A support must be available based on ancillary data to confirm and correctly interpret the PSI measurements. Furthermore, there are also specific issues, depending on the different adopted PSI techniques (PS-InSAR, SBAS, IPTA, SPN, CPT, StaMPS) that have to be carefully accounted for and possibly corrected or avoided using suitable methods.

We will concentrate here on PS-InSARn (Ferretti et al. 2000, 2001; Colesanti et al. 2003) displacement measurements, as an example of such issues. For this type of PSI analysis, the main open issues are: (1) the correct reconstruction of the actual displacement vector, (2) the problem of low-density of PSs over non-urban areas, (3) the link between surface and subsurface displacements, (4) the space averaging of point measurements. The problem of reconstructing the actual displacement vector, or at least of correctly interpret the measured one, is due to the fact that PSI analysis is based on velocities measured along a versor codirectional to the satellite line-of-sight (LOS). This means, in general, that we only measure a component of the whole displacement, unless the actual displacement versor $\hat{\mathbf{u}}_\mathbf{a}$ is codirectional with the LOS vector $\hat{\mathbf{u}}_{\mathbf{LOS}}$. Another important corollary of this, often negliected, is that with the PSI techniques, in theory, is not possible to measure displacements occurring along the direction $\hat{\mathbf{u}}_\mathbf{n}$ normal to the $\hat{\mathbf{u}}_{\mathbf{LOS}}$. The direction of $\hat{\mathbf{u}}_{\mathbf{LOS}}$ depends on the satellite we are using and on the orbit. Usually, SAR space platforms cover a given area both in descending and in ascending orbit. This offers a good opportunity to look at a given hillslope under two different view angles (Fig. 5).

The combined use of ascending and descending geometry implies an increase in image elaboration costs, but allows for the reconstruction of 2 important components of the actual displacement vector $\mathbf{V}$: the vertical component $\mathbf{V_Z}$ and the horizontal E–W component $\mathbf{V_X}$. Being the orbit of SAR satellites polar, it is

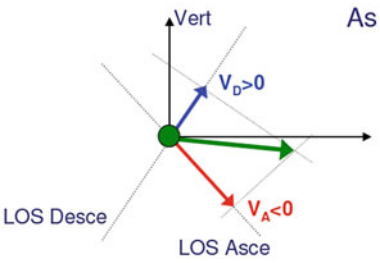

Fig. 5 LOS displacements of the same area observed along two different orbits. The actual vector $\mathbf{V}$ (*green*) is decomposed and only the two LOS components $\mathbf{V_D}$ and $\mathbf{V_A}$ are measurable

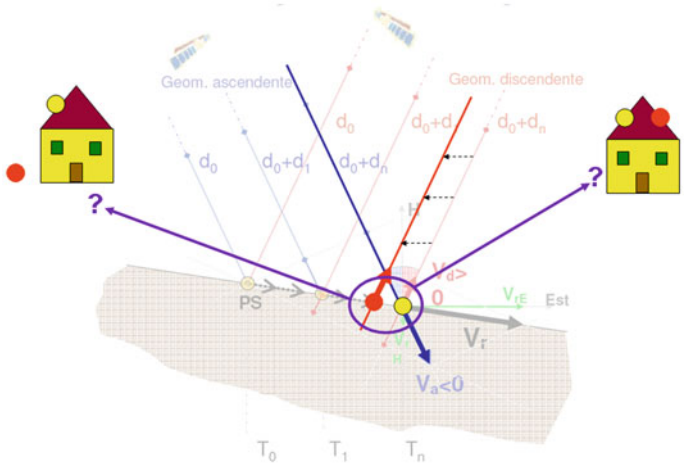

Fig. 6 The problem of vector decomposition in case of decoupling of ground reflectors for different SAR orbits. In the case of a given object reflecting in both geometries (*right example*) the vector decomposition can be safely carried out. The opposite case (*left example*), might generate errors depending on whether the 2 points (*red* and *yellow*) are moving with the same behaviour or not

unfortunately impossible to estimate the component of displacement along the N–S direction on the azimuth plane. However, different orbits, having different look angles with respect to the topographic surface, do not usually measure exactly the same target since the backscattering characteristics of a given ground object are rarely good in both directions. For this reason, the decomposition of the two LOS vectors along the know components $\mathbf{V_Z}$ and $\mathbf{V_X}$ must be carried out with care.

The Fig. 6 exemplifies this concept. Very seldom a given object is capable of backscattering with high coherence the radar signal from both orbits. Therefore, for the vector decomposition and $\mathbf{V_Z} - \mathbf{V_X}$ reconstruction, we are forced to use two different stable PS reflectors in close proximity, one from the ascending and one from the descending geometry. This process, called PS-coupling, can be very delicate since the persistent scatterers to be joined together must behave in the same way with respect to displacement pattern in time (Fig. 6).

For this reason, it is not recommended to just average velocities in space, nor to automatically couple PS points on the sole basis of their distance. Additionally, in the case of landslides, even a geostatistical approach based on variogram analysis may be deceiving, because of the uncorrelated nature of mass movements at many scales. Differently from other ground movements such as soil subsidence, where the displacement vector module is strongly autocorrelated in space (see e.g. Lu et al. 2012), landslides are characterized by velocities almost spatially constant within their boundary that suddenly drop to zero outside it.

A possible solution is to carefully compare PSI time series of candidate couple points before actually using them for vector decomposition (Fig. 7).

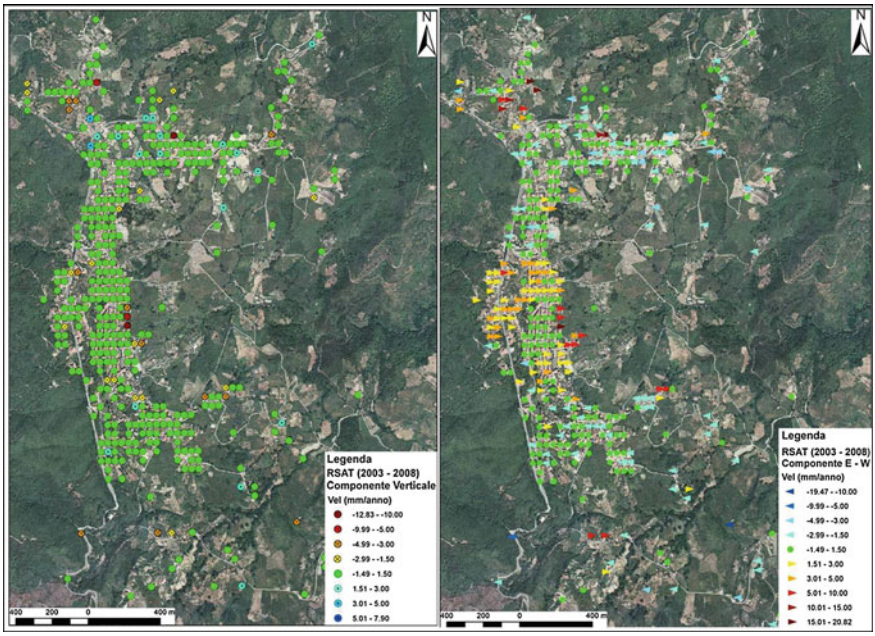

Fig. 7 A successful case of vector decomposition in the two components $\mathbf{V_Z}$ and $\mathbf{V_X}$ in Southern Italy (Calabria region)

One of the major drawbacks of the PS-InSAR™ method, the low density of PS in non-urbanized areas, is being at least partially overcome by the SqueeSAR™ technique, developed by Novali et al. (2009). Another important issue is the need of local underground displacement measures (such as inclinometer readings) to compare the PSI-based surface velocities with the actual 3D vector at different depths in the landslide body. Finally, often the PS-InSAR™ information, which is by nature local, needs some averaging in space to obtain pseudo-continuous maps of average displacement (Fig. 8). To do this for landslides, where the horizontal component $\mathbf{V_X}$ is seldom unimportant, a correct PS 2-orbit coupling and vector decomposition has to be carried out before interpolation. Thence, a correct scheme of statistical averaging must be selected, after an analysis of the local autocorrelation properties of the $\mathbf{V_X}$ and $\mathbf{V_H}$ vectors.

3.2 Ground-Based DInSAR: A Case Study for Early Warning

The use of GB-InSAR covers quite different purposes. Mainly they are centered on the nearly-continuous observation of a given unstable slope for early-warning, failure forecasting or emergency management.

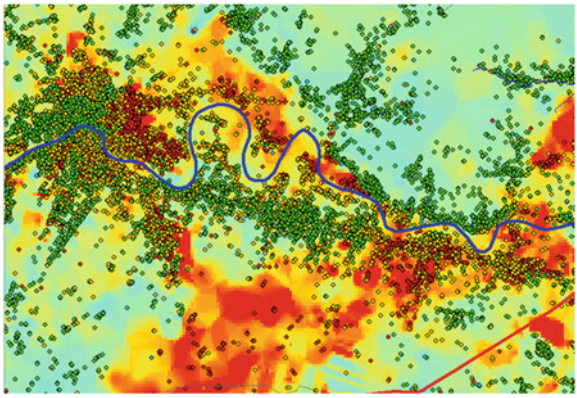

Fig. 8 Ground displacement pseudo-continuous map obtained in the Arno river basin (Tuscany, Central Italy) after vector decomposition and autocorrelation analysis

Several examples of such application are available in the literature (Casagli et al. 2010). A specific successful case which is a good example is the one related to the Mt. Beni rock slide, located in Central Italy, also reported by Gigli et al. (2011). The activity of this unstable slope, that was already involved in rock falls that led to the closure of the quarry at its base at the beginning of 1990s, experienced a sudden acceleration in 2002, when several large cracks were seen developing in the upper part of the slope. The geology of the rock mass is made up of a basal marl-layered limestone overlain by a typical ophiolitic series encompassing, from bottom to the top, basalt breccias, ophiolitic breccias and jointed massive basalts. This setting, and the jointing of the upper basalt layer, favour the development of a perimeter crack system that seemed to isolate a possible unstable mass of about 1–2 M m^3. For this reason, in order to establish a real-time all-weather warning system, a GB-InSAR was installed in place together with other in situ traditional monitoring systems (mainly distometer bases across the perimeter cracks) (Fig. 9).

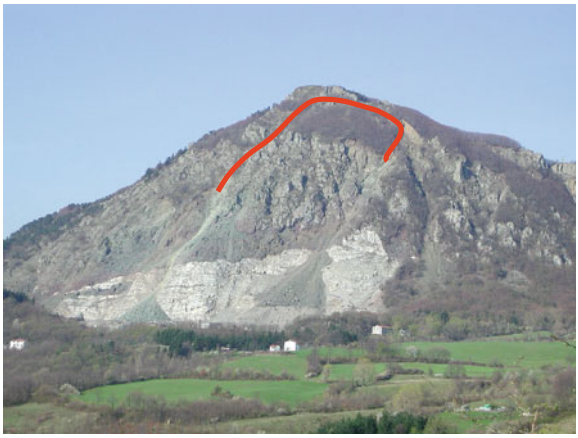

Fig. 9 Image showing the situation at Mt. Beni in April 2002, at the beginning of the GB-InSAR monitoring. The *red line* depicts the approximate position of the main perimeter crack system

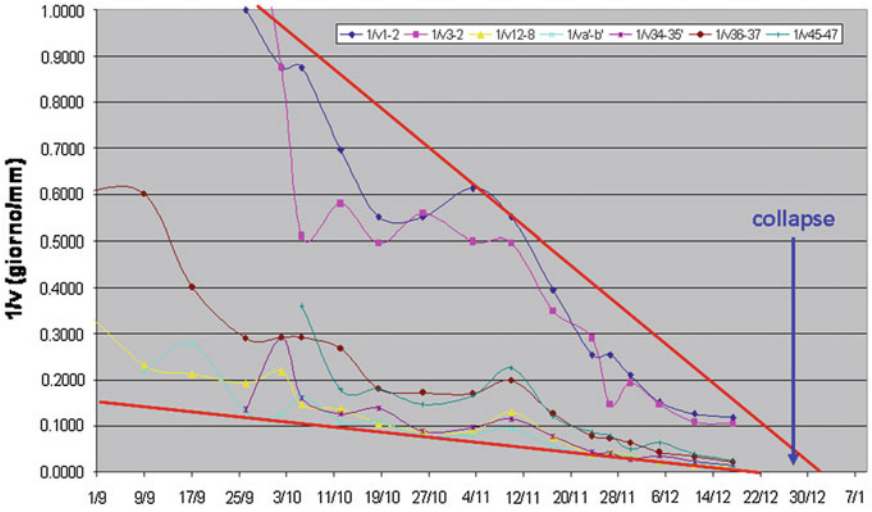

Fig. 10 Prediction of the failure time by the inverse velocity method. The data used for this analysis (both from distometer bases and GB-InSAR) allowed the prediction of the instant of failure with an error of less than 24 h, thus enabling early warning measures

The GB-InSAR apparatus was of the LiSA type and was installed in front of the main slope, at a distance of about 2 km. The analysis of SAR data highlighted the presence of 3 main zones affected by major displacements, where the installation of in situ devices was impossible due to the high velocity of deformation, ranging, for the period of monitoring between 5th and 19th of May 2002, from 4.8 to 10.6 mm/day (Gigli et al. 2011). The joint analysis of InSAR, distometer bases and modelling data allowed for a continuous surveillance of the slide and for the prediction of the failure using the inverse velocity method (Fig. 10).

The GB-InSAR cumulated displacements over the aforementioned period are depicted in Fig. 11, where the different zones of the rock mass are evidenced in their peculiar behaviour.

The main collapse involved a rock mass of about 0.5 Mm^3 and took place on December 28, 2002, after a preliminary localized failure of about 20,000 m^3 occurred on December 14, 2002. The final configuration of the slope is depicted in Fig. 12.

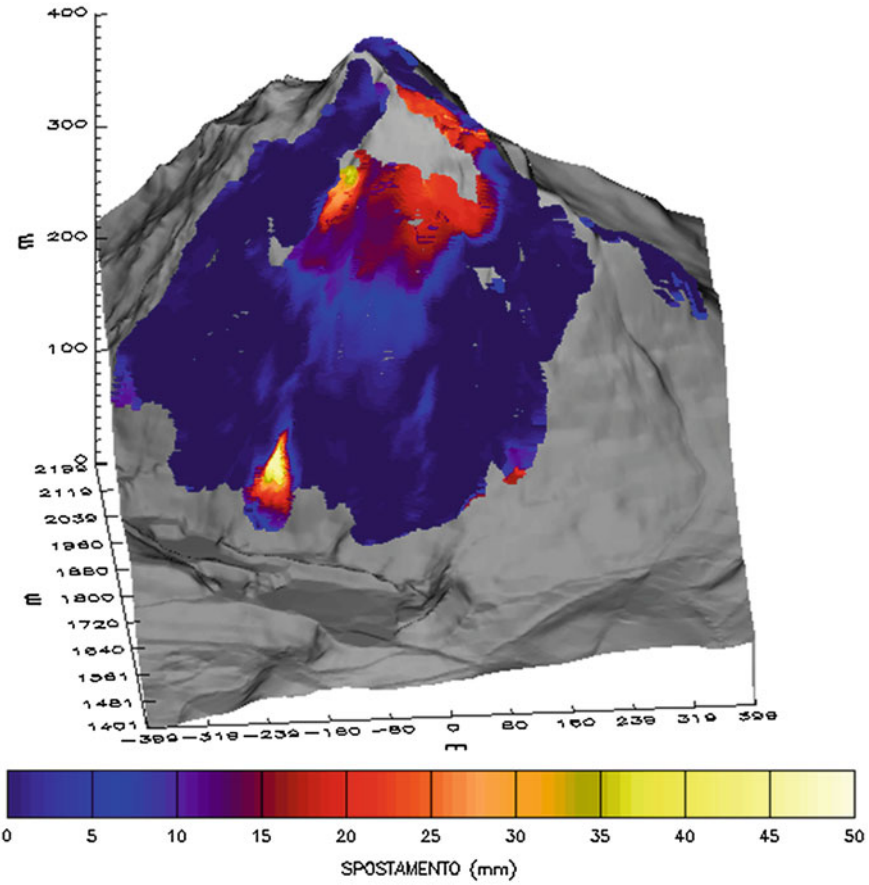

Fig. 11 GB-InSAR cumulated displacement at Mt. Beni in the period between 5th and 19th of May 2002

Fig. 12 Mt. Beni after the main collapse on December 28, 2002

4 Conclusions

We have seen some important characteristics and issues related to the use of radar interferometry in landslide hazard and risk analysis, at several levels. Our conclusions would like to point out some key lessons learned in our experience so far: (1) the analysis at the basin scale using PSI techniques must be carried out by using ancillary data on topography (DEM, orthophoto, satellite optical images) and taking care of correct displacement vectors starting from LOS measurements; (2) the maximum detectable velocities are still limited but are steadily increasing due to the continuous development of new space-borne SAR platforms; (3) where tailored slope-scale application of SAR interferometry are needed, GB-InSAR apparatus should be adopted for a real-time monitoring in early warning applications.

References

Berardino P, Fornaro G, Lanari R, Sansosti E (2002) A new algorithm for surface deformation monitoring based on small baseline differential SAR interferograms. IEEE Trans Geosci Remote Sens 40:2375–2383

Canuti P, Casagli N, Catani F, Falorni G, Farina P (2007) Integration of remote sensing techniques in different stages of landslide response. In: Sassa K, Fukuoka H, Wang F, Wang G (eds) Progress in Landslide Science, Springer, Berlin, pp 251–260

Casagli N, Catani F, Del Ventisette C, Luzi G (2010) Monitoring, prediction, and early warning using ground-based radar interferometry. Landslides 7:291–301

Catani F, Farina P, Moretti S, Nico G, Strozzi T (2005) On the application of SAR interferometry to geomorphological studies: estimation of landform attributes and mass movements. Geomorphology 66(1–4):119–131

Colesanti C, Ferretti A, Prati C, Rocca F (2003) Monitoring landslides and tectonic motions with the permanent scatterers technique. Eng Geol 68:3–14

Crosetto M, Biescas E, Duro J, Closa J, Arnaud A (2008) Generation of advanced ERS and envisat interferometric SAR products using stable point network technique. Photogram Eng Remote Sens 74:443–450

Cruden DM, Varnes DJ (1996) Landslide types and processes. In: Turner AK, Schuster RL (eds) Landslides investigation and mitigation, Special Report 247. Transportation Research Board, National Research Council, Washington DC, pp 36–75

Farina P, Colombo D, Fumagalli A, Marks F, Moretti S (2006) Permanent scatterers for landslide investigations: outcomes from the ESA-SLAM project. Eng Geol 88:200–217

Ferretti A, Prati C, Rocca F (2000) Nonlinear subsidence rate estimation using permanent scatterers in differential SAR interferometry. IEEE Trans Geosci Remote Sens 38:2202–2212

Ferretti A, Prati C, Rocca F (2001) Permanent scatterers in SAR interferometry. IEEE Trans Geosci Remote Sens 39:8–20

Gigli G, Fanti R, Canuti P, Casagli N (2011) Integration of advanced monitoring and numerical modeling techniques for the complete risk scenario analysis of rockslides: the case of Mt. Beni (Florence, Italy). Eng Geol 120:48–59

Hooper A, Zebker H, Segall P, Kampes B (2004) A new method for measuring deformation on volcanoes and other natural terrains using InSAR persistent scatterers. Geophys Res Lett 31:L23611

Hooper A, Segall P, Zebker H (2007) Persistent scatterer InSAR for crustal deformation analysis, with application to Volcan Alcedo, Galapagos. J Geophys Res 112:B07407

Lanari R, Mora O, Manunta M, Mallorqui JJ, Berardino P, Sansosti E (2004) A small-baseline approach for investigating deformations on full-resolution differential SAR interferograms. IEEE Trans Geosci Remote Sens 42:1377–1386

Lu P, Casagli N, Catani F, Tofani V (2012) Persistent scatterers interferometry hotspot and cluster analysis (PSI-HCA) for detection of extremely slow-moving landslides. Int J Remote Sens 33(2):466–489

Massonnet D, Feigl KL (1998) Radar interferometry and its application to changes in the earth's surface. Rev Geophys 36:441–500

Mora O, Mallorqui JJ, Broquetas A (2003) Linear and nonlinear terrain deformation maps from a reduced set of interferometric SAR images. IEEE Trans Geosci Remote Sens 41:2243–2253

Novali F, Ferretti A, Fumagalli A, Rocca F, Prati C, Rucci A (2009) The second generation PSInSAR approach: SqueeSAR. In Proceedings of FRINGE 2009, 30 November–4 December 2009, Frascati, Italy (European Space Agency), CD-ROM

Rosen PA, Hensley S, Joughin IR, Li FK, Madsen SN, Rodriguez E, Goldstein RM (2000) Synthetic aperture radar interferometry. Proceedings of the IEEE, 88, pp 333–382

Rott H, Scheuchl B, Siegel A, Grasemann B (1999) Monitoring very slow slope movements by means of SAR interferometry: a case study from a mass waste above a reservoir in the Ötztal Alps, Austria. Geophys Res Lett 26:1629–1632

Strozzi T, Wegmuller U, Keusen HR, Graf K, Wiesmann A (2006) Analysis of the terrain displacement along a funicular by SAR interferometry. IEEE Geosci Remote Sens Lett 3:15–18

Tarchi D, Casagli N, Moretti S, Leva D, Sieber AJ (2003) Monitoring landslide displacements by using ground-based radar interferometry: application to the Ruinon landslide in the Italian Alps. J Geophys Res 108(B8-2387):101–114

Xia Y, Kaufmann H, Guo XF (2004) Landslide monitoring in the three Gorges area using D-InSAR and corner reflectors. Photogram Eng Remote Sens 70:1167–1172

Relative Factors of Beihei Highway's Ground Deformation Interpretation Based on Remote-Sensing Imagery Technology

Chunjiao Wang, Wei Shan, Ying Guo, Zhaoguang Hu and Hua Jiang

Abstract Beihei Highway is located in the northern region of the Lesser Khingan Range, near the southern permafrost border of northeast China, which belongs to permafrost belt of high latitudes. The effect of global warming and other natural factors, coupled with urbanization and socio-economic developments has led to continuous melting and structural changes in the permafrost bed and has caused the southern border of the permafrost zone to shift northwards. These changes aggravated the instability of the southern area of the permafrost, one of which is the collapse of a highway embankment which occurred along the Beihei Highway. What threatens the security of the Beihei Highway is that many landslides exist on the highway and most of these landslides are unstable. Remote sensing imagery data from LANDSET ETM + and ENVISAT ASAR were used to study the environmental impact of the highway roadbed slope instability in sensitive and domain area of permafrost degenerate zone and to get the basis for assessment and early warming of deformation, destabilization and other disasters. The authors interpreted and extracted ground temperature, soil moisture and other factors relative to highway deformation. From local survey records, information obtained from weather station and historical imagery from GOOGLE EARTH shows that there is a comparative analysis with interpreted consequences, which can commendably reflect practical ground surface situation and show correlation of various factors. Result may show interpreted consequences' accuracy for using remote sensing techniques and its fundamental importance for monitoring and early warning deformation disasters caused by climate change and permafrost degradation.

Keywords Remote sensing · Permafrost · Temperature · Moisture · Interpretation

C. Wang · W. Shan (✉) · Y. Guo · Z. Hu · H. Jiang
Northeast Forestry University, Harbin, Heilongjiang 150040, China
e-mail: Shanwei456@163.com

W. Shan et al. (eds.), *Landslides in Cold Regions in the Context of Climate Change*, Environmental Science and Engineering, DOI: 10.1007/978-3-319-00867-7_14,

1 Introduction

Northeast China is not only a unique permafrost region, but is also the second largest permafrost belt in China. Total area covered by the permafrost is approximately 400,000 km^2 (Chang and Jin 2013). The Permafrost region is divided into three based on topography: (1) scattered islands to island talik, (2) discontinuous permafrost, and (3) continuous permafrost. The most characteristic underlying surface is the vast forest and snow, which influences the surface temperature of permafrost and the function of ice melt in the underlying season. In China's northeast Singanense and the Russian Transbaikalia areas, significant local temperature deformation is mainly caused by many factors such as snow, vegetation, moisture, landform and atmospheric inversion. These contribute to form different high altitude permafrost and polar sing-an-baikalian permafrost.

In the past 50 years, northeast region of China has witnessed progressive upward trend in air temperature which is higher than that of national average increase. Air temperature all the year round trends toward higher, as well. It has been projected that within the next 50–100 years, northeast permafrost will greatly degenerate due to the effect of increased climate change. This will lead to gradual change in weather conditions and influence northward recession and shrinking of the permafrost belt (Zhou et al. 2000). Weather forecast and predictions hinted that the present trend of events will inadvertently lead to a rise in temperature of the permafrost belt, which will lead to retreat of the glacial layers, causing reduction in thickness and instability of the permafrost belts. These changes imply that unstable and seasonal permafrost area will increase. Meanwhile, this shows that permafrost degradation in northeast China can cause adverse changes in the ecological environment, such as atrophy of wetland ecosystems, landslides, melt lake and frozen mud flow and other geological disasters, coupled with destruction of municipal buildings and infrastructures (Wei and Jin 2011).

In Heilongjiang province of China, urbanization and industrialization has increasingly led to the construction and development of cities, towns, municipalities and highways under the seasonally frozen layers of permafrost which extend to the northern mountain area underlain by permafrost. Human activity has also increased within the area. Frozen ground near the southern boundary is very sensitive to climatic and environmental changes. The degree of instability of engineering structures in the area is increasing daily due to permafrost melting and transportation security has become a very serious issue. A whole section of embankment collapse events and many landslide disasters have occurred due to civil engineering works carried out when construction work on the Beihei highway began in 1999 (Zhang and Hou 2009). Further widening and expansion of the Beihei highway to dual carriageway in 2009 led to increased instability of the slope sections which showed developing zones of weakness. However, the highway expansion cannot be abandoned owing to its significance to the ever growing population as it poses a major transportation issue that needs urgent attention. Since 2009, field investigations, geological surveys, soil temperature monitoring,

moisture and pore pressure monitoring coupled with other disaster prevention engineering assessments have been carried out on areas affected by slope instability and landslides. However, based on discrete points, monitoring method cannot get region-wide surface temperature, soil moisture, elevation, slope and other data; the interpretation of these data can only grasp the macro-regional environmental changes, carry out the evaluation and discriminant of the unstable region.

Based on LANDSET ETM +, ENVISAT ASAR data source in remote sensing image, application of thermal infrared remote sensing, radar remote sensing method for land surface temperature and soil moisture inversion analysis, combined with field investigation, weather station data and history of Google Earth image were analyzed and compared; preliminary research results were obtained.

2 Methods and Results

1. Land surface temperature inversion

Using six Landsat ETM + image scenes to land surface temperature inversion, dates in which the data were acquired are: 20110503, 20110604, 20110823, 10111010, 20120521, 20120622.

Vegetation coverage F_v, is obtained by using the decomposition of mixed pixels method, the entire image class was divided into water, vegetation and buildings. The specific calculation formula is as follows:

$$F_v = (NDVI - NDVI_s)/(NDVI_v - NDVI_s) \tag{1}$$

According to the experience from previous research, the remote sensing image is divided into three types: water, towns and natural surface. Radiation rate of water-like assignment is 0.995, the emissivity estimation of natural surface and towns according to the type (2, 3) to calculate respectively:

$$\varepsilon_{surface} = 0.9625 + 0.0614F_V - 0.0461F_V^2 \tag{2}$$

$$\varepsilon_{building} = 0.9589 + 0.086F_V - 0.0671F_V^2 \tag{3}$$

In the formula, $\varepsilon_{surface}$ and $\varepsilon_{building}$ represents the emissivity of the natural surface and town.

Satellite sensor receives the thermal infrared radiation brightness value L_λ which consist of three parts: the atmospheric upwards radiation brightness $L\uparrow$, satellite sensor received energy of the ground radiation brightness after the atmosphere and reflected energy of atmospheric radiation after downward reaching the ground. Satellite thermal infrared radiation of sensor receives the brightness value of the equation can be written as (radiative transfer equation):

$$L_\lambda = [\varepsilon \cdot B(T_s) + (1 - \varepsilon)L\downarrow] \cdot \tau + L\uparrow \tag{4}$$

ε is the surface emissivity, T_s is the surface true temperature, $B(T_s)$ is the Planck's law to the blackbody thermal radiation intensity in T_s, τ is atmospheric transmittance in thermal infrared band. Radiation brightness $B(T_s)$ of blackbody with temperature T in thermal infrared band is:

$$B(T_s) = [L_\lambda - L\uparrow - \tau \cdot (1-\varepsilon)L\downarrow]/\tau \cdot \varepsilon \tag{5}$$

after getting the radiation brightness of blackbody with temperature T in thermal infrared band, according to Planck's formula of inverse function, the surface land true temperature T_s was calculated:

$$T_s = K_2/\mathrm{In}(K_1/B(T_s) + 1) \tag{6}$$

Ground temperature inversion result diagram is shown in Figs. 1, 2, 3, 4, 5, 6.

2. Soil moisture inversion

Soil inversion using ten ENVISAT ASAR historical images of the study area and data acquisition date are 20040128, 20040616, 20040825, 20041208, 20050216, 20050323, 20051123, 20051228, 20050308, and 20070117.

The original ASAR image acquisition of backscattering coefficient extraction and the calculation formula is as follows:

$$\sigma^0 = \frac{\langle A^2 \rangle}{K} \sin\theta \tag{7}$$

In the formula: A is intensity on DN images; θ is radar incidence angle, K is the absolute calibration constant (Bao and Liu 2006).

Based on dielectric properties of soil with different water content, the radar echo signal were also found to be different. Establishing the relationship between back scattering coefficient and soil moisture according to radar parameter (Han and

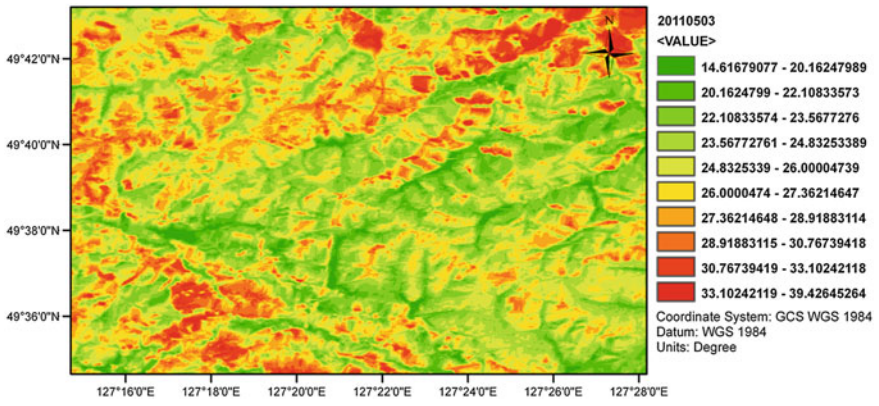

Fig. 1 Temperature inversion results in 20110503

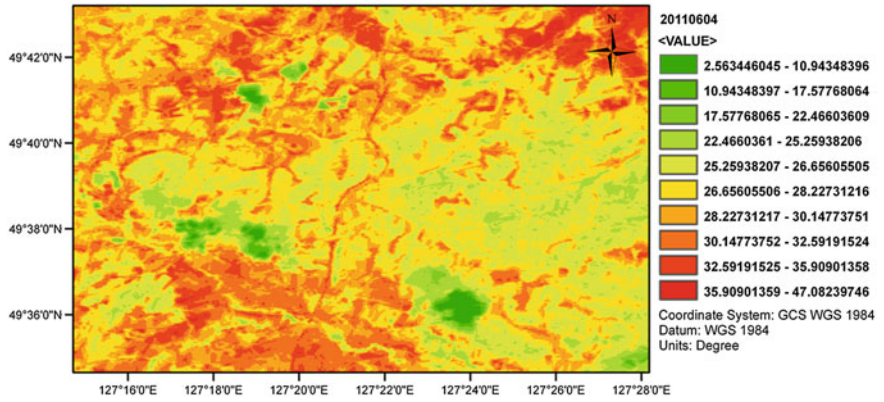

Fig. 2 Temperature inversion results in 20110604

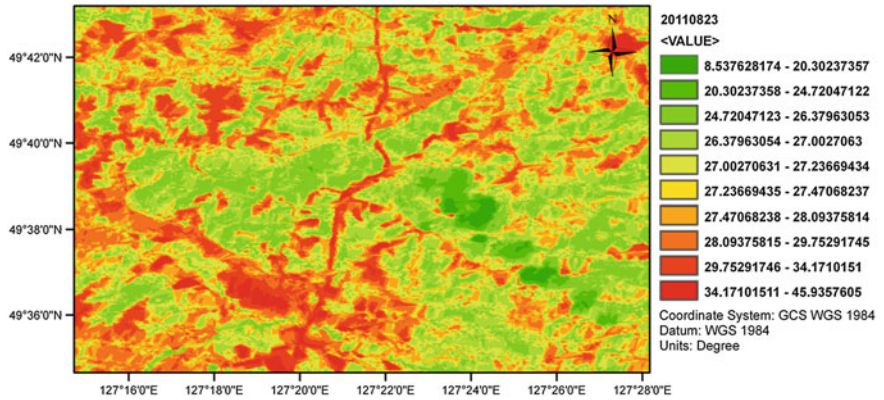

Fig. 3 Temperature inversion results in 20110823

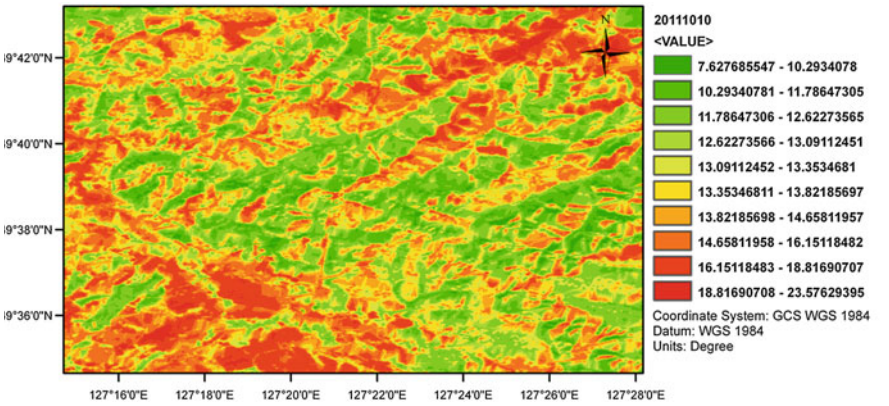

Fig. 4 Temperature inversion results in 20111010

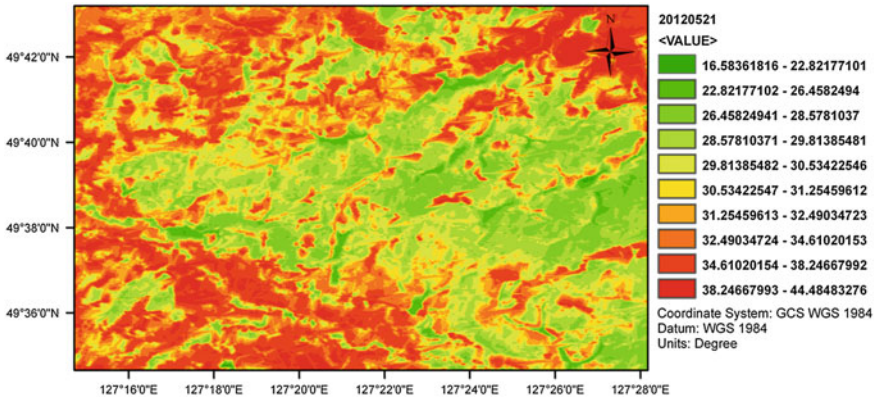

Fig. 5 Temperature inversion results in 20120521

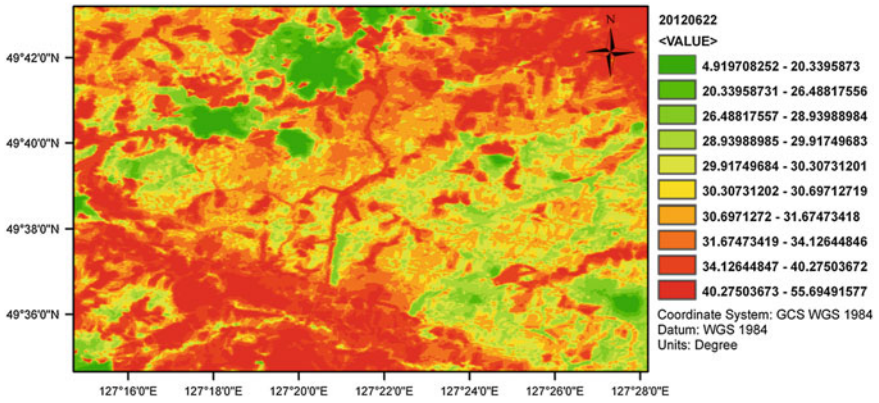

Fig. 6 Temperature inversion results in 20120622

Peng 2012). The experiential formula between back scattering coefficient and soil moisture wasapplied (Jin 2011):

$$\sigma^0 = A + Bm_v \tag{8}$$

Because there is no water content of soil reference data in the study area, soil moisture inversion for the relative variation.

Soil moisture inversion results as shown in Figs. 7, 8, 9, 10, 11, 12, 13, 14, 15, 16.

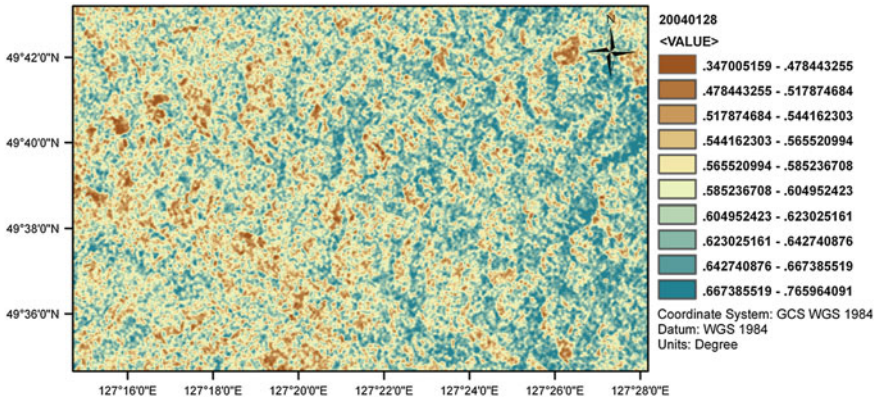

Fig. 7 Soil moisture inversion result in 20040128

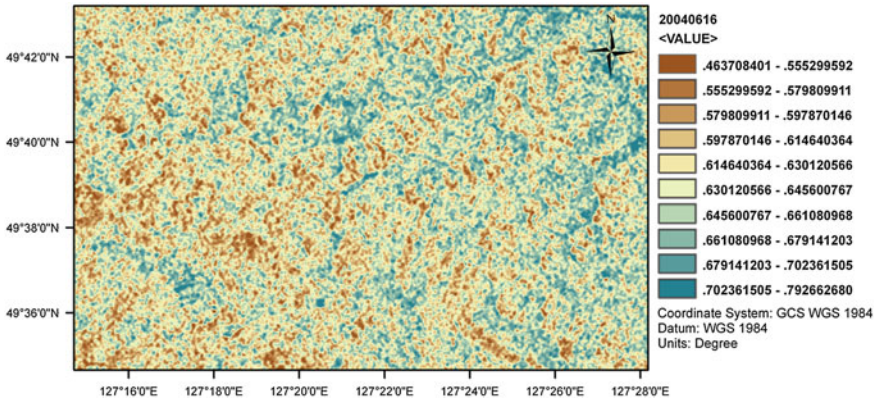

Fig. 8 Soil moisture inversion result in 20040616

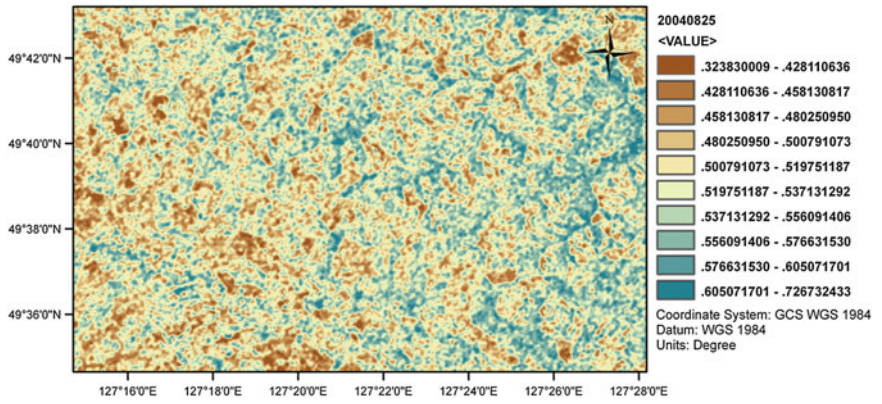

Fig. 9 Soil moisture inversion result in 20040825

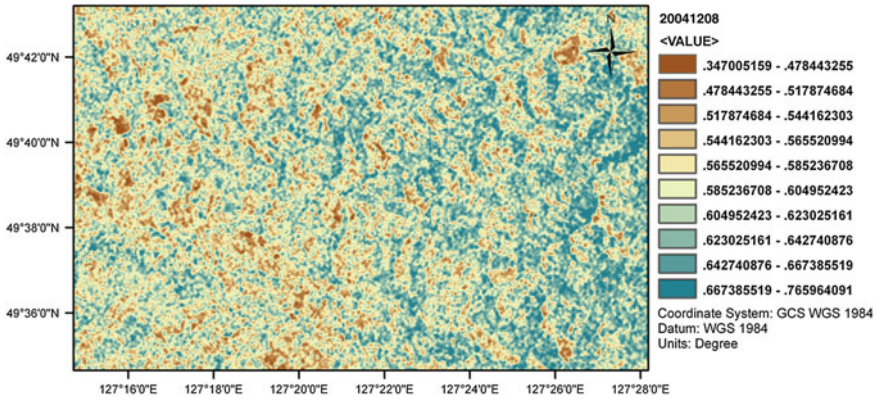

Fig. 10 Soil moisture inversion result in 20041208

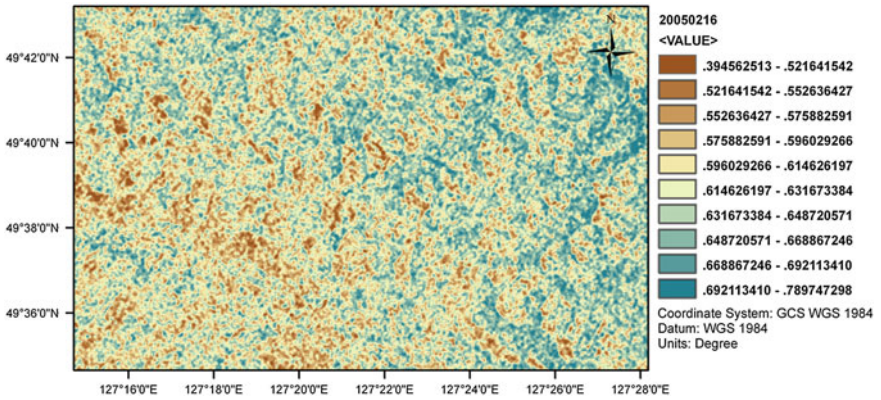

Fig. 11 Soil moisture inversion result in 20050216

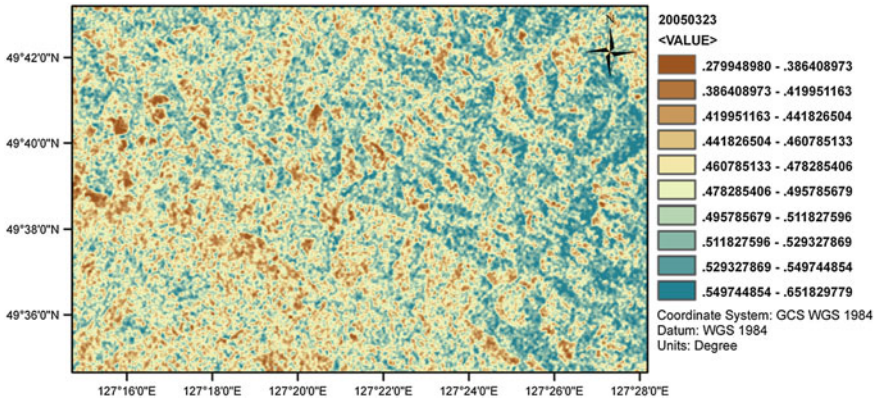

Fig. 12 Soil moisture inversion result in 20050323

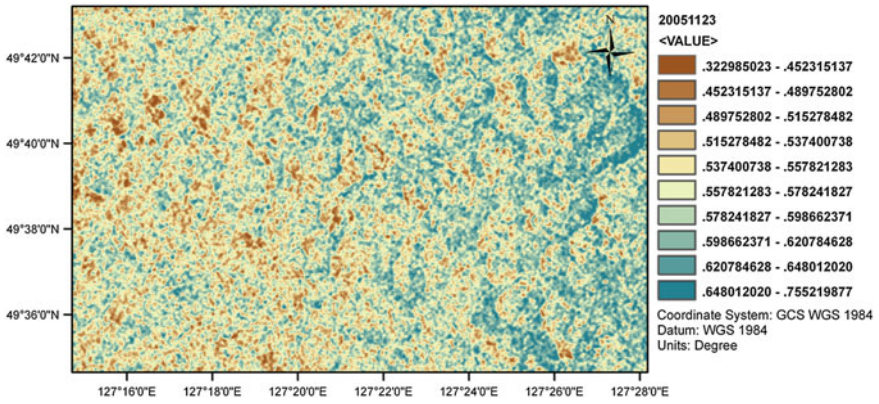

Fig. 13 Soil moisture inversion result in 20051123

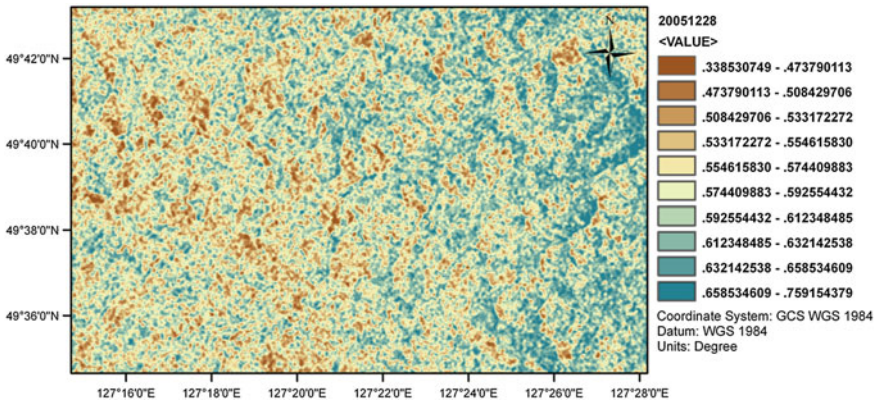

Fig. 14 Soil moisture inversion result in 20051228

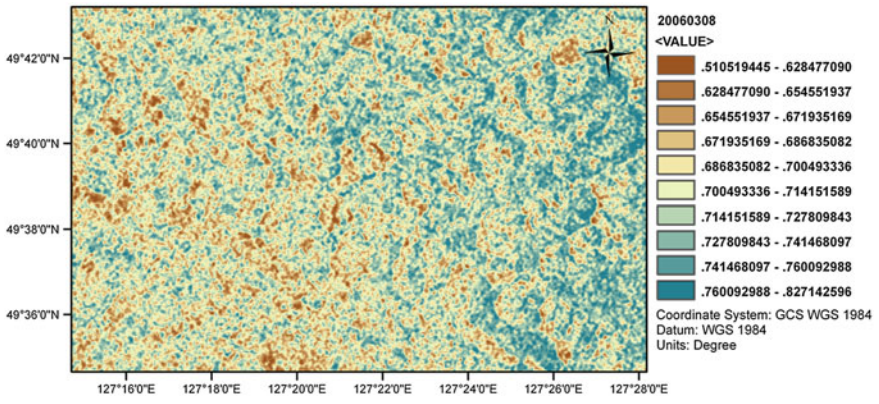

Fig. 15 Soil moisture inversion result in 20060308

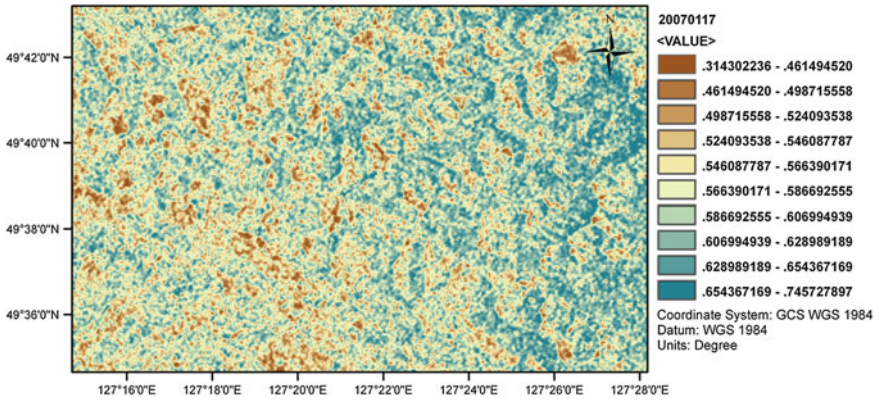

Fig. 16 Soil moisture inversion result in 20070117

3 Discussion

Picking 10 values from typical point 1(p1) to point 5(p5), what can be seen from GOOGLE EARTH is that p1, p1-1 and p1-2 are located in a depressed area while p2 and p2-1 are on the highway pavement. P3, p3-1 are selected in the cleuch and on the end of the cleuch. Drill data shows that there is permafrost near p4 area. Figure 17

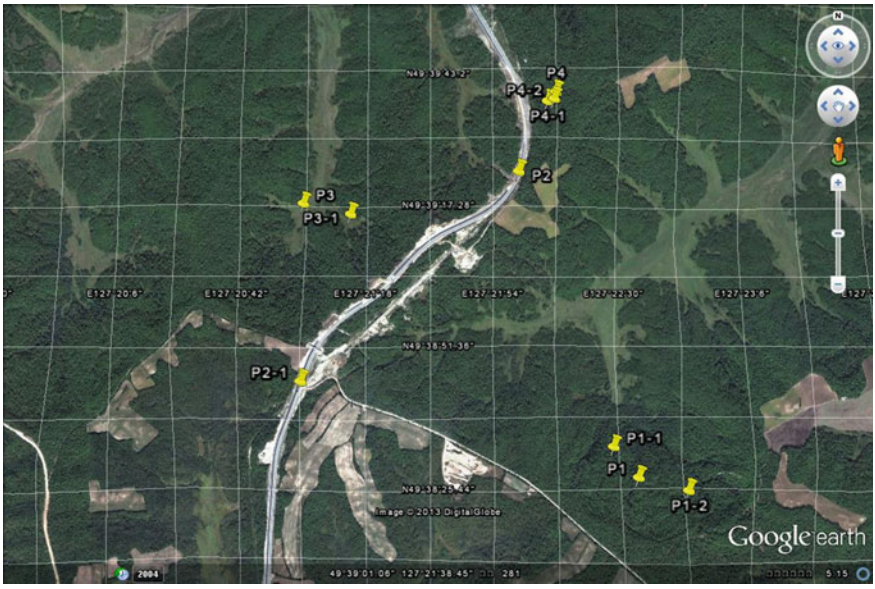

Fig. 17 The position map of selected points

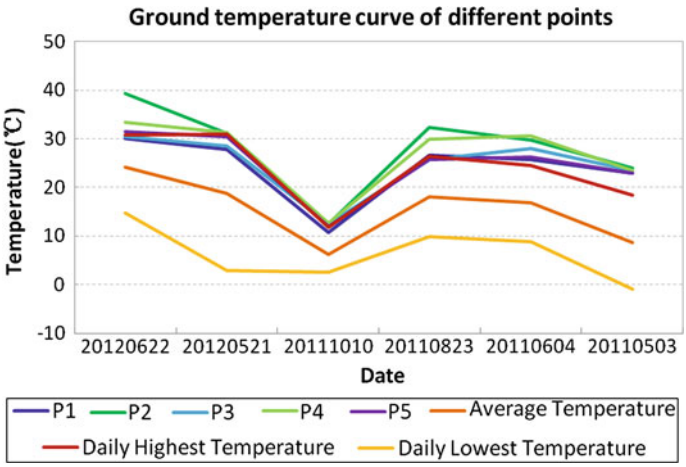

Fig. 18 Ground temperature curve at different points

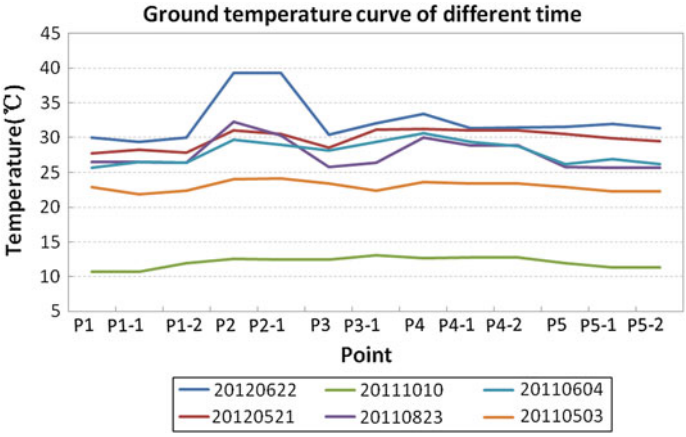

Fig. 19 Ground temperature curve at different time interval

shows point location map. Figure 18 shows ground temperature at different points. Figure 19 shows ground temperature at different time interval. Figure 20 shows soil moisture at different points. Figure 21 shows soil moisture at different time interval.

Result obtained from comparison of data between Sunwu meteorological station and interpretation data shows similar changing tendency of ground temperature. The change of soil moisture and relative atmospheric moisture has no obvious uniformity. The position of p1 can be seen in Fig. 22. Analysis of data obtained from Google Earth imagery shows that this area is an erosion depressed area of high permafrost deposits. The ground temperature value of p1 curve in

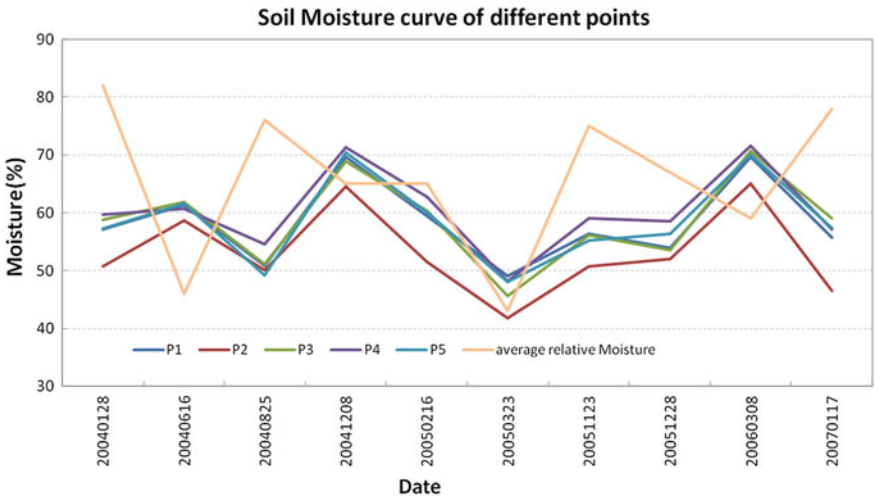

Fig. 20 Soil moisture curve at different points

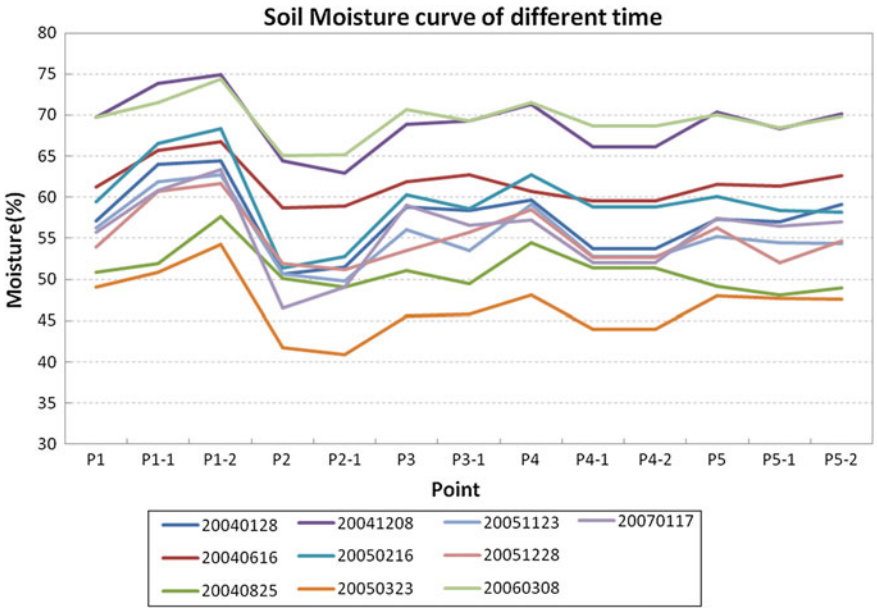

Fig. 21 Soil moisture curve of different time interval

Fig. 18 is lower than that of other points in the area. The soil moisture values of p1, p1-1 and p1-2 curves in Fig. 21 are higher than other points. This area has wet and cold characteristics which confirms the above assertion. P2, located on the highway, whose ground temperature value changes with change in atmospheric

Fig. 22 Google Earth image of P1 subsidence area in 2010

temperature, with rate of increase and decrease higher than other points, the seasonal changing characteristic is notable. The moisture value is low. Interpretation values of p2 are in according with actual situation. Compared with p3 and p4, the ground temperature and soil moisture value are all similar. The p4 is located in frozen ground area and p3 is located in cleuch area. The cleuch in the study area often have frozen ground; this indicates that the data is reasonable.

4 Conclusion

Space remote sensing technology can be used to acquire numerous ground temperature, soil moisture and other relative information in regional scale. Firstly, proposed to make use of remote sensing in study area for getting deformation relative factors. The preliminary results can be got. The result can reflect the actual situation, and the factors have certain relativity. Application of earth observation technology in China's low altitude, high latitude, isolated and complex geological permafrost region and disaster-prone areas is important for environmental monitoring, to know and handle highway and environmental degradation in permafrost sensitive areas which has significant meaning for assessment and early warming on deformation, slide, instability and other disaster of sub-grade, slope and highway domain.

References

Bao YS, Liu LY (2006) Using ASAR images to monitor soil moisture and wheat cover. J Remote Sens 10(2):264–265 (in Chinese)

Chang XL, Jin HJ (2013) Review of permafrost monitoring in the northern greater Da hinggan mountains, Northeast China. J Glaciol Cryopedology 35(1):93–94 (in Chinese)

Han Z, Peng F (2012) Southern tidal flat of the Yangtze Estuary quantitative study of soil moisture based on ENVISAT ASAR. Marine Sci Bull 31(2):163–165 (in Chinese)

Jin X (2011) High resolution SAR image information extraction of bare soil and soil moisture inversion exploration. Zhejiang University Master's Degree Thesis, p 56

Wei Z, Jin HJ (2011) Permafrost change prediction in Northeast China under the conditions of climate change. Sci China 41(1):74–84 (in Chinese)

Zhang JZ, Huo M (2009) Northeast isolated permafrost distribution characteristic and its roadbed design strategies. Chin Foreign Highw 29(6):28–30 (in Chinese)

Zhou YW, Guo DX, Qiu GQ (2000) Geocryology in China. Science Press, p 450 (in Chinese)

Geotechnical and Geophysical Characterization of Frozen Granular Material

Anna Maria Ferrero, Alberto Godio, Maria Migliazza, Luigi Sambuelli, Andrea Segalini and A. Théodule

Abstract Degrading or thawing permafrost has been identified as being an issue of national importance with respect to its potential for causing severe damages or even loss of lives in densely populated Alpine regions due to climate change (Gruber et al. 2004; Gruber and Haeberli 2007). On this basis, a joint study was initiated by the Safe Mountain Foundation (Fondazione Montagna Sicura, Cormayeur, Italy) and some universities to investigate variations in geotechnical behaviour of the Alpine permafrost caused by changes in temperature. Permafrost is found in the Alpine regions at elevations higher than 2,500 m above sea level, depending on the location and exposure of the slope. Its mechanical features are determined by the combined effect of ice and soil particles. The water content can have an important influence on the shear resistance of the frozen soil: if the water content is low, the ice will not be able to include the soil particles. However, if it is very high, the resistance will be determined above all by the ice itself (Andresland 1987). Temperature is another driving factor that can influence the mechanical behaviour of ice (Fish and Zaretsky 1997). On this basis, this work concentrates on analysing the geotechnical and geophysical behaviour of the dispersed moraine deposits found in Alpine areas, which have been subjected to different climatic conditions due to the effect of high temperatures. The work concentrates on the

A. M. Ferrero
Earth Sciences Department, University of Torino, via Valperga Caluso 10128 Torino, Italy

A. Godio · L. Sambuelli
DIATI—Technical School of Torino, Corso Duca degli Abruzzi 10128 Torino, Italy

M. Migliazza (✉)
Earth Sciences Department, University of Milan, via Luigi Mangiagalli 34, 20133 Milan, Italy
e-mail: mariarita.migliazza@unimi.it

A. Segalini
DICATeA, University of Parma, Parco Area delle Scienze, 181/a 43124 Parma, Italy

A. Théodule
Safe Mountain Foundation, Vilar de la Palud, Courmayeur, AO, Italy

W. Shan et al. (eds.), *Landslides in Cold Regions in the Context of Climate Change*, Environmental Science and Engineering, DOI: 10.1007/978-3-319-00867-7_15,

geotechnical and geophysical characterization of two different glacial deposits present in the Aosta Valley region; the first one generated by the Tsanteleina glacier (Rhêmes Valley, 2,690 m a.s.l.), and the second one surrounding the Blu lake (Ayas Valley, 2,214 m a.s.l.). The characterization was carried out at different scales: laboratory-scale analysis using representative granular materials and field in situ investigations, geotechnical and geophysical testing. The geotechnical measurements were performed using photographic dimension analysis of the deposit, coupled with seismic and electrical surveys. Specimens were collected, remolded, saturated, and kept in a cooler in the laboratory. The specimens were later subjected to laboratory tests to evaluate the geomechanical strength properties of the materials using (mono-axial compressive strength and Young modulus) and geophysical (P and S wave velocities) behaviour of this kind of soils are affected by temperature variations under 0 °C (−35/−5 °C).

Keywords Frozen granular material · Permafrost · Geophysical characterization · Laboratory testing · Geotechnical characterization

1 Introduction

The cryosphere (snow, ice and permafrost), in high mountain areas, is particularly vulnerable to variations in temperature due to the effect of climate change.

These changes, in particular, the increase in air temperature, are reflected on rainfall regime, with greater display of summer drought, and on the distribution and persistence of glaciers and permafrost.

Another important aspect of climate change in high mountain areas is the development of potentially dangerous, natural instabilities connected with thawing of permafrosts and glacial dynamics. This is even more obvious in the Alpine region where, due to latitude and altitude effects, glaciers and permafrosts are often in frigid conditions, that is, at temperatures at or below the freezing point of water.

Series of investigations conducted on the Alps in the Aosta Valley region (CENSI_CRO 2009) showed the main contributing factors to such phenomenon is management of structures at high altitudes.

Analysis of soil samples collected from these sites is complicated because of various factors which include:

- The presence of permafrost which modifies the mechanical behaviour of the ground,
- The presence of unfrozen water in different quantities, depending on the season and on the depth of the ground;
- The triggering of ice-flows, due to thawing of the surface layers of the permafrost caused by excavations or climatic disturbances;

- The impossibility of obtaining complete samples due to elevated grain size distribution variability of typical material of the moraine zone;
- Logistic difficulties in transport and local analyses of the material.

For these reasons, degrading of the permafrost can lead to remarkable damage and loss of human lives in the most densely populated alpine zones (Gruber et al. 2004; Gruber and Haeberli 2007) and this has led the Safe Mountain Foundation in Courmayeur, Italy, the University of Parma and the Politecnico di Torino to set up an experimental study in order to perform a geotechnical and geophysical characterization of the permafrost zones. Permafrost is found in areas above 2,500 m, and it varies in function of the location and exposition of the slope.

The mechanical behaviour of permafrost layers is determined by combined action of ice and particles of the ground and it is affected to a great extent by the ice content in the mixture (Andresland 1987). For this reason, the resistance of the ice and ice mixture is affected by temperature (Fish and Zaretsky 1997).

The difficulties involved in accessing and sampling the zones subject to permafrost have led to a preference for the use of in situ measurement techniques, such as geophysical measurements, which make it possible to measure indicator parameters on the deposits. These parameters are then calibrated with the mechanical characteristics of the materials.

The present work is focused on carrying out laboratory tests on samples frozen at different temperatures. Both geophysical and geomechanical tests have been carried out in order to determine correlations between the representative magnitudes of the phenomenon, in order to apply these correlations in the interpretation of the in situ measurements.

Geophysical laboratory measurements involved the ultrasonic measurements of the compressional and shear wave velocities observed on samples at different temperatures. The data set are used to estimate the (dynamic) mechanical parameters of two different frozen soils. The sampling was conducted in two different sites: the first area was created by the Tsanteleina glacier, above the Granta Parei in the Rhemes Valley (2,690 m a.s.l.) and the second area surrounds the Blue Lake in the Ayas Valley (2,214 m a.s.l.).

Ice also contains mineral salts, which affects the melting temperature. This can be defined as a eutectic mixture of substances—a mixture of substances whose melting point is lower than that of the individual substances that make up the mixture. In the phase diagram, it is identified as a point that corresponds to an invariant equilibrium. A eutectic mixture, at a determined pressure value, is characterized by a well-defined weight relationship between its constituents and a well-defined temperature value. One example of this is a mixture of ice and salt (H_2O at the solid state and NaCl); ice melts at 0 °C, and salt melts at 804 °C, while their eutectic mixture melts at −21.3 °C.

The two solid phases (ice and NaC1) and the liquid phase are present in equilibrium at the same time at the eutectic point. The velocity of seismic waves is also conditioned by the composition of the mixture at different temperatures (Spetzler and Anderson 1968). Moreover, the Vp and the Vs in pure ice are not

influenced by the temperature of the pure ice. Distilled water was therefore used in the present research to make up the samples utilized in the laboratory in order to have a better comprehension of the in situ phenomena through geophysical measurements.

2 Geographical and Geological Setting

Aosta valley is located in the northwestern part of Italy in the western Alps. Sampling was conducted in two different sites (Fig. 1). The first area was formed by the Tsanteleina glacier, above the Granta Parei in the Rhemes Valley (2,690 m a.s.l.) and the second area surrounds the Blue Lake in the Ayas Valley (2,214 m a.s.l.).

Going up on the valley from the southwest to the northwest, the most important structural systems of the valley can be found. These structures were deformed by the collision between the European and African plates. Also observed are outcrops of orthogneisses, eclogite mica schists, gabbros, metagranites and the Mesozoic tectum of the Austrian-Alpine system of Paleo-African origin (Fig. 2). After this system, there are metasedimentary covers of oceanic origin (calc-schists, marbles and quartzites) and oceanic metabasites (serpentinites, amphibolites, metagabbros and prasmites) of the Piedmont area of calc-schist with Greenstones at the bottom of which are continental and oceanic sequences, corresponding to the southern

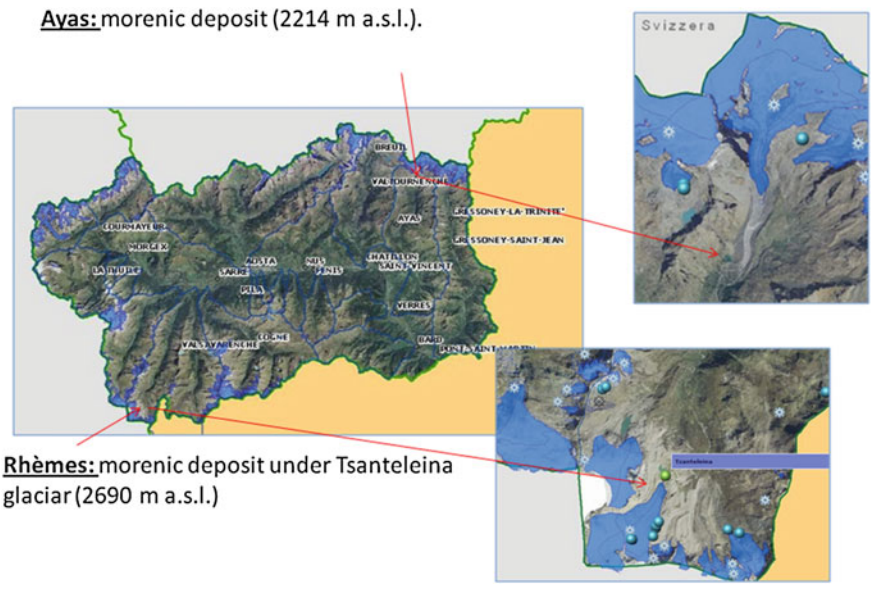

Fig. 1 Test site location

continental margin of the European plate also known as the Pennidic System. During the latest phase of the Alpine orogeny, the Austrian-Alpine and Pennidic nappe system translated over the Ultrahelvetic and Helvetic systems which are

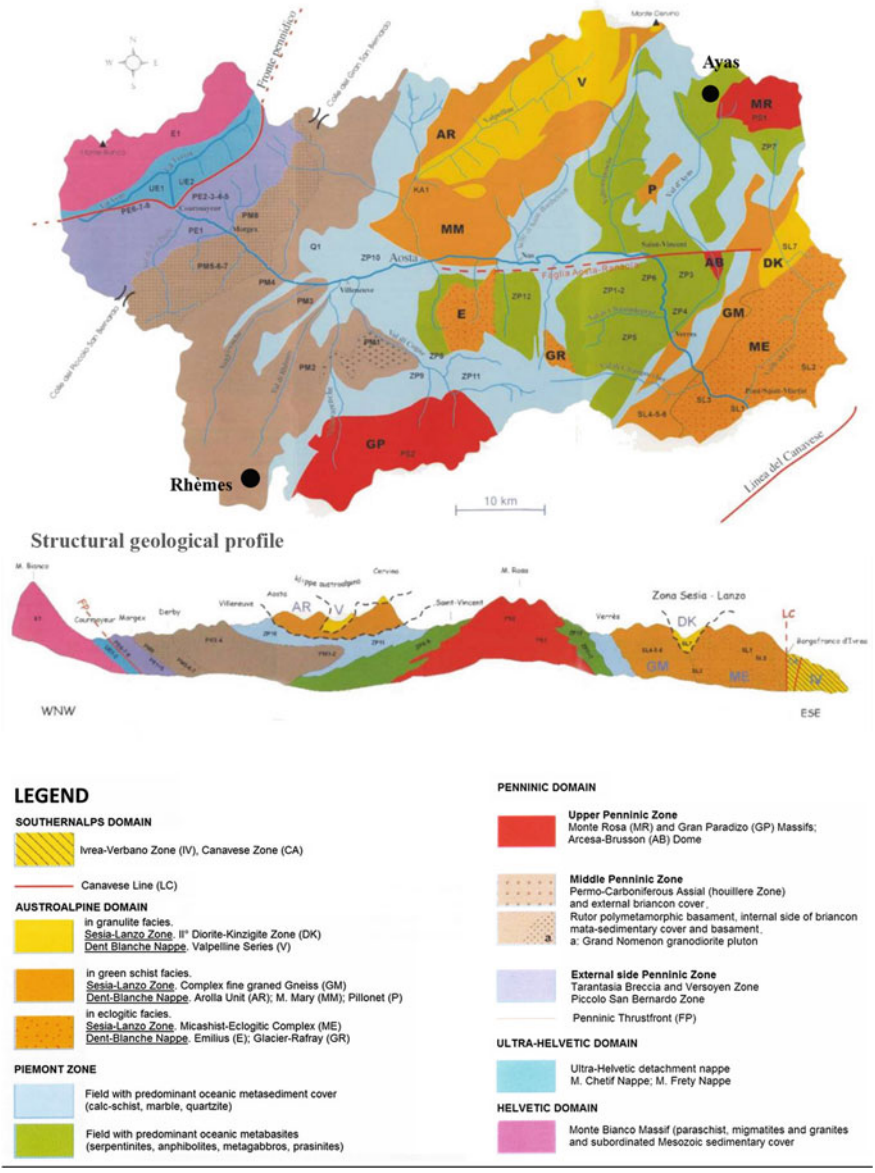

Fig. 2 Geological and Structural map of Valle d'Aosta region (after Bonetto and Gianotti 1998)

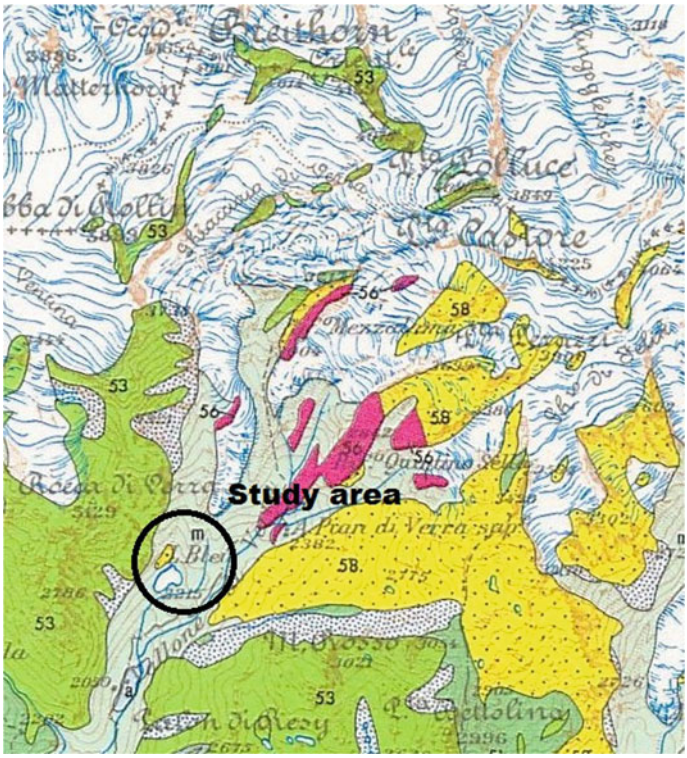

Fig. 3 Details of the Geologic Map of the Valle d'Aosta region (G. Elter, 1987) depicting the area surrounding the Val d'Ayas *Blue Lake*. Legend: m = undifferentiated till; 53 = serpentine; 58 = micaschists; 56 = metagranite and gneiss

composed of crystalline basement rocks of the European continent (Mnt. Bianco massif), and on the related sedimentary cover (Fig. 3).

Concerning the Val di Rhèmes sampling area adjacent to the Granta Parei, it can be pointed out that (Fig. 4) the moraine terrain is composed of gneisses, cleavelandite, mica schist, quartzite and graphite schist (grey, 43), brilliant schist (light blue, 44), limestone and dolomites (yellow, 38).

3 Geotechnical Characterization

The tests conducted in the laboratory first involved classification of sample materials according to the Unified Soil Classification System (USCS). Atterberg limits and granulometric curves were determined for both materials (Fig. 4). The specimens from Rhèmes shows a average liquid and a plastic limit of 15 and 11 %,

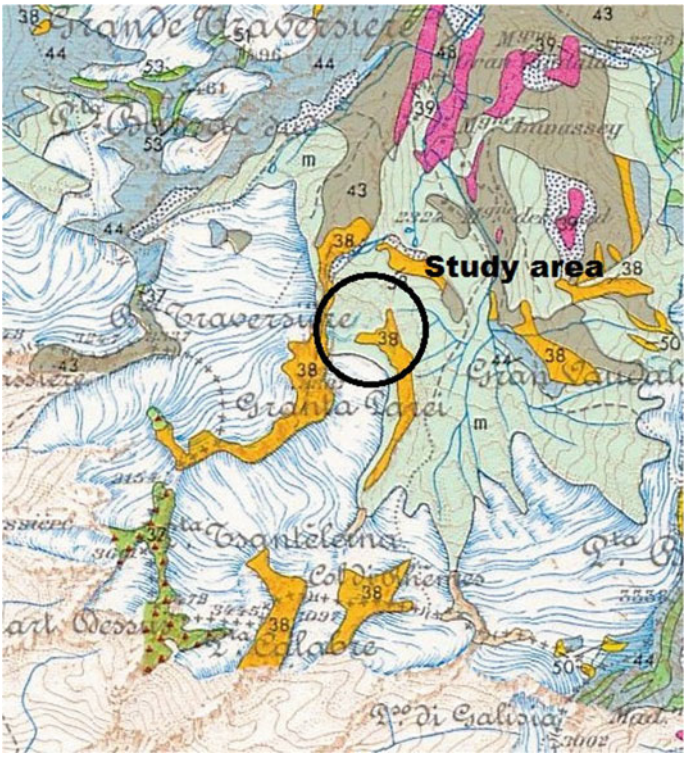

Fig. 4 Details of the Geologic Map of the Valle d'Aosta region (G. Elter, 1987), depicting the area surrounding the High Rhèmes Valley's Granta Parei. Legend: m = undifferentiated till; 38 = limestones and dolostones; 43 = micaschists and gneiss

while the liquid limit and plastic limit of samples from Ayas are 24 and 16 %, respectively.

The unified soil classification system (USCS) shows that soil materials from Ayas are well graded fine to coarse sands (SW), while those from Rhèmes are silts of low plasticity (ML) (Fig. 5).

Uniaxial compression tests were conducted on the samples at different temperatures (between −2 and −28 °C) and vertical displacement, normal load and temperature were measured by means of a thermocouple. The tests were carried out with an MTS press, equipped specifically to conduct controlled deformation tests, at the Materials laboratory of Parma University. The tests were conducted on 100 mm diameter and 200 mm high cylindrical shaped samples made up of sieved granular material of maximum size of 5 mm in order to keep the ratio between the samples and maximum dimension of the particles equal to 1:20. All the samples were prepared and frozen under constant temperature in a controlled chamber. The obtained results are shown in Table 1.

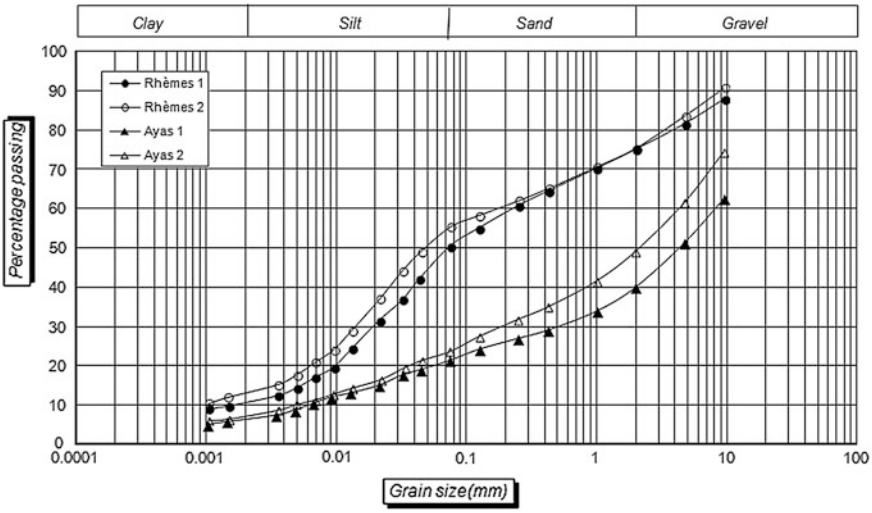

Fig. 5 Grain size distribution curve

Table 1 Features and results of Uniaxial tests on frozen specimens (where w is the water content; T is the temperature, $\Delta\sigma_{p-r}$ is the difference between peak and residual strength, Ed is the deformation modulus computed at the strain level reported)

Specimen	W [%]	T [C]	Displ rate [mm/s]	Peak strength [kPa]	Peak strain [%]	Residual strength [kPa]	$\Delta\sigma_{p\text{-}r}$ [kPa]	Ed max [MPa]	Strain level [%]
A1_1	33.7	−6	0.018	4,251	1.05	3,277	974	1,085	0.29
A1_2	27.3	−5.5	0.018	3,679	1.16	2,922	757	1,074	0.25
A2_1	30.5	−13	0.018	11,669	1.23	6,847	4,822	2,543	0.30
A2_2	32.6	−14	0.018	10,397	1.33	7,001	3,396	2,201	0.50
R1_1	27.6	−5.5	0.018	3,162	2.07	3,162	0	1,719	0.03
R1_2	24.7	−4.8	0.018	2,928	1.56	2,928	0	775	0.37
R2_1	32.2	−14	0.018	10,050	1.36	7,178	2,872	2,634	0.00
R2_2	31.4	−13	0.018	11,959	1.39	6,835	5,124	2,484	0.32

Although some authors (Arenson 2002) have pointed out that some glaciers are not usually completely saturated and circulation of water inside them is one of the reasons for their rapid thawing as air temperature rises; only completely saturated samples have been considered in this test campaign.

The reason for this is that a segregation phenomenon of the finer parts of a deposit can be observed in the deeper parts of the deposit, and this is accompanied by the formation of less permeable material and, consequently, less circulation of water.

4 Ultrasonic Laboratory Measurements

The main goal of the acoustic laboratory test was to evaluate the variation of both P and S wave velocities in frozen artificial soil samples in temperature range of −30 to −5 °C.

The use of ultrasonic wave velocity measurements in estimating the physical properties of frozen soils is a well established technique (e.g. Timur 1968; Zimmerman and King 1986; Carcione and Seriani 1998; Sheng et al. 2003).

Measurements of ultrasonic P and S wave velocities (v_p and v_s) have been carried out under constant load and different temperatures on the two samples A1 (Ayas) and R1 (Rhemes). The measurement chain consisted of: a CNS Electronic LTD P.U.N.D.I.T. pulse generator; two CNS LTD P and S wave transmitter/receivers with a nominal frequency of 150 kHz; a CNS LTD commuting box to switch between P and S wave; two CNS LTD amplifiers (8.5 dB for P waves and 10 dB for S waves); a Le Croy WaveJet 314 oscilloscope with a USB port through which the signal have been stored for later processing. The signals were sampled at 50 MHz with a record length of 200 μs. All the tests were done with an aluminum foil between the probes and the sample and by applying an axial load in order to enhance the acoustic coupling of S wave transducers. A specifically developed software, written in Matlab®, allows for ultrasonic pulse travel time reading, spectral analysis, comparison between P and S wave signals and storage of the read travel times.

5 Obtained Results

The obtained results, in terms of stress–strain curves, are reported in Fig. 6 for samples of the two different sites. The results, in terms of strength and strain, obtained with variations in temperature are shown in Fig. 7.

The first obvious observation seems to be a decrease in strength and stiffness as temperature is increased, but, in reality, a real variation of the behaviour of the ice material was recorded which showed ductile behaviour at temperatures closes to zero and fragile behaviour as temperature diminished. Even the shapes of the samples after rupture seemed to be remarkably different. At low temperature, localized rupture zones appears along clearly visible planes, while the samples shows diffused strain for temperatures close to zero.

The strain at rupture was also influenced to a great extent by temperature, from values of about 2 %, for low temperatures, up to 15 % for temperatures close to zero. This aspect seems to be particularly important from applicative point of view for the definition, for example, of in situ monitoring systems.

The acoustic measurements were analyzed both in time and frequency domain to estimate the travel time and frequency content of the signal. A preliminary inspection of the signal at the oscilloscope permitted to evaluate the signal to noise

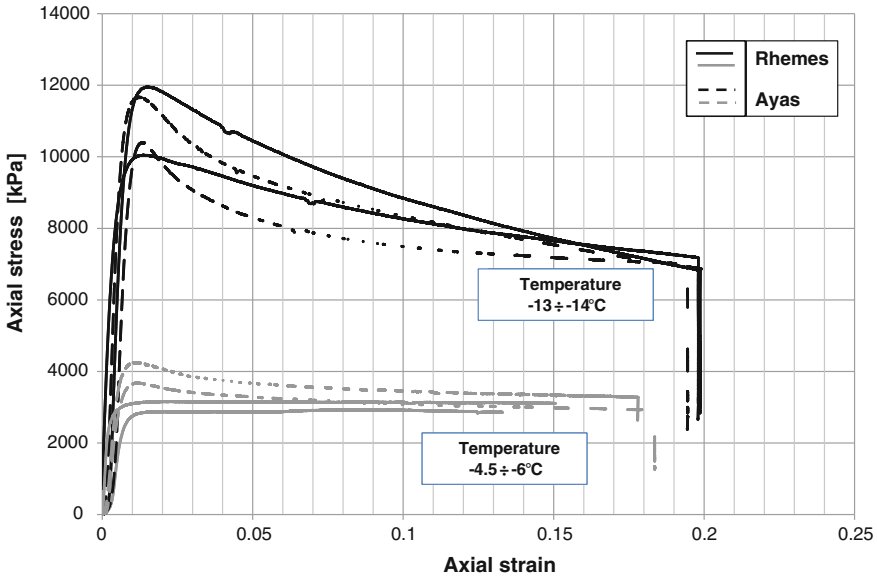

Fig. 6 Stress-strain curves obtained for the samples of Ayas Valley and Rhèmes Valley

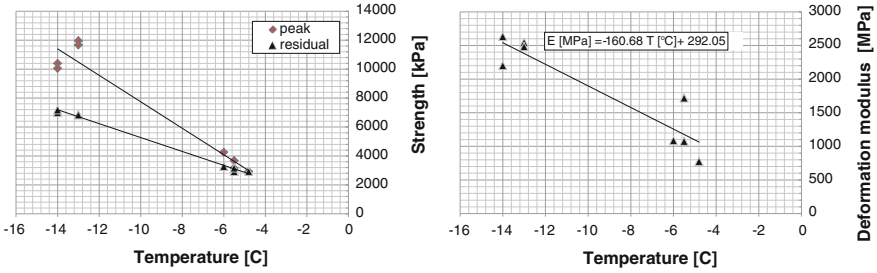

Fig. 7 Specimen temperature versus peak and residual Strength (*left*) and deformation modulus Ed (*right*) obtained by the uniaxial compressive tests on both Ayas and Rhèmes samples

ratio; they have been further stored and the power spectral density (PSD), with the aim of estimating the dominant transmitted frequency, has been calculated. Figure 8 shows the PSD's of some signals related to P and S waves collected at −5 °C. According to the probes characteristics, the dominant frequencies are in the range of 50 and 150 kHz.

The travel-time related to P and S waves at each temperature has been picked and both the velocities have been calculated.

The P wave velocities range from 4,100 m/s (at −5 °C) to about 4,500 m/s at lower temperature on the samples of the first site (Ayas); the sample of the second site are in the range of 4,300 m/s to 4,800 m/s. Shear wave velocities have similar trend. We observe values in the range between 2,100 m/s and 2,600 m/s for Ayas

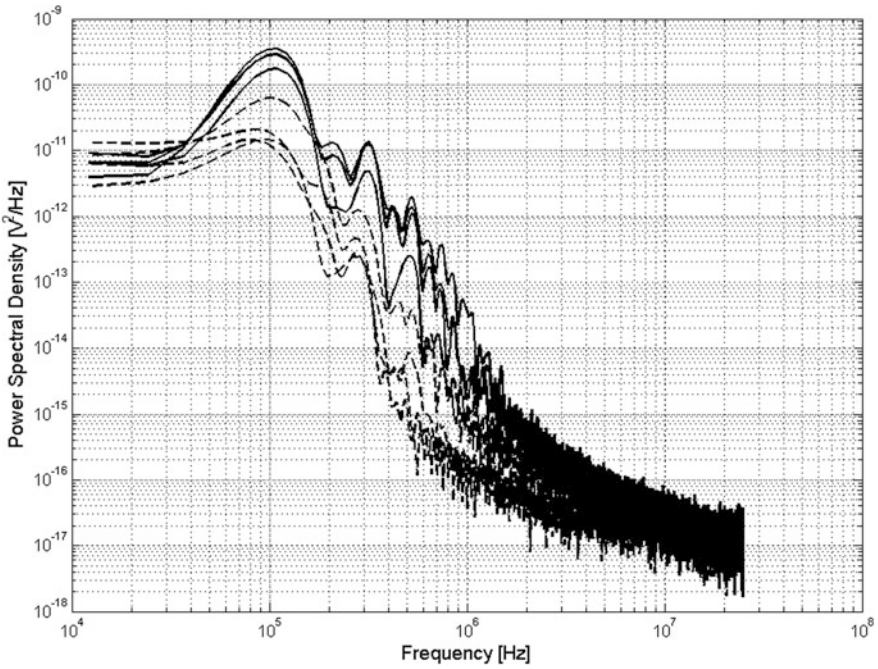

Fig. 8 Power spectral density of some signals related to P (Solid line) and S (dashed line) waves obtained at a temperature near −5 °C

soil material, and 2,100–2,500 m/s for soil material of the Rheme site. The plots of the P and S wave velocities versus the temperature are shown in Fig. 9 for the Ayas and Rhemes sites. The straight line interpolating curves and equations are also presented. All of them show a negative gradient with increasing temperature from −30 to −5 °C.

By using the well known formula of elasticity theory, Poisson dynamic ratio v_{dyn}, Young dynamic modulus E_{dyn} and shear dynamic modulus G_{dyn} were calculated and plotted against temperature with interpolating straight lines and equations.

$$v_{dyn} = \frac{\frac{1}{2}\left(\frac{v_p}{v_s}\right)^2 - 1}{\left(\frac{v_p}{v_s}\right)^2 - 1} \tag{1}$$

$$E_{dyn} = \rho v_p^2 \left(\frac{1 - v_{dyn}}{(1 + v_{dyn})(1 - 2v_{dyn})} \right) \tag{2}$$

$$G_{dyn} = \rho v_s^2 \tag{3}$$

where ρ is the density of the sample in kg m^{-3}.

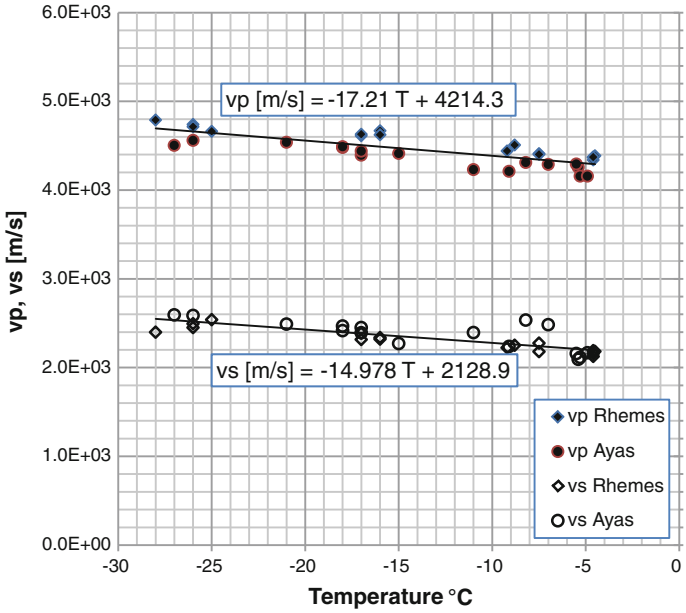

Fig. 9 Variation of V_p and V_s with temperature in the Ayas and Rhemes samples. The interpolating *straight lines* are also shown

The dynamic elastic moduli, E and G (Fig. 10) of the two sites, show a negative gradient with temperature, in accordance with the literature (Wang et al. 2006).

Poisson coefficient shows a slight increase with temperature in the range of 0.27–0.33. This can be related to increase of free water content in the samples as temperature increases.

In Fig. 10, the curves of the pure ice are also shown according to the formula suggested by Gammon et al. (1983). The discrepancies of the gradients are due to the presence of unfrozen water and small fraction of gas (air) in our samples that inadvertently had a strong effect, as far as the dynamic compressive modulus is concern (Timur 1968; Grant et al. 1999; Christ and Park 2009).

6 Conclusions

The conducted tests show how ice deposits loose strength and become more strained as temperature increases, thus, determining a remarkable variation of the stability conditions of a slope.

The laboratory measurements have pointed out a discrete variability in the strain properties of the materials for changes in temperature. In particular, the compression modulus in dynamic conditions shows a gradient of about −300 to

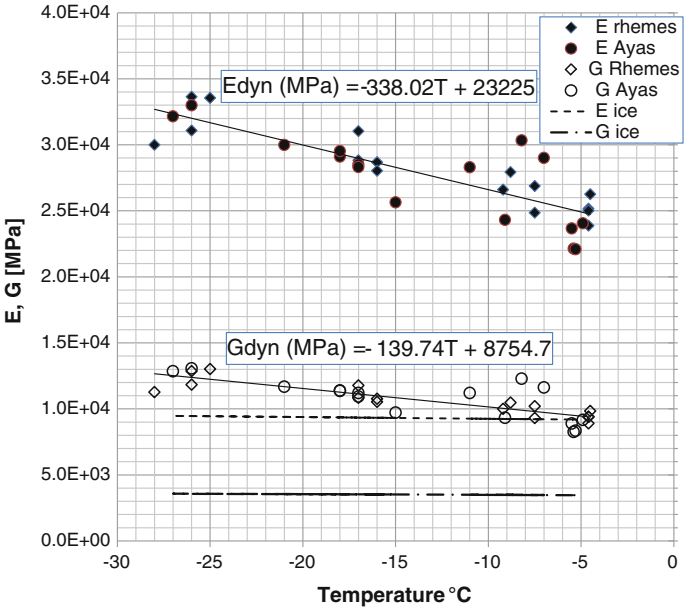

Fig. 10 Variation of G_{dyn} and E_{dyn} with temperature in the Ayas and Rhemes samples. The interpolating straight lines and the trends referred to the pure ice (*dashed lines*) are also shown

−400 MPa/°C for an increase in temperature of −30 to −5 °C. The dynamic shear modulus is characterized by gradients which ranged between −130 and −200 MPa/°C for the same conditions. In particular, both dynamic elastic moduli with increasing temperature from −30 to −5 °C show negative gradients which varies from −300 to −400 MPa/°C (E_{dyn}) and from −130 to −190 MPa/°C (G_{dyn}).

The corresponding value obtained from laboratory unconfined static compression test is −160 MPa/°C for the deformation modulus.

The different strain modalities and the different strain values upon rupture caused by variations in temperature should be taken into consideration in the design and modelling of in situ monitoring systems and in the case of interactions with buildings (for example, mountain shelters, the pillars of chairlifts etc.) in order to evaluate the compatibility of the strains in the foundation ground with the functioning of the structures.

Acknowledgments This comprehensive study was funded in the framework of the interreg European project GlaRiskAlp (2007–2013 Operational programme for cross-border cooperation Italy—France, Alps—ALCOTRA).

References

Andersland OB (1987)—Frozen ground engineering. Ground engineering reference book, Bell FG (Ed), Butterworth

Arenson Lukas Urs (2002)—Unstable alpine permafrost: a potentially important natural hazard—variations of geotechnical behaviour with time and temperature. Swiss federal institute of technology Zurich

Carcione JM, Seriani G (1998) Seismic and ultrasonic velocities in permafrost. Geophys Prospect 46:441–454

CENSI_CRO (2009) Censimento dei Crolli in Roccia in alta quota. Relazione tecnica finale Ing. Michèle Curtaz. Available on line, in Italian

Christ M, Park J (2009) Ultrasonic technique as tool for determining physical and mechanical properties of frozen soils. Cold Reg Sci Technol 58:136–142

Fish A, Zaretsky Y (1997)—Ice strength as a function of hydrostatic pressure and temperature. Cold Reg Res Eng Lab, Hanover N.H

Gammon PH, Kiefte H, Clouter MJ, Denner WW (1983) Elastic constants of artificial and natural ice samples by Brillouin spectroscopy. J Glaciol 29(103):433–460

Grant SA, Boitnott GE, Tice AR (1999)—Effect of dissolved NaCl on freezing curves of Kaoloinite, Montmorillonite and sand pastes. US Army Corps of Engineers Cold region Research & Engineering Laboratory, Special Report 99–2

Gruber S, Haeberli W (2007)—Permafrost in steep bedrock slopes and its temperature related destabilization following climate change. J Geophys Res, 112:F02S18

Gruber S, Hoetzle M, Haeberli W (2004)—Permafrost Thaw and Destabilisation of Alpine Rock Walls in the hot summer of 200. Geophys Res Lett

Sheng Y, Peng W, Wen Z (2003)—Physical properties of frozen soils measured using ultrasonic techniques. Permafrost, Phillips, Springman, Arenson (eds), pp 1035–1038

Spetzler H, Anderson L (1968) The effect of temperature and partial melting on the velocity and attenuation in a simple binary system. J Geophys Res 73(18):6051–6060

Timur A (1968) Velocity of compressional waves in porous media at permafrost temperature. Geophysics 33(4):584–595

Wang D, Zhu Y, Ma W, Niu Y (2006) Application of ultrasonic technology for physical–mechanical properties of frozen soils. Cold Reg Sci Technol 44:12–19

Zimmerman RW, King MS (1986) The effect of the extent of freezing on the seismic velocities in unconsolidated permafrost. Geophysics 51(6):1285–1290

A Rapid Stability Evaluation Method of Collapse in Sliding-Type Slopes

Shi-wei Shen, Lei Nie, Sun-lin Dai and Yan Xu

Abstract The principal features of sliding-type collapse, one of the most common failure modes in highway slope instability, are the existence of gently inclined joints or soft strata and tensile cracks on top of the slopes. Based on six major contributing factors of sliding-type collapses along the Ji'an-Gumalin Highroad slopes, a quick stability evaluation system was proposed to analyze the stability of slopes in different working conditions. The result shows that in its natural state, the collapsed masses are less stable, while under the influence of precipitation and seismicity, the collapsed masses are unstable, and factor of safety is lower due precipitation effect.

Keywords Sliding-type collapse · Influent factors · Rapid stability evaluation method

1 Introduction

As one of the major failure modes in slope engineering, slope collapse is usually accompanied with complex geological condition, cracked rock mass, and characteristic failure modes. In recent years, many scholars and researchers have done lots of research on various aspects. Zhao Jianjun and Liu Weihua from Chengdu Technology University have studied the characteristics of joints on the slope with statistical method and summarized the failure mechanics. They built an evaluation system using limit equilibrium method, and using method of interacting relationship matrix, weights of different parameters were fixed, which showed a quick stability evaluation system. Tian Qinyan from Zhongnan University studied

S. Shen (✉) · L. Nie · S. Dai · Y. Xu
College of Construction Engineering, Jilin University, Changchun, 130026 Jilin, People's Republic of China
e-mail: 69896116@qq.com

W. Shan et al. (eds.), *Landslides in Cold Regions in the Context of Climate Change*, Environmental Science and Engineering, DOI: 10.1007/978-3-319-00867-7_16,

fractural rock slopes with the key block theory, and proposed a stability evaluation system used presently in slope stability studies. Also, Xie Qiyong, Yan E'chuan, Quan Fenwen, Duan Haipeng, Yu Zihua, Huo Xiangyu, and Ling Bisheng discussed the different aspects of fractural slopes including engineering geologic conditions, influencing factors of fractural rock slopes' stability, analysis of failure mechanisms, and the stability evaluation. Shen Shiwei chose six major influencing factors of sliding-type collapse as research content and built up a rapid evaluation model for Ji'an-Gumaling collapse, then compared the result with traditional static force analysis method.

As for the collapse of slopes, due to their abruptness, it is important for the engineers to finish the stability evaluation in as short time as possible, even make the judgment in the field. This paper proposes a rapid evaluation system. Through the confirmation of weights of different parameters by experience and theoretical calculation, rapid stability evaluation method can be taken in the field.

2 Failure Mechanism of Slope's Sliding-Type Collapse

With the existence of weak structural planes beneath unstable rock masses, and tensile cracks on the back edge, slopes tend to show a creep and tension-crack motion. At the onset, groundwater infiltrates from the cracks into the slopes and weakens the soft structural plane. The water pressure and the gravity of the rock masses contribute to the creep slide of the slope. As the displacement reaches to a certain value, the collapse of the slope occurs. This type of collapsed mass can be divided into three parts: tensile crack zone, locked zone, and creep zone. The schematic figure of the sliding collapse is shown in Fig. 1.

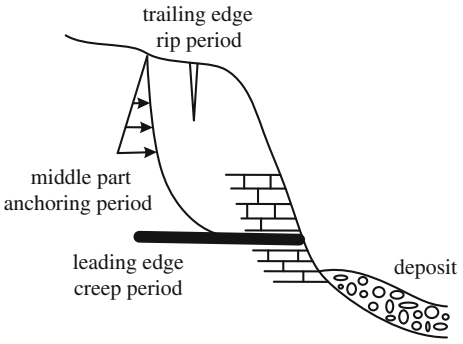

Fig. 1 Schematic figure of the sliding collapse

3 Influent Factors of Stability in Sliding-Type Collapse Slopes

The sliding-type collapse of slopes has a complex and various contributing factors. For consideration of engineering geological condition, physical and mechanical properties of rocks and the inducing factors of the circumstance, the evaluating variables are as follows:

1. Depth of the tensile crack. As for the sliding-type collapse, the process of the slope failure can be described as: the transfixion of tensile crack and weak sliding plane, deformation of unstable rock mass towards the free face, and the final collapse of slopes. Therefore, the depth of tensile crack on the back edge of slopes is an important factor in stability evaluation: the deeper the cracks, the weaker slopes are.
2. Dip angle of sliding plane. The sliding plane of the slope determines the failure process, and can be seen as a significant factor. From mechanical model of the sliding mass, it is obvious that with a higher dip angle, the deformation of rocks is accessible and the factor of safety is lower.
3. Mechanical properties of the structural plane. The shear resistance of the structural plane plays an important role in the stability evaluation of all kinds of slopes. Obviously, the lower the shear resistance, the weaker the slope becomes.
4. Degree of rocks weathering. Weathering degree of unstable rocks represents the fissures and mechanical properties of rocks. The stability of slopes is weak with a low anti-weathering ability rocks.
5. Underground water. Underground water is the primary inducing factor of the surrounding environment to the stability of slopes. Research has shown that the probability of collapse happening in rainy period is much higher than any other time. The precipitation causes the accumulation of groundwater in the fissures of rocks, applies a horizontal water pressure to the collapse mass, and weakens the mechanical properties of rock masses, which all have a negative effect on the slope's stability.
6. Unloading relaxation. Cracks from the unloading relaxation have largely determined the distribution of collapse rocks. Slopes with a high degree of unloading relaxation are broken, easily infiltrated by water, and have high failure probability.
7. Other inducing factors. There are some other influencing factors in the evaluation of slope's stability, including seismic and artificial explosion. The dynamic load opens the fissures, looses the structural plane and leaves the rock disjointed and susceptible to failure.

In summary, influencing factors of sliding-type collapse are interrelated, variance from one factor leads to changes in other factors. And the stability of slopes is the combining influence of these variables.

4 A Rapid Assessment Method for Sliding Collapses

Stability of dangerous rock mass of sliding-type collapse can be calculated using the static analysis method, but in practical engineering, it usually needs to be determined by technicians at the scene when a rapid assessment method is needed.

The rapid assessment method for the stability of dangerous rock mass is conducted on the basis of rapid assessment index system which can be summarized as: (1) description of the dangerous rock mass characteristics; (2) establishment of qualitative rapid assessment index system; (3) rapid stability assessment of the dangerous rock mass; (4) index assignment; (5) quantitative rapid stability assessment of the dangerous rock mass.

4.1 Introduction of the Relational Matrix for the Interaction Between Indicators

The key controlling factors for sliding collapses include: depth of rear edge cracks (F1), inclination angle of the sliding surface (F2), mechanical properties of the structural plane (F3), degree of rock mass efflorescence (F4), groundwater (F5) and unloading flabby condition, which interact to form the rapid stability assessment index system of the sliding dangerous rock mass. For qualitative stability analysis of the dangerous rock mass, mutual relationship between indicators have to be taken into consideration which is usually characterized with the relational matrix that tends to determine the importance of stability analysis of the dangerous rock mass by analyzing the contribution and the interactive strength between these indicators.

The interactive relational matrix in stability assessment of the dangerous rock mass sets the key controlling factors (F1–F6) on the main diagonal while the relationship between every two factors on the sub-diagonal (Fig. 2).

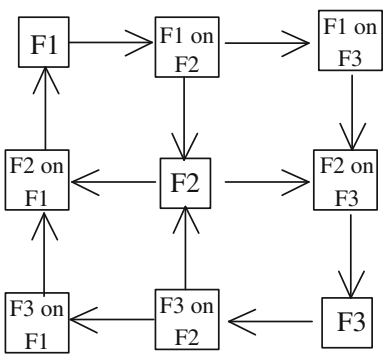

Fig. 2 Interaction in the relational matrix

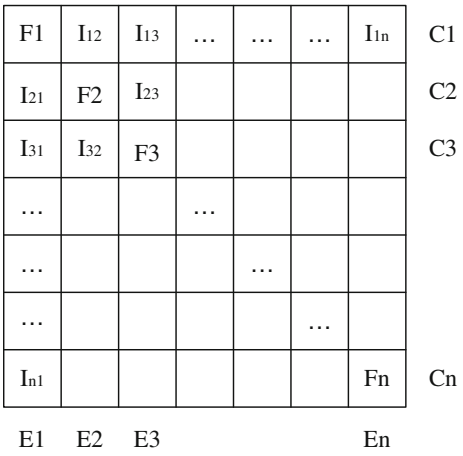

Fig. 3 Relational matrix of the interaction between multi-factors

Each element in the matrix is given different values which ranges from 0 to 4 based on the interaction strength, of which 0 means no effect, 1 means a weak effect, 2 means equal effect, 3 means stronger effect and 4 means strongest effect. The value of each element is presented as I_{ij}, and the value of Fi affecting Fj shows 0 on the main diagonal, so the relational matrix is shown in Fig. 3

In practical engineering, the activity index is introduced to mean various contributions of each factor to the system:

$$k_i = \frac{C_i + E_i}{\sum_{i=1}^{n}(C_i + E_i)} = \frac{C_i + E_i}{\sum_{i=1}^{n}\sum_{j=1}^{n} I_{ij}} \tag{1}$$

In the matrix, the key controlling factors are set on the main diagonal of which each indicator on the line means the influence on other indicators which on the rank means the influence exerted by other indicators on one indicator. The key controlling factors include depth of the rear edge crack (F1), inclination angle of the sliding surface (F2), mechanical properties of the structural plane (F3), degree of rock mass efflorescence (F4), groundwater (F5) and unloading flabby condition. On the non-main diagonal, the indicators are valued from 0 to 4 based on the influence degree by the experts half quantitative value method (Table 1).

Table 1 Valves of the interaction of the relational matrix

	I_{i1}	I_{i2}	I_{i3}	I_{i4}	I_{i5}	I_{i6}	C_i	k_i (%)
I_{1i}	**F1**	0	2	3	4	1	10	18.27
I_{2i}	0	**F2**	1	1	2	1	5	6.73
I_{3i}	1	1	**F3**	3	3	2	10	22.12
I_{4i}	1	0	4	**F4**	2	1	8	18.27
I_{5i}	4	1	3	2	**F5**	0	10	21.15
I_{6i}	3	0	3	2	1	**F6**	9	13.46
E_i	9	2	13	11	12	5		100.00

Table 2 Value of each indicator

Values	Rules	Values	Rules	Values	Rules
(F1) rear edge crack depth		(F2) sliding surface inclination		(F3) structural plane mechanical properties	
0	<0.1 slope height	0	<20°	0	Stronger
1	Medium	1	20° to 60°	1	Strong
2	>0.5 slope height	2	>60°	2	Low
(F4) rock mass efflorescence degree		(F5) groundwater		(F6) unloading flabby condition	
0	Low	0	No water	0	Weak
1	Medium	1	Medium	1	Medium
2	High	2	High	2	High

4.2 Value of Each Indicator

To quantitatively evaluate the stability of the dangerous rock mass, each indicator needs to be valued according to the interaction, influence and relationship. And because the six key controlling factors above are all qualitative, each indicator must be calculated after quantified in accordance with uniform standards.

Using the expert half quantitative valve method to value each indicator on various occasions and establish 3-standards of value: 0 means low contribution, 1 means contribution and 2 means high contribution. Rapid assessment indicators of the dangerous rock mass are quantized as shown in Table 2 according to the characteristics of various indicators and their influence on the stability of the rock masses.

4.3 Calculation and Classification of the Instability Indicators

To calculate the stability of the dangerous rock mass as the equation following, we determined the weight of each indicator according to the matrix and determined the single factor classification index with the qualitative analysis method.

$$UMII = \lambda_i \sum_{i=1}^{n} k_i \cdot \frac{F_i}{2} \tag{2}$$

where F_i is the ith single factor classification index; k_i is weight of the ith indicator; λ_i is correction coefficient of rainfall or earthquake.

UMII is a variable which is also called instability index of rock mass. It is calculated from the influencing factors that can evaluate the stability of the

Table 3 Classification about stability of the dangerous rock mass

Level of stability	Degree of stability	Index of instability UMII
IV	Stable	<25
III	More stable	25–50
II	Understable	50–75
I	Instability	>75

dangerous rock mass. λ is the correction factor of rainfall and earthquake, under natural conditions usually used 1.0. There are six master control factors of unloading relaxation representing the effect of earthquake on the stability of the dangerous rock mass. The correction factor of weak relaxation, middle relaxation and strong relaxation is 1.0, 1.2 and 1.5. It is through mechanical properties of the structural plane to represent the effect of the rainfall on the stability of the dangerous rock mass. The correction factor of weak rainfall, middle rainfall and strong rainfall is 1.0, 1.2 and 1.5.

To quantitatively describe the degree of stability of the rock mass, the stability of the dangerous rock mass is graded on the basis of computational formula (2). According to the standard adopted for the classification of rock mass by Huang Da, it divided the degree of stability into four levels: stable, more stable, understable and unstable. Combined with engineering practice, on the basis of the UMII, get the classification about stability of the dangerous rock mass such as Table 3.

The rapid assessment system of rock mass stability for sliding collapses based on rapid evaluation index system, which used the method of qualitative and semi quantitative to quick judge the stability of rock mass. During the evaluation, the first thing was to research engineering geological conditions of rock mass. Study on the interaction of each evaluation index, and make qualitative analysis of rock mass. Then get the value of evaluation index, and make quantitative analysis. The process can be divided into four steps and described as follows: (1) description of the dangerous rock mass characteristics; (2) establishment of the qualitative rapid assessment index system; (3) index assignment; (4) quantitative rapid assessment of the stability of the dangerous rock mass. It can be seen from above process, accuracy analyzed the engineering geological condition of rock mass is the basis of rapid evaluate stability. Get the reasonable values of evaluation index is the significant effect on quantitative evaluation.

5 Practical Engineering Case

The study area is located in the K6+965 section, on the right side of Jian-Gumaling highway, as shown on the cross-section (Fig. 4). The slope angle is 70°, and the slope height is 20 meters. The rock composing the slope is highly fragmented and

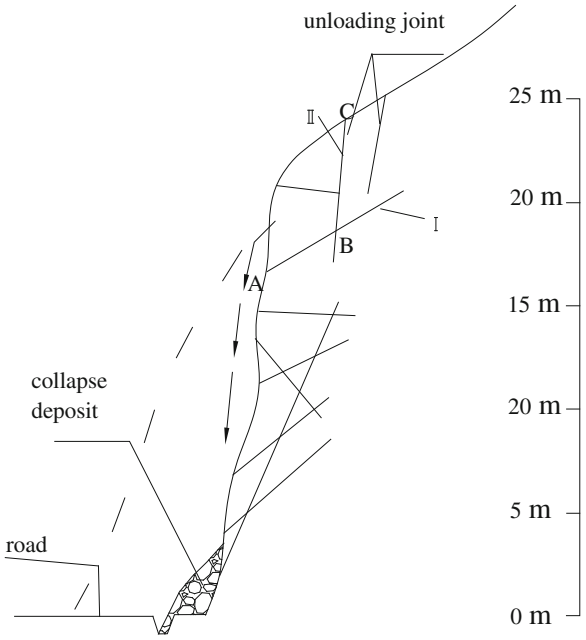

Fig. 4 Longitudinal cross section of K6+965 highway landslide

intensely weathered. The lithology of the layer is mainly dominated by the early Yanshan granite, between which thin layers of mudstone are deposited. The rock units in the slope are dominated by joint fissures which are divided into three groups, 195°∠75°, 115°∠36°, 285°∠65°, otherwise the tailing edge crack is about 2 meters deep, the dip angle of the sliding surface is 36°; the rock density is 2.72 g/cm^3 with cohesion of the shear surface of 2.8 kPa, and friction angle of 11°. The main six controlling parameters for the rapid evaluation system were chosen, and values of the parameters are given according to quantitative values in Table 2, and list the result in Table 4.

According to the interaction matrix in Table 1, assuming correction factor to be 1.5 under the condition of rain, and assuming the correction factor is 1.2 under the condition of earthquake, we got the dangerous rocks instability index values (UMII) under different working conditions, as shown in Table 5.

As is shown in Table 5, K6+965 section is understable under the natural working condition, and is unstable in rainy working condition and earthquake working condition, and the stability is worse in rainy condition compared with earthquake condition.

Table 4 Rapid evaluation parameter table of Jian-Gumaling highway typical section

Specific conditions	Quantitative value	Specific conditions	Quantitative value	Specific conditions	Quantitative value
(F1) trailing edge crack depth		(F2) dip angle of the sliding surface		(F3) mechanical characteristic of structure surface	
2 m	0	36°	1	C = 2.8 kPa $\phi = 11°$	2
(F4) weathered degree of rock		(F5) groundwater condition		(F6) The unloaded and relaxed state	
Badly weathered	2	Crack is not full of water	1	Medium unloading	1

Table 5 Dangerous rocks instability index values under different working conditions

Different working conditions	Nature working condition	Raining working condition	Earthquake working condition
Instability index (UMII)	68.06	107.45	81.35
Stability classification	Understable	Instable	Instable

6 Conclusion

According to the research, we got this conclusion:

1. Sliding-type landslide is mainly composed of pull-crack in the tailing edge, locked soil layer in the middle part and creep at the front end, while the main failure mode is creep-pull crack.
2. The main factors influencing the stability of sliding-type landslides are depth of the tailing edge crack, dip angle of the sliding surface, mechanical characteristics of the structural surface, degree of weathering of the rockmass, groundwater condition, and the unloaded and relaxed state.
3. The research process of the sliding rockmass rapid stability evaluation system can be summarized as: (a) characteristic description of dangerous rockmass; (b) establishment of dangerous rockmass rapid stability evaluation system; (c) qualitatively evaluate the stability of the dangerous rockmass; (d) evaluate index assignment; (e) quantitative rapid stability evaluation of the dangerous rockmass.
4. The result obtained from Jian-Gumaling highway sliding-type landslide indicates that the section is understable under natural condition, and is unstable under the effect of rainfall and earthquake, and increases under intense rainfall effect compared with the earthquake condition.

References

Duan HP, Zhao JJ, Ju NP (2008) Analysis of deformation process and deformation mechanism of fragmentation structure rock slope. Sub-grade Eng 139(4):170–172

Huo YX, Huang RQ, Ju NP (2009) Deformation mechanism and stabilization measures of broken granitic rock slope that experienced WENCHUAN earthquake. J Eng Geol 17(3):317–321

Ling BS, Zheng JZ (2009) Stability analysis and support design of high and deep phyllite cut slope in fragmentation structure. J Geol Hazards Environ Preserv 20(2):33–36

Liu EH (2008) Study on stability, movement characteristics and countermeasures of potential unstable rockmass in high-steep slope. Doctoral Dissertation of Chengdu University of Technology, China

Quan FW (2004) Mechanism and treatments of rock slope of fragmentation structure. Highway 6:8–12

Shen SW (2010) Research on the geological environment and slope stability of mountain area in southeastern of Jilin Province. Doctoral Dissertation of Jilin University, China

Tian QY (2003) Theory of block rock mass slope collapse monitoring and prediction and its application. Doctoral Dissertation of Center South University, China

Xie QY, Rao YA, Wu L (2004) Stability analysis of fragmental rockmass slope at Yinshan mausoleum of Yue mausoleum. Soil Eng Found 18(4):7–9

Yan EC, Dai GZ, Liu CX (2005) Stability analysis and treatment design of a loosen structure road cutting rock slope. Rock Soil Mech 26(supp):257–260

Yu ZH, Yan EC, Dai GZ (2005) Stability analysis and treatment design of a loosen structure road cutting rock slope. J Highw Transp Res Dev 22(9):137–140

Zhao JJ (2007) Study and application on rapid slope stability evaluation method for highway. Doctoral Dissertation of Chengdu University of Technology, China

Part V
Case Study on Landslide in Cold Region

Glacier Retreat, Lakes Development and Associated Natural Hazards in Cordilera Blanca, Peru

Adam Emmer, Vít Vilímek, Jan Klimeš and Alejo Cochachin

Abstract Cordillera Blanca is the heaviest glacierized tropical range in the world. Due to the global climate change, most of glaciers are retreating and thinning. Glacier retreat leads to the formation and development of all types of potentially hazardous glacial lakes (bedrock-dammed, moraine-dammed, and ice-dammed). Potential hazardousness of glacial lakes is strongly interconnected with dynamic slope movements: (1) sudden release of water from glacial lakes (also known as glacial lake outburst floods—GLOF) is mainly caused by dynamic slope movement into the lake (about 80 % in the Cordillera Blanca); (2) released water may easily transform into debris-flow or mud-flow, thanks to its high erosion and transport potential. Based on field study and remotely sensed images, this contribution documents glacier retreat in the Cordillera Blanca with regards to formation and development of new potentially hazardous glacial lakes, which evolve mainly in elevations of about 4,600–5,000 m a.s.l. We introduce and describe three hazardous events associated with glacier retreat in the last decade: (a) sudden release of water from moraine-dammed Lake Palcacocha in 2003; (b) sudden release of water from bedrock-dammed lake No. 513 in 2010; and (c) sudden release of water from bedrock-dammed Lake Artizon Alto and

A. Emmer (✉) · V. Vilímek
Department of Physical Geography and Geoecology, Faculty of Science,
Charles University in Prague, Albertov 6, 128 43 Prague 2, Czech Republic
e-mail: aemmer@seznam.cz

V. Vilímek
e-mail: vit.vilimek@natur.cuni.cz

J. Klimeš
Institute of Rock Structure and Mechanics, Academy of Sciences of the Czech Republic,
V Holešovičkách 41, 182 09 Prague 8, Czech Republic
e-mail: jklimes@centrum.cz

A. Cochachin
Unidad de Glaciologia y Recursos Hidricos, Authoridad National de Agua Av.
Confraternidad Internacional 167, Huarás, Peru
e-mail: acochachin@hotmail.com

W. Shan et al. (eds.), *Landslides in Cold Regions in the Context of Climate Change*,
Environmental Science and Engineering, DOI: 10.1007/978-3-319-00867-7_17,

subsequent moraine dam failure of downstream situated Lake Artizon Bajo in 2012. The first and third events were caused by landslides of lateral moraines (which are often non-
consolidated and nearly vertical) into the lakes. The second event was caused by ice- and rockfall into the lake. These events illustrate that various natural hazards (dynamic slope movements, floods) associated with glacier retreat in the Cordillera Blanca are closely linked and represent actual threats to urbanization and safety of lives and property.

Keywords Natural hazards · Glacier retreat · Dynamic slope movements · GLOFs · The Cordillera Blanca

1 Introduction

Impact of climate change to glacier retreat and thinning (downwasting) and associated natural hazards in high mountain areas has been described by O'Connor and Costa (1993) and more recently, by Clague et al. (2012). Glacier retreat is closely tied with various types of natural hazards which have potential to cause significant damages. These include direct and indirect dynamic slope movements (Richardson and Reynolds 2000a), catastrophic floods following sudden water release from any type of high mountain lake (Costa and Schuster 1988), earthquakes following intense ice loss (deglaciation-induced earthquakes) (Harrison et al. 2006), and also, changes in runoff regime followed by droughts (Mark 2002). These apparently disparate natural hazards are in fact naturally linked. Based on remotely sensed photographs and field study conducted in 2010, 2011 and 2012, this contribution brings three examples of ties (links) among glacier retreat, selected glacial lake development (Fig. 1), various types of dynamic slope movements and outburst floods in the Cordillera Blanca mountain range (Peru).

Richardson and Reynolds (2000a) distinguishes between direct and indirect dynamic slope movements associated with deglaciation. Direct dynamic slope movements associated with deglaciation are snow/ice avalanches, while indirect are mass re-organizing paraglacial processes affecting steep sided valleys—e.g. rock avalanches and landslides. This phenomenon of indirect dynamic slope movements associated with deglaciation is also called "landslide response to post-Little Ice Age glacier retreat and thinning" (Holm et al. 2004). Together, these two groups of dynamic slope movements represent the most frequent trigger of sudden and often catastrophic water release from glacial lakes in the Cordillera Blanca—80 % overall of which 45 % are direct and 35 % indirect dynamic slope movements into the lake. The remaining 20 % of sudden water release from glacial lakes in the Cordillera Blanca are due to earthquakes and flood waves from lakes situated upstream (Emmer and Cochachin 2013). A sudden water release from any type of glacial lake irrespective of its cause is called a "Glacial lake outburst

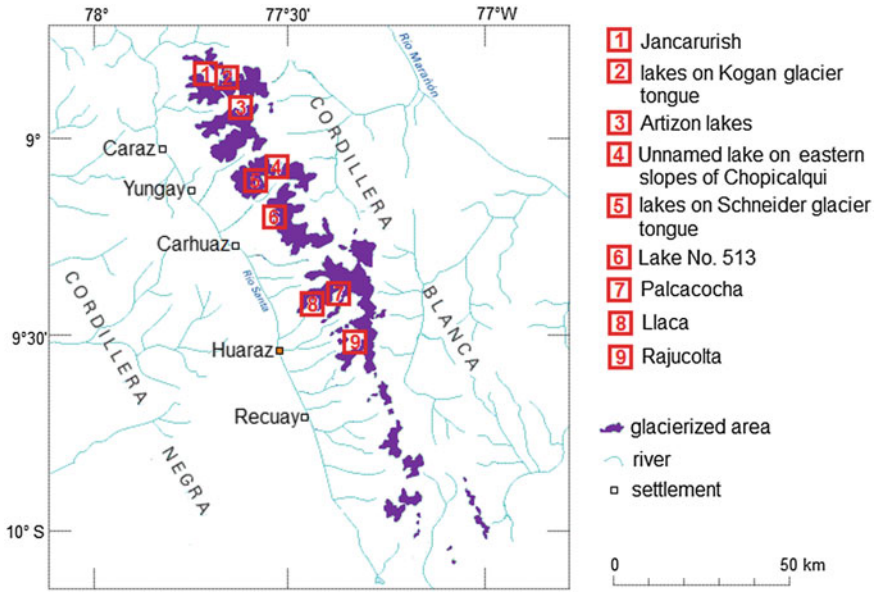

Fig. 1 The Cordillera Blanca and the location of lakes mentioned in this paper (*base map* USGS)

flood" (GLOF). A GLOF may result from failure or overflow of a glacial lake dam and, thanks to its high erosion and transport potential, may easily transform into flow movement (e.g. debris-flow or mud-flow). These events claimed thousands of lives during the 20th century, and caused significant damage in the Cordillera Blanca. The most catastrophic was the moraine-dam failure of lake Palcacocha in 1941 and the moraine-dam failure of lake Jancarurish in 1950 (Zapata 2002).

2 Study Area: The Cordillera Blanca

The Cordillera Blanca is located in the northcentral Andes, in the Ancash region of Peru (8.5°–10°S; 77°–78°W). This mountain range is part of the Cordillera Occidental (Western Cordillera). The Cordillera Blanca is the highest Peruvian mountain range with sixteen peaks over 6 000 m a.s.l. and also the most heavily glacierized tropical range in the world, with present glacier extent of about 600 km^2 (Georges 2004). This figure represent approximately one fourth of worldwide extent of tropical glaciers (Ames and Francou 1995). The western part of the Cordilllera Blanca is drained by Rio Santa into the Pacific Ocean, while the eastern part is drained by Rio Marañon and then by the Amazon River into the Atlantic Ocean (Fig. 1). The geological structure is very complicated and differs from south to north as well as from east to west. The upper parts of the Cordillera Blanca are underlain by granitic intrusions, but there are also parts which are

underlain by extrusive vulcanic rocks such as andesitic rocks and tuffs or sedimentary rocks such as sandstones and shales (Wilson et al. 1995). The Cordillera Blanca is an active seismic region, where large earthquakes occur (e.g. 1970 earthquake with M7.7), cause significant damages and also initiate various types of natural hazards such as dynamic slope movements or GLOFs (Lliboutry et al. 1977). The main fault zone extends approximately 210 km through the western slopes of this range.

2.1 Glacier Retreat

The Cordillera Blanca had been glacierized several times in geologic history and the glacier extent was much more extensive during the late Pleistocene and Holocene (Mark 2002; Vilímek 2002). Clear evidence of past glacier extent such as massive moraines, U-shaped valleys and striations can still be found in reliefs, kilometers away from the present position of glaciers. The last significant glacier advance happened during the so called "Little Ice Age"—a relatively cold period, which culminated (according to lichenometric dating and ice-core data from Huascarán glacier) from 1590 to 1720 and less extensively from 1780 to 1880 (Thompson et al. 2000; Solomina et al. 2007). Since the end of the Little Ice Age, glaciers started to retreat and new glacial lakes began to form and develop.

Moraines that formed during the Little Ice Age mark the maximal glacier extent during this period, but there is no appropriate evidence for the subsequent glacier retreat during the 19th Century. Glaciers of the Cordillera Blanca have been inventoried several times in the 20th Century and the trend of retreat and thinning is obvious. Georges (2004) reconstructed the extent of glaciers in the 1930s to 800–850 km^2, based on the first aerial photographs of this region. According to remotely sensed photographs of this area in the 1970s, the extent of glaciers decreased in 40 years to 723 km^2 (Ames and Francou 1995). The latest investigation demonstrated that the extent of glaciers was about 600 km^2 at the beginning of the 21st Century (Georges 2004). These numbers show that glacier extent has decreased by about one fourth since the 1930s. The total volume of glaciers can also be assumed to have decreased in this period, due to downwasting. This intense glacier retreat and thinning is visible on all glaciers within the Cordillera Blanca; nevertheless, there are some differences in the rates of glacier retreat. Areal and volumetric glacier retreat is mostly controlled by various combinations of the following factors:

1. Meteorological regime—solar radiation—energy for glacier thawing is mostly gained from solar radiation, thus a very important characteristic is the total number of hours of sunshine in a year and aspect of slopes and its exposition (see below) (Oerlemans and Knap 1998; Mark 2002)
    - temperatures and precipitation (e.g. Huggel et al. 2004)—every part (valley) of the Cordillera Blanca has a specific meteorological regime, but in general,

sites with higher temperatures and/or lower precipitation have greater rates of glacier retreat

2. Topographic setting—aspect—aspect is generally considered as one of the most important non-climatic characteristics influencing rate of glacier retreat, because it is closely connected with hours of solar radiation. Glaciers with an eastern aspect have the highest rate of glacier retreat within the Cordillera Blanca, while glaciers with southwestern aspect have lower rates of glacier retreat (Mark 2002)
   - exposure—exposition is a second topographical characteristic, which controls rate of solar radiation. That is, sites which are often shaded by surrounding terrain receive less solar radiation than exposed sites.
3. Glacier characteristics—area (volume) of glacier—Larger glaciers have a greater volume of ice and lower initial rates of retreat and thinning; larger ice bodies are able to resist for a long time (Kaser 1995)
   - debris coverage—the role of debris cover on glacier retreat is not uniform. On one handglacier tongues covered by a thick debris layer are able to resist the direct impact of solar radiation and thus may persist for a longer time in lower altitudes (in the form of buried ice). On the other hand glacier tongues covered by a thin debris layer thin easily, due to heat exchange between the ice body and dark debris with a higher heat capacity and lower albedo (Richardson and Reynolds 2000b).

The number of glacial lakes in the Cordillera Blanca during the 20th Century increased with a decrease in the extent of the glacierized area (Table 1). The first inventory of lakes was presented by Concha (1951) who showed that there were 230 lakes of significant size at the beginning of the 1950s, of which most of the glacial lakes in altitudes between 4,250 and 4,600 m a.s.l. Morales et al. (1979) updated the overall number of lakes of significant size to 267. Portocarrero (1995) summarised 899 lakes in the Cordillera Blanca and now there are more than one thousand of lakes overall (see Table 1), and new lakes form and develop in the altitudes between 4,600 and 5,000 m a.s.l.

Table 1 Decreasing extent of glacierized area and increasing number of lakes since 1930 within the Cordillera Blanca

Years	Glacier extent (km^2)	Number of lakes	References
1930	800–850	–	Georges (2004)
1951	–	230 (lakes of significant size)	Concha (1951)
1970	723	267 (lakes of significant size)	Ames and Francou (1995); Morales et al. (1979)
1995	–	899 (overall)	Portocarrero (1995)
2000	600	–	Georges (2004)
2012	<600	>1,000 (overall)	This study

2.2 Typology of Glacial Lakes

A glacial lake is a lake, whose basin was excavated by glacial erosion, dammed by a glacier body or moraine or some combination of these. A number of typologies of (glacial) lakes for different purposes and regions have been created e.g. by Hutchinson (1957), or later by Kalff (2002) or Janský et al. (2006). Typology of lakes within the Cordillera Blanca with regard to its potential hazardousness was first presented by Concha (1951). One of the most common typologies is one that divides glacial lakes according to the material which forms the lake dam. This typology generally distinguishes between:

1. bedrock-dammed lakes;
2. moraine-dammed lakes; and
3. ice-dammed lakes.

The first and second types easily reach a significant volume of accumulated water (from 10^6 to 10^7 m^3) within the Cordillera Blanca, while the third type does not.

Bedrock-dammed lakes form in depressions excavated by glacial erosion after its retreat. The dam of the lake is composed of solid rocks, and thus is considered to be stable (Huggel et al. 2004). Therefore, dam breach is not a possible scenario for sudden water release, unlike the dam overflow. This type of lake is very common within the Cordillera Blanca, but they are often insignificant in size. Of course, there are some which exceed a volume of 10^6 m^3 (e.g. lake No. 513, lake Auquiscocha or lake Churup), but most of them do not.

Concha (1951) distinguished between bedrock-dammed lakes with direct contact with a glacier and without contact with a glacier, because direct contact with a glacier and the possibility of it calving into the lake and producing displacement waves is a very important characteristic in the potential hazardousness of the selected lake. New bedrock-dammed lakes evolve in present days, some of them evolve in hanging valleys mostly at altitudes ranging between 4,600 and 5,000 m a.s.l. An example of a new, rapidly growing bedrock-dammed lake is an unnamed lake situated beneath the eastern slopes of Chopicalqui massif (6,354 m a.s.l.). This lake enlarged its area between 2003 (Fig. 2a) and 2011 (Fig. 2b) more than two times. The volume of accumulated water, which is available for sudden water release, is also increasing rapidly. The maximum length of the lake was more than 500 m in 2011 and there is a great potential for further growth following glacier retreat.

Moraine-dammed lakes are most frequently formed behind moraines after glacier retreat. This type represents the largest lake in the Cordillera Blanca. The volume of accumulated water may exceed 10^7 m^3. Some examples are Lakes Jancarurish (12,322 $\times$ 10^6 m^3; Fig. 3a); Rajucolta (17,546 $\times$ 10^6 m^3; Fig. 3b), and Placacocha (17,325 $\times$ 10^6 m^3; Fig. 3c), which are all dammed by massive moraines formed during the Little Ice Age at elevations between 4,250 and 4,600 m a.s.l. All these examples of very large contemporary moraine-dammed lakes within the Cordillera Blanca had produced GLOFs in history (Rajucolta in

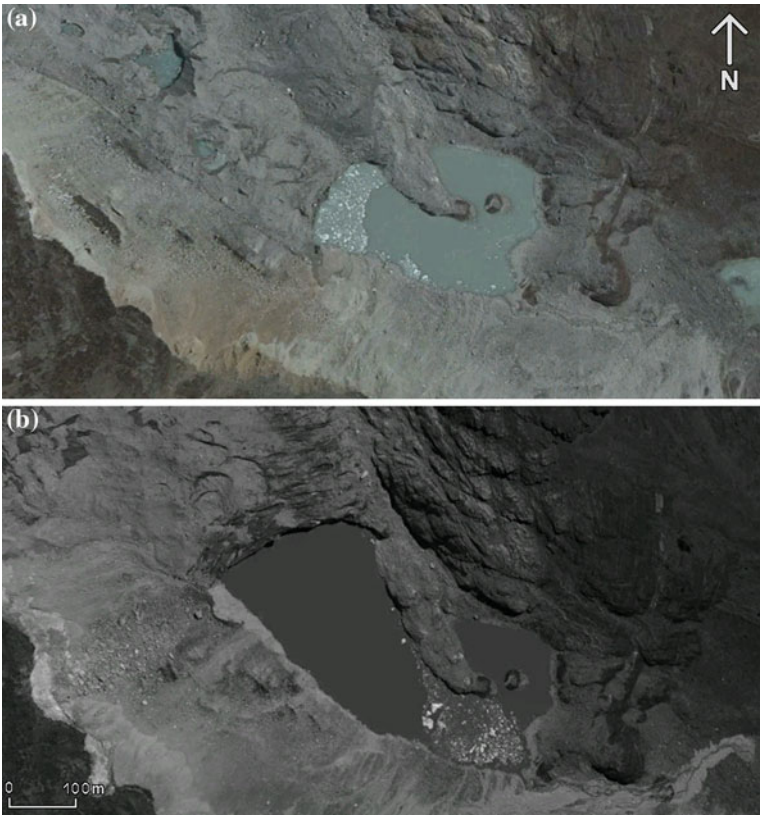

Fig. 2 Unnamed growing bedrock-dammed lake beneath the eastern slopes of Chopicalqui massif. Part **a** was taken in 2003, while part **b** was taken in 2011. Clear evidence for a small outburst flood after overflowing the dam following glacier calving or landslide of lateral moraine into the lake is visible in part **b** (*Source* Google Earth Digital Globe 2013)

1883; Palcacocha in 1941 and 2003; and Jancarurish in 1950) (Zapata 2002). The height of LIA moraine dams may exceed one hundred meters and their slopes are frequently very steep and unstable. Richardson and Reynolds (2000a) showed that lakes formed behind LIA moraines are potentially dangerous because they are dammed by unconsolidated and poorly sorted material which enhances dam failures, and at the same time, they are often in direct contact with the glaciers (icefalls into the lake represent the most frequent trigger for outburst floods). Clague and Evans (2000) showed that moraine-dammed lakes most commonly fail at the beginning of glacier retreat. The Cordillera Blanca is an example of this scenario.

Concha (1951) divided moraine-dammed lakes of the Cordillera Blanca into more categories. The first distinction is between moraine dams with steep slopes and moraine dams with gentle slopes, but no critical value is given, thus the

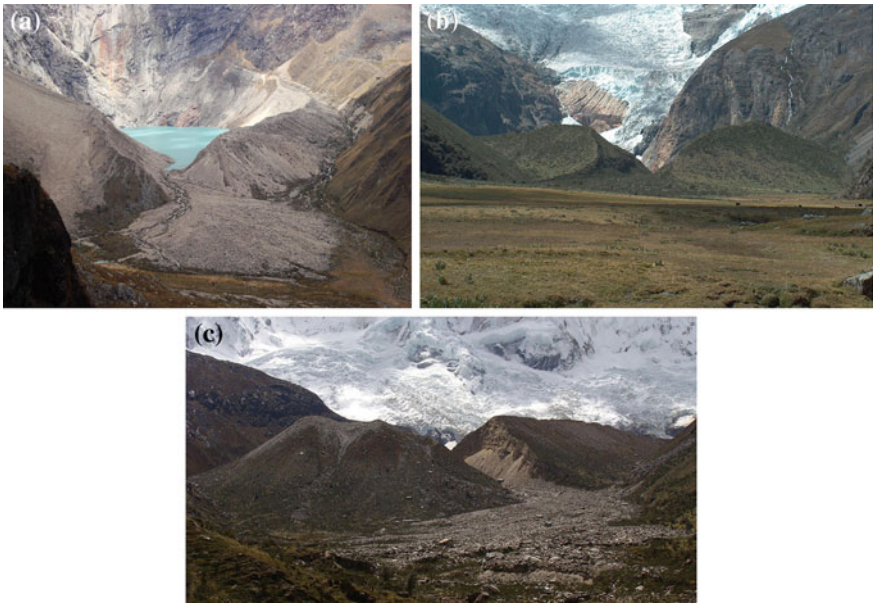

Fig. 3 Examples of failed moraine dams within the Cordillera Blanca. Part **a** shows the moraine dam of lake Jancarurish in de Los Cedros valley (failed in 1950), part **b** the moraine dam of lake Rajucolta in the Rajucolta valley (failed in 1883) and part **c** the moraine dam of lake Palcacocha in the Cojup valley (failed in 1941)

classification is quite subjective. The second distinction, in the case of bedrock-dammed lakes, is between moraine-dammed lakes with direct contact with glaciers and without direct contact with glaciers. These two characteristics in a simplified way reflect potential hazardousness of moraine-dammed lakes. That is, the slope of a moraine dam reflects its potential to failure and contact with glaciers reflects the possibility of icefall into the lake to trigger its failure.

Ice-dammed lakes are generally considered as one of the less stable types of lakes (Korup and Tweed 2007). Various subtypes of ice-dammed lakes were defined by Costa and Schuster (1988) according to the position of the lake in relation to the glacier. Only one subtype of ice-dammed lakes is represented in Cordillera Blanca—supraglacial lakes. This subtype of ice-dammed lakes is a product of surface glacier melting and evolves directly on the glacier tongue body. Merging of small lakes may produce a large one, but obvious instability of ice dams limit the possibility of development of supraglacial lakes of significant size. If glacier tongue is surrounded by moraines, merging of supraglacial lakes usually foregoes to formation of moraine-dammed lake.

There is no ice-dammed lake of significant size in the Cordillera Blanca at the moment, because these most frequently appear after damming of a lateral valley by an advancing glacier in the main valley, or after damming of the main valley by an advancing glacier from a lateral valley (Costa and Schuster 1988); but there is a

high number of small supraglacial lakes that developed on glacier tongues with gentle slopes. Maximal perimeter of these lakes is in the order of tens of meters and the estimated volume of accumulated water reaches 10^4 m^3. Example of a site with a large number of ice-dammed lakes (subtype supraglacial lakes) is the tongue of Kogan glacier (Fig. 4a), beneath the northern slopes of Quitaraju massif (6,036 m a.s.l.). Development of these lakes indicates intense thinning of the Kogan glacier. The glacier tongue is not surrounded by a terminal moraine and thus the formation of a moraine-dammed lake by merging of small supraglacial lakes is not a possible scenario, in contrast to the tongue of Schneider glacier (Fig. 4b) beneath the eastern slopes of Huascarán Sur massif (6,768 m a.s.l.). The debris-covered tongue of Schneider glacier is surrounded by moraines, so there is a potential for future development of a significant moraine-dammed lake by merging of small supraglacial lakes.

3 Case Studies

Three examples illustrate the interconnections between glacier retreat, dynamic slope movements and potential hazards posed by developing glacial lakes. These events occurred in the last decade and caused material damages in affected valleys.

3.1 Lake Palcacocha 2003 Event

Lake Palcacocha is situated at the upper part of Cojup valley, which is oriented in the NE-SW direction under the Nevado Palcaraju (6,274 m a.s.l.) and Nevado Pucaranra (6,165 m a.s.l.). Terminal and lateral moraines were formed during the little ice age glacier advance, and with glacier retreat after this period a moraine-dammed lake formed and continued to expand. On 13rd December 1941, the moraine dam failed, probably after an icefall into the lake which produced a displacement wave, and the wave eroded the outflow of the dam (Oppenheim 1946). The volume of water released was estimated to be between 8×10^6 m^3 (Evans and Clague 1994) to 10^7 m^3 (Vilímek et al. 2005). The resultant glacial lake outburst flood transformed into debris flow, travelled down the valley, and invaded the city of Huaráz, where it claimed about 6,000 lives and destroyed one third of the whole city (Lliboutry et al. 1977). Currently, Lake Palcacocha is dammed by a basal moraine with two artificial dams (Fig. 5a) and its volume reached $17{,}325 \times 10^6$ m^3 during the 20th Century due to continuing glacier retreat (Vilímek et al. 2005).

A small GLOF was produced from Palcacocha Lake during March 19th 2003 by a planar landslide which crashed into the lake. The probable triggering factor was the over-saturation of the moraine material by precipitation. The 2003 landslide occurred in the inner part of the left lateral moraine adjacent to the glacial

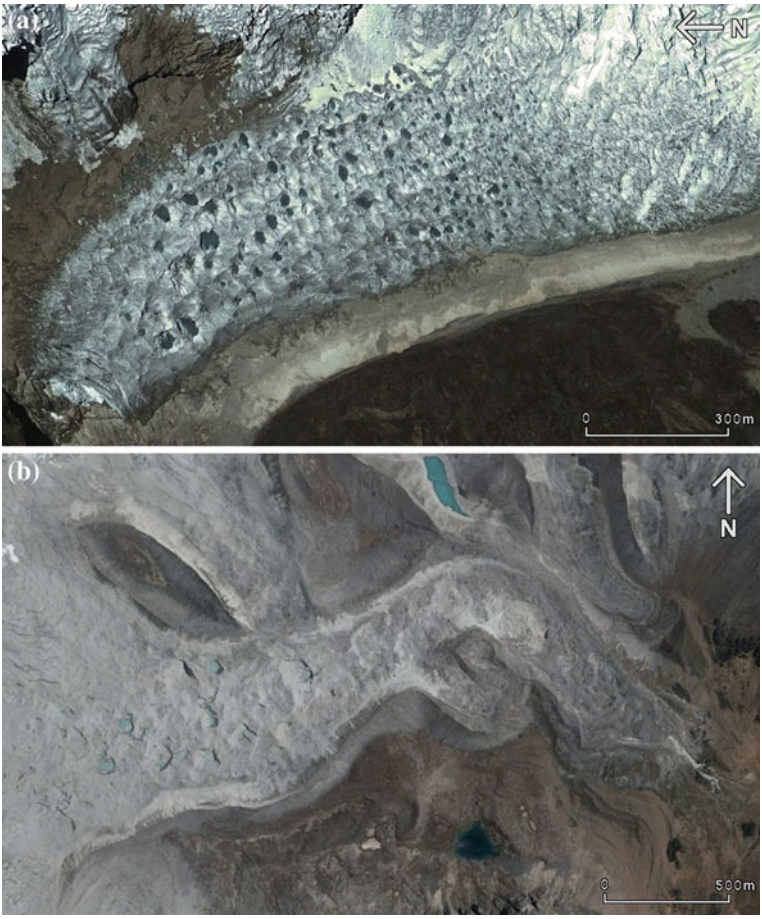

Fig. 4 Tongues of Kogan glacier in 2012 (part **a**) and Schneider glacier in 2003 (part **b**) with tens of small supra-glacial lakes. The debris-covered tongue of Schneider glacier is surrounded by moraines and thus there is a potential for future formation and development of a moraine-dammed lake (*Source* Google Earth Digital Globe 2013)

tongue—in the location where prominent drop-offs of the moraine slope were identified on the 1970 aerial pictures (Vilímek et al. 2005). These features were also seen during fieldwork in 2003 (Zapata et al. 2003), and we assume that these might have played an important role in water infiltration and in the evolution of the planar sliding plane of the landslide. The landslide hits partly the glacial tongue. The volume of the slope movement was estimated to be about 50,000–75,000 m^3. A displacement wave which was created in the lake was at least 8 m high. The wave reached the frontal dam of Palcacocha Lake and after overtopping, it created a small GLOF in Cojup stream and Quilcay River. Fortunately large damages were avoided, nevertheless the water treatment plant for Huarás, capital city of Ancash

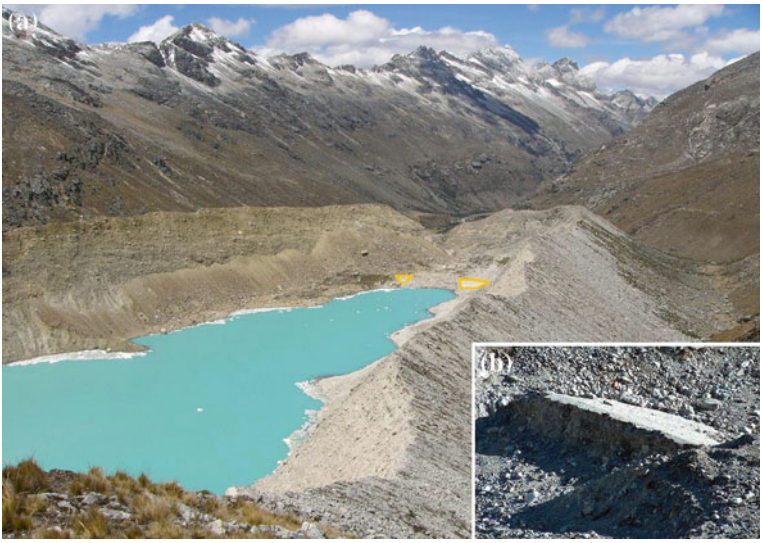

Fig. 5 View on lake Palcacocha with two artificial dams (*highlighted by the orange line*); steep nearly vertical lateral moraines are visible on both sides surrounding the lake. The detail picture (Part **b**) was taken after the 2003 event and captures the damaged artificial dam

department, was blocked by sediment-laden currents and also an aritificial dam of the lake was partly damaged (Fig. 5b). The landslide left no significant accumulation on the lakeshore. A secondary debris flow originated from the highly saturated material from the upper part of the moraine slope and produced a small accumulation cone. Field mapping around the glacial lake showed that the right lateral moraine on the opposite side of the lake shows signs of rather fresh but smaller planar landslides.

The most active parts of the entire inner slopes are those adjacent to the glacial tongue.The adjacent slopes became distabilized as the glacier retreated (Vilímek et al. 2005). This condition finally led to the landslides. Slopes without glacial support are turning towards a more stable profile based on the mechanical properties of the moraine material. This led to a gradual decrease in the inner moraine slopes and to the accumulation of moraine material in the lake. Evans and Clague (1994) mentioned with respect to high mountain slopes that the slope instability could persist after glacier retreat for perhaps hundreds of years. Comparison of remotely sensed data showed that the main phase of the glacial tongue retreat did not happend since 1970 (Vilímek et al. 2005). As a result of these processes, the maximal width of the lake is in the part adjacent to the glacial tongue.

The precise role of landslides in glacial retreat is not clear, but field investigations in 2004, after the March 2003 landslide, proved that part of the glacial tongue was destroyed and broken to small ice blocks by the landslide. The impact of these landslides might have contributed to glacier's disintegration in the past and therefore to its more rapid thawing. Our recent research in this area is focused

on calculation of slope stability in moraines and on geophysical profiling, because other moraine blocks are distinguishably separated into left lateral moraine. The precise detachment zones have to be fixed to calculate their volumes.

3.2 Lake No. 513 2010 Event

The Lake No. 513 is a bedrock-dammed lake which is the largest of a group of three lakes situated in the central part of the Cordillera Blanca beneath the western slopes under Mt. Hualcán (6,122 m a.s.l.) with a water level of 4,437 m a.s.l. These slopes are formed by steep rock-walls fully covered by glaciers. This area consists of intrusive rocks formed from sharp modelled peaks and crests. Lithologically, they are composed of coarse-grained granodiorites and tonalites. Several hanging ice blocks were identified during our field inspection (2010 and 2011) as well as from satellite images. Ice and rock falls originating from similar settings represents devastating disasters in the Cordillera Blanca many times in the past (e.g. Zapata 2002; Klimeš et al. 2009). Frontal parts of the glaciers in the lake surrounding terminate in the altitude between 4,600 and 4,800 m a.s.l. depending on local morphology. However, the longest tongue reached the lake with an ice-fall crossing a 150 m high rocky step. Lake No. 513 is classified as a bedrock-dammed lake, before the artificial lowering of the water level, a combined bedrock and moraine dam was formed here after the glacier retreat. Now the moraine crest does not hold any water, which is entirely contained behind solid rocks.

During the 1970 earthquake in Ancash Peru, an ice avalanche from the eastern wall of the Hualcán mountain crashed into Lake Librón in the Huichajanca valley, in the Marañón River basin (Zapata 2002). Another event from Lake No. 513 happened in 1991 and was described by Carey et al. (2012). In April 11th 2010 a large block of glacier together with rocks, crashed from the southwestern part of Mt. Hualcán slope (Fig. 6a) into Lake No. 513 and part of the lake water overflowed the dam and created a GLOF in the Chucchún River valley, a right tributary to the Santa River. During this event some houses, roads, bridges and an important water treatment facility were destroyed, fortunately no fatality was recorded. The rather low extent of damage is due to the fact that the valley is not densely populated and some villages were out of reach of the debris flow. The debris flow went into the city of Carhuaz as well, but again only limited damages occurred. However, from geomorphologic point of view, this event was rather strong, because a large amount of material was transported down the valley. Lateral erosion was documented inside the valley (Fig. 6b) as well as large blocks accumulated at several places in the valley where stream power decreased (Fig. 6c). However, for the case of larger rock- or ice-fall into the lake, a much more serious disaster is likely to occur within the area in the near future.

Fig. 6 Part **a** shows Hualcán massif above Lake No. 513; the source area of 2010 ice and rock avalanche is *highlighted* by *orange circle*. Part **b** shows a part of Chucchún valley with dominance of erosional processes and part **c** shows a part of valley with dominance of accumulation processes

3.3 Lakes Artizon Alto and Artizon Bajo 2012 Event

Lakes Artizon Alto and Artizon Bajo are situated in a head of Artizon valley, which is a left-sided tributary of the Santa Cruz valley in northern part of the Cordillera Blanca. This is a part of the Rio Santa basin which drains into the Pacific Ocean. The Artizon valley is oriented to the North and is surrounded by three conspicuous peaks—Nevado Artesonraju (6,035 m a.s.l.) from the south-west, Nevado Parón (5,600 m a.s.l.) from the South, and Nevado Millisraju (5,500 m a.s.l.) from the East. The event which occurred on 8th February 2012 is one of the most recent GLOF events in the Cordillera Blanca, and it affected four lakes and two valleys. The sequence of important events in the formation and development of the Artizon lakes is reinterpreted below:

1. Glacier retreat was followed by formation and development (deepening) of the Artizon lakes; moraine-dammed lake Artizon Bajo is about 300 m long and 140 m wide with volume of accumulated water, 333,000 m^3 (Huaman 2001);

bedrock dammed Lake Artizon Alto is about 750 m long and 200 m wide, with a significant rock peninsula which divides the lake into two sub-basins (Fig. 7a)

2. Continuing retreat and thinning of the glacier tongue above the Lake Artizon Alto to the altitude of about 4,800 m a.s.l.
3. Steep lateral moraines are no longer supported by the glacier body and thus they are predisposed to slope movements; in 2001 it was recommended to lower the water level of Lake Artizon Bajo due to the possibility of landslides into Lake Artizon Alto (Huaman 2001)
4. On 8th February 2012, a landslide of the left lateral moraine (approximate volume in order of 3–8 $\times$ 10^5 m^3) into Lake Artizon Alto occurred (Fig. 7b), generating a displacement wave
    - the direct trigger of the landslide is not exactly known, but a probable trigger is precipitation (according to SENAHMI precipitation measurements in Yungay and Pamabamba, both about 25 km far from Arteson valley), there was intense precipitation during the last few days before this event)
    - another common trigger of dynamic slope movements in the Cordillera Blanca is earthquake, but according to the USGS earthquake archive, there was no earthquake on 8th February 2012 in the northern part of the Cordillera Blanca
    - we suggest that a moraine landslide may have occurred due to precipitation in combination with degradation caused by ice core melting.
5. The displacement wave following the landslide entered into the lake and overflowed the bedrock dam of Lake Artizon Alto and reached Lake Artizon Bajo.
6. The moraine dam of Lake Artizon Bajo was overflowed and a "positive feedback" effect caused a breach and moraine dam failure; the flood wave from Lake Artizon Alto increased its overall volume of about 2 $\times$ 10^5 m^3 water from Lake Artizon Bajo.
7. Escaped water transported a large amount of moraine material and significantly affected the Artizon valley (erosion in the upper part of the valley and deposition in the form of an alluvial fan in the mouth of the valley into the Santa Cruz valley. The central part of the Santa Cruz valley was also affected, mostly by accumulation processes, sand bar formation, and partial transfer of stream channel (Fig. 7c).
8. The released volume of water reached and then was partly absorbed by landslide-dammed lake Jatuncocha in the Santa Cruz valley; also material influx into the lake was significant, the lake was shortened by about 80 m and the lake area also decreased.
9. There was also minor damage to the artificial dam of Lake Jatuncocha due to increased flow rate.

Fig. 7 Lakes Artizon Alto and Artizon Bajo in 2003 before (part **a**) and in 2012 after (part **b**) the 2012 GLOF event. The *orange highlighted line* represents the extent of the glacier. Please note the significant glacier retreat. The *yellow color* in part **b** represents the accumulation of landslide of a lateral moraine, which entered the lake Artizon Alto on 8th February 2012. Part **c** demonstrates the dominant processes in the valleys Artizon and Santa Cruz after water release (*red color*—parts of the valley with erosion processes dominant; *green color*—parts of the valley with accumulation processes dominant) (*Source* Google Earth Digital Globe 2013)

10. Increased flow rate from Lake Jatuncocha with no sediment load eroded part of Santa Cruz valley before reaching another landslide-dammed lake (Lake Ichiccocha).
11. The rest of the flood wave was absorbed by Lake Ichiccocha.

In the affected valleys (the Artizon and Santa Cruz), we may generally distinguish between areas where erosion processes are prevalent and areas where accumulation processes are prevalent. Erosion processes are prevalent on the steeper parts of the valley, while accumulation processes are prevalent on the flatter parts (Fig. 7c), except for a short flat part of the Santa Cruz valley beneath the Lake Jatuncocha which was eroded by increased flow rate from this lake, because all transported material was retained in the Jatuncocha Lake basin. The stream banks in the steeper upper part of Artizon valley are more prone to slope movements after the incision of the stream channel (undercutting the slopes), thus there is a possibility of future slope movements and formation of a landslide-dammed lake. An alluvial fan that was originally 300 m wide on the flatter part of the Artizon valley has been extended to 500 m wide by transported material. The position of the stream channel in the Santa Cruz valley has been changed by the accumulation of sediment bars. This example shows how a local landslide into the lake may subsequently affect valleys and lakes, which are kilometers away.

4 GLOFs: A Manageable Hazard??

The region of the Cordillera Blanca is relatively densely populated, so there is urgent need to manage various natural hazards including GLOFs following sudden release of water from any type of glacial lake. As shown above, occurence of GLOF is a highly complex question which is strongly linked with other types of natural hazards, mainly with dynamic slope movements or large earthquakes. These hazards are difficult to quantify or to predict precisely in time, thus it is not possible to completely prevent hazards associated with sudden release of water from glacial lakes. Richardson and Reynolds (2000a) listed three phases of glacial hazard management: the first phase is identification of a potential hazard, followed by hazard assessment (second phase), and ideally, the third phase is hazard mitigation. Thanks to ongoing formation and development of all types of glacial lakes in the Cordillera Blanca, it is important to reassess their potential hazards thoroughly. Potential hazard identification and reliable assessment are crucial steps in risk estimation and effective management (Fig. 8).

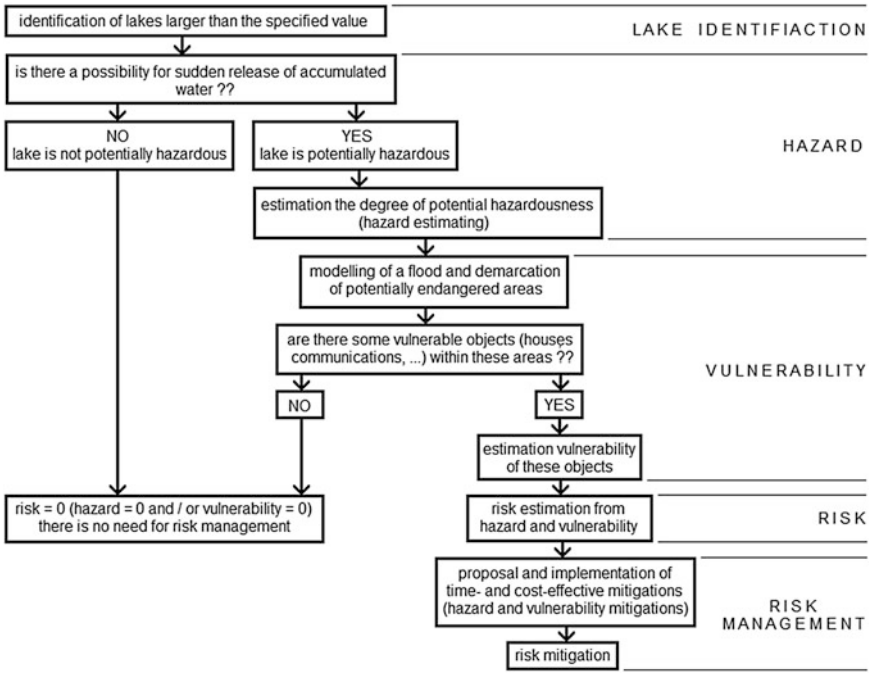

Fig. 8 Schematic procedure for GLOF risk management [According to: Huggel et al. (2004); Hegglin and Huggel (2008); Richardson (2010), and Shrestha (2010)]

4.1 Hazard Assessment

New potentially dangerous lakes are forming and developing (Klimeš 2012), and existing lakes are rapidly changing their characteristics. It is highly important to realize that potential hazardousness of glacial lakes is changing significantly during short time periods, because high mountain environment is one of the most dynamic natural environments worldwide. The previous examples of Lake Palcacocha and Lake No. 513 showed that GLOFs may occur even from a lake on whose dam has been remediated, and which was considered as safe. Lake Palcacocha changed from a "safe lake" to one producing a GLOF in 30 years between the 1970′s and 2003 (Vilímek et al. 2005). During this period, the glacier retreated about 1,000 m. This intense deglaciation led to rapid increase of water volume accumulated in the lake. Also, lateral moraines with steep slopes were uncovered and thus ready for landslide into the lake (2003 event). These are remarkable changes, and also the reason why the results of hazard assessment should be reevaluated after a certain period of time.

There are two phases of GLOF hazard assessment. The first phase aims at estimating the possibility of sudden water release from any given glacial lake, while the second phase aims at modelling the flood wave downstream, determining

the endangered areas, estimating the probability of debris-flow occurrence and the probable maximal travel distance (Huggel et al. 2004). There are a number of methods for GLOF hazard assessment, but these events in Cordillera Blanca differ in some ways from other world regions. These differences consist in share and representation of causes of sudden water release and also in high number of remedial work applied on dams in the Cordillera Blanca (see Sect. 4.2 Hazard mitigation). This is necessary to be accounted for in precise hazard assessment for glacial lakes within the Cordillera Blanca (Emmer and Vilímek, 2013).

4.2 Hazard Mitigation

Lakes of the Cordillera Blanca are famous for the high number of remedial projects (Carey 2005), which have been implemented since the 1940s. There are about forty glacial lakes with dams that have been remediated (Reynolds 2003). Three different types of remedial works were most commonly applied on glacial lakes within this region:

1. Open cut—Open cut is carried out by countersinking the outlet of lakes which do not have a solid rock dam (moraine-dammed lakes). The countersunken outlet is usually combined with artificial dam construction, but sometimes is not (e.g. Lake Arhueycocha). Open cut cannot be applied to bedrock-dammed lakes, therefore in this case tunnels are used (see below) to lower the water level permanently. Open cut allows the water level to be decreased and thus reduces the volume of accumulated water.
2. Artificial dam—The main purpose of an artificial dam is to increase dam freeboard and thus enable the dam to be resistant against displacement waves generated by dynamic slope movements into the lake. Most significant glacial lakes within the Cordillera Blanca were remediated by a combination of a concrete outflow and an artificial dam [e.g. Lake Llaca (Fig. 9a), or Lake Rajucolta (Fig. 9b)]
3. Tunnel—Tunnels are used to decrease and limit the water level of bedrock-dammed lakes (e.g. Lake No. 513; Fig. 9c), or of moraine-dammed lakes with a naturally high freeboard but without a natural surface outflow (e.g. Lake Safuna Alta).
4. Siphon—Siphons are used to lower the water level before remedial work is done (usually before open cut countersink or tunnel excavation is carried out), however this is not a permanent solution. Figure 9d shows siphons installed in 2011 to lower the water level of Lake Palcacocha.

As shown above, sudden water release from Lake Palcacocha and Lake No. 513 occured despite the fact that they had been remediated. These lakes were chosen to be remediated, because they were adjudged to be potentially hazardous, and thus remedial work was done. If remedial work had not been done, the volume of released water would have been much larger and thus the impacts would have been

Fig. 9 Examples of remedial works. Part **a** shows artificial dam and concrete outlet of lake Llaca in the central part of the Cordillera Blanca; dam freeboard is 12 m. Part **b** captures ongoing work on the dam of lake Rajucolta in 2004. Part **c** shows the entrance to the tunnel excavated in the bedrock dam of lake No. 513 (*red arrow*). Part **d** shows six siphons installed in fall 2011 to drain and lower the water level of lake Palcacocha

more catastrophic. Water released from lakes of remediated dams should not be interpreted as failure of the remedial works, but as improvement in hazard assessment, because it is not entirely possible to prevent GLOFs only by remedial work on the lake dam. Also, vulnerability mitigation such as urban planning based on demarcation of potentially endangered areas should be done to eliminate fatalities and significant material damages.

5 Conclusions

The number of potentially hazardous lakes within the Cordilllera Blanca is increasing due to the ongoing glacier retreat and parallel glacial lake formation and development in this heavily glacierized tropical range of the world. Furthermore, the number of lakes is currently estimated to be more than one thousand within this region and this number is still increasing. There are three types of glacial lakes within the Cordillera Blanca which evolve with glacier retreat in altitudes between

4,600 m a.s.l. and 5,000 m a.s.l. These are: (1) bedrock-dammed lakes; (2) moraine-dammed lakes; and (3) ice-dammed lakes. Significant lakes, having volumes exceeding 10^6 m^3 of accumulated water, are of the first and second type, while ice-dammed lakes do not reach this volume in the Cordillera Blanca. All types of glacial lakes may produce glacial lake outburst floods, nevertheless lakes dammed by Little Ice Age moraines are generally supposed to be potentially the most hazardous in these days, because they are dammed by unstable moraines and are frequently close to the present glaciers and the volume of accumulated water is often great. Floods from any type of glacial lake are most commonly caused by dynamic slope movements into the lake, producing displacement waves, which breach or overflow the lake dam. The slope movements can be either direct or indirect, and are associated with deglaciation. Dynamic slope movements are mostly icefalls from hanging or calving glaciers or landslides of newly exposed lateral moraines. These events claimed thousands of lives and caused significant material damage within the Cordillera Blanca since the end of the Little Ice Age. Presented examples of Lake Palcacocha, Lake No. 513 and Lakes Artizon Alto and Artizon Bajo showed that the threat of GLOF is real and will require appropriate and continued attention well into the 21st Century when glacier retreat continues and even accelerates.

Acknowledgments The authors would like to thank Prof. Richard Crago (Bucknell University) for the consultation and staff of Authoridad National de Agua (Huaráz) for scientific and logistic support. The Grant agency of the Czech Republic (Project GACR P 209/11/1000) and Grant agency of the Charles University (Project GAUK No. 70413) are acknowledged for financially supporting this project.

References

Ames AM, Francou B (1995) Cordillera Blanca—glaciares en la historia. Bulletin de l'Institut Français d'Études Andines 24(1):37–64

Carey M (2005) Living and dying with glaciers: people's historical vulnerability to avalanches and outburst floods in Peru. Global Planet Change 47(2–4):122–134

Clague JJ, Evans SG (2000) A review of catastrophic drainage of moraine-dammed lakes in British Columbia. Quaternary Science Reviews, 19:1763-1783

Clague JJ, Huggel C, Korup O, McGuire B (2012) Climate change and hazardous processes in high mountains. Revista de la Asociación Geológica Argentina 69(3):328–338

Concha JF (1951) Origen de las Lagunas. Corporación Peruana del Santa, División de Geología y Seguridad de Lagunas, Huaraz (Peru), p 4

Costa JE, Schuster RL (1988) The formation and failure of natural dams. Geol Soc Am Bull 100:1054–1068

Emmer A, Cochachin A (2013) Causese and mechanisms of moraine-dammed lake failures in the Cordillera Blanca, North American Cordillera and Himalaya. AUC Geographica 48(2) (in press)

Emmer A, Vilímek V (2013) Review article: Lake and breach hazard assessment for moraine-dammed lakes: an example from Cordillera Blanca (Peru). Natural Hazards and Earth System Science, 13:1551–1565. doi:10.5194/nhess-13-1551-2013

Evans SG, Clague JJ (1994) Recent climatic change and catastrophic geomorphic processes in mountain environments. Geomorphology 10:107–128
Georges C (2004) The 20th century glacier fluctuations in the tropical Cordillera Blanca, Peru. Arct Antarct Alp Res 36:100–107
Harrison S, Glasser N, Winchester V, Haresign E, Warren C, Jansson KA (2006) Glacial lake outburst flood associated with recent mountain glacier retreat, Patagonian Andes. Holocene 16(4):611–620
Hegglin E, Huggel C (2008) An integrated assessment of vulnerability to glacial hazards—a case study in the Cordillera Blanca, Peru. Mt Res Dev 28:299–309
Holm C, Bovis M, Jacob M (2004) The landslide response of alpine basins to post-little Ice Age glacial thinning and retreat in southwestern British Columbia. Geomorphology 57:201–216
Huaman AC (2001) Estudio de vulnerabilidad y seguridad física de la laguna Artizon Bajo. Instituto National de Recursos naturales (INRENA), Unidad de Glaciologia y Recursos Hidricos, Huaráz, p 46
Huggel C, Haeberli W, Kääb A, Bieri D, Richardson S (2004) An assessment procedure for glacial hazards in the Swiss Alps. Can Geotech J 41:1068–1083
Hutchinson EG (1957) A Treatise on Limnology, vol 1, geography, physics and chemistry. Wiley, New York, p 1015
Janský B, Šobr M, Yerokhin S (2006) Typology of high mountain lakes of Kyrgyzstan with regard to the risk of their rupture. Limnol Rev 6:135–140
Kalff J (2002) Limnology, inland water ecosystem. Prentice-Hall, Inc., New Jersey 592
Kaser G (1995) Some notes on behaviour of the tropical glaciers. Bull. Inst. fr. Études andines, 24:671–681
Klimeš J (2012) Geomorphology and natural hazards of the selected glacial valleys, Cordillera Blanca, Peru. AUC Geogr 47(2):25–31
Klimeš J, Vilímek V, Omelka M (2009) Implications of geomorphological research for recent and prehistoric avalanches and related hazards at Huascaran, Peru. Nat Hazards 50(1):193–209
Korup O, Tweed F (2007) Ice, moraine and landslide dams in mountainous terrain. Quatern Sci Rev 26:3406–3422
Lliboutry L, Morales BA, Pautre A, Schneider B (1977) Glaciological problems set by the control of dangerous lakes in Cordillera Blanca, Peru. I. Historical failures of moranic dams, their causes and prevention. J Glaciol 18:239–254
Mark BG (2002) Observations of modern deglaciation and hydrology in the Cordillera Blanca. Acta Montana, ser. A Geodyn 19(123):23–36
Morales BA, Zamora MC, Ames AM (1979) Inventario de lagunas y glaciares del Perú. In: Boletín de la Sociedad Geológica del Perú, Parte III, Lima, pp 63–82
Oerlemans J, Knap WH (1998) A 1 year record of global radiation and albedoin the ablation zone of Morteratschgletscher, Switzerland. J Glaciol 44(147):213–238
O'Connor JE, Costa JE (1993) Geologic and hydrologic hazards in Glacierized basins in North America resulting from 19th and 20th century global warming. Nat Hazards 8:121–140
Oppenheim V (1946) Sobre las lagunas de Huaráz. In: Boletin de la sociedad geologica del Peru, Sociedad geologica del Peru, Lima, pp 68–80
Portocarrero CR (1995) Proyecto prioritario del afianzamiento hídrico del rio Santa. Hidrandina S.A., Huaraz (Peru), p 28
Reynolds JM (2003) Development of glacial hazard and risk minimisation protocols in rural environments. Methods of glacial hazard assessment and management in the Cordillera Blanca, Peru. Reynolds Geo-Sciences Ltd., Flintshire, p 72
Richardson SD, Reynolds JM (2000a) An overview of glacial hazards in the Himalayas. Quat Int 65(66):31–47
Richardson SD Reynolds JM (2000b) Degradation of ice-cored moraine dams: implications for hazard development. In: Debris-Covered Glaciers, Proceedings of a workshop held at Seattle, Washington, USA, September 2000, The Netherlands, pp 187–197

Richardson SD (2010) Remote sensing approaches for early warning of GLOF hazard in the Hindu Kush—Himalayan region. Uniten Nations International Strategy for Disaster Reduction (UN/ISDR), 35 pp

Shrestha AB (2010) Managing flash flood risk in the Himalayas; informational sheet #1/10. International Centre for Integrated Mountain Development (ICIMOD), Kathmandu (Nepal), p 4

Solomina O, Jomelli V, Kaser G, Ames A, Berger B, Pouyaud B (2007) Lichenometry in the Cordillera Blanca, Peru: "Little Ice Age" moraine chronology. Glob Planet Change 59:225–235

Thompson L, Mosley-Thompson E, Henderson K (2000) Ice-core paleoclimate records in tropical South America since the las glacial maximum. J Quat Sci 15:377–394

Vilímek V (2002): Paleogeographical evolution of central Andes. Acta Montana, ser. A Geodyn 19(123):7–21

Vilímek V, Zapata ML, Klimeš J, Patzelt Z, Santillán N (2005) Influence of glacial retreat on natural hazards of the Palcacocha Lake area, Peru. Landslides 2:107–115

Wilson J, Reyes L, Garayar J (1995) Geología de los cuadrángulos de Pallasca, Tayabamba, Corongo, Pomabamba, Carhuaz y Huari. Boletín No. 16—1967 Actualizado por la Dirección de la Carta Geológica Nacional a 1995, Boletín No. 60, Serie A Carta Geológica Nacional, INGEMET, Lima, p 64

Zapata ML (2002) La dinamica glaciar en lagunas de la Cordillera Blanca. Acta Montana 19(123):37–60

Zapata ML, Gómez RJL, Santillán NP, Espinoza HV, Huamaní AH (2003) Evaluacion del estado de los glaciares en la cabecera de la laguna Palcacocha. Informe tecnico, INRENA, INGEMMET, Huaraz, p 23

Case Study on the Kokkawa Landslide Caused by Snowmelt

Hideaki Marui and Yoshihiko Koizumi

Abstract This paper presents comprehensive study of the process and mechanism of the 7th March 2012 Kokkawa landslide in Japan. The landslide has the following dimensions; average width of 150 m, maximum length of about 500 m. The depth of the sliding surfce is about 20 m. The volume of the sliding soil mass is estimated to be 750,000 m^3. Although no one was killed or injured, several house were completely destroyed by the sliding soil mass. In addition, a lot of inhabitants of neighbouring houses had to be evacuated. The Kokkawa landslide occurred in Joetsu City, which is located in the southwestern part of Niigata Prefecture. Many deep-seated landslide events have been recorded in the past in Joetsu City area. The area is also characterized by long and heavy bouts of hazardous snow falls. A lot of snow accumulation was observed in the vicinity of the landslide area during winter season. Clearly the landslide was triggered by snowmelt. The soil layer above the geological formation border probably contained high amount of water due to antecedent snowmelt before the occurrence of the landslide. It was remarkably observed that the sliding soil mass has long travel distance and high velocity at the early stage of the movement.

Keywords Snowmelt · Travel distance · Drainage · Topography · Landslide hazard assessment

H. Marui (✉)
Research Institute for Natural Hazards and Disaster Recovery, Niigata University, Nishi-Ku, Ikarashi-Ninocho 8050, Niigata 950-2181, Japan
e-mail: maruihi@cc.niigata-u.ac.jp

Y. Koizumi
Department for Erosion and Torrent Control, Niigata Prefectural Government, Chuo-Ku, Shinko-Cho 4-1, Niigata 950-8575, Japan

W. Shan et al. (eds.), *Landslides in Cold Regions in the Context of Climate Change*, Environmental Science and Engineering, DOI: 10.1007/978-3-319-00867-7_18,

Fig. 1 Location map of the study area

1 Introduction

On 7 March 2011, a landslide occurred at Kokkawa in Joetsu City in southwestern part of Niigata Prefecture. Although no one was killed or injured, several houses were destroyed by the sliding soil mass. In addition, inhabitants of the neighbouring houses had to be evacuated. Average length and width of the landslide is 500 m and 150 m, respectively. The depth of the sliding surface is about 20 m, while the volume of displaced soil mass is estimated to be 750,000 m^3. (Fig. 1 Location map), (Fig. 2 Overview of the landslide area from the head scarp), (Fig. 3 Front view of the landslide)

2 Characteristics of the Kokkawa Landslide

2.1 Topography and Geology of the Landslide Area

The landslide occurred at Kokkawa district, located at the western margin of the gently inclined Higashi-Kubiki hillslope areas, facing the Takada plain. The height of the location is about 200 m above sea level. The geology around the landslide area is divided into two units, namely Upper Pleistocene conglomerate layer, the Saruhashi Formation and Lower Pliocene mudstone layer, the Sugawa Formation. The upper conglomerate layer is permeable while the lower mudstone layer is impermeable. Therefore, the groundwater supplied by snowmelt was stored in the soil layer above the boundary of the geological formation. The probable explanation is that snowmelt water infiltrated into the permeable upper conglomerate layer, pushing out groundwater along the boundary between the upper permeable Saruhashi Formation and lower impermeable Sugawa Formation. Geological

Fig. 2 Overview of the landslide area showing the head scarp

Fig. 3 Front view of the landslide

structure composed of two different strata could easily cause a landslide at this geological formation boundary. Majority of the soil mass of the upper Saruhashi layer are significantly weathered and contains certain percentage of fine materials. This layer could easily trap groundwater and hardly drain groundwater. As a result, it seems that the sliding soil mass possessed high water content and high mobility. The Fig. 4a–d shows the highly movable behaviour of the sliding soil mass.

2.2 Specific Features of the Location

In order to specify the topographic location of the landslide, it is necessary to identify the original topography of the area concerned. As shown in Fig. 3, the

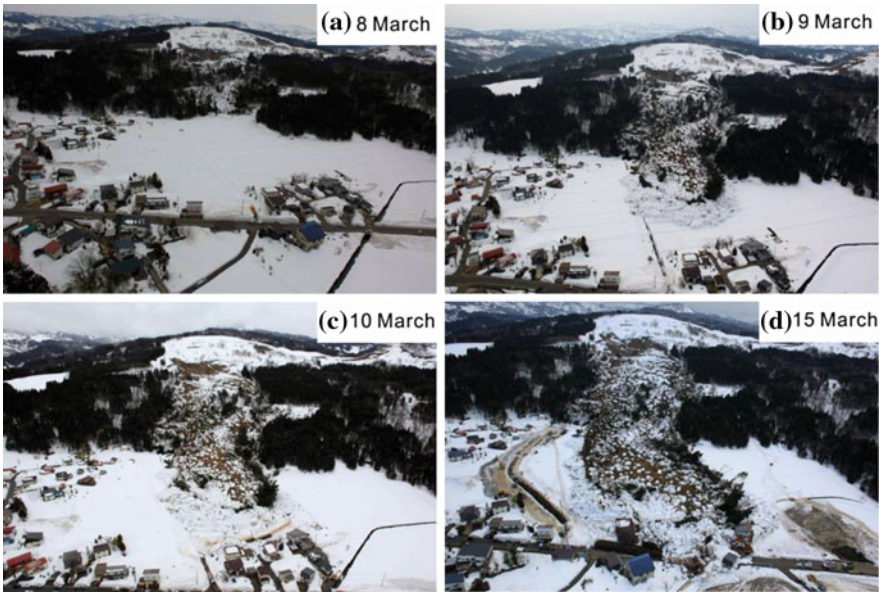

Fig. 4 **a–d** Movement of displaced soil mass

current landscape just behind the landslide shows a relatively gentle hillslope without forest cover. It is considered that the current landscape of the area is artificially changed by stone quarrying activities. The original topography of the area is shown in Fig. 5 which is interpreted by aerial photos taken in 1985. Typical topographic features of a landslide such as "steep head scarp", "gentle slope area after sliding" and "marginal accumulation of slid soil mass" are easily visible. In relation to the location of the recent Kokkawa landslide, clear valley topographies can be observed at both side margins of the long and narrow landslide topography. The existence of such valley topographies suggest that infiltrated groundwater could be easily supplied into the soil layer of the landslide.

2.3 Travelling Process of Sliding Soil Mass

In the first photograph a, of Fig. 4, the sliding soil mass was still on the slope on 8 March, next day after the landslide occurrence. In the second photograph b, the upper part of the sliding soil mass was moved away from the slope margin on the very gentle fluvial plane on 9 March. In the third photograph c, the upper part of the displaced soil travelled towards the inhabited areas on 10 March. Although sand bags were set in front of the displaced soil, it was of no use at all to protect the houses. In the fourth photograph d, the upper part of the displaced soil finally

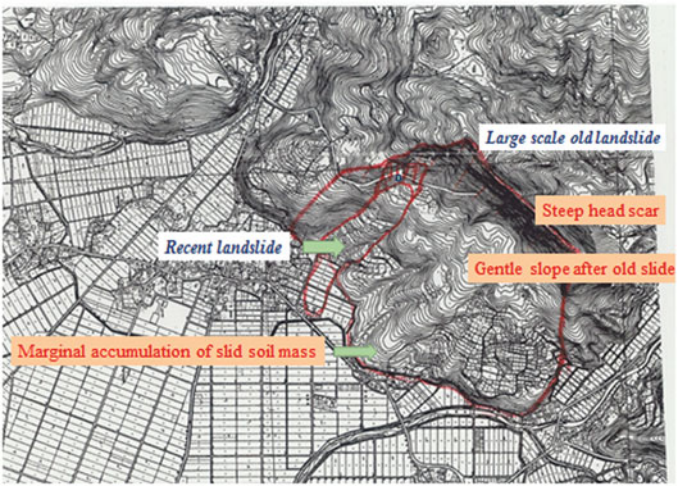

Fig. 5 Original topography of old large scale landslide

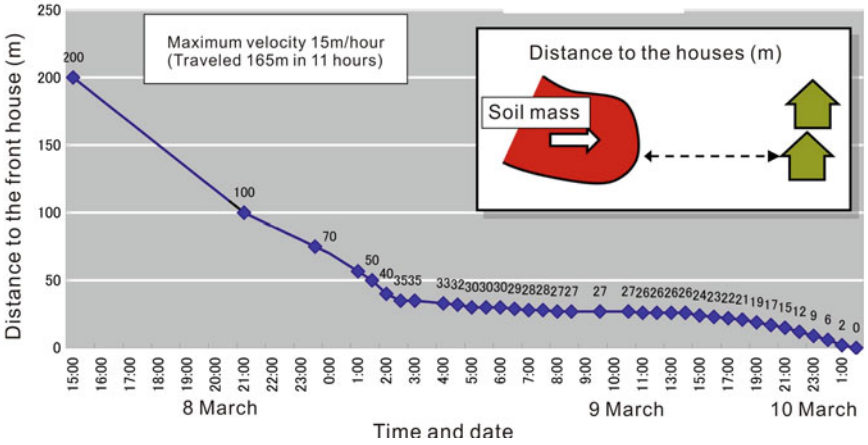

Fig. 6 Variation of travelling velocity of soil mass

reached the road and several houses in the inhabited areas were completely destroyed on 15 March. The upper part of the displaced soil travelled 250 m with maximum velocity of approximately 15 m/h. After 2 weeks the soil mass was finally stopped. Detailed variation of travelling velocity of front part of the displaced soil is shown in Fig. 6.

2.4 Soil Properties of the Sliding Zone

In order to detect the sliding surface, several boreholes were drilled in the sliding soil mass. Soil properties of the sliding zone were investigated. Soil samples taken from the sliding zone show the following physical properties. The liquid limit shows high value of 67.1 %. The plastic limit is 32.1 %. The plasticity index is 35.0. The residual shear strength parameters were measured by ring shear test. The residual ϕ is 19.8° and the residual c is 8.2 kPa. When compared with usual values of residual ϕ of sliding zone of landslides in the neighbouring areas, the residual ϕ around 20° is rather high value. Therefore, it is necessary to evaluate significant effects of high pore water pressure in order to explain occurrence of the Kokkawa landslide.

2.5 Weather Conditions

Snow accumulation of the area concerned in the year was relatively higher than normal. The weather conditions recorded by the nearest meteorological station at Sekiyama in Myoko City is shown in Fig. 7. As shown in the figure, the air temperature had risen suddenly and exceeded 10 °C 2 days before the occurrence of the landslide. At the same time, the measured depth of the snow cover decreased rapidly. It suggests that the landslide was mainly triggered by snowmelt (Figs. 7, 8).

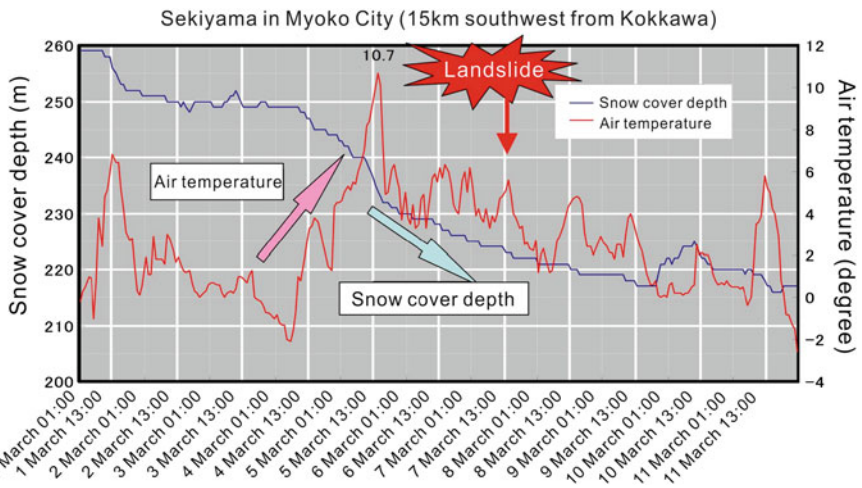

Fig. 7 Weather conditions at the nearest meteorological station

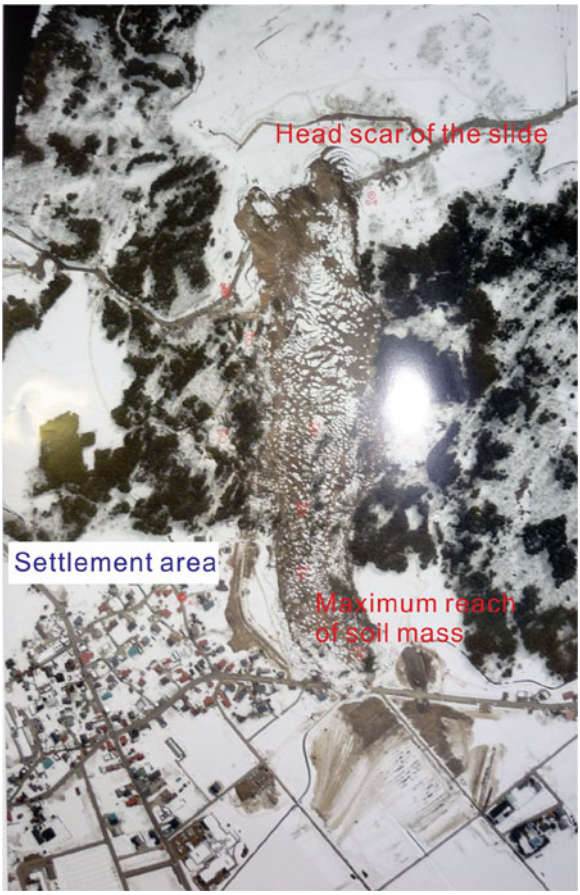

Fig. 8 Aerial photograph of Kokkawa landslide (provided by Niigata Prefectural Government)

3 Countermeasures for Stabilization

3.1 Emergency Operations

It was urgently needed to arrange the following emergency operations to mitigate damage by the sliding soil mass (Fig. 9).

1. In order to restrain the active movement of the sliding soil mass, it was necessary to drill a lot of horizontal boreholes for drainage of groundwater from the landslide body and also soil layer behind the head scarp. In addition, it was also necessary to construct open channels to divert surface water in order to avoid infiltration of surface water into landslide body.
2. In order to protect houses in settlement areas, retaining walls, vertical barriers and embankments were constructed to regulate the travelling course of the top part of the displaced soil mass.

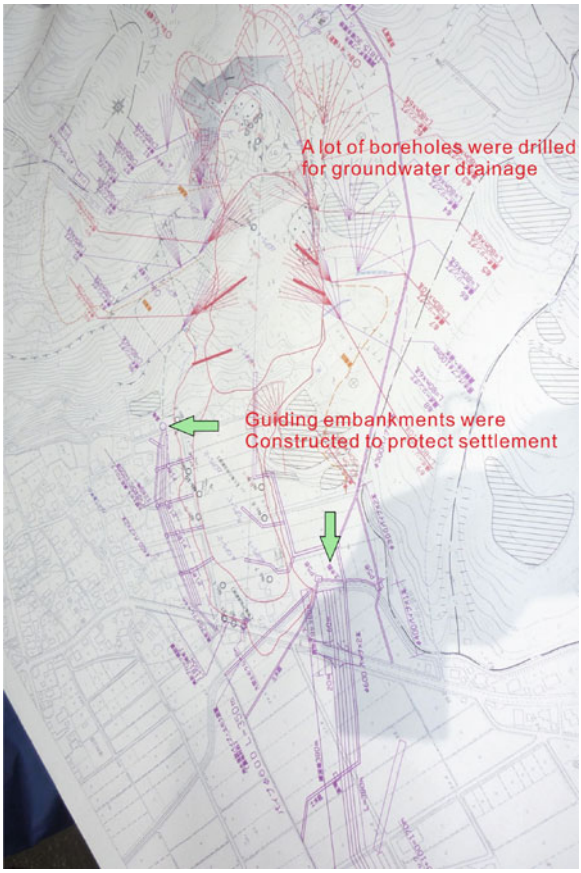

Fig. 9 Countermeasures for stabilization (provided by Niigata Prefectural Government)

3. Continuous real time monitoring of behaviour of the displaced soil mass were carried out. For such monitoring 10 GPS receivers and several vertical extensometers were installed in the landslide body.
4. Groundwater drainage with several horizontal boreholes functioned effectively and the movement of the top part of the sliding soil mass stopped two weeks after the occurrence of the landslide.

3.2 Permanent Countermeasures

During the early stage after occurrence of the landslide, it was impossible to install any permanent countermeasures on the landslide area because of high water content of the soil mass in the area. Many weeks after installation of several horizontal boreholes, certain amount of groundwater stored in the soil layer behind the head scarp and within the displaced soil was gradually drained. This was

followed by stepwise designing and construction of permanent countermeasures including:

1. Cutting and reshaping the unstable steep slope near the head scarp.
2. Drilling and installation of vertical drainage wells to lower groundwater level within the slope.
3. Construction of channels for surface water drainage and subsurface conduits for draining of shallow groundwater.
4. Construction of retaining walls at the top margin of the displaced soil mass.

3.3 Monitoring of Movement of Soil Mass

Although the displaced soil mass ceased to move several weeks after the occurrence of the landslide, it is important to install continuous real time monitoring system for possible movements of the displaced material and also on possible successive slides just behind the landslide area in the next rainy season. For the case of unforeseen additional landslide occurrence, it is necessary to install early warning system pending the completion of permanent countermeasures.

4 Concluding Remarks

1. The main triggering factor of the Kokkawa landslide is considered to be significant amount of groundwater supply by snowmelt.
2. Compared with other landslides in neighbouring areas, the residual internal friction angle (ϕ) of the sliding zone of the Kokkawa landslide shows rather high value.
3. It is necessary to evaluate significant effects of high pore water pressure in order to explain occurrence of the Kokkawa landslide.

Acknowledgments The authors are thankful to the Department of Torrent and Erosion Control of Niigata Prefectural Government for practical arrangement for field visit and also for provision of technical materials like aerial photographs and topographical maps.

Debris Flow on a Seasonally Frozen Rupture Surface at Moose Lake, British Columbia

Marten Geertsema, Menno van Hees, Marta Chiarle and Jennifer Hayek

Abstract In early month of November 2007, a 1.4 km debris flow initiated on a steep south-facing slope above Moose Lake in Mount Robson Provincial Park, British Columbia. Snow meltwater was likely concentrated along a shallow seasonally frozen rupture surface, generating high pore water pressure. The debris flow bifurcated into two concentrated gullies before distributing as a debris flood on a snow-covered fan. The debris flow crossed a twin pipeline corridor and came to rest in a ditch against a highway berm. There was no damage to infrastructure. In many ways, the landslide resembles skin flows described in permafrost zones.

Keywords Debris flow · Debris flood · Seasonal ice · Snow · South-facing slope · British Columbia

1 Introduction

Shallow flows, common in permafrost areas around the world have been studied in detail. Water from snowmelt and rainfall concentrates along the upper boundary of permafrosts in the active layer, generating high porewater pressures and thaw consolidation (McRoberts and Morgenstern 1974, Leibman 1995, Lewkowicz and Harris 2005). Less well known are shallow landslides that occur in a similar fashion over seasonally frozen ground (Guo and Shan 2011; Shan et al. 2012). In this chapter we briefly describe an example of the latter case.

M. Geertsema (✉) · M. van Hees · J. Hayek
Ministry of Forests, Lands and Natural Resource Operations, Prince George, BC, Canada
e-mail: marten.geertsema@gov.bc.ca

M. Chiarle
Consiglio Nazionale delle Ricerche—Istituto di Ricerca per la Protezione Idrogeologica U.O.S, Torino, Italy

W. Shan et al. (eds.), *Landslides in Cold Regions in the Context of Climate Change*, Environmental Science and Engineering, DOI: 10.1007/978-3-319-00867-7_19,

2 Study Area

The 2007 Moose Lake landslide occurred on the Rocky Mountains of Mount Robson Provincial Park in British Columbia (Figs. 1, 2, 3). The steep slopes of Mount Robson are composed of shallow colluvium and till overlying a moderately consolidated bedrock. The lower slopes are composed of granular materials derived from alluvial and colluvial sediments.

In 2004, the area was deliberately burnt. The purpose of burning the forest was to enhance biodiversity within the park, by re-establishing a natural fire regime. Thus, there were no live trees on the initiation and transport zone of the landslide.

The bedrock of the Rocky Mountains is variable with a complicated structure. In the Moose Lake area, limestone and sandstone interbeds of the Gog Group, overlie the Miette shales and mudstones (Murphy 1990).

Climatic condition of the region at 1,000 m asl are 2.7 °C mean annual temperature (MAT) and 1,108 mm mean annual precipitation (MAP), and at 1,600 m asl yields an MAT of 0.6 C and MAP of 1,108 mm (Wang et al. 2010).

Linear infrastructure at the base of the slope includes twin buried pipelines, the Trans-Canada Highway, and the Canadian National Railway.

Fig. 1 Location map showing the Moose Lake landslide (*red star*)

Fig. 2 Landslide (*red polygon*) shown on the North side of Moose Lake. Local weather stations are 5 and 20 km west of the landslide, respectively. Google image—North at top

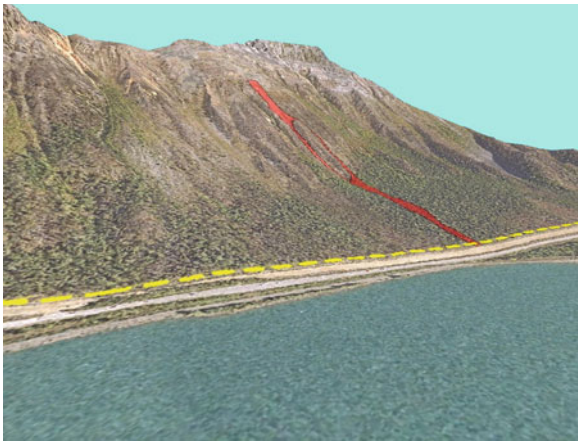

Fig. 3 Orthophoto draped over a 5 m DEM showing the 2007 Moose Lake landslide in *red*. The *yellow dashed line* depicts a buried twin pipeline. Beside this is the Trans Canada Highway, and the CN railway. Moose Lake is in the foreground

3 Landslide

3.1 Landslide Geometry

The landslide initiated at an elevation of 1,650 m asl, dropping 600 m over a surface distance of 1.4 km, and formed a travel angle of 25.4° (Figs. 2, 3). The landslide began as a rotational debris slide at the main scarp, merely 30 m long, and then transformed into a steep, shallow flow, some 50 m wide and 400 m long, along a 33.5° slope. The landslide had travelled a vertical distance of 225 m by this time. Mud was splashed up to 6 m high on trees (Fig. 4). Here the landslide debris was very thin, ranging from less than one to three decimetres in thickness (Fig. 5), in some cases still covering an ice-rich frozen horizon in April 2008.

Fig. 4 Mud splashed up to 6 m high (*red arrow*) on trees just above where the landslide bifurcates into two paths. Debris cover is up to three decimetres thick here. View down slope. Photo M. Geertsema

Fig. 5 Thin, decimetre thick debris cover (*gray*) over frozen reddish surface soil. Movement was extremely shallow and very rapid. Photo M Geertsema

Next, the flow bifurcated into two shallow channels, travelling up to 470 m along a 32° slope, dropped another 250 m in elevation. The channels ranged from 7 to 15 m in width. The flows rejoined near the base of the steep slope and travelled the remaining 550 m as a low energy debris flow through dense vegetation on a snow-covered fan with slope angle of 11°.

In all, the long flow covered an area of 5.4 ha involving a mere volume of 10,000–15,000 m^2. This is in sharp contrast to landslides of similar length in British Columbia with volumes two orders of magnitude greater (Geertsema et al. 2006).

3.2 Landslide Timing

We discovered the landslide after a snow avalanche cleared its track on the 29th of March 2008. Tire tracks over the debris where the distal end of the landslide covered a buried pipeline indicates it happened much earlier, just after the early season snow in the beginning of November 2007 (Figs. 6, 7). The fresh debris was likely hidden by a thin snow cover when crossed, and thus went unnoticed. The snow cover was however thin enough to allow an imprint of the wheel tracks to be made. Construction work along the pipeline corridor was suspended for the winter and did not resume until sometime after our observations in 2008. We conclude that the landslide likely happened around 4–6 November, but was not visible until the following spring, due to the snow falls that would have obscured the deposit.

3.3 Landslide Mechanism

The steep south-facing surfaces on the northern hemisphere is subject to greater daily temperature amplitudes than the low angle slopes on cooler aspects (Hall et al. 2005; Noetzli et al. 2007; Harris et al. 2009). Moreover, the forest canopy on the fan provided more shade than the steep slope above with its charred trees

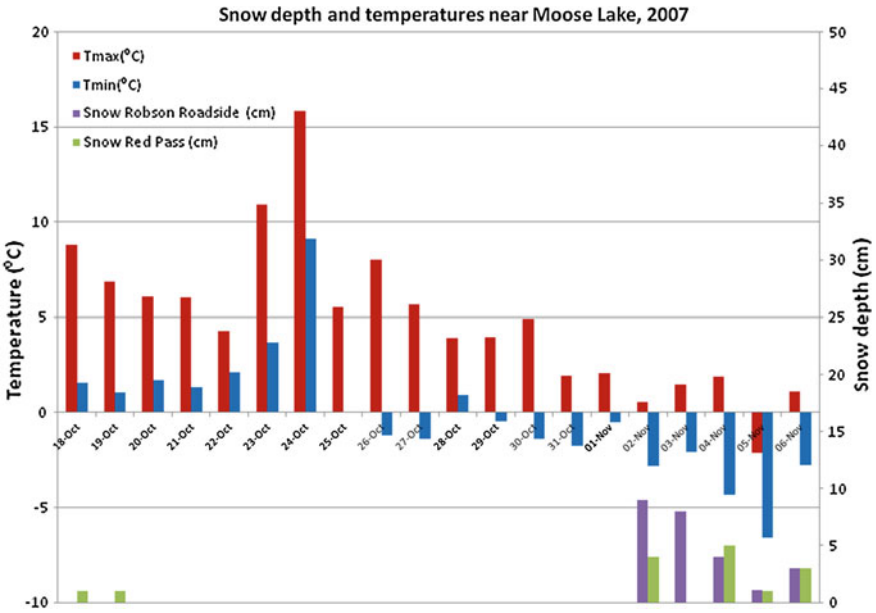

Fig. 6 Snow depth and daily maximum and minimum air temperature near the Moose Lake landslide

Fig. 7 Pre-season tire tracks over the landslide deposit. This likely happened when there was thin snow cover—sufficient to hide the deposit, but not enough to prevent impressions in the wet mud

Fig. 8 Collapsing debris surface under differentially melting basal snow on the depositional fan. Photo M. Geertsema

(standing, but without needles). Figure 6 gives local snow accumulation and temperature distribution of the location along the highway. While the snow gradually melted on the steep slope due to radiative heating, it accumulated on gently inclined slopes in the forest. Temperatures on the upper slope would likely have been colder and hotter than indicated in Fig. 6 due to the combined influences of lapse rate and increased radiative heating. This would have resulted in both snow melting and shallow soil freezing on the upper slope.

The small rotational movement at the crown of the landslide occurred first. This may have loaded a shallow layer of saturated soil overlying a frozen horizon, driving up pore pressures. Both thaw consolidation and pore pressure increase (McRoberts and Morgenstern 1974), combined with the undrained loading effect (Hutchinson and Bhandari 1971) of the first movement, likely triggered the rapid flow.

Although the forest fire effect (removal of tree needles) may have contributed to radiative heating and cooling, we saw no field evidence of water repellency. We supect rises in piezometric levels were likely caused by shallow (10–20 cm deep) frozen layers based on observations of lateral scarps and lingering frozen layers at the time of our field visit.

The flow energy dissipated on the gently inclined fan with slope angle of 11°. Figure 8 shows an interesting morphology of the collapsing debris with radiating cracks due to differential melting of the underlying snow layer.

4 Conclusions

Seasonally frozen ground on steep south-facing slopes in British Columbia can pose a serious geotechnical hazard, particularly when vegetative cover is removed. These slopes are subject to more extreme temperature fluctuations than slopes on other aspects and as such, experience more repeated freezing and thawing.

At the Moose Lake landslide, thawing surface soil and snowmelt contributed to thaw consolidation and soil saturation. Snowmelt water concentrated along shallow frozen layers (several decimetres in the Moose Lake landslide). Once initial movement takes place, undrained loading causes sufficiently high pore water pressure to initiate failure. Fortunately, the landslide's energy dissipated on a snow-covered fan prior to encountering linear infrastructure.

Acknowledgments We are grateful to Dr. Jeannette Noetzli for constructive anonymous reviewers of this chapter.

References

Geertsema M, Clague JJ, Schwab JW, Evans SG (2006) An overview of recent large catastrophic landslides in northern British Columbia, Canada. Eng Geol 83(1):120–143

Guo Y, Shan W (2011) Monitoring and experiment on the effect of freeze-thaw on soil cutting slope stability. Procedia Environ Sci 10:1115–1121

Hall K, Arocena JM, Boelhouwers J, Liping Z (2005) The influence of aspect on the biological weathering of granites: observations from the Kunlun Mountains, China. Geomorphology 67(1):171–188

Harris C, Arenson LU, Christiansen HH, Etzelmüller B, Frauenfelder R, Gruber S, Vonder Mühll D (2009) Permafrost and climate in Europe: monitoring and modelling thermal, geomorphological and geotechnical responses. Earth Sci Rev 92(3):117–171

Hutchinson JN, Bhandari RK (1971) Undrained loading, a fundamental mechanism of mudflows and other mass movements. Geotechnique 21(4):353–358

Leibman MO (1995) Cryogenic landslides on the Yamal Peninsula, Russia: preliminary observations. Permafrost Periglac Process 6(3):259–264

Lewkowicz AG, Harris C (2005) Morphology and geotechnique of active-layer detachment failures in discontinuous and continuous permafrost, northern Canada. Geomorphology 69(1):275–297

McRoberts EC, Morgenstern NR (1974) The stability of thawing slopes. Can Geotech J 11(4):447–469

Murphy DC (1990) Geology of Canoe River map area (83D), British Columbia–Alberta. Geological Survey of Canada, Open file report, 2324

Noetzli J, Gruber S, Kohl T, Salzmann N, Haeberli W (2007) Three-dimensional distribution and evolution of permafrost temperatures in idealized high-mountain topography. J Geophys Res 112(F2):F02S13

Shan W, Zhang CC, Guo Y (2012) Mechanism of shallow slide on soil road cutting slope during spring in seasonal frozen region. Appl Mech Mater 178:1258–1263

Wang T, Hamann A, Spittlehouse D (2010) ClimateWNA_4.62

Assessment of Landslide Hazards in a Typical Tundra of Central Yamal, Russia

Artem Khomutov and Marina Leibman

Abstract This chapter presents an assessment of cryogenic landslide hazard study based on differentiation of landscapes in Central Yamal. Analysis of landslide pattern shows that all recent cryogenic landslides are located on concave slopes. As concave slopes from our opinion are being modified from ancient landslides, it means that recent landslides occupy ancient landslide slopes. Recent landslide impact differs within the same landscape complexes appearing on different geomorphic levels of the central Yamal. Generally, this impact increases from low to high geomorphic levels. Landscape complexes are divided into five groups according to predicted cryogenic landslide hazard degree. Grouping of landscape complexes is based on differentiation of landscape conditions more or less favourable for cryogenic landslides and on the latest cryogenic landslide occurrence. Landslide distribution within a landscape unit determines its sensitivity to landslide recurrence; the larger the area of disturbance by recent landslide, the more sensitive is a landscape complex subdivided within the study site. At the same time, directly disturbed by the latest landslides areas within a landscape unit are considered non-hazardous because the re-occurrence of cryogenic landslides on such locations in coming centuries is mostly improbable.

Keywords Cryogenic landslides · Cryogenic translational landslides · Landscape complexes · Landscape map · Landslide impact · Map of the landslide hazard

A. Khomutov (✉) · M. Leibman
Earth Cryosphere Institute, Siberian Branch of Russian Academy of Sciences,
Tyumen, PO Box 1230 625000, Russia
e-mail: akhomutov@gmail.com

W. Shan et al. (eds.), *Landslides in Cold Regions in the Context of Climate Change*, Environmental Science and Engineering, DOI: 10.1007/978-3-319-00867-7_20,

1 Introduction

Cryogenic landslide is a major surface process controlling landscape dynamics in Central Yamal.

A methodological base for the study of active surface processes in specific arctic landscapes of the cryolithozone is found in publications by Burn (Burn and Lewkowicz 1990; Burn and Zhang 2009), Ermokhina (2009; Ermokhina and Ukraintseva 2003), Harris (Harris and Lewkowicz 1993, 2000), Kizyakov (2005; Kizyakov et al. 2006), Leibman (1994, 1995, 1997, 2001, 2005; Leibman and Kizyakov 2007), Lewkowich (1988, 1990), Melnikov (1983; Melnikov et al. 1974, 2004); Moskalenko (2003, 2006), Rebristaya (Rebristaya et al. 1995); Smetanin (2006), Streletskaya (Streletskaya and Leibman 2002), Ukraintseva (Ukraintseva et al. 1992, 2000, 2003), Vasiljevskaya (Vasiljevskaya et al. 2004), and many others.

Cryogenic landslide is the most active geomorphic process in areas with widespread occurrence of tabular ground ice (Leibman 2005). Development of cryogenic landslides in areas of shallow occurrence of tabular ground ice should be considered as the most hazardous type of slope instability. Landslides on such slopes can re-occur even in events of slight increase in summer temperatures combined with minimal technogenic disturbance (Leibman and Kizyakov 2007; Burn and Zhang 2009).

Slopes with seasonal underground ice formed at the base of the active layer in certain combination of climatic factors over a period of several years are less sensitive to the impact (Leibman 1997). Cryogenic landslide along such ice surfaces (cryogenic translational landslides or active-layer detachments) can re-occur at the same site once in a few hundred years (Leibman et al. 2003). However, this periodicity is not fixed in time, and adjacent areas may be affected by these processes during other periods of significant increase in summer precipitation and simultaneous increase in temperature. Cryogenic translational landslides (CTL) are the largest in size and in mass; this is why they are so hazardous.

Assessment of the landslide hazard in different areas, including permafrost zone, is contemporarily one of the most important tasks of scientists. To determine the risks of landslide processes, scientists use qualitative estimates based on identification of sites with different landslide activation characteristics (Kazakov and Gensiorovskii 2008). To ensure landslide control during construction, assessment of landslide situation is carried out using qualitative and quantitative methods which include description of geomorphological and hydrogeological conditions, engineering geological sections of landslides, mapping of landslide occurrence based on field and remote sensing data, and measurements along with geophysical surveys in areas affected by landslides (Postoev et al. 2008). There are examples of the landslide risk as one of the dangerous cryogenic processes assessed using a numerical score to determine landslide occurrence probability (Chehina et al. 2004).

During the period after catastrophic activation of cryogenic landslide on the Yamal Peninsula, many scientists were involved in cryogenic landslide research, such as landslide morphology, distribution and association with different

landscapes, geomorphic and lithological complexes. Theory of cryogenic landslide process was established, mechanism was studied and cryogenic landslides were classified by Leibman (1994, 1995, 1997, 2004, 2005; Leibman et al. 2003; Leibman and Kizyakov 2007). Certain features of soil and vegetation cover on slopes disturbed by landslides were described under the leadership of Rebristaya, Leibman, Ukraintseva and Streletskaya (Rebristaya et al. 1995; Leibman 1997; Leibman and Streletskaya 1997; Ukraintseva and Leibman 2007; Ukraintseva et al. 2003 and many others). Distribution of landslides in Bovanenkovo gas field was analyzed using remote-sensing data and GIS technique (Leibman et al. 1997; Drozdov and Ukrainrseva 2000; Ukraintseva et al. 2005). Result of this analysis was extrapolated for the entire tundra subzone of the northern part of western Siberia (Ukraintseva 2008). For the study area, one of the first attempts to estimate the potential hazard of cryogenic landslide activation was undertaken by Ukraintseva (Ukraintseva et al. 1992). In a qualitative expert judgement based on analysis of changes in slope morphology of the Bovanenkovo gas field. Expert judgement is proposed as a kind of rapid assessment and alternative to quantitative methods requiring long-time special stationary observations (Garagulya and Parmuzin 1980; Ershov 1989; Guidelines 1981). Ermokhina (2009; Ermokhina and Ukraintseva 2003; Ermokhina and Myalo 2012) assessed probability of landslide process activation on the Yamal Peninsula using vegetation as an indicator of land surface processes. Because of active exploration of gas on the northern gas fields beneath the cryolithozone which is characterized by active surface processes, wider application of digital airborne and space borne data related to assessment of landslide hazards becomes a timely issue.

2 Study Area

Estimation of the landslide hazard was carried out at the Vaskiny Dachi key site located in the watershed of the Se-Yakha and Mordy-Yakha rivers in the Central Yamal area of alluvial-lacustrine-marine plains and terraces (Fig. 1).

The study area is a hilly plain with narrow watersheds and long gentle slopes. The highest elevation (up to 58 m altitude), is found within flat-topped remnants of the Salekhardskaya Plain. The territory is intensely dissected by narrow river valleys and gullies. Erosion channels depend on the amount of potential relief energy, therefore, the deepest ravines are dissecting high geomorphic levels. The dissection depth on the Salekhardskaya and Kazantsevskaya plains is up to 50 m. Most of the territory (about 60 %), is represented by gentle slopes with gradient up to 7°; slopes with gradient between 7° and 50° (observed maximum in the area) occupy approximately 10 % of the area; and the remaining 30 % include floodplains, lake depressions, and narrow-topped ridges (Leibman et al. 2003).

Active slope processes are typical of the outliers of marine terraces composed of ice-rich deposits with tabular ground ice. Thermocirques develop on the slopes with shallow occurrence of tabular ground ice, and transform into landslide cirques as the tabular ground ice is exhausted (Leibman 2005).

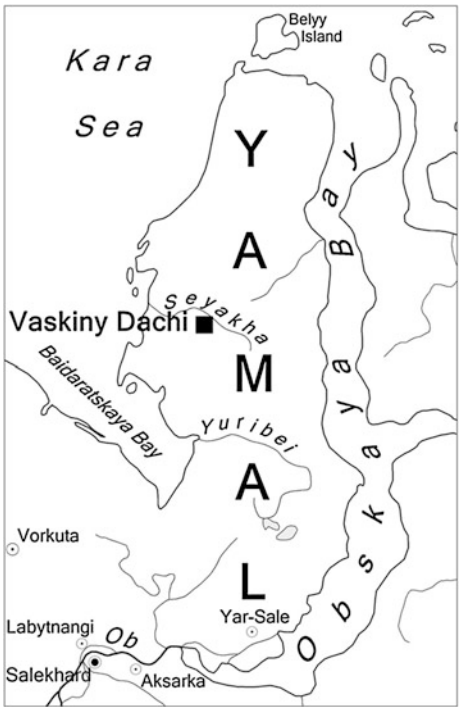

Fig. 1 Location map of Vaskiny Dachi key site on Central Yamal

From landscape point of view, Vaskiny Dachi key site is located in moss and lichen-dominated tundra subzone, and gradually changes into low-shrub tundra (Trofimov 1975), in bioclimatic subzone D according to circumpolar arctic vegetation map (CAVM Team 2003; Walker et al. 2005, 2009, 2012).

Dense dwarf birches (Betula nana) are widespread on the watersheds. The well-drained hilltops is occupied by dwarf shrub-moss-lichen communities. On gentle poorly drained slopes, compared to well-drained ones, low shrubs and dwarf shrubs are well developed and mosses predominate. On convex tops and windy hill slopes, shrub-moss-lichen communities with spot-medallions are predominant. River valleys, thermocirques, and landslide cirques with thick snow cover are characterized by willow thickets [shrub height corresponds to average snow cover thickness (Leibman 2004)]. Sedge and sphagnum bogs and flat-topped polygonal peatlands are common on flat and concave (saddles) surfaces of watersheds and terraces, in the river valley bottoms, on low lake terraces and in other depressions.

3 Methods

From our point of view, expert approach based on a CTL origin in the region of interest, combined with landscape approach best suits assessment of cryogenic landslide hazard. Main attention is given to the cryogenic landslides of 1989 as a

large-scale landslide event which provided enough data for both conceptual and statistical output.

We offer special landscape zoning suitable for analysis of landslide hazard. Firstly, geomorphic levels with specific geology, topography, and slope length were subdivided, according to Leibman and Kizyakov (2007). Higher geomorphic levels provide greater amplitude of the relief, longer slopes, and respectively probability of large-scale landslide process (Leibman 2005). Then, landforms where cryogenic landslide activation is probable were assigned. Separated were subhorizontal surfaces and bottoms where cryogenic landslide formation is impossible, and tops where landslides are improbable. Estimation of landslide hazard on the slopes is based on previously developed conceptual models of cryogenic landslide process (Leibman and Kizyakov 2007). Analysis of landslide pattern shows that all recent cryogenic landslides are located on concave slopes (Fig. 2). As concave slopes on our opinion results from ancient landslides, it means that recent landslides occupy ancient landslide slopes (Leibman 2005). But new landslides are less probable on concave slopes already affected by recent landslides than on concave slopes with only ancient landslides. The conditions for new landslides have developed on some sites differing in size (from the first few meters to hundreds of meters, depending on the age of CTL located on the slopes affected by old CTL). These conditions include thick organic canopy on the surface and high degree of cryodiagenesis of sandy and silty loam active layer deposits.

Landslide hazard is the probability of surface disturbance due to slope displacement ("outflow of material zone"), formation of landslide shear surface ("transit zone"), and deposition of the displaced material ("accumulation zone"). From landscape point of view, the process of landslide activity affects all types of landforms. Watershed edges are affected in the zone of outflow, resulting in detached cracks in the watershed and subsidence due to suffusion. The slope surface in the transit zone is exposed, leading to the activation of thermoerosion. Saline clay is exposed on the surface, resulting in specific vegetation succession.

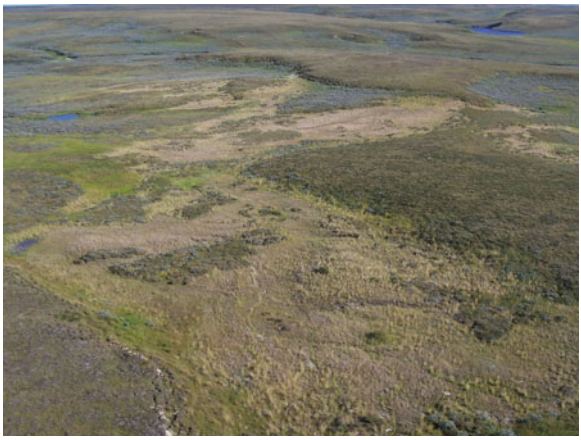

Fig. 2 Cryogenic translational landslides of 1989. Vaskiny Dachi key site

The landslide body is unloaded at the lower part of the slope, into the valley, or gully in the accumulation zone. This leads to change of hydrological regime, blocking of slope and valley water flow and forming of backwater lakes with thermokarst activation (Gubarkov 2009; Gubarkov and Leibman 2010).

The suggested method of assessment of landslide hazard uses analysis of recent landslide impact on landscapes. To elaborate this method we used an integrated landscape approach (Khomutov and Leibman 2010) combined with the concept of cryogenic landslide mechanisms (Leibman 2001; Leibman and Kizyakov 2007; Leibman and Egorov 1996), in contrast to previously suggested method of landslide hazard assessment on slopes (Leibman 1994, 1995), based on indexing of slopes according to their steepness and length, as well as differences in geological cross-section composition. In proposed new version of assessment, the full range of landscape factors directly or indirectly affecting the probability of cryogenic landslide activation was included.

To analyze recent landslide impact, nineteen landscape complexes were subdivided within main landforms (hill tops, slopes of various gradient and valley bottoms) (Fig. 3, Table 1).

Distribution of CTL that of 1989 were mapped and their number and area calculated within each of nineteen landscape units.

All landslides were combined into three groups depending on their coverage area: less than 0.002 sq.km, from 0.002 to 0.01 sq. km, and more than 0.01 sq. km. Cryogenic landslide is attributed to a particular landscape complex if the landslide body has descended directly from the surface of this landscape complex, starting from the upper point of the block displacement edge, even assuming that the contour of this landscape complex directly limited by landslide shear surface while landslide body deposited within the next landscape complex.

4 Results

4.1 Recent Landslide Impact

At Vaskiny Dachi, most of the largest landslides (with area of more than 0.01 sq.km, and up to 0.08 sq.km each), are found on poorly drained lengthy, gentle and concave ancient-landslide-affected slopes, and sub-horizontal hummocky-tussocky slopes adjacent to the hilltops.

Landslides with an area of 0.002–0.01 sq.km are generally linked to all the landscape complexes, more often to landslide-affected concave shrubby slopes. Single landslides of this type occur on rather drained sub-horizontal slopes with hummocky and tussocky tundra adjacent to hilltops, and drainage hollows, ravine, gully, and small stream valley slopes.

Small landslides, with area less than 0.002 sq.km, are widely distributed on steep slopes of ravine and stream systems and are frequently linked to boundaries

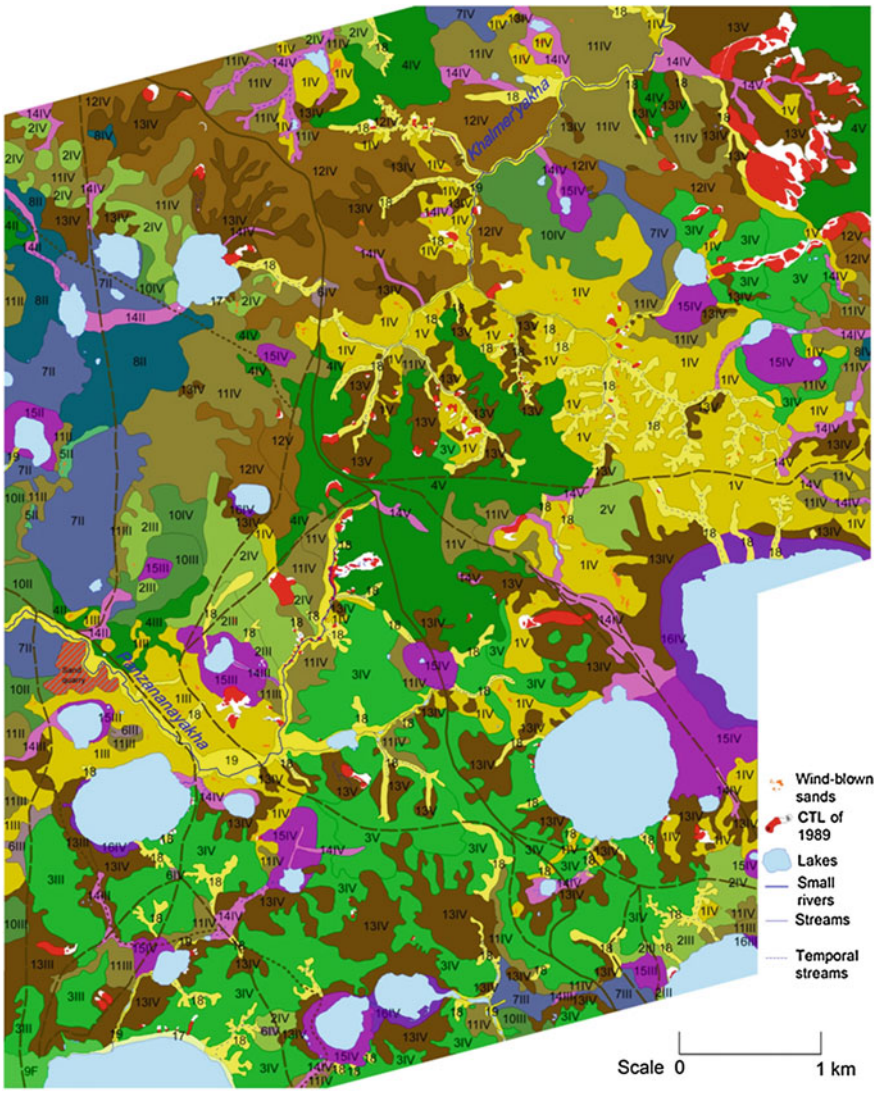

Fig. 3 Vaskiny Dachi landscape map. 1III–15IV—landscape complexes

between these landscape complexes and rather drained edges of sub-horizontal watersheds undercut by ravines and stream valleys, as well as lake depressions.

Recent landslide impact differs within the same landscape complexes appearing on different geomorphic levels: V marine plain, IV coastal-marine plain, III alluvial-marine plain, II river terrace, Mordy-Yakha river flood plain. Landscape complexes are associated in five groups according to the recent landslide impact

Table 1 Landscape pattern of Vaskiny Dachi

Drainage	Relief	Landscape complexes	Landscape unit ##	Area, %/recent landslide impact, % of landscape				
				V	VI	III	II	F
Rather drained	Convex tops	Rolling subhorizontal watersheds (convex hill tops and their slopes) with polygonal dwarf shrub-herb-lichen tundra with wind-blown sands on sandy and silty soils, alternate with herb-shrub-moss tundra on silty and clayey soils	1	4,1/3,6	6,0/2,9	1,4/6,2	–	–
	Subhorizontal tops	Flat subhorizontal watersheds with hummocky herb-dwarf shrub-moss-lichen and tussocky shrub-herb-moss tundra on silty and clayey soils (locally with wind-blown sands)	2	0,4/0,0	2,3/0,2	0,9/1,5	–	–
		Flat subhorizontal watersheds with herb-shrub-moss tundra on silty and clayey soils, with patches of polygonal herb-shrub-lichen-moss tundra on sandy and silty soils	3	1,8/8,0	10,1/0,6	1,2/0,0	–	–
		Flat subhorizontal watersheds with hummocky-tussocky shrub-herb-moss tundra on silty and clayey soils	4	5,9/7,4	1,3/0,6	0,4/0,0	0,2/0,0	–
		Peripheral zone of flat subhorizontal surfaces with hummocky polygonal herb-dwarf shrub-moss-lichen tundra on silty soils (locally with wind-blown sands)	5	–	–	–	0,1/0,0	–
	Deflation forms	Wind-blown sands (within polygons 1, 2, 5)		0,1/0,0				
Poorly drained	Subflat surfaces	Flat slightly slopping surfaces with herb-moss-shrub tundra on silty and clayey soils	10	–	1,4/0,0	0,7/0,0	0,6/0,0	–
	Gentle slopes	Flat gentle slopes with tussocky herb-grass-moss willow thickets (dwarf birch presented) on clayey soils	11	0,4/0,0	9,3/0,0	0,6/0,0	0,5/0,0	–
		Flat gentle slopes with tussocky shrub-sedge-sphagnum communities on silty and clayey soils	12	0,5/20,5	7,1/1,2	–	–	–
	Concave landslide-affected slopes	Concave gentle slopes with ancient landslide shear surfaces, with herb-grass willow thickets on clayey and saline clay soils	13	4,3/15,9	9,0/0,7	1,3/4,1	–	–
		Cryogenic translational landslides of 1989 overgrown to a various degree: landslide bodies (a) with partly degraded typical vegetation on silty and clayey soils; landslide shear surfaces (b) with pioneer grass groups on saline clay		2,2/100,0				

(continued)

Table 1 (continued)

Drainage	Relief	Landscape complexes	Landscape unit ##	Area, %/recent landslide impact, % of landscape				
				V	VI	III	II	F
Periodically wet	Hollows	Drainage hollows with cottongrass-sedge-moss communities on clayey soils	14	0,3/6,7	2,2/0,1	0,2/0,0	0,4/0,2	–
	Concave bottoms and depressions	Khasyreis with mostly dwarf shrub-lichen communities on more drained sites (with peaty silty and peat soils), with cottongrass-sedge-moss willow thickets and dwarf shrub-sedge-sphagnum bogs on wetter sites (with peaty clayey and peat soils)	15	–	2,5/0,0	0,6/0,0	0,2/0,0	–
		Low lake terraces with tussocky sedge-moss communities on peaty silty and clayey soils	16	–	1,1/0,0	0,1/0,0	–	–
		Lake beaches with fragmentary cottongrass-arctophila communities on sands	17	0,1/0,0				
	Ravine and valley complex	Ravines and gullies with flat wet cottongrass-sedge-moss bottom and steep hummocky-tussocky slopes with herb-moss willow thickets and dwarf birch on clayey soils	18	4,4/0,9				
		Small stream valleys with herb-moss willow beds on clayey soils	19	1,6/2,3				
	Subhorizontal flat surfaces	Flat rear zone of flood plain with tussocky sedge-moss and sedge-cowberry-moss communities on clayey soils	9	–	–	–	–	0,2/0,0
Wet		Flat subhorizontal surfaces with flat-topped polygonal cloudberry-sedge-lichen-sphagnum peatland on peaty silty, clayey and peat soils	6	–	0,1/0,0	0,1/0,0	–	–
		Flat subhorizontal surfaces with dwarf shrub-sedge-sphagnum and cottongrass-sedge-moss bogs with patches of flat-topped polygonal peatland on peaty silty and clayey soils	7	–	0,6/0,0	0,4/0,0	3,0/0,0	–
		Flat subhorizontal surfaces with cottongrass-sedge-moss bogs on silty and clayey soils	8	–	0,1/0,0	–	1,9/0,0	–
		Lakes		8,0/0,0				
Natural-technogenic disturbances		Sand quarry		0,2/0,0				
		Tracks actively used for all-terrain vehicle pass	—	–				
		Tracks not used recently or rarely used for all-terrain vehicle pass	– -	–				
		Tracks used for reindeer sleds only	- - - -	–				

NOTE V—Fifth Marine plain, *IV*—Forth Coastal-marine plain, *III*—Third Alluvial-marine plain, *II*—Second river terrace, *F*—Mordy-Yakha river flood plain

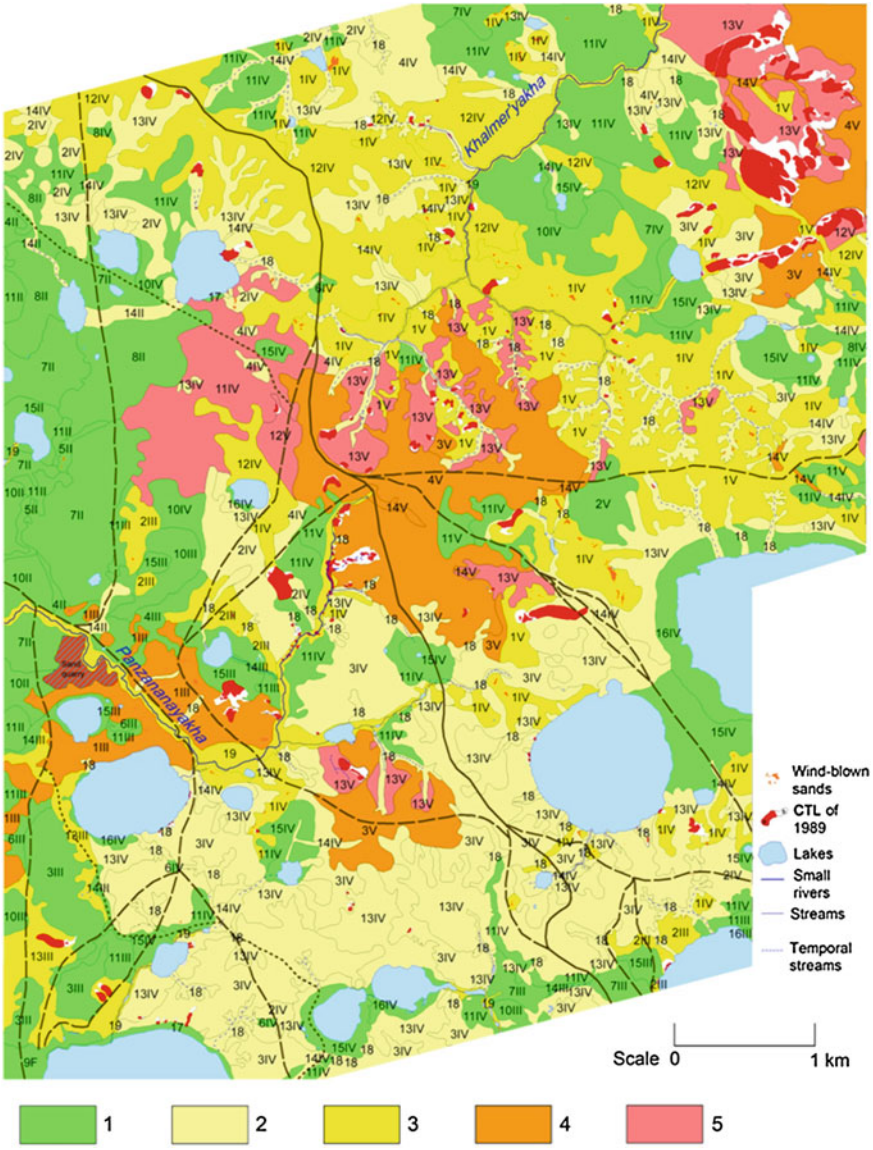

Fig. 4 Map of recent landslide impact within subdivided landscape complexes. Degree of recent landslide impact: 1—none (0 %), 2—low (0–1 %), 3—mean (1–5 %), 4—high (5–10 %), 5—largest (10 % and more)

(Fig. 4, Table 2). Generally, impact of recent landslides on landscape complexes increases from low (II–III) to high (IV–V) geomorphic levels.

The largest landslide impact occurred on concave ancient-landslide-affected slopes (unit 13, Table 1) and gentle slopes with tussocky shrub-sedge-moss cover

Table 2 Degree of recent landslide impact (1) and cryogenic landslide hazard (2) of Vaskiny Dachi landscapes[a]

2 1	Impossible	Minimal	Average	Serious	Maximal
None (0 %)	7II, 7III, 7IV, 8II, 8IV, 9F, 15II, 15III, 15IV, 16III, 16IV, 17, CTL of 1989	3III,4II, 4III, 5II, 6III, 6IV, 10II, 10III, 10IV	2 V, 11II, 11III, 14III	11IV, 11 V	–
Low (0–1 %)	–	2IV, 3IV, 4IV	14II	14IV, 18	13IV
Mean (1–5 %)	–	2III	1IV, 1 V, 12IV	19	13III
High (5–10 %)	–	–	3 V, 4 V	1III, 14 V	–
Largest (>10 %)	–	–	–	–	12 V,13 V

[a] According to Table 1 and Figs. 4 and 5; II, III, IV, V, F—See note under Table 1

(unit 12, Table 1) on the V marine plain. These landscape units have been affected by the CLT of 1989 landslide event on the area of 16 and 20 %, respectively.

Though in general, watersheds are not affected by landslides, landslide impact here may result from those landslides on concave slopes and steep slopes of drainage hollows, ravines and small stream valleys affect edges of the watershed landscapes.

High recent landslide impact occurred on flat watersheds with shrub-moss tundra (unit 3, Table 1), with hummocky-tussocky tundra (unit 4, Table 1), and in drainage hollows (unit 14, Table 1) on the V marine plain, as well as on rolling watersheds (unit 1, Table 1) of the III alluvial-marine plain. Mean recent landslide impact occurred on rolling watersheds (unit 1, Table 1) on V and IV plains and flat watersheds with hummocky and tussocky tundra (unit 2, Table 1) on III alluvial-marine plains due to the cryogenic landslides on boundaries of these landscapes with gullies, ravines, small streams valleys, and deep lake basins. Small stream valleys (unit 19, Table 1), despite large number of small landslides, are also characterized by mean recent cryogenic landslide impact as well as concave landslide slopes (unit 13, Table 1) on III alluvial-marine plain and flat gentle slopes (unit 12, Table 1) on IV coastal-marine plain. Ravines and gullies (unit 18, Table 1) are characterized by low recent landslide impact because the area of small landslides affecting steep ravine slopes is insignificant. On II river terrace drainage hollows (unit 14, Table 1) are characterized only by a low recent landslide impact due to a single landslide descended into the lake basin as a result of cutting the surface by vehicle track. All other landscape complexes on all levels are not affected by recent landslides.

Recent landslide impact on landscape complexes does not exceed 20 %. Therefore, the surfaces that are free of recent landslides and can be affected by cryogenic landslides in nearest future at least amount to 80 % of each landscape unit. The activation of cryogenic landslides in the next 300 years is improbable

(Leibman and Kizyakov 2007) on the surfaces affected by recent landslides because active layer did not form on the landslide shear surfaces overgrown with pioneer vegetation and characterized by unformed organic horizon and often by active thermoerosion.

4.2 Cryogenic Landslide Hazard

Landscape complexes affected by recent landslides are considered sensitive to landslide process: the more sensitive, the larger the area affected by CTL of 1989. Parts of the landscape complexes without recent landslides are most hazardous from the point of view of possible landslide activation. According to this principle and based on analysis of recent CTL coverage within different landscape complexes and geomorphic levels, landscape complexes are associated into five groups of hazard degree: ***impossible***, ***minimal***, ***average***, ***serious*** and ***maximal*** (Fig. 5, Table 2), based on estimation of geomorphic features, slope steepness, drainage, microrelief, vegetation associations and former landslide activity.

Impossible hazard degree is on low, mostly wet peatlands (units 7–9) as well as khasyreis (unit 15), lake terraces (unit 16) and beaches (unit 17). Landslide shear surfaces and bodies of 1989 are also included in this group because of very low probability of repeated landslide process in nearest future.

Landscapes with ***minimal*** hazard of cryogenic landslide are all rather drained flat subhorizontal watersheds (units 2–5), including flat-topped polygonal peatlands (unit 6), and poorly drained subflat surfaces (unit 10) on all geomorphic levels except the V marine plane.

Convex hill tops and their slopes (unit 1) on the IV and V plains, flat subhorizontal watersheds (units 2–4) on the V marine plain, gentle slopes adjacent to the higher geomorphic levels with well-developed moss cover (unit 12) as well as gentle slopes with mostly mossy willow thickets (unit 11) and drainage hollows (unit 14) on II river terrace and III alluvial-marine plain are in ***average*** hazard degree group. Probability of small-scale landslide process increases in immediate proximity of rather drained rolling hill tops, subhorizontal watersheds and lake depression slopes.

Lengthy shrubby slopes with small gradient (unit 11) on the IV and V plains rather favourable for vast landslides are in ***serious*** hazard degree group. Ravines, gullies and small river valleys are included in the group of ***serious*** hazard of cryogenic landslide process because of high potential of small-scale landslides on steep unevenly drained concave shrubby slopes. Landslide hazard on steep sides of drainage hollows (unit 14) on the IV and V plains is also higher than on similar landscapes of lower geomorphic levels because of deep dissection.

Maximal hazard of cryogenic landslide is assigned to concave shrubby slopes (unit 13) being ancient landslide shear surfaces; for landslide cirques and slopes, except landslide shear surfaces of 1989 where thermoerosion and thermokarst are still active due to the effect of landslide.

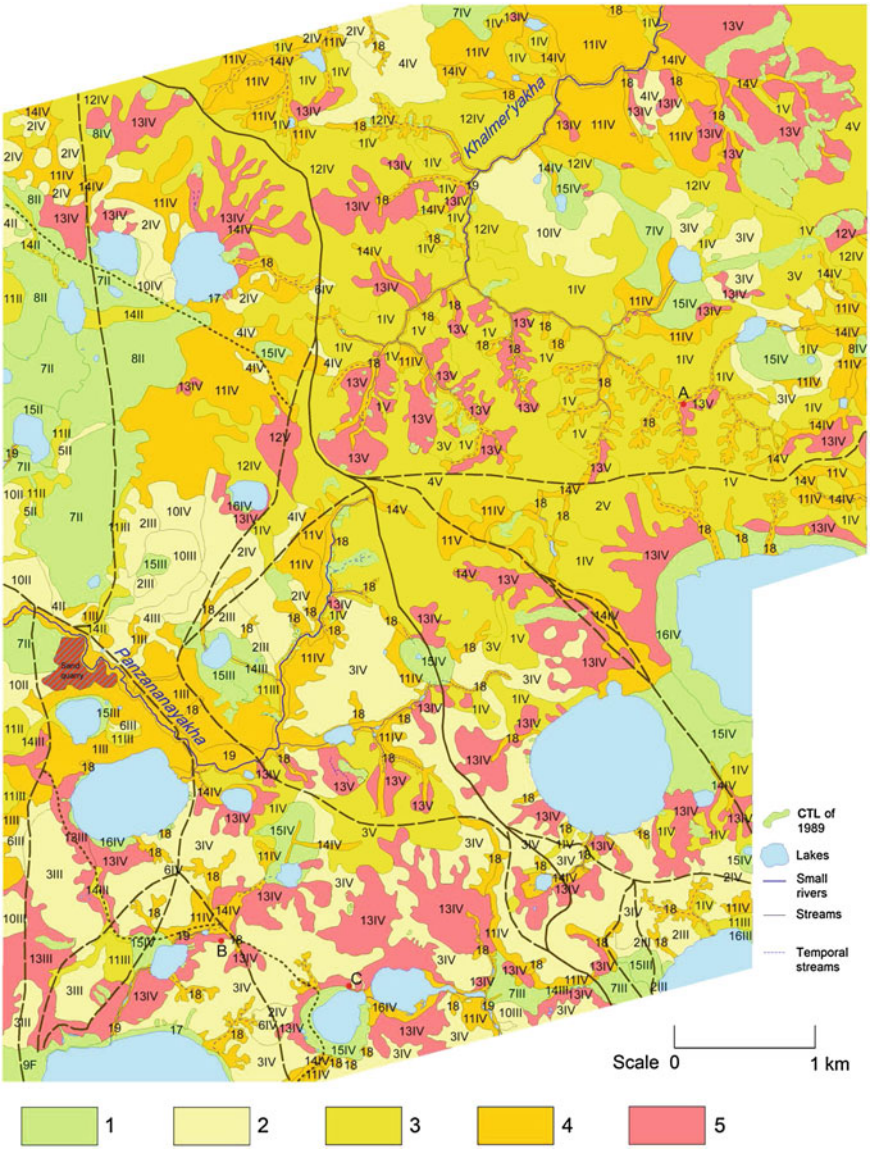

Fig. 5 Map of cryogenic landslide hazard within subdivided landscape complexes. Degree of cryogenic landslide hazard: 1—impossible, 2—minimal, 3—average, 4—serious, 5—maximal

Artificial sand quarry is not of a high landslide hazard now because it is abandoned and partly revegetated. There are only processes of bogging and thermokarst within excavations and deflation on surrounding sandy banks. Only steep slopes of these banks cut by a river are favourable for small-scale landslide

process. Also, cryogenic landslides could be triggered by vehicle tracks across slopes. Tracks crossing ravine heads could activate thermoerosion resulting in its turn in landslide process.

Maximal hazard of cryogenic landslide remains on concave shrubby slopes (unit 13) of all geomorphic levels. Hazard of large-scale landslide process on gentle shrubby or partly shrubby slopes (units 11 and 12) increases from lower to higher geomorphic levels. Hazard of small-scale landslide process on tentatively horizontal surfaces (units 1–4) increases if deeply dissected by ravine and small stream valleys, but without obvious relation to their geomorphic level.

5 Discussion

Existing and applied in the Central Yamal landslide risk assessment methods are qualitative or semi-quantitative in nature. Ukraintseva et al. (1992) identified natural complexes on the map characterized by the development of recent cryogenic processes, including slope ones, as a results of field surveys and expert judgement using analysis of landscape structure and engineering and permafrost changes. Her map of 1:100000 scale covers the III alluvial-marine plain and river terraces. Prediction of slope-process activation is based on the distribution of recent processes (the more widely and evenly distributed processes are the more risky is the area). This method does not take into account our findings that the same area can become a scene for new landslides only after several hundred years, excluding cases close to surface location of massive ground ice. This method was suggested and applied in the Bovanenkovo gas field where it is acceptable because of low topography (from III alluvial-marine plain to Se-Yakha river floodplain). Ermokhina (2009) estimated the likelihood of re-occurrence of landslides on landslide slopes based on the degree of recovery of vegetation. Her methods concentrated on ancient landslide slopes and did not assess other surfaces.

South of Bovanenkovo in the area of research station Vaskiny Dachi with much more complicated geomorphology, high geomorphic levels, deeper in general massive ground ice position in the section, and much lower degree of anthropogenic impact, different approach is needed and suggested in this chapter. Also based on relatively similar understanding of the process activation reasons, we suggest quantitative analysis of process coverage which was made possible by long-term detailed field study of landslide distribution and different mechanisms of its development (Leibman and Egorov 1996; Leibman et al. 2003; Khomutov and Leibman 2010). Also recently much more detailed remote-sensing data became available which in cooperation with field survey of landscape structure allowed quantitative analysis with the addition of detailed landscape approach. Map of recent landslide impact (Fig. 4) shows the degree of surface disturbance by recent landslides. The higher the degree, the more sensitive is a landscape complex to cryogenic landslide process. At the same time areas directly affected by recent landslides are attributed to low landslide risk, as the repetition of the landslide

process can not be on the surface with immature active layer and low degree of re-vegetation. The map of cryogenic landslide hazard (Fig. 5), being compared with other landslide prediction maps show that in general, the area of potential landslide risk match. However, our map accesses landslide hazard in much more detail and is based on a longer and much more detailed ground truth and high-resolution remote-sensing data interpretation. During the 2012 field investigation, we observed two newly formed cryogenic landslides (Figs. 6 and 7) and thermocirque (Fig. 8), most probably activated by CTL. Cryogenic landslide A (see Fig. 5) is formed on the steep slope of the ravine (unit 18) and the upper part of the landslide shear surface belongs to concave landslide slope (unit 13). Cryogenic landslide B (see Fig. 5) initiated on flat sub-horizontal surface (unit 3) near the edge to concave slope with willow thickets (unit 13). Thermocirque C (see Fig. 5) activated on shrubby concave slope (unit 13). Thus, all the cryogenic landslide objects observed in 2012 are directly related to the landscape complexes characterized by

Fig. 6 Small cryogenic translational landslide (A) on ravine slope, detected in 2012 field season

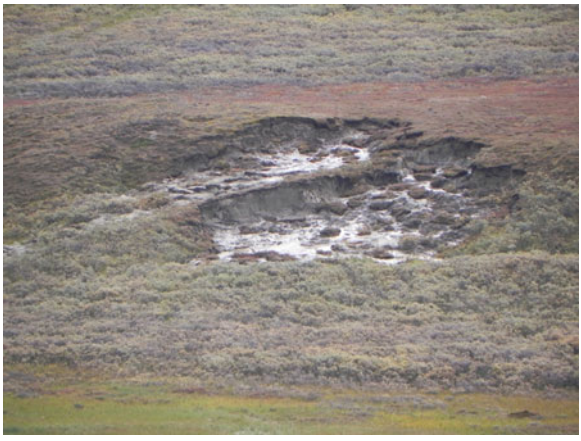

Fig. 7 Cryogenic landslide (B) on watershed edge to concave shrubby slope, detected in 2012 field season

Fig. 8 Thermocirque (C) on concave shrubby slope, detected in 2012 field season

maximal landslide hazard degree according to the suggested method, which proves the applicability of the suggested method.

6 Conclusions

Method of cryogenic landslide hazard analysis is based on quantitative assessment and expert judgment of recent landslide distribution and their parameters in different landscapes.

Recent landslide impact on landscape complexes determines response of these landscapes to potential landslide activation depending on the area affected by these landslide events within each landscape.

Surfaces affected by these landslides are not at risk of being activated by cryogenic landslides because ice-bearing transient layer has not developed at the bottom of the "new" (after the active layer detachment) active layer.

The application of this method revealed the following:

Very high cryogenic landslide hazard on concave shrubby slopes is characteristic of all geomorphic levels except Mordyakha river flood plain and II river terrace.

Risk of large-scale landslides process on gentle shrubby to partly shrubby slopes increases from low to high geomorphic levels. Small-scale landslides process on sub-horizontal surfaces increase with degree and depth of dissection by ravine and small stream valleys independent of geomorphic level.

Landscapes in the Key area are characteristic of the typical tundra in the north of western Siberia. Therefore, the method tested at the Key site can be applied to other plains of typical tundra zone with widely distributed tabular ground ice triggering cryogenic landslides, north of Yuribey River as indicators of evolution of hazardous slope processes ongoing since the Late Holocene.

The application of cryogenic landslide hazard analysis using recent landslide impact study and based on landscape approach is quite effective due to low labor costs. If high resolution satellite images for the area of interest are available, the method described in this chapter is easy to apply with result of preliminary field investigations. Field work is needed just to refine local features for correct remote delineation of landforms and vegetation cover on the landscape base map. The combination of the suggested landscape method with the phyto-indication method

suggested by Ermokhina (2009) surely allows for the most accurate prediction of landslide activation, but is connected with more detailed field study.

Acknowledgments This study was possible, thanks to the integration grants No. 122 and No. 144 of the SB RAS, department of education and science of Tyumen Region, Grant No. 583-DON, and the presidential council for grants, Science School Grant No. 5582.2012.5 to the Earth Cryosphere Institute SB RAS.

References

Burn CR, Lewkowicz AG (1990) Retrogressive thaw slumps. Canadian Geographic 34(3):273–276

Burn CR, Zhang Y (2009) Permafrost and climate change at Herschel Island (Qikiqtaruq), Yukon Territory, Canada. J Geophys Res 114:F02001. doi:10.1029/2008JF001087

CAVM Team (2003) Circumpolar arctic vegetation map conservation of arctic flora and fauna (CAFF) Map No. 1. US Fish and Wildlife Service, Anchorage, AK

Chehina IV, Rivkin FM, Ivanova NV, Koreisha MM, Popova AA (2004) Construction of estimation maps of natural risk of cryological processes on the Varandei Peninsula coast. In: Cryosphere of oil-and-gas bearing provinces. Abstracts of international conference, Tyumen, pp 112

Drozdov DS, Ukrainrseva NG (2000) Map of natural geosystems of Bovanenkovo gas field (landscape map). In: Melnikov ES (ed) ECI SB RAS (in Russian)

Ermokhina KA (2009) Phyto-indication of exogenous processes in the tundras of Central Yamal. Candidate dissertation. Moscow University, Moscow, 24 pp (in Russian)

Ermokhina KA, Myalo EG (2012) Phytoindicators of landslide disturbances in the Central Yamal. In: Drozdov DS, Romanovsky VE (eds) Tenth international conference on permafrost. Translations of russian contributions. The Northern Publisher, Salekhard, Russia, 2:531–536

Ermokhina KA, Ukraintseva NG (2003) Ecosystem response on dynamics of cryogenic landslides in the subarctic tundras (Yamal Peninsula). In: Arctic-alpine ecosystem and people in a changing environment. Book of abstracts. Polar Environmental Centre, Tromsø, Norway, p 97

Ershov ED (ed) (1989) Geocryology of the USSR. Western Siberia. Nedra, Moscow, 454 pp (in Russian)

Garagulya LS, Parmuzin SYu (1980) Signs of assessment of stability to changes of natural factors and technogenic impact in the permafrost area. In: Permafrost study, vol 19. Moscow State University, Moscow, pp 56–58 (in Russian)

Gubarkov AA (2009) Interrelation of hydrologic and cryogenic processes in the basins of small rivers and on the Kara sea coast. Candidate dissertation. Tyumen, 18 pp (in Russian)

Gubarkov AA, Leibman MO (2010) Bead-shaped channel forms as evidence of paragenesis of cryogenic and hydrological processes in the small-river valleys of Central Yamal. Earth Cryosphere, XIV(1):41–49 (in Russian)

Grechishchev SE (ed) (1981) Guidelines for prediction of cryogenic physical-geological processes developing in the exploited areas of the Far North. VSEGINGEO, Moscow, 78 pp (in Russian)

Harris C, Lewkowicz AG (1993) Form and internal structure of active-layer detachments slides, Fosheim Peninsula, Elsmere Island, Northwest Territories, Canada. Canadian Journal of Earth Sciences 30(8):1708–1714

Harris C, Lewkowicz AG (2000) An analysis of the stability of thawing slopes, Ellesmere Island, Nunavut, Canada. Canadian Geotechnical Journal 37(2):449–462

Kazakov NA, Gensiorovskii YuV (2008) Exogenous geodynamic and fluvial processes in the low-mountain area of the Sakhalin Island as the risk factors for “Sakhalin-2” oil and gas

pipelines. Environmental Geoscience: Engineering Geology, Hydrogeology, Geocryology 6:483–496 (in Russian)
Khomutov AV, Leibman MO (2010) Landscape pattern and cryogenic landslide hazard analysis on Yamal Peninsula, Russia. In: Thermal state of frozen ground in a changing climate during the IPY. Abstracts from the Third European Conference on Permafrost. The University Centre in Svalbard, pp 254
Kizyakov AI (2005) Dynamics of the thermodenudation processes on the coast of Yugorsky Peninsula. Earth Cryosphere IX(1):63–67 (in Russian)
Kizyakov AI, Leibman MO, Perednya DD (2006) Destructive relief-forming processes at the coasts of the Arctic plains with tabular ground ice. Earth Cryosphere X(2):79–89 (in Russian)
Leibman MO (1994) Cryogenic landslides and their interaction with linear constructions on Yamal Peninsula Russia. In: Smith DW, Sego DC (eds) Proceedings of the 7th International Cold Regions Engineering Specialty Conference, Edmonton, pp 865–869
Leibman MO (1995) Preliminary results of cryogenic landslides study on Yamal Peninsula, Russia. Permafrost and Periglacial Processes 6(3):259–264
Leibman MO (1997) Cryolithilogical peculiarities of the seasonally thawed layer on slopes in relation to the landslide process. Earth Cryosphere I(2):50–55 (in Russian)
Leibman MO (2001) Procedures and results of active-layer measurements in marine saline deposits of Central Yamal. Earth Cryosphere V(3):17–24 (in Russian)
Leibman MO (2004) Mechanisms and stages of slope cryogenic process formation in the western sector of Russian Arctic. In: Relief forming processes: theory, practice, research methods. Materials of XXVIII Plenum of Geomorphic Commission, Novosibirsk, pp 160–162 (in Russian)
Leibman MO (2005) Cryogenic slope processes and their geoecologic consequences under the tabular ground ice distribution. Doctor of science dissertation, Tyumen, 40 pp (in Russian)
Leibman MO, Egorov IP (1996) Climatic and environmental controls of cryogenic landslides, Yamal, Russia. In: Senneset K (ed) Landslides. Balkema Publishers, Rotterdam, pp 1941–1946
Leibman MO, Kizyakov AI (2007) Cryogenic Landslides of the Yamal and Yugorsky Peninsulas. Earth Cryosphere Institute SB RAS, Moscow, 206 pp (in Russian)
Leibman MO, Kizyakov AI, Sulerzhitsky LD, Zaretskaya NE (2003) Dynamics of the landslide slopes and mechanism of their development on Yamal Peninsula, Russia. In: Proceedings of the Eighth international conference on permafrost, Zurich. A.A.Balkema Publishers, Rotterdam, Netherlands I:651–656
Leibman MO, Streletskaya ID (1997) Land-slide induced changes in the chemical composition of active layer soils and surface-water run-off, Yamal Peninsula, Russia. In: Iskandar IK, Wright EA, Radke JK, Sharratt BS, Groenevelt PH, Hinzman LD (eds) Proceedings of the international symposium on physics, chemistry, and ecology of seasonally frozen soils, Fairbanks, Alaska, June 10–12, 1997, CRREL Special Report 97–10, CRREL, Hanover, pp 120–126
Leibman MO, Streletskaya ID, Konyakhin MA (1997) Assessment of surface dynamics at Bovanenkovo gas field (Central Yamal Peninsula) during the period 1949 to 1990. Geomorphology 2:45–48 (in Russian)
Lewkowich AG (1988) Slope Processes. In: Clark MJ (ed) Advances in periglacial geomorphology. Wiley, Chichester, pp 325–368
Lewkowich AG (1990) Morphology, frequency and magnitude of active-layer detacment slides, Foshein Island, N.W.T. In: Pergelisol-Canada, Permafrost-Canada. Proceedings of the fifth canadian permafrost conference, Centre d'etudes nordique, University Laval, Collection Nordicana, Quebec, vol 54, pp 111–118
Melnikov ES (ed) (1983) Landscapes of cryolithozone of West Siberian gas province. Nauka, Novosibirsk, 163 pp (in Russian)
Melnikov ES, Leibman MO, Moskalenko NG, Vasiliev AA (2004) Active-layer monitoring in the cryolithozone of West Siberia. Polar Geography 28(4):267–285

Melnikov ES, Veisman LI, Kritsuk LN et al. (1974) Landscape indicators of engineering-geocryological conditions of West Siberia North and their interpretive features. Nedra, Moscow, 132 pp (in Russian)

Moskalenko NG (2003) Interaction between vegetation and permafrost in different bioclimatic zones of western part of Russian Arctic. Earth Cryosphere VII(4):14–20 (in Russian)

Moskalenko NG (ed.) (2006) Anthropogenic changes of ecosystems in West Siberian gas province. ECI SB RAS, 358 pp (in Russian)

Postoev GP, Lapochkin BK, Kazeev AI, Nikulshin AS (2008) Natural and human-induced processes assessment of landslide hazard at the construction sites. Environmental Geoscience: Engineering Geology, Hydrogeology, Geocryology 6:547–557 (in Russian)

Rebristaya OV, Khitun OV, Chernyadjeva IV, Leibman MO (1995) Dynamics of vegetation on the cryogenic landslips in the central part of the Yamal Peninsula. Botanical Journal 80(4):31–48 (in Russian)

Smetanin NN (2006) Geoecological assessment of oil-gas area of West Yamal based on analysis of geosystem structure. Candidate dissertation. ECI SB RAS, Tyumen, 23 pp (in Russian)

Streletskaya ID, Leibman MO (2002) Cryogeochemical interrelation of massive ground ice, cryopegs, and enclosing deposits of Central Yamal. Earth Cryosphere VI(3):15–24 (in Russian)

Trofimov VT (ed) (1975) Yamal Peninsula (Engineering-geological outline). Moscow University Press, Moscow, 280 pp (in Russian)

Ukraintseva NG, Leibman MO (2007) The effect of cryogenic landslides (active-layer detachments) on fertility of tundra soils on Yamal Peninsula, Russia. In: Schaefer, Schuster, Turner (eds) Conference presentations from the 1st North American Landslide Conference Vail Colorado June 3–8 2007. Landslides/slope instability AEG Special Publication, 23 Omnipress (Conference CDROM), pp 1605–1615

Ukraintseva NG (2008) Vegetation response to landslide spreading and climate change in the west siberian tundra. In: Proceedings of the ninth international conference on permafrost, University of Alaska Fairbanks, vol 2, 1793–1798

Ukraintseva NG, Leibman MO, Sreletskaya ID (2000) Peculiarities of landslide process in saline frozen deposits of Central Yamal, Russia. In: Bromhead E et al. (eds) Landslides in research, theory and practice. Proceedings of the Eighth International Symposium on Landslides. Cardiff, UK. Thomas Telford, London, vol 3, pp 1495–1500

Ukraintseva NG, Shuvalova EM, Smetanin NN (2005) Cryogenic translational landslides on area of Bovanenkovo gas field: distribution, features, consequences. In: Third Conference of Russian Geocryologists. Moscow, vol 2. University Book Publisher, Moscow, pp 178–185 (In Russian)

Ukraintseva NG, Shuvalova EM, Vasiliev AA (1992) Assessment of potential hazard of slope processes activation on area of Bovanenkovo gas field. In: Grechischev SE (ed) Methods of research of cryogenic physical-geological processes. VSEGINGEO, Moscow, pp 109–113 (in Russian)

Ukraintseva NG, Streletskaya ID, Ermokhina KA, Yermakov SYu (2003) Geochemical properties of plant-soil-permafrost system at landslide slopes, Yamal, Russia. In: Proceedings of the eighth international conference on permafrost, Zurich, vol II. A.A. Balkema Publishers, Rotterdam, Netherlands pp 1149–1154

Vasiljevskaya VD, Grigorjev Ya V, Pogozheva Ye A (2004) Indexes of stability, degradation and self-recovery for tundra soil-vegetation cover. Earth Cryosphere, VIII(1):53–63 (in Russian)

Walker DA, Epstein HE, Raynolds MK, Kuss P, Kopecky MA, Frost GV, Daniëls FJA, Leibman MO, Moskalenko NG, Matyshak GV, Khitun OV, Khomutov AV, Forbes BC, Bhatt US, Kade AN, Vonlanthen CM, Tichy L (2012) Environment, vegetation and greenness (NDVI) along the North America and Eurasia Arctic transects. Environmental Research Letters 7:015504

Walker DA, Leibman MO, Epstein HE, Forbes BC, Bhatt US, Raynolds MK, Comiso JC, Gubarkov AA, Khomutov AV, Jia GJ, Kaarlejarvi E, Kaplan JO, Kumpula T, Kuss P, Matyshak G, Moskalenko NG, Orekhov P, Romanovsky VE, Ukraientseva NG, Yu Q (2009)

Spatial and temporal patterns of greenness on the Yamal Peninsula, Russia: interactions of ecological and social factors affecting the Arctic normalized difference vegetation index. Environmental Research Letters 4:045004

Walker DA, Raynolds MK, Daniëls FJA, Einarsson E, Elvebakk A, Gould WA, Katenin AE, Kholod SS, Markon CJ, Melnikov ES, Moskalenko NG, Talbot SS, Yurtsev BA and the other members of the CAVM Team (2005) The circumpolar Arctic Vegetation Map. Journal of Vegetation Science 16(3):267–282

Cryogenic Landslides in Paragenetic Complexes of Slope and Channel Processes in the Central Yamal Peninsula

Anatoliy Gubarkov, Marina Leibman and Maria Andreeva

Abstract The paper discusses the development of a number of cryogenic and channel processes, as well as their paragenetic complexes. In small river basins, these complexes form (a) landslide-affected slopes and landslide cirques, (b) river valleys. Up to half of the small river basins' area in the upstream is subject to cryogenic process. The vast majority (80 %) of these processes are cryogenic landslides. Other slope processes are interconnected to cyclicity of cryogenic landslide. They appear between the landslide cycles, lasting between 200–400 years. Cryogenic landslides within paragenetic complexes are rapid and violent process. Thermoerosion and thermokarst develop between the active phases of cryogenic landslides. These processes can be considered to be accompanying slow processes. Lowering of the surface per landslide cycle is on average of 0.9 m in the upper part of the slope and up to 1.6 m in the lower part. This corresponds to surface denudation of 4–6 mm per year. Subsequent processes of thermoerosion and thermokarst are responsible for lowering the surface to significantly higher degree (0.6–1.05 m).

Keywords Paragenesis of processes · Cycle of processes · Cryogenic landslides · Thermoerosion · Landslide cirque · River valley · River channel processes

A. Gubarkov (✉)
Tyumen State Oil–Gas University, Volodarskiy str., 38, Tyumen, Russia 625000,
e-mail: agubarkov@rambler.ru

M. Leibman · M. Andreeva
Earth Cryosphere Institute SB RAS, PO Box 1230 Tyumen, Russia 625000,

W. Shan et al. (eds.), *Landslides in Cold Regions in the Context of Climate Change*, Environmental Science and Engineering, DOI: 10.1007/978-3-319-00867-7_21,

1 Introduction

Cryogenic landslides in the Central Yamal Peninsula are one of the most common processes (Ananieva 1997; Baulin et al. 1996, 2003; Baranov and Posnanin 1999; Leibman et al. 2003). There are cryogenic landslides of shearing and flowing mechanisms named accordingly (Kaplina 1965; French 1976, 1998; Lewkowicz 1990; Harris and Lewkowicz 1993; Leibman et al. 2003).

The majority of cryogenic processes are characterized by relation to one or more associated processes (Ershov 1989; Washburn 1979). In the upper reaches of small rivers, slope processes are the most common. One of them is cryogenic landslide process which leads to the formation of landslide cirques (Leibman et al. 2003).

Cryogenic landslides in the central Yamal are one of the most common processes. A large area of slope surfaces is influenced by landslides along with other cryogenic processes. The closest paragenetic relations exist between the cryogenic landslides and thermoerosion (Gubarkov and Leibman 2007). Immediately after cryogenic landslide event, melting of ground ice and the formation of a new active layer starts. Against this background, active become erosion and thermoerosion of thawed permafrost by water flows, generated by rainfall and snowmelt. Observations show that erosion/thermoerosion of the shear surfaces formed after the last extensive cryogenic landslides in 1989, continued for more than 20 years, as they are unevenly and slowly re-vegetating (Ermokhina 2009).

It is known that cryogenic landslides are cyclical and take place once between 200 and 400 years, which is an average of 300 years (Leibman et al. 2003). Each landslide cycle is accompanied by erosion/thermoerosion which leads to the formation of landslide cirques of different sizes and depths. With an increase in the number of cryogenic landslide cycles on the same surface, the depth of landslide cirques increases. Sequential impact of cryogenic landslides and thermoerosion on the slopes leads to a certain surface denudation. The depth of concavity depends on the geomorphic level and geocryological conditions.

Most of the slopes in the valleys of small rivers with headwaters on the III–V marine terraces were formed by paragenetic complexes of cryogenic and hydrological processes (Gubarkov and Leibman 2010). Most often, the leading slope process in the formation of the valleys is cryogenic landslides. Cryogenic landslides belong to the rapid exogenous processes (Sukhodrovsky 1979; Leibman et al. 2003). Speed of their movement on the same territory is swift as compared to the phases that separate them. Slow processes are also involved in the denudation of surface that is exposed by cryogenic landslides. Only a certain combination of factors can prepare the next cycle of cryogenic landslide. The main processes between cycles of landslides are mud flows and thermoerosion, while in the case of exposure of tabular ground ice, is referred to as thermodenudation.

Earlier studies of the upper, middle and lower reaches of the small River Panzananayakha located in the central Yamal Peninsula at the research polygon "Vaskiny Dachi" showed differences in the complexes of cryogenic processes

between each portion of the river valley (Gubarkov and Leibman 2010). In the valley of Panzanana-yakha river, each of the aforementioned cryogenic processes developed most intensively on a particular section of the river (in the upper, middle and lower reaches), depending on hydrology, geocryological and geomorphological factors. Due to the narrowness of the valley, the regular cryogenic landslide in the upper reaches has a significant impact on the hydrological regime of the river, forming dammed parts of the channel with temporary flowing reservoirs. The impact of cryogenic landslides on the valley in the middle and lower reaches was not detected; they do not form dammed reservoirs. This is because the landslide body did not reach the river bed due to the greater width of the valley as compared to the upstream. In these parts of the river, manifestation of thermokarst in the valley and the mainstream can be found (Everdingen 1998; Drozdov 2004; Surkov and Tarbeeva 2012).

The purpose of this paper is study the development of separate cryogenic and channel processes, and their paragenetic complexes, resulting in the formation of (a) landslide slopes and landslide cirques and (b) river valleys.

2 Research Methods

Remote sensing, land-based regime, and route monitoring and measurements were used for the study of cryogenic and hydrological processes. The studies covered a variety of natural systems. The largest system is a river basin. The objects of study were two small rivers at "Vaskiny Dachi", located on the watershed of Se-Yakha and Mordy-Yakha main Yamal's rivers. Within the basin areas allocated are most active manifestations of cryogenic landslides and paragenetically associated processes.

General analysis of the influence of cryogenic landslides, thermokarst and thermoerosion on the width of the valley bottoms was undertaken. Land-based methods helped establish the type of processes or their paragenetic complexes. High-resolution satellite imagery of the river valleys of Panzanana-yakha and Halmer-yakha rivers were used in the analysis. Established were the main morphometric characteristics of the processes and landforms that affect the width of the bottom of the valley in the upstream.

The sequence and intensity of processes in an asynchronous (sequential) paragenetic complex of cryogenic landslide process and thermoerosion were under a detailed study within a separate cryogenic landslide. A mechanism for transformation of cryogenic landslide shear surfaces under the influence of thermoerosion, surface runoff and thermokarst subsidence of permafrost during the formation of a new active layer have been established.

For the study of the cyclic effects of cryogenic landslides and subsequent erosion lowering of the surface, two landslides with different lengths, width and number of sliding cycles on the same surface were selected. We have chosen three reference landslide shear surfaces, with the number of cycles 1, 3 and 5. The time

of landslide shear surface formations were estimated to be 20, 600–1,200 and 1,000–2,000 years, respectively. Cryogenic landslide age is set according to the direct observation of the process in the field, starting from 1989, using radiocarbon studies (Leibman et al. 2003) and remote sensing of the surface area (Gubarkov and Leibman 2012).

For the study of paragenetic processes and cyclicity, a special technique of morphometric measurements was developed. It aims at determining the depth of cutting-into the shear surface of cryogenic landslides or landslide cirque, in relation to the directly adjacent areas of undisturbed slopes (Fig. 1a, b). For the same profiles within the landslide shear surfaces, the depth of erosion and thermoerosion troughs were measured.

All measurements of gullies and ravine morphometry were conducted in three cross-sections laid through the landslide shear surfaces in the upper, middle and lower cross-sections (Fig. 1a). The upper cross-section on the cryogenic landslide shear surface is laid in 10–15 m from the edge of the material mobilization area. The middle cross-section is linked to the transit zone and the lower one is located in the mouth part, the accumulation zone. In the absence of a full cycle of erosion on the landslide shear surfaces, the measurements were performed in an abbreviated form.

We studied the influence of cryogenic landslides on the change of active layer depth. Active layer measurements were carried out on six landslide shear surfaces of cryogenic landslides, within the erosion network and on the adjacent stable slope surface. Active layer measurements were carried out along three profiles in the upper, middle and lower part of cryogenic landslide as indicated in Fig. 1.

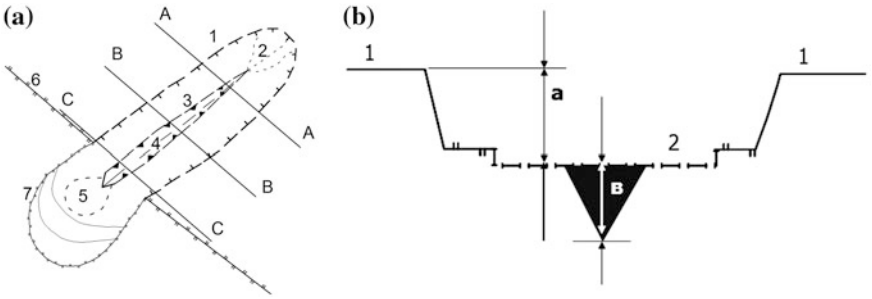

Fig. 1 **a** Scarp of a cryogenic landslide; 2—erosion network; 3—ravine; 4—thalweg of the ravine; 5—debris cone of the ravine; 6—edge of the slope; 7—landslide body; A–A—the upper cross-section; B–B—the middle cross-section; C–C—the lower cross-section. **b** Morphometric parameters measured on the shear surfaces of landslides along the cross-sections A–A, B–B and C–C: 1—Undisturbed surface adjacent to the cryogenic landslide; 2—shear surface; 3—erosion trough; *a*—the depth of the shear surface of cryogenic landslide relative to the adjacent slope; *B*—the depth of erosion trough

3 Results and Discussion

3.1 Cryogenic Landslide Process in the Basins (Valleys) of the Small Rivers

Dokuchayev (1878) was the one to draw attention to the change in the width of river valleys in Russia. At present, the main causes of changes in the river valleys have been established (Simonov 1972; Karasev and Khudyakov 1984). The following factors are the leading ones: tectonic, glacial, landfall and accumulative. The impact of cryogenic processes on change of the river channel width in the Yamal Peninsula is mainly noted in their upper reaches (Baulin et al. 2003 and others).

In the upper reaches of the rivers originating on the high geomorphologic levels (marine terraces) cryogenic slope processes, such as cryogenic landslides, become important. The cryogenic landslide materials enter the riverbeds, cover them and, in some cases, part of the valleys of small river as well. When the stream water is dammed, ponds are formed with heavily processed shores, which lead to the widening of the bottom of the river valley. Since the study area is located in a zone of continuous permafrost, expansion of the river valley is also due to thermokarst accompanied by local slope processes.

In the upper reaches of the Panzanana-yakha and Halmer-yakha rivers, the valleys are shaped by a number of cryogenic processes (Fig. 2). Thus, the area of cryogenic landslides on the Panzanana-yakha river make up 39 %, on the Halmer-yakha river 18 %, on hasyreis and lakes 7 and 8 %, in each valley respectively, in thermoerosion ravines 4 and 11 %. On the edges and upper parts of slopes in the Halmer-yakha valley, sandy hollows result from deflation (2 % coverage), which is absent in the upper reaches of the Panzanana-yakha river. The rest of the valleys belongs to the flat surfaces and slightly sloped watershed areas without active cryogenic processes (50 and 61 %). Area ratio shows that the percentage of cryogenic landslides is the largest within surfaces of upstream river basins subject to cryogenic processes.

Research on the valley banks in the upper reaches of the rivers showed that their formation is highly dependent on time, frequency and place of cryogenic landslide location. The field and remote-sensing materials indicate that cryogenic landslide shear surfaces could be divided into three groups: ancient, old, and modern. The oldest surfaces in the study area are under the age of 1,800–2,200 years (Leibman et al. 2003). Cryogenic landslide surface ratios are distributed as follows: The ancient surfaces in the valley of Panzanana-yakha river occupy 61 % of the total area of cryogenic landslides, in the Halmer-yakha river valley they are absent; old surfaces occupy 25 and 92 %, modern −14 and 8 %, respectively.

In the valleys of the rivers under study, distribution of the surface area controlled by cryogenic processes is very different. Leading process in the valleys of both rivers are cryogenic landslides. Area and length of the ravine system in the Halmer-yakha river valley are increasing, indicating a more active thermoerosion

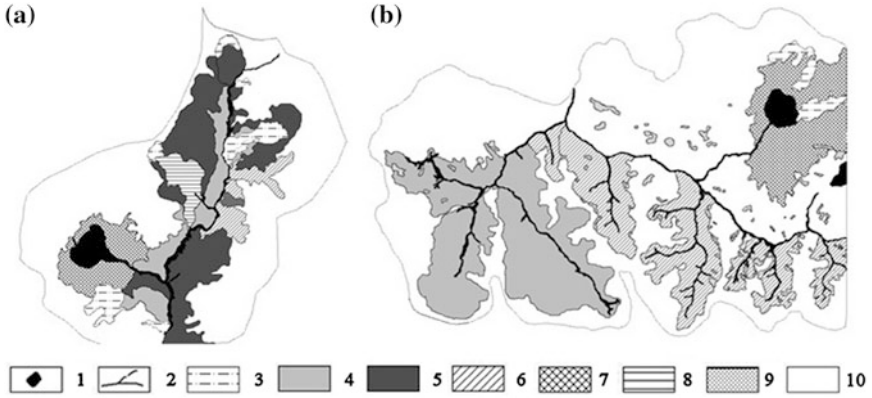

Fig. 2 Upper reaches of the Panzanana-yakha (*A*) and Halmer-yakha (*B*) river basins. *Key* 1—lakes; 2—permanent and temporary streams; 3—modern cryogenic landslides; 4—middle aged cryogenic landslide surfaces; 5—ancient cryogenic landslide surfaces; 6—ravine network; 7—hasyreis; 8—outlier without active denudation; 9—areas of deflation; 10—watershed area

as compared to the Panzanana-yakha river valley. The significant specific feature of the upper reaches of the Halmer-yakha river is deflation, mainly distributed in the edge part of ravine network in the form of local windblown sand hollows.

There are 4 types of cryogenic landslides that differ in age and location relative to each other in the Panzanana-yakha river valley. On the slopes, they can be situated without affecting older shear surfaces and bodies of cryogenic landslides being landslides of first order (type 1; Yemelyanova 1972). They can "nest" into each other, landslides of second order (type 2; Yemelyanova 1972), overlap the previous cryogenic landslides, multilevel landslides (type 3; Makkaveev 1971) and form terraces, stepped landslide (type 4; Timofeev 1978). The valley of the Halmer-yakha river is characterized by landslides of only type 1.

Comparison of landslides in the Panzanana-yakha and Halmer-yakha river valleys showed that different types of landslides could influence both the slopes and the bottoms of the channels of small river valleys. Impact on slopes without affecting the bottom of the river is due to types 1 and 3 of landslides on the Panzanananyaha river. Landslides regulating the channel run and width of the river bottom are types 2 and 4 on the Panzanana-yakha river and type 1 on the Halmer-yakha river. The shape of the slopes, their drainage, turbidity of water flows, erosion and thermoerosion is determined by cryogenic landslide processes. At the bottom, cryogenic landslides form dams and determine the width of the valley bottom and channel runoff in the small rivers.

According to the results of high-resolution satellite imagery interpretation for Panzanana-yakha river valley in the upstream, the width of the valley bottom was measured every 100 m from the source to the middle reaches of the river at every point. Analysis of the data showed that the bottom, depending on one or several principal and related cryogenic processes could be divided into seven sites (Table 1).

Table 1 Number of site, cross-section and morphometric characteristics of the Panzanana-yakha river valley

No. of site	No. of cross-section	Distance from the river source, m	Width of the river valley bottom, m
1	1–3	0,2	3,7
2	3–7	0,6	17,6
3	7–9	0,9	5,7
4	9–14	1,1	11,0
5	14–18	1,7	25,1
6	18–21	2,0	18,9
7	21–22	2,1	11,9

Depending on the intensity, sequence and duration of cryogenic processes, the width of the river bottom changes. On sites with cryogenic landslides, width of the river valley narrows by 2–3 times compared to cryogenic landslides dammed and flooded areas. Unlike Panzanana-yakha river, there are no dammed water bodies at the bottom of the Halmer-yakha river valley, which resulted to minor differences in the width of the bottom along the entire river channel.

High activity of cryogenic landslide process and accompanying parageneti-cally-related processes led to increased turbidity of the water flow, most clearly seen in the middle and lower reaches of the river. In the middle reaches, there is a sharp decrease in turbidity compared to the upstream. Maximum turbidity in the upper reaches for the observation period in 2007 is 5,120 g/m^3, Table 2, while in the middle reaches, it did not exceed 3 g/m^3 and increased to 33 g/m^3 towards the river mouth. Similar relations were observed in the previous years of observation.

Table 3 shows the total volume of rock involved in sediment runoff in the Panzanana-yakha river basin over four years of observation, during the predominance of slow cryogenic processes between active phases of cryogenic landslide process. It suggests that, all types of processes in the valley move around 80 m^3 of deposits per year.

During cryogenic landslide process, one landslide alone in the valley is able to move ten times more material from the slopes into river beds. In 1989, the volume of the largest landslide in the Panzanana-yakha river valley was 6,000 m^3, which is 75 times greater than the total annual solid runoff during the entire periods between landslide cycles. In the same year the landslide volume in the Halmer-

Table 2 Hydrological characteristics of the Panzanana-yakha river for 2005–2008

Years	Maximum water discharge, l/s		Maximum turbidity, g/m^3	
	In the upper reaches	In the lower reaches	In the upper reaches	In the lower reaches
2005	1	15	15	10
2006	3	60	61	17
2007	5	90	5,120	33
2008	15	360	3,180	28

Table 3 Volume of sediment (m^3), transported into the bottom of the Panzanana-yakha river valley in 2005–2008 by the cryogenic landslides, erosion and thermoerosion (debris cones) and channel processes (river bank downfalls) and their percentage in the valley

River channel	Landslide materials	Debris cones of the ravine network	Channel processes	Sum	%
Upstream	15,7	134	0	150	47
Middle	11.2	0	57	68.2	21
Downstream	5.4	0	95	100	32
Amount	32.3	134	152	318	100
%	10.2	42	47,8	100	

yakha river valley was about 800 thousand m^3, which is more than 10 thousand times greater than the average annual sediment runoff. Such volumes of sediment yield from the riverbed by water flows last for a long time. In fact, the river channel runs at a new level that is several meters higher than the previous level.

Cryogenic landslides form dammed lakes that exist for years and increase the time of water exchange in small rivers up to 10 times (Gubarkov & Leibman 2010). Thus, even a single cryogenic landslide can regulate the water flow of small watercourses for several years.

During the existence of "dams", the dammed lakes accumulate different amounts of material from ravine network. This amount depends on the lifetime of the "dam" and amount of suspended matter yielded into the dammed lake. After breaking of the "dam", not the entire layer of accumulative sediment is eroded at the bottom of the dammed lake. The remaining sediment forms steps in the channel, which when vegetated, becomes resistant to erosion. In the upper reaches of the Panzanana-yakha river, 7 vegetated steps and 3 newly formed non-vegetated steps were discovered. Height of the formed steps increased downstream from 1.2 to 1.9 m. This is due to a combination of factors, ranging from the source to the middle reaches of the river. Increase in height of the steps downstream to the boundary between the upper and middle reaches of the river is connected to the initial stage of formation of thermokarsts along the river channel. Height difference occurs with the formation of hydraulic jump and the removal of washed out sediment. A significant factor in the formation of steps is temporary to permanent streams flowing into the mainstream at the step toe. They provide higher removal of sediment, additional influx of turbulent heat in the lower part of the step, standing water in the hydraulic jump have warming effect on permafrost.

Studies have revealed the relationship between cryogenic and hydrological processes affecting small river valleys in the upper reaches and determining their morphometric and hydro-morphometric characteristics. From the combination of slope cryogenic manifestations (especially landslides and thermoerosion) processes, the upper reaches of small rivers are characterized by complex relationships, resulting to cryogenic complexes of landforms and channel forms, united in a system of paragenetic complexes.

4 Study of Landslide Shear Surfaces

As mentioned above, landslide shear surfaces are modified by thermoerosion and thermokarst processes. Length of landslides and their location on the slope determine the intensity of thermoerosion and depth of the gullies and ravines. In general, the longer the landslide and the steeper the slope, the more intense is thermoerosion. However, intensive thermoerosion at the top and middle of the slope is accompanied by accumulation at its foot. In the absence of permanent erosion of the cone (at the sea coast or river channel), the slope can be stabile for a long time, which is typical of the ancient landslide shear surfaces.

Since 1989 gullies and ravines formed on shear surfaces of cryogenic landslides up to 1–2 m deep. The measurement results are shown in Table 4.

Complete cycle of erosion processes, including the pronounced zones of mobilization, transit and accumulation of sediment is identified on 4 landslide shear surfaces (cryogenic landslides 1–4, Table 4), which are the longest. On the shear surfaces of cryogenic landslides 5–9 (Table 4), the landslide material blocks the accumulation zone, so that the debris cone is not formed and the measurement of erosion parameters becomes impossible. Cryogenic landslides 10 and 11 are the shortest, the body of landslide blocks the transit zone. Erosion and thermoerosion in the area of substance mobilization is less pronounced.

The average value of the shear surface depth in relation to the stable surface of the slope increases slightly downslope. The average depth of erosion troughs

Table 4 Depth of the shear surfaces of cryogenic landslides (m) in relation to the surrounding slopes and depth troughs and gullies (m) in relation to the shear surface in the upper, middle and lower cross-sections in landslide cirques

Landslide #	Depth of the shear surface in cross-sections			Depth of troughs and gullies in cross-sections			Cycle of erosion
	Upper	Middle	Lower	Upper	Middle	Lower	
1	−3.3	−3.8	−9.5	−1.2	−1.2	−0.2	Complete
2	−0.5	−3.1	−2.5	−0.5	−2.1	−0.4	
3	−3.5	−2.5	−0.5	−1	−1.1	−0.8	
4	−4.2	−3.4	−2.2	−1.2	−1.2	−0.3	
5	−5.7	−5.7		−0.2	−1.5		Incomplete
6	−2.1	−1.8		0	−0.2		
7	−1.7	−2.3		−0.2	−1.7		
8	−3.7	−5.8		−1.2	−0.1		
9	−5.3	−6.2		−0.1	−1		
10	−3.7			−1			Minimum
11	−5.3			−0.9			
Average	−3.5	−3.8	−3.9	−0.7	−1.1	−0.4	
Minimum	−0.5	−1.8	−1.5	0	−0.1	−0.2	
Maximum	−5.7	−6.2	−9.5	−1.2	−2.1	−0.8	
Amplitude	−5.2	−4.4	−8.0	−1.2	−2	−0.6	

(gullies and ravines) deepens gradually from the upper cross section to the middle cross-section from 0.7 to 1.1 m. From the middle cross-section to the lower cross-section, the trough depth decreases to 0.4 m. It is due to the higher water flow speed in the upper part of the shear surface and its decrease in the lower part where debris cone is formed.

Complete cycle of erosion network on slopes with pronounced areas of substance mobilization, sediment transport and accumulation on a slope foot is possible only when the entire landslide body left the shear surface. If there is a small displacement of the landslide body and sufficient drainage area above the shear surface, short shallow erosion troughs are formed (e.g., cryogenic landslides 10 and 11). With a significant shift of the landslide body, but not along the entire length of the slope, the formation of gullies to the depth of 1.5–1.7 m without formation of pronounced debris cone on the shear surface is possible (cryogenic landslides 5–9). Removal of sediment on such slopes is due to the infiltration of runoff through the active layer and land cover or transit of suspended particles through the landslide material with the formation of a debris cone downslope from the body of a landslide.

Analysis of the relationship between the depth of gullies and ravines and the depth of the shear surface in the slope for four full-course cryogenic landslides (cryogenic landslides 1–4, see Table 4) showed different trends in the upper, middle and lower parts of the shear surface. The upper cross-sections are characterized by increased depth of troughs and increased depth of the landslide shear surface (Fig. 3).

Given that the flow rate and water content determined by the catchment area is less in the upper cross-sections compared to the middle and lower cross-sections, the main control belongs to the slope gradient. The inflow of moisture from the seasonally thawed layer of the surrounding surface may be of certain importance as well. The deep shear surfaces exceeding 5 m (see Table 4), are areas of increased snow accumulation. On the one hand, melting snow leads to increased runoff which inadvertently reduces the vegetative period and prevents consolidation of the shear surface by vegetation.

In the middle cross-sections, the relationship between the depth of erosion formed on the shear surface of cryogenic landslides and the depth of shear surface against the stable slope is virtually absent (Fig. 4), occupying an intermediate position between the positive relation in the upper cross-section and negative in

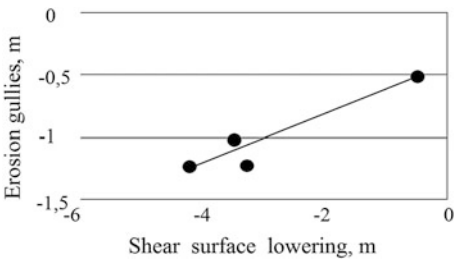

Fig. 3 The relation between the depth of the gullies and ravines and depth of the shear surface in a landslide cirque related to the surrounding slope, the upper cross-section of the shear surfaces, cryogenic landslides 1–4

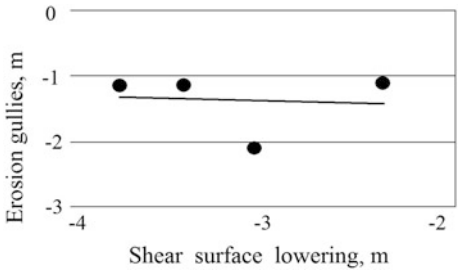

Fig. 4 The relation between the depth of the gullies and ravines and depth of the shear surface in a landslide cirque related to the surrounding slope, the middle cross-section of the shear surfaces, cryogenic landslides 1–4

the lower cross-section (Fig. 5). There is a slight decrease in erosion trough depth with increasing depth of the shear surfaces relative to the adjacent slopes. This is due to sediment load in the runoff, limiting the transport energy even in terms of increased water content at the lower cross-section in comparison with the upper cross-section.

Opposite trend is observed in the lower cross-section (Fig. 5). Reduction in the depth of erosion troughs with increasing depth of the shear surface relative to the adjacent slopes is well defined. Changing the slope gradient from steep on the shear surface to flat at the slope foot for the full cycle of erosion on long cryogenic landslides, leads to the predominance of accumulation over erosion and formation of debris cones in the lower cross-sections of these landslides. Trough depth is reduced from 1.2 to 0.2–0.8 m, indicating a sharp decrease of the erosion potential of runoff.

On the shear surfaces of the full erosion cycle, there are two types of erosion-accumulative processes. Processes of the first type lead to a sharp increase in the depth of ravine (erosion) from the upper cross-section to the middle and as precipitous drop in the ravine depth from the middle cross-section to the lower (accumulation). This type of erosion and accumulation processes is typical of cryogenic landslide 2. The second type of erosion and accumulation processes is even distribution of depth along the upper and middle cross-sections and a sharp decrease in depths in the lower cross-section (cryogenic landslides 1, 3, and 4).

For the first type of erosion and accumulation processes (cryogenic landslide 2), the upper cross-section is characterized by erosion of mild intensity. In the middle cross-section, erosion is followed by slope processes on the sides of the ravine; accumulative processes in the lower cross-section remain. The second type of erosion and accumulation processes leads to the preservation of erosion landforms in the upper cross-sections and the predominance of accumulation in the middle cross-section and increased accumulation in the lower cross-section.

Measurement of depth of the erosion forms revealed the following: formation of erosion network of full cycle with marked zones of mobilization, sediment transport and accumulation on the slope is possible in the case of complete deletion of the landslide body from the shear surface. At partial removal of landslide materials, only some forms of erosion-accumulative relief are formed on the shear surfaces.

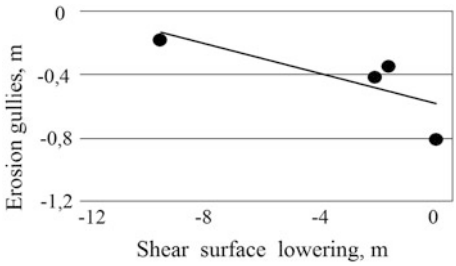

Fig. 5 The relation between the depth of the gullies and ravines and depth of the shear surface in a landslide cirque related to the surrounding slope, the lower cross-section of the shear surfaces, cryogenic landslides 1–4

There is a correlation between the depth of erosion formed on the shear surface and the depths of the shear surface against the surrounding slopes. This dependence is directly proportional to the area of substance mobilization; and is inversely proportional to the accumulation zone. In the upper cross-sections, we observed an increase in erosion trough depth with increase in depth of shear surfaces. This is due to a greater potential energy of the relief at deep cuts, which creates conditions for the maximum realization of erosive potential of the water flow in the absence of suspended sediment in the water coming from the catchment area.

In the lower cross-sections, there is a decrease in the depth of erosion troughs with an increase in the depth of the shear surfaces. This is due to an increase in total suspended solids coming from the high side walls surrounding the deep shear surface. As a result of the maximum water content of runoffs in the lower cross-section, the removal of suspended solids does not occur, as their amount exceeds the erosive potential of water flow.

At the increase of the relief depth in the middle cross-section, the depth of gullies neither increase nor decrease, as here patterns identified for the upper and lower cross-sections compensate each other. Though the water content of the runoff is higher than that of the upper cross-section, erosion does not increase because erosion potential is spent on transit of the suspended sediment.

General relationship between shear surface depths and erosion troughs of a cryogenic landslide is shown in Fig. 6. The scheme suggests that the greater the number of landslide cycles on the same surface (forming a landslide cirque), the lesser the potential for the development of thermoerosion in the bottom of the landslide cirques. Erosion potential shifts up the slope; that is, the possibility of thermoerosion landforms development is preserved only due to the increase in their length up the slope.

Because of cryogenic landslide process, subsequent erosion and thawing of ground ice at the formation of a new active layer causes subsidence of the surface by a certain degree. Figure 7 shows the shear surface and the depth of erosion troughs in it for a different number of landslide cycles. Initial landslides on the surfaces not exposed to cryogenic landslide process earlier are up to 1.8 m deep against the undisturbed slope surface. The depth of thermoerosion trough does not exceed 0.2 m. Landslides embedded into each other with the formation of a landslide cirque are examined on the example of one of the landslides on the bank

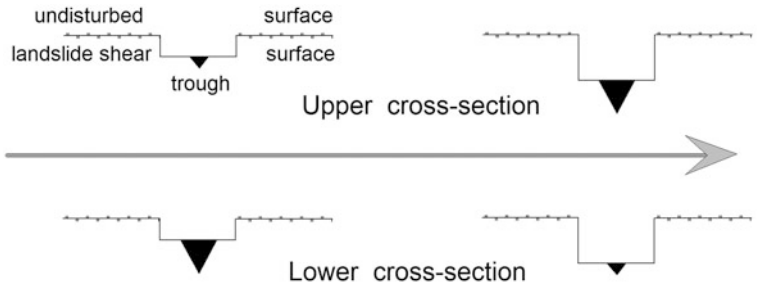

Fig. 6 Direction and intensity of the water flow cutting of erosion-thermoerosion type of on the shear surfaces of the cryogenic landslides. *Key* 1—Undisturbed surface adjacent to the cryogenic landslide; 2—shear surface; 3—erosion trough

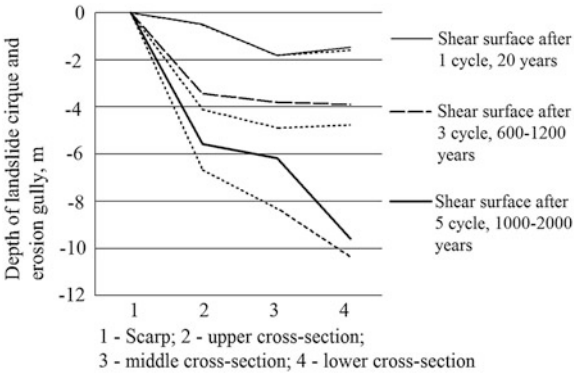

Fig. 7 Relation of the depth of shear surfaces to a number of landslide and erosion cycles in the landslide cirques

of the Panzanana-yakha river. Satellite image shows three shear surfaces of different ages. Their width is slightly different and the length varies significantly (Fig. 8). As a result of the three landslide cycles and the same number of erosion cycles, overall lowering of the surface amounts to 4.2 m, which means that each landslide and erosion cycle, lowers the surface to 1.2–1.3 m over a period of 200–400 years (Leibman and Kizyakov 2007). The surface which underwent at least 5 cycles of landslide process was lowered by 9.5 m, i.e., each landslide cycle deepened it by 1.9 m. It is possible that additional lowering of this surface was due to thermokarst, thawing of underground ice and subsequent subsidence.

Depths of landslide cirques and the number of landslide cycles (according to Leibman and Kizyakov 2007; Gubarkov and Leibman 2012) allows for calculating the value of the surface lowering in time intervals that make up these cycles (200–400 years). Compared were upper-middle and lower cross-sections of a landslide cirque given 3 or 5 landslide cycles (Table 5). There is little difference in the rate of surface lowering for all the cross-sections in a 3-cycle case ranging

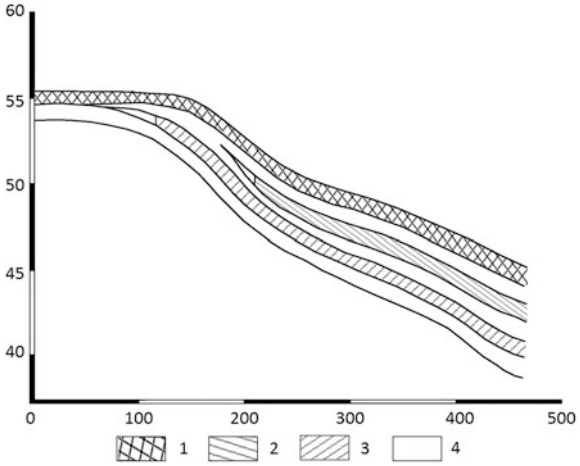

Fig. 8 Landslide and erosion cycles in the landslide cirque in the Panzanana-yakha river valley. *Key*: 1, 2, 3—900, 600, 20 year old landslide cycles, respectively; 4—erosion cycles separating landslide cycles

Table 5 The average depth (m) of the of landslide cirque bottoms for 1 landslide cycle

Number of cycles	Period, years	Cross-section		
		Upper	Middle	Lower
3	600–1200	−1.17	−1.27	−1.30
5	1,000–2,000	−1.14	−1.24	−1.90
Average	200–400	−1.15	−1.25	−1.60

between 1.17 and 1.30, and increasing from upper to lower cross-section (Table 5). Taken a 5-cycle case, the range of lowering depths is 1.14–1.90. Such an increase in the lowering rate for the lower cross-section may be associated with intense thermokarst.

Measurements of thicknesses of 156 landslide materials at the site "Vaskiny Dachi" showed that each landslide cycle is responsible for 0.3 to 1.0 m, averaging 0.55 m lowering of the landslide cirque surface. Therefore, its lowering due to erosion and thermokarst subsidence has an average range of 0.6 m in the upper part of the slope and 1.05 m in the lower part (see Table 5). Cryogenic landslide process triggers other processes that produce thermodenudation of the same intensity in the upper cross-section and twice as intensive in the lower cross-section.

The averaged value of surface lowering through alternating the main parage-netically associated slope cryogenic processes for three to five landslide cycles is 3.8–6.0 mm per year (Table 6). The middle and lower parts of the slopes have greater potential of lowering compared to the upper part of the slope. The obtained

Table 6 The average denudation (mm) for different number of cycles of landslide process and thermoerosion

Number of cycles	Period, years	Cross-section		
		Upper	Middle	Low
3	600–1200	−3.9	−4.2	−4.3
5	1,000–2,000	−3.8	−4.1	−6.3

values are close to the estimate of denudation obtained by Voskresensky (2001) for the Arctic Plains, which he estimated to be 6 mm per year.

Cryogenic landslides change the slope topography and thus, lead to subsequent lowering of the shear surface due to erosion and thermokarst that create conditions for increased snow accumulation, which leads to an increase in the depth of the active layer. Increased seasonal thawing due to the warming action of dammed by landslide materials water in summer. In reservoirs dammed by landslides, there is thermokarst subsidence. In gullies and ravines, cut deep into the shear surfaces of cryogenic landslides, we observe increased snow accumulation, which prevents freezing in winter, but also contributes to increased thawing in summer (Voskresenskiy 2001). In addition, the gullies and ravines experience temporary warm influence of runoffs in summer during rainfall.

Measurements of the active layer on the shear surfaces of cryogenic landslides, erosion network and on adjacent undisturbed surface were conducted on 6 landslide shear surfaces. Measurements were carried out along the profiles shown on Fig. 1. The average depth of the active layer on the shear surfaces exceeds the depth of active layer at the adjacent undisturbed surface by 43 %. Erosion network on the shear surface increases the depth of thawing by additional 10 %. The maximum difference in the depth of thaw is noted in the middle cross-section of the shear surfaces, where it may be two or more times deeper (Fig. 9). Given the

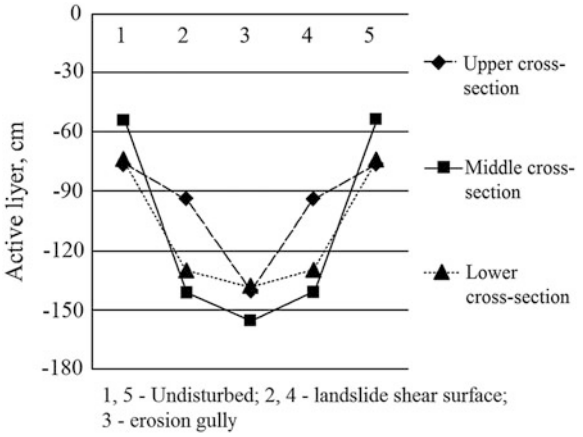

Fig. 9 Averaged active layer depth on the shear surfaces of cryogenic landslides, in ravines and adjacent undisturbed surface in a landslide cirque with three cycles of landslide process

warming impact in areas of erosion or damming of water, thawing can increase up to three times compared to the adjacent undisturbed surface.

Wider landslides or landslide cirques allow snow redistribution from the central part towards the scarp and side walls where increased snow accumulation may be observed. In such cases, we observe the maximum thaw near the scarp and side wall foot.

5 Conclusions

Cryogenic landslide process is a process that determines the formation of slopes and bottoms of the upper reaches of small river valleys. The volume of landslide materials per active phase in the cycle of cryogenic landslides may exceed the total annual volume of all sediment transfer by all other cryogenic and channel processes by 10,000 times.

Depending on the location in the Panzanana-yakha river valley, landslides are divided into two groups: (a) those that impacts only on the slopes with no impact on the bottom of the river, and (b) regulating channel run and width of the bottom of the river.

In the river valleys, the bottom width of which depends on the cryogenic landslides, two main types of the valley are observed: (a) erosion portions of the valley bottom narrowed by the landslide materials, and (b) expanded, flooded or waterlogged portions of the valley bottom dammed by the landslide process.

Damming of water flow in channels of small rivers by cryogenic landslide materials increases the time of water exchange by an order of magnitude, which is one of the main conditions for the development of river-channel thermokarst.

The main factors of landslide cirque formation are cryogenic landslide processes, thermoerosion and thermokarst. The rate of these processes varies. Cryogenic landslide process is a rapid process, thermoerosion has an active phase and gradually slows down; thermokarst belongs to the slow cryogenic processes.

Denudation in the formation of landslide cirques by various cryogenic processes consists of two components. The first process is cryogenic landslide process, the contribution of which is about half of the total lowering of the surface in the upper part of the slope and about a third—in the lower. Subsequent processes are thermoerosion and thermokarst, which lowers the surface even more.

Lowering of surface in the landslide cirques per landslide cycle (200–400 years) on the average makes 0.9 m in the upper part of the slope and up to 1.6 m in the lower part. This corresponds to the denudation of 4–6 mm per year.

References

Ananieva GV (1997) Especially engineering permafrost northern segment of the projected route of the railway Ob-Bovanenkovo. In: Results of basic research of the Earth Cryosphere in the Arctic and Subarctic. Nauka Publisher, Novosibirsk, 1997, pp 116–123 (In Russian)

Baranov AV, Posnanin VL (1999) Thermoerosional processes. In Erosion processes of Central Yamal. Gomel Publisher. St. Petersburg, pp 176–188 (in Russian)

Baulin VV, Aksenov VI, Dubikov GI (1996) Engineering-geological monitoring of Yamal oil- and gas-fields. In: V. II. Geocryological conditions of Bovanenkovsky gas-fields assimilation. IPOS SO RAN, Tyumen, pp 240 (in Russian)

Baulin VV, Dubikov GI, Aksenov VI (2003) Permafrost conditions Harasavey and Kruzenshternovsky gas condensate fields (Yamal Peninsula). Geos Publisher, Moscow, pp 180 (in Russian)

Dokuchayev VV (1878) Ways of formation of river valleys of the European Russia. St. Petersburg, pp 127 (in Russian)

Drozdov DS (2004) Information and cartographical modeling of natural and technogenic environments in a geokriologiya. Dissertation. Earth Cryosphere Institute SB RAS, Tyumen, pp 49 (In Russian)

Ermokhina KA (2009) Phyto-indication of exogenous processes in the tundras of Central Yamal. Dissertation. Moscow University, Moscow, pp 24 (In Russian)

Ershov ED (1989) Geocryology of the USSR. Western Siberia. Nedra Publisher, Moscow, pp 454 (in Russian)

Everdingen RO (1998) Multi-language glossary of permafrost and related ground ice terms, version 2. IPA, pp 161–167

French HM (1976) The Periglacial Environment. Longman, London, p 309

French HM (1998) Permafrost, real estate and climate change: the case of Thompson, Northern Manitoba, Canada. Biuletyn Peryglacjalny, pp 35–44

Gubarkov AA, Leibman MO (2007) Erosion processes on the share surfaces of cryogenic landslides: a case study at Vaskiny Dachi Station. Proceedings of the International Conference "Cryogenic Resources of Polar Regions", Salekhard, Russia, June 2007 II:136–138 (in Russian)

Gubarkov AA, Leibman MO (2010) Bead-shaped channel forms as an evidence of paragenesis of cryogenic and hydrological processes in the small-river valleys of central Yamal. Kriosfera Zemli (The Earth Cryosphere). XIII 1:41–49 (In Russian)

Gubarkov AA, Leibman MO (2012) Cryogenic and hydrological processes in the small-river valleys of Central Yamal. In: Processes of self-organization in erosion-channel systems and dynamics of river valleys. Tomsk. www.channel2012.ru/congeo.htm. (In Russian)

Harris C, Lewkowicz AG (1993) Micromorphological investigations of active-layer detachment slides, Ellesmere Island, Canadian Arctic. In: Proceedings of the 6th International Conference on Permafrost, Beijing, China. S. China University of Technology Press, pp 232–237

Kaplina TN (1965) Cryogenic slope processes. Nauka Publisher, Moscow, 296 pp (In Russian)

Karasev MS, Khudyakov GI (1984) River systems: on the example of the Far East. Nauka Publisher, Moscow, pp 143 (in Russian)

Leibman MO, Kizyakov AI, Sulerzhitsky LD, Zaretskaya NE (2003) Dynamics of the landslide slopes and mechanism of their development on Yamal peninsula Russia Permafrost. In: Phillips M, Springman SM, Arenson LU (eds) Proceedings of the 8th international conference on permafrost. Zurich 21–25 July 2003. Balkema, Lisse, pp 651–656

Leibman MO, Kizyakov AI (2007) Cryogenic Landslides of the Yamal and Yugorsky Peninsulas. Earth Cryosphere Institute SB RAS, Moscow-Tyumen, pp 206 (in Russian)

Lewkowicz AG (1990) Morphology, frequency and magnitude of active-layer detachment slides, Fosheim Peninsula, Ellesmere Island, N.W.T. In: Burgess MM, Harry DG, Sego DC (eds) Proceedings of the 5th Canadian permafrost conference, Quebec, June 1990. Laval University, Quebec, Collection Nordicana No. 54, 1990, pp 111–118

Makkaveev AA (1971) The dictionary on hydrogeology and engineering geology. Nedra Publisher, Moscow, pp 216 (in Russian)
Simonov YuG (1972) Regional geomorphological analysis. Nauka Publisher, Moscow State University, Moscow, pp 252 (in Russian)
Sukhodrovsky VL (1979) Exogenous transformation of relief in the permafrost zone. Nauka Publisher, Moscow, pp 280 (In Russian)
Surkov VV, Tarbeeva (2012) AM Bead-shaped channel forms in the small-river valleys of central Yamal. In: Processes of self-organization in erosion-channel systems and dynamics of river valleys. Tomsk, www.channel2012.ru/congeo.htm. (In Russian)
Timofeev DA (1978) Terminology of a denudation and slopes. Nauka Publisher, Moscow, pp 242 (in Russian)
Voskresenskiy KS (2001) The modern relief-forming processes on plains of the northern Russia. Moscow State University, Moscow, 264 (In Russian)
Washburn AL (1979) Geocryology: a survey of periglacial processes and environments. E. Arnold, London pp 406
Yemelyanova EP (1972) Main regularities of landslide processes. Nedra Publisher, Moscow, pp 310 (in Russian)

Editors Biography

Dr. Wei Shan is a Professor in Northeast Forestry University, China. He is a board member of the International Consortium on Landslides (ICL) and network coordinator for landslides in cold regions. His main research interest is in geo-environmental disasters in cold regions.

Dr. Ying Guo is an Associate Professor in Northeast Forestry University, China. She is Alternate Representative of the International Consortium on Landslides (ICL) and coordinator secretary of ICL Landslides in Cold Regions Network. Her research interest mainly is in hydrogeology and slope protection engineering in cold regions.

W. Shan et al. (eds.), *Landslides in Cold Regions in the Context of Climate Change*, Environmental Science and Engineering, DOI: 10.1007/978-3-319-00867-7,

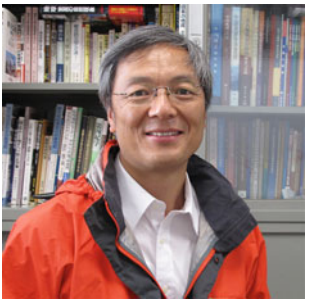

Dr. Fawu Wang is a Professor in the Department of Geoscience and Director of Research Center on Natural Disaster Reduction of Shimane University, Japan. His current research interest covers submarine landslides, landslide dams, landslides triggered by earthquake and water level variation, and landslide problems under the context of climate change.

Dr. Hideaki Marui is director of the Research Institute for Natural Hazards and Disaster Recovery of Niigata University and professor in the section of Mechanical Analysis on Disasters. He has been involved in a lot of research activities of the Japan Landslide Society. In recent years, Niigata Region has experienced a series of natural disasters such as earthquakes, floods, heavy snow falls. Most of such phenomena have strong relationship with landslide occurrence. He has been targeting various types of landslides. Landslides caused by snowmelt are one of the most important issues of his research activities.

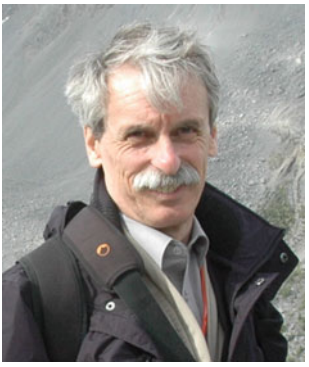

Dr. Alexander Strom is a head of Seismic hazard assessment department of the Geodynamic Research Center—branch of the JSC "Hydroproject Institute". His main research interests are on paleoseismology, on active faults affecting engineering structures and on mechanisms of large-scale bedrock landslides formation and motion.